Deltares

Morphological model for the River Meuse

Sambeek-Grave v0.8

enabling delta life

foto: RWS/J.v.Houdt

Morphological model for the River Meuse

Sambeek-Grave v0.8

Authors
Willem Ottevanger
Victor Chavarrias
Amgad Omer

\coverPhoto{...}

Morphological model for the River Meuse

Sambeek-Grave v0.8

Client	Rijkswaterstaat
Contact	Arjan Sieben, Roy Frings, Siebolt Folkertsma
Reference	
Keywords	Meuse, Sambeek, Grave, D-HYDRO, SMT, morphology

Document control

Version	v1.0
Date	2024-04-18
Project number	11209261-002
Document ID	11209261-002-ZWS-0008
Pages	183
Status	final

Author(s)

	Willem Ottevanger	Deltares

Summary

Recent events, such as the flood in July 2021 in the Meuse River in which large changes in bed level posed problems to infrastructure, have shown that up-to-date morphodynamic models are essential to aid in evaluation of measures and policy choices.

The Meuse River at present does not have a validated numerical model for morphodynamics. To uniformise the approaches on the Rhine and the Meuse, a plan was developed for the construction of a two-dimensional morphodynamic model of the Meuse which builds on the recently developed hydrodynamic D-HYDRO model of the Meuse. The current report shows the development of the version v0.8 model for the reach between Sambeek and Grave. The simulation has undergone a 1D calibration, using the sedimentation volume in the summerbed lowering at rkm 155. Therefore, this model should not yet be used for studies.

The morphodynamic model uses the Simulation Management Tool (SMT) to speed up the computation. An original flow time of 4 years reduced to 22.5 days, enabling the computation to run in just over 33 hours.

The model uses a locally refined mesh in the main channel. The hydrodynamics of the model compare reasonably to water-level-slope and velocity measurements. The division of the flow between the main channel and floodplain show expected behaviour, but are not verified as measurements do not exist.

An exploratory data analysis reveals the width-averaged changes in the bed level from measurements during the period after the summerbed lowering.

A discharge-dependent parameter investigation shows the behaviour of the model and reveals that the water level does not match the steering water level at Mook for low discharges, indicating that the Q-h boundary condition does work correctly. Furthermore, the calibration procedure of the hydrodynamic model yields friction coefficients that cannot be explained from the physical point of view and that cause unrealistic patterns of sediment transport.

The model calibration consists of the offline computation of transport conditions for the period between July 2014 and June 2018, where the volume of sediment deposited in the summerbed lowering is used as a calibration goal. Finally after different morphological computations reasonable agreement was found, except for the downstream reach near the weir of Grave where the model predicted sedimentation, whereas the measurements show a decrease in bed level. Further investigation is required to understand what causes this difference.

The model settings and underlying assumptions are discussed, and an outlook for further model investigation are provided.

Contents

List of Tables

List of Figures

1 Introduction

1.1 Background and motivation

The Meuse River, at present, does not have a validated two-dimensional numerical model for morphodynamics.

The current assessment of morphodynamic change can follow from:
- expert judgement from the local river authority
- WAQUA simulations in combination with the offline post-processing tools WAQMORF
- Ongoing development of a similar tool for D-HYDRO called D-FAST Morphological Impact.
- The large scale 1D model by Berends *et al.* (2020).

The above analyses offer only order of magnitude values, and are restricted to a single measure. When considering system-wide measures an up-to-date morphodynamic model is needed for river management issues such as:
- project design of interventions in/along the summer bed (normalisation, sediment management),
- impact assessment for evaluation of measures (river engineering assessment framework / licensing),
- analyses of/after monitoring in pilots (sediment management, eroding banks, river widening such as by longitudinal dams, etc.),
- system analyses for long-term scenarios with management variants, e.g. for IRM (Integraal RivierManagement – Integrated River Management) so that estimates can be made of the morphological development on the different river functions.

To align the approaches on the Rhine and the Meuse, a plan was developed for the construction of a two-dimensional morphodynamic model of the Meuse which builds forward on the recently developed hydrodynamic D-HYDRO model of the Meuse (De Jong, 2021). This development is ongoing for the Rhine model as well.

Development of the morphodynamic model using D-HYDRO is desired, since it is foreseen that the new sixth generation hydrodynamic model (De Jong, 2021) will soon replace the current fith generation WAQUA hydrodynamic model. It therefore makes sense to align the software for the morphodynamics as well.

1.2 Objective

The objective of this project is the development of a new modelling instrument that simulates the complex spatial riverbed dynamics in the Meuse river, enabling us to predict developments and effects of interventions in the riverbed, examine options for long-term (2050-2100) management and policy decisions, and thus shape the river management of the future.

1.3 Current report

The current report describes the setup of the morphodynamic model version 0.8 for the reach between Sambeek and Grave. This model has undergone a 1D calibration for the sedimentation in the summerbed lowering, but has not undergone a 2D calibration yet. Therefore the model should not be used in studies yet.

2 Approach for model setup

In 2019, Spruyt and Ottevanger developed a plan of action for the development of the morphological model for the Meuse. Based on this, they present a general approach, which foresees a model development in several steps. These steps are extended as follows for this project:

- v0 This version is a basic model that contains the most important functionality, with the main goal to have a running but not yet too complex model.
- v1 Building on v0, the first model version is a version which covers similar functionality as is provided for the Rhine by the existing DVR (Duurzame vaardiepte Rijndelta) model. Moreover, the model is based on the latest available data and insights.
- v2 The second model version is based on v1 but extended with new functionality to make the model suitable for more types of applications (e.g. finer grids, exchange of sediment between main channel and flood plains, bank erosion processes, etc.).
- v3 The third model version is used to develop new insights and functionality.

Table 2.1 shows the development of the model according to the different phases and an overview of the progress in the past years.

2.1 Background

The hydrodynamic model set up by De Jong (2021) includes the Meuse from Lixhe to Keizersveer. Different weir operations are incorporated in the model. Moreover to calibrate the model different model versions have been setup. These represent the river geometry in the years 1995, 2012, 2014 and 2019. In these years, different floods occurred which enable the validation for the high discharge events.

2.2 Activities prior to 2023

An initial model setup was carried out by Ottevanger *et al.* (2020).

In 2021, a pilot reach in the Common Meuse (in Dutch: Gemeenschappelijke Maas, also Grensmaas) was identified near Meers. The location of Meers was modelled by carrying out multiple simulations. The current status of the Meers model is that there are still differences in the results between sequential and parallel runs. Although many runs were performed and different software bugs were resolved, the differences remain at this location. It is hypothesized that the inherent sensitivity of the system (geometry, mathematical formulations and the numerical translation thereof) lead to differences which can be large with respect to an initial perturbation.

Since 2022, the reach of Sambeek-Grave was selected as a second pilot location. This location is well suited as there is a large-scale measure (summer-bed lowering) which has been implemented and the bed level is measured every year. Moreover, the reach has a lower slope and it appears that models of the low-slope rivers are found to be less sensitive, compared to the steeper river reaches like the Meers model. This is demonstrated by findings in a model of the Western Scheldt and different schematic river models.

2.3 Overview of the activities

The table below describes the model development steps per sub category, and the present status of the different reaches of the Meuse. For legibility the following abbreviations have been introduced:

- EK: Eijsden-Keizersveer,
- LiK: Lixhe-Keizersveer,
- ML: Monsin-Lixhe,
- LB: Lixhe-Borgharen,
- BL: Borharen-Linne,
- LR: Linne-Roermond,
- RB: Roermond-Belfeld,
- BS: Belfeld-Sambeek,
- SG: Sambeek-Grave,
- GL: Grave-Lith,
- LK: Lith-Keizersveer.

Table 2.1 Steps in model development

activity areas	associated activities	model version	2020	2021	2022	2023
data collection	• Collection of all data needed to set-up a model, e.g. boundary conditions, calibration data hydrodynamics and sediment transport and morphology, bed composition, etc.	v0,v1	EK - v0, Meers - v0	SG	SG, Li-K	SG v0.8, LR v0.5, RB v0.5, BS v0.5, GL v0.5, LK v0.5
morphodynamic model schematization: towards a well-working basic model (v0)	• set-up of a first running model including: a. dynamic river bed b. representative initial bed elevation (e.g. smoothing of bed forms) c. suitable roughness formulation for morphology d. sediment (grain sizes and sediment layers, with focus on active/upper layer) e. secondary flow f. first choice of transport formula and parameters (uncalibrated) g. non-erodible and less erodible layers h. suitable grid resolution • testing phase v0 model, identification of problems and modification of the schematization accordingly	v0		SG SG - v0.5 EK EK	SG - lokale 20m	SG LR, RB, BS, GL, LK - 20m
extending the basic model to a v1 model	• more sophisticated description of a. main channel roughness b. composition and thickness of underlayers, including non-erodible layers • set-up of a dredging and dumping module • testing phase v1 model, and iterative modification of model schematization if necessary	v1			SG	(sed.trans. including separate roughness) SG (fully mobile)

(continues on next page)

Table 2.1 – continues from previous page

activity areas	associated activities	model version	2020	2021	2022	2023
development of methodologies and tools for running the model	• approach and tools for model simulation (i.e. Simulation Management Tool) • strategy for model spin-up • strategy and tools for model evaluation and presentation of results • strategy and tools for simplification of model set-up and improving reproducibility	v0,v1	EK, EK - v0	SG - Too coarse	SG - Local 20 m	Improvement of restart to seconds Submodels based on standard simulations Start on user manual
model calibration and validation	• calibration and validation strategy • adapting the hydrodynamic model to make it suitable for morphodynamic simulations • hydrodynamic validation • *offline* calibration giving a first estimate of morphological response based on the flow field in the hydrodynamic simulations • 1D morphodynamic calibration and validation (focusing on width-averaged, large-scale and long-term trends) • 2D morphodynamic calibration and validation (focusing on 2D patterns in the river bed, such as bank patterns and bend profiles) • validation of dredging and dumping module	v1		2014-2018	2014-2018 remove weirs 50000 m3/year, Influence of fixed layers	2014-2018 20 m submodels SG v0.8, LR v0.5, RB v0.5, BS v0.5, GL v0.5, LK v0.5 Jump at SG lowering Analysis of statistical output of bed level changes
exploring model uncertainties	• influence of unknown physical variables (e.g. roughness in transport, bed composition, active layer thickness) • influence of model settings (e.g. initial geometry/composition and boundary conditions) or modelling concepts (e.g. Hirano model) • influence of simulation strategy and approaches (e.g. methods for optimizing simulation time, schematization of the hydrograph, choice of simulation period)	v1-v3				
development of modeling strategies and development for future use of the model	• identifying types of application and requirements • development of strategies for application of the model (e.g. choice of scenarios, choices • for model settings and geometry, type of interventions)	v1-v3				

(continues on next page)

Table 2.1 – continues from previous page

activity areas	associated activities	model version	2020	2021	2022	2023
	• identifying needs for further development of the model schematization (including needs for knowledge development and data requirements) • implementation and testing					
verification of model application	• testing the model application in test cases of a. effect of interventions b. planning study (*planstudie*) c. (long-term) forecast of system behaviour • improvement of the model schematization, modeling strategies, methodologies and tools based on the outcomes of the test cases	v1-v3				
implementation of new functionality in D-HYDRO	• Identifying requirements of new functionality • functional design of needs • design of implementation • implementation and testing • updating user manuals	v2-v3				
reports			Ottevanger *et al.* (2020)	Ottevanger *et al.* (2021); Ottevanger (2021)	Ottevanger and Chavarrias (2022b,a)	Ottevanger *et al.* (2024a,b)
related work				Chavarrias (2021)	Chavarrias and Ottevanger (2022)	

3 Model setup

3.1 Introduction

For the development of the model the large scale model of De Jong (2021) is used as a basis. This model is based on the Baseline schematisation j19_6-w2. The construction of the model in general is explained in Ottevanger *et al.* (2021). In this report, differences related to this main setup are explained.

The location between Sambeek and Grave, is well suited for calibration of the numerical model. This is because it shows the response of the river bed due to the summerbed lowering in the reach. Meijer (2020a,b) compiled an overview of the measured yearly bed levels for the Meuse River. This information was aggregated into different polygon sections, in which the average development can be seen. Figure 3.1 shows the measured evolution of the summer-bed-averaged river bed.

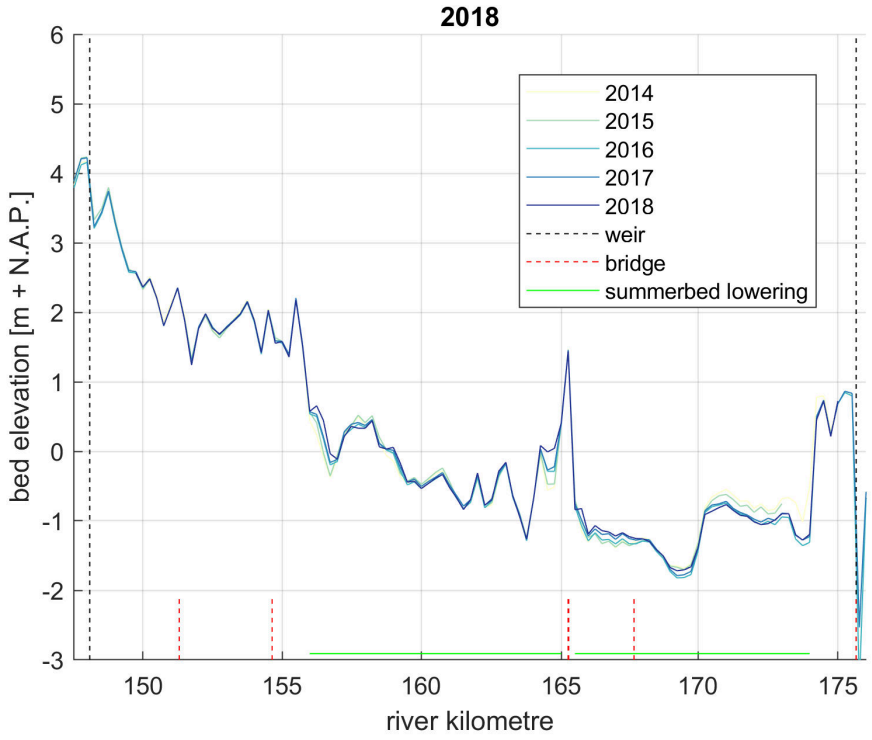

Figure 3.1 Bed level development averaged over the main channel (L3R3) Meijer (2020a,b)

3.2 Location

The river stretch Sambeek-Grave is located between river kilometer (rkm) 147 and rkm 175. Grabbing immediate attention is the meander bend cut-off at Boxmeer, which was shortened in 1980 (Tolman, 1987). The bend cut-off was a component of a plan developed by Lely (1926) developed to assist in the rapid conveyance of water in the case of floods. Both the shortening and the removal of the sharper bends aid in this. As an added benefit, the maneuvering for shipping was also improved. Figure 3.2 shows the original situation. Figure 3.3 shows the design, which shortened the river by roughly 1.6 km. Figure 3.4 shows the current situation. In addition, in 1942 the Beersche weir got closed off when constructing the railway from Venlo to Nijmegen (Figure 3.5). Prior to the closure the Traverse Beersche Maas would get inundated during floods.

Besides that, different channels also characterise this region, such as the connection to the Mookerplas and the Maas-Waal canal which allows passage between the Maas and the Waal. Another is the Niers river which attaches to the main channel.

Besides what can be seen from above the reach has also been subject to different flood mitigation measures in the course of the Maaswerken (see Figure 3.6). An important measure was the lowering of the river bed in the stretch between Sambeek and Grave. This happened between rkm 155 and 174 in 1996 and 1997 as a first phase (pilot project), and later in a second phase in 2012 (rkm 156-167) and 2015 (rkm 168-174).

In addition, different nature rehabilitation measures, such as removal of bank protection, are recently completed or are planned in the coming years. An evaluation of the past 10 years of the development of the nature-friendly banks was done by Chrzanowski *et al.* (2019); Chrzanowski and Buijse (2019). An overview of the locations is shown in Figure 3.7.

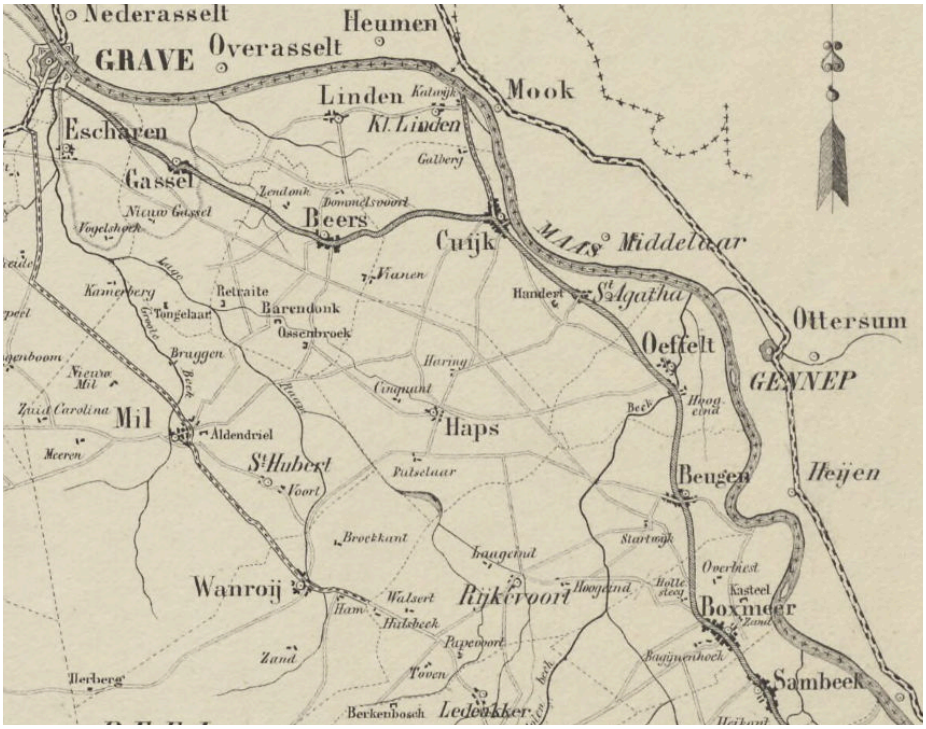

Figure 3.2 Bends at Heijen (in lower right corner) as drawn by Kuypers and Osch (1853). Accessed from https://uu.georeferencer.com

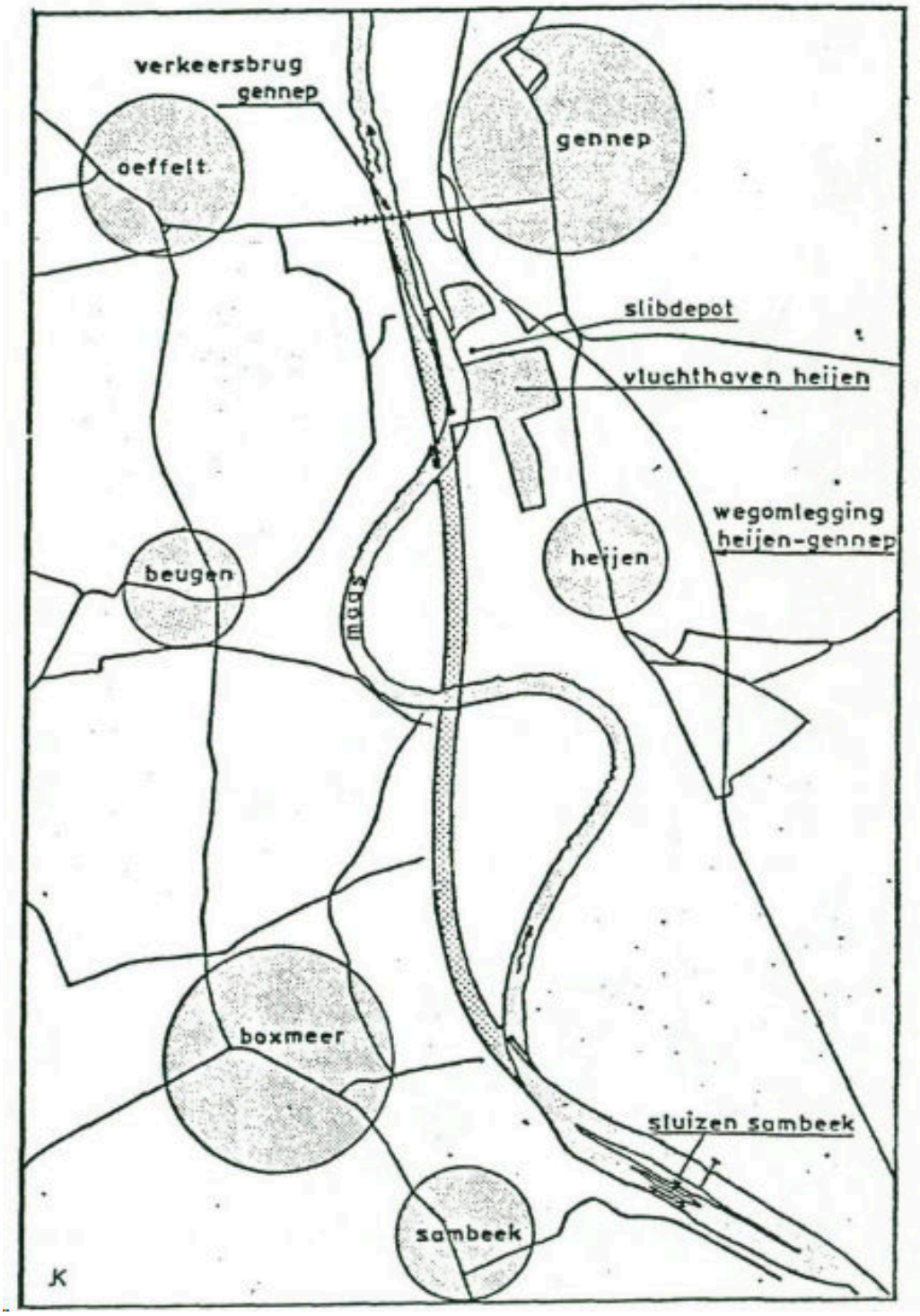

Figure 3.3 Illustration of the bend cut-off as shown in RWS, Directie Limburg (1979)

Figure 3.4 Current layout for the reach Sambeek-Grave

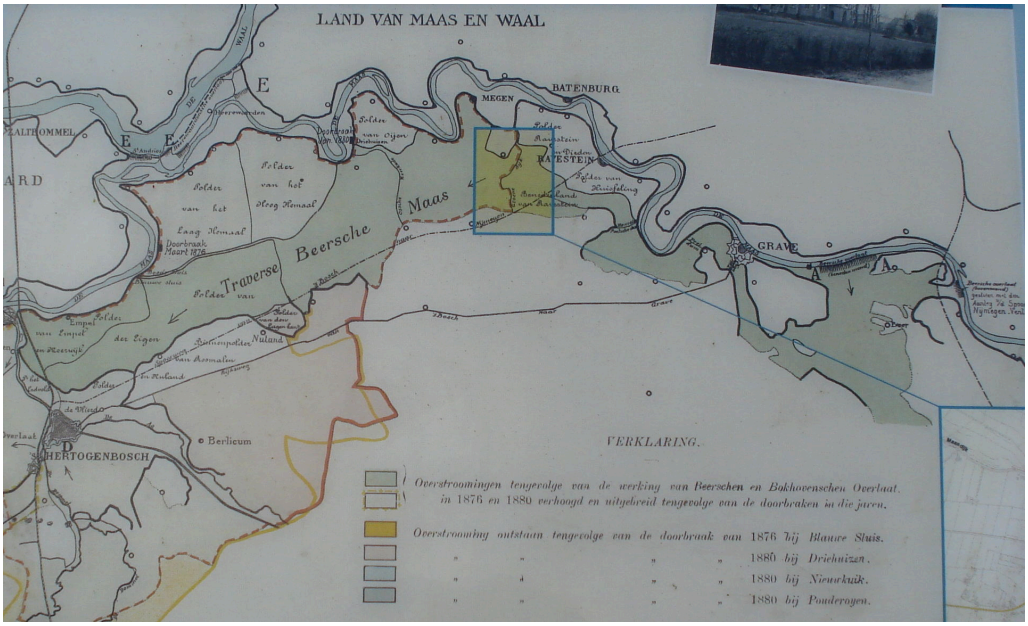

Figure 3.5 The former Beersche weir (at A) and the Traverse Beersche Maas (in green)

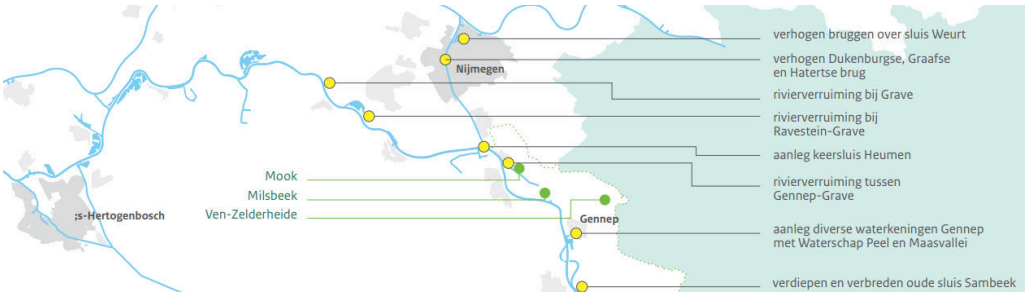

Figure 3.6 Overview of measures for the Maaswerken, source: https://puc.overheid.nl/rijkswaterstaat/doc/PUC_165412_31/

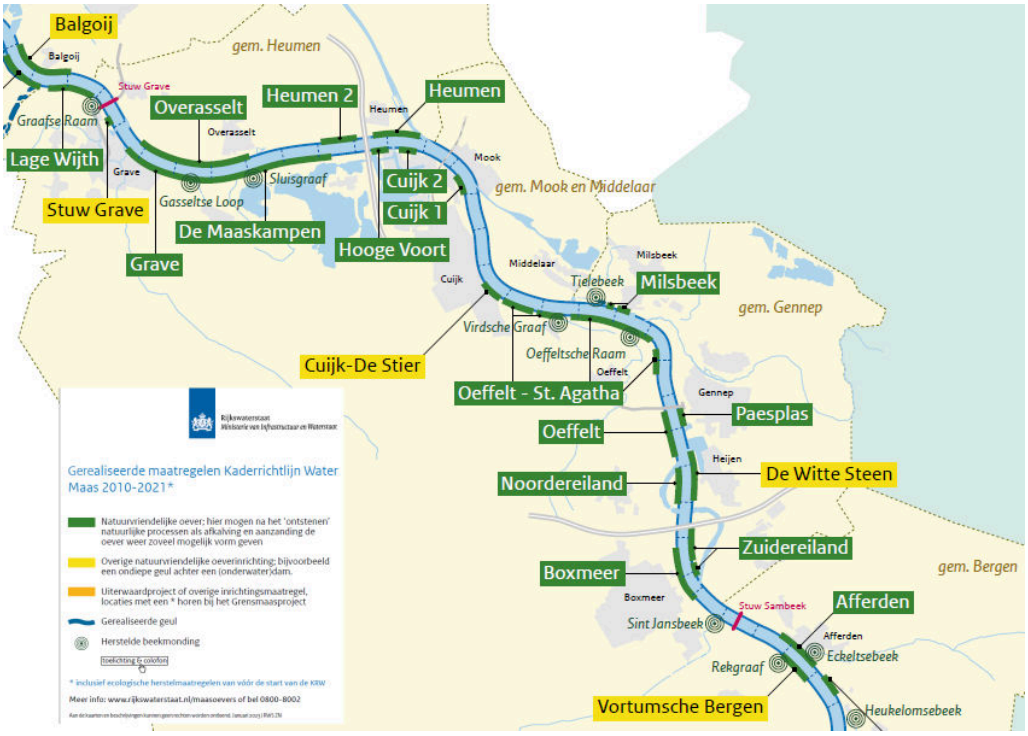

Figure 3.7 Overview of nature rehabilitation measures in the reach Sambeek-Grave. https://open.rijkswaterstaat.nl/publish/pages/178556/klikbare_kaart_gerealiseerde_maatregelen_krw_maas_2010-2021.pdf

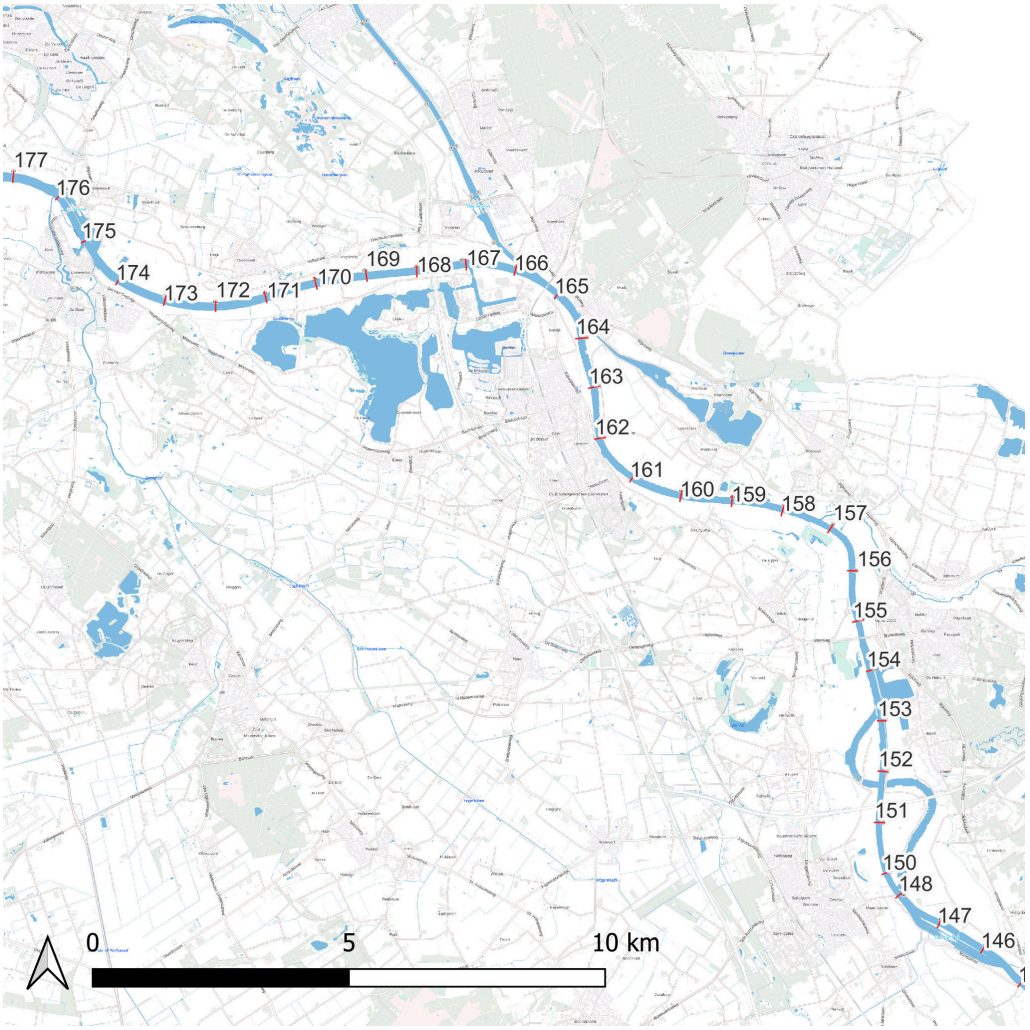

Figure 3.8 Location of river kilometres

3.3 Structures

The water level in the reach between Sambeek and Grave is strongly influenced by the operation of weir Grave, which has to maintain specific water levels for navigation. Mook is the central point in this stretch, on which the water level is maintained at 7.91 m w.r.t N.A.P by adjusting the gates at Grave for low discharges until roughly 950 m^3/s. For higher discharges the water level of 7.25 m w.r.t. N.A.P. at Grave is used as a set point. This can be seen in Figure 3.9. Based on the head difference in the betrekkingslijnen, the weir operation was also checked as a function the discharge. Figure 3.10 illustrates the corresponding discharges for the weir operation, similar to the water levels in Figure 3.9.

Besides, the weirs there are also three locks (at Mook connecting to the Mookerplas, at Heumen connecting to the Maas Waal canal and at Cuijk connecting to the Kraaienbergse Plassen). These all close when the water level at Mook exceeds 8.30 m+N.A.P (see De Jong (2021) for details).

Within the reach there are different bridge crossings:

- MA_151.31_A77-Maasbrug-Boxmeer
- MA_154.64_N264-Maasbrug-Gennep
- MA_165.25_Fietsbrug-Mook
- MA_165.26_Spoorbrug-Mook
- MA_167.65_A73-Maasbrug-Heumen
- MA_175.65_N324-John-S-Thompsonbrug-Grave

At Mook, the railway and bicycle bridge are known to have a bed protection which will act as a fixed layer in the model. The most downstream of these bridge crossings coincides with the location of the weir at Grave.

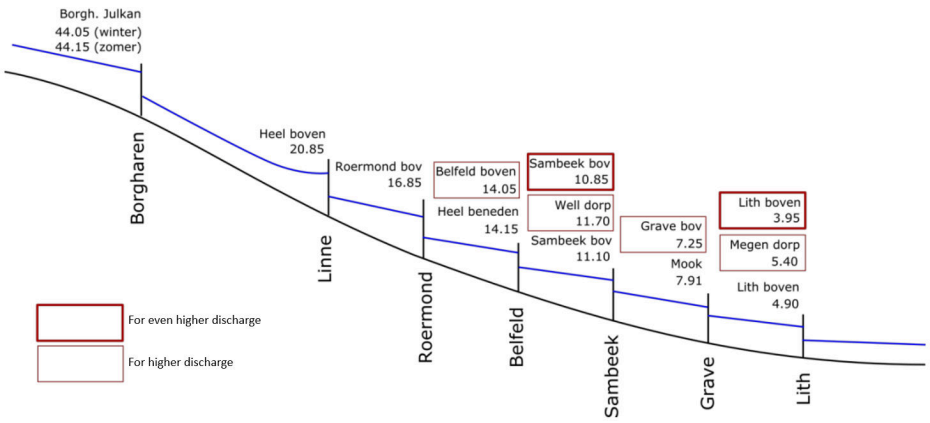

Figure 3.9 Water levels for weir operation on the Meuse (adapted from De Jong (2021))

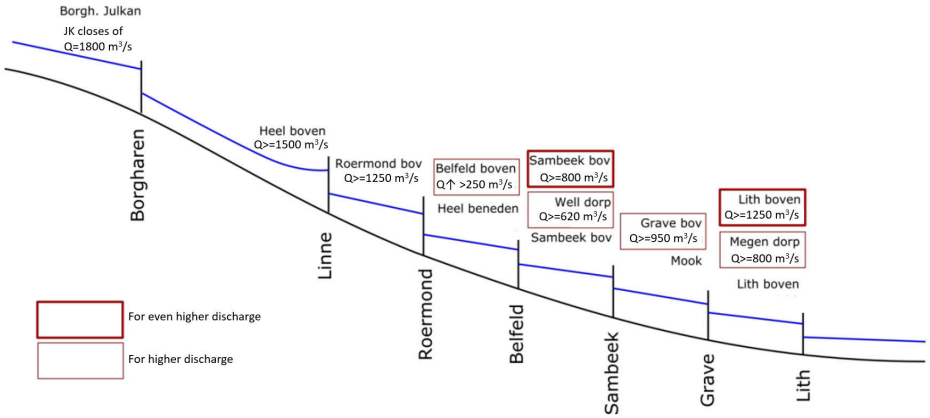

Figure 3.10 Discharges associated with the steering water levels for weir operation on the Meuse (adapted from De Jong (2021))

3.4 Grid

At some locations the morphologically active portion of the grid was only 3 grid cells in the transverse direction (cf. De Jong (2021)). Therefore the grid was refined along the main channel by a factor two, to have enough cells in the transverse direction in the morphologically active region.

To generate the refined grid the curvilinear section was followed and within this polygon the grid was refined a factor two. At the transition zones a single row was sacrificed to have the triangles at the connecting interface to have better grid properties (viz. smoothness and orthogonality). A small stretch of the resulting grid is shown in Figure 3.11.

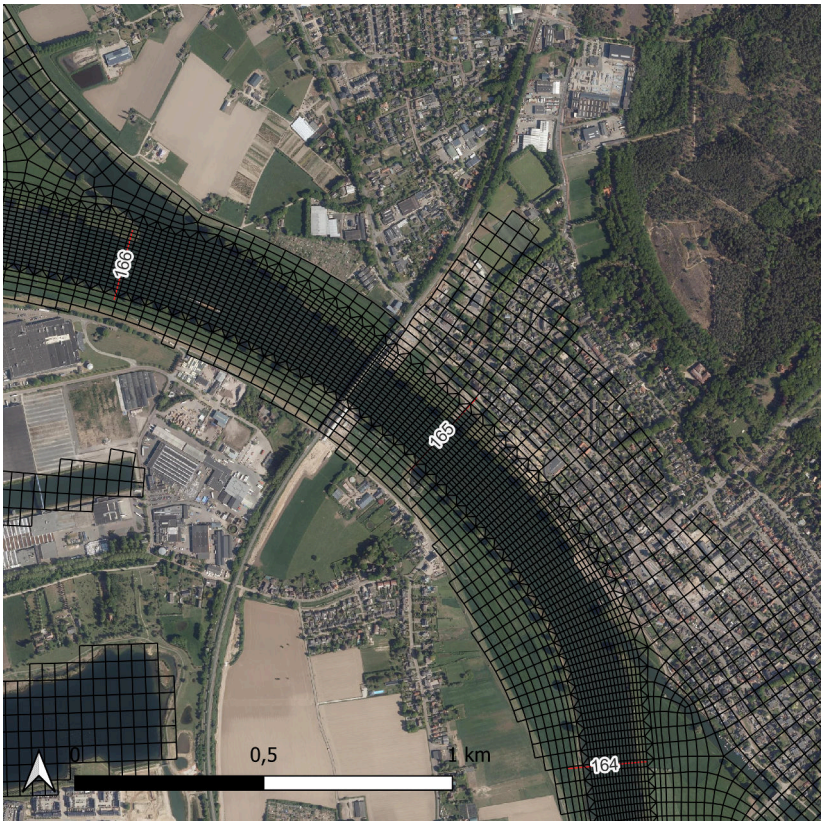

Figure 3.11 Example grid with refined summerbed at near Mook.

3.5 Bed level

As the model is intended for calibration purposes, the bed level is based on the 2014 situation. In the initial hydrodynamic and sediment transport computations this is based on the Baseline schematisation j14_6-v14 (Rijkswaterstaat and Deltares, 2022). At a later stage it was discovered that there was a mistake in the schematisation of the summerbed lowering just upstream of the weir at Grave (measure ma_zbgra14_a1 added a dredging of 1.5 m depth, whereas this should have been a dredging up till the level 1.5 m + N.A.P.). In the later versions of the model, this was replaced by the yearly multi-beam measurement data at a 1x1 grid (JMP2014). This will be fixed in a subsequent edition of the Baseline database j14_6. The initial bed level is shown in Figure 3.12.

There is also a j19 bed level available as an initial condition, however this will not be reported in the current document. This is important for future applications of the model, related to a near current schematisation.

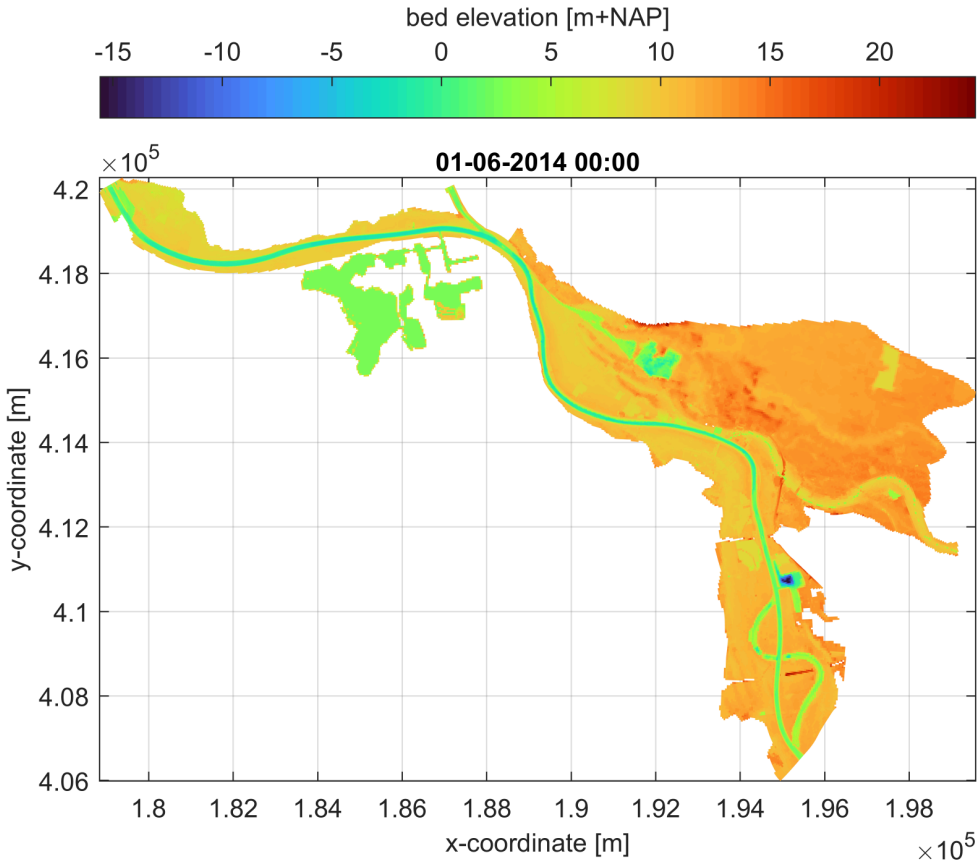

Figure 3.12 Bed level at the start of the simulation (considered to be at 1-6-2014).

3.6 Boundary conditions

To simplify the challenges for the morphodynamic model, the interaction with weirs steered by D-RTC Real Time Control was deliberately excluded from the model. Instead, the influence of the weir is taken into account in the downstream boundary condition.

At the downstream end, a stage discharge relation is used. This stage discharge relation is based on the 'Betrekkingslijnen' Rijkswaterstaat Zuid Nederland (2019). To illustrate the relation, the 'Betrekkingslijnen' and measured data at 2014 at Grave Boven are plotted versus the discharge at Venlo (with a time shift of 17 hours). This leads to a striking Q-h relation, which leads to a lowering of the water level for increasing discharges below 1000 m^3/s, and subsequently increasing for higher discharges. This is due to the operation of the weir at Grave (as explained in Section 3.3).

At the upstream part of the reach near Sambeek a discharge condition is applied. This discharge condition is based on the measurements at Venlo (cf. Figure 3.14).

Subsequently a schematic discharge wave is created for use with the simulation management tool (SMT, cf. Yossef *et al.* (2008); Ottevanger *et al.* (2020)). The approach used is similar to Yossef *et al.* (2008), in which the hydrograph is modelled through a set of constant discharge simulations with varying morphological factor, rather than a dynamic hydrograph. The schematic hydrograph is shown in Figure 3.15.

In the current report the discharge sequence in the SMT was done according to a different method than is currently considered best. It is currently considered better to use physical cutoff points in the flow to distiguish between the different flow regimes (see Sieben (2023)).

In the current report the discharge sequence was derived as follows:

First an integer partitioning of half days was sought where the following integer programming problem was solved:

$$\min_x f^T x \qquad \text{subject to} \begin{cases} x \text{ are integers} \\ A_{eq}x = b_{eq} \\ 1 \leq x \leq 100 \end{cases} \tag{3.1}$$

where $A_{eq} = [320, 160, 80, 40, 20, 10, 5]$, $b_{eq} = 365 \cdot 2$, and $f = [\frac{1}{320}, \frac{1}{160}, \frac{1}{80}, \frac{1}{40}, \frac{1}{20}, \frac{1}{10}, \frac{1}{5}]$.

The above equation partitions the year into different periods which sums to exactly a mulitple of the half days in a year b_{eq}. By reducing the factor f for large A_{eq}, the preference is to find larger blocks than smaller blocks which will be better in the next steps when converting this to a discharge sequence. By setting an upper and lower bound for the periods it enforced that each period occurs at least once.

When using 7 categories, the optimal value of x was found as: [1, 1, 2, 1, 1, 2, 2], which splits the year into 10 different periods which are a multiple of half days. Sorting the periods from small to large results in the following cumulative time periods [160, 240, 280, 320, 340, 350, 355, 360, 362.5, 365]. These values were used to find a cumulative discharge percentile in the discharge sequence of Venlo between 2014 and 2018.

Secondly, the following cumulative discharges are subsequently found

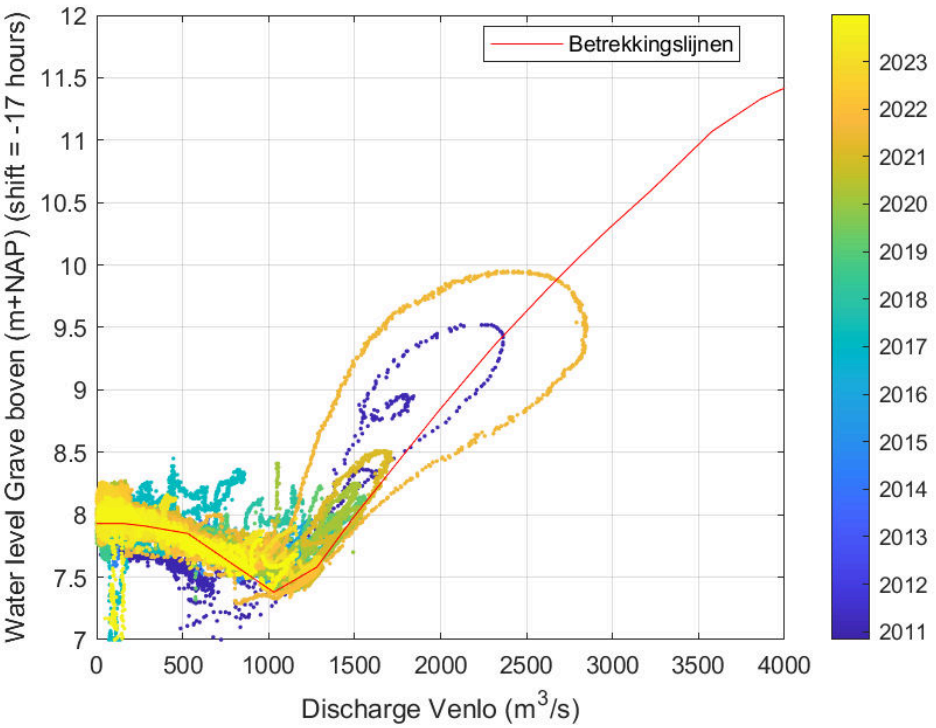

Figure 3.13 Stage discharge relation at Grave boven, based on the 'Betrekkingslijnen', and water level measurements in comparison to the discharge at Venlo shifted by 17 hours.

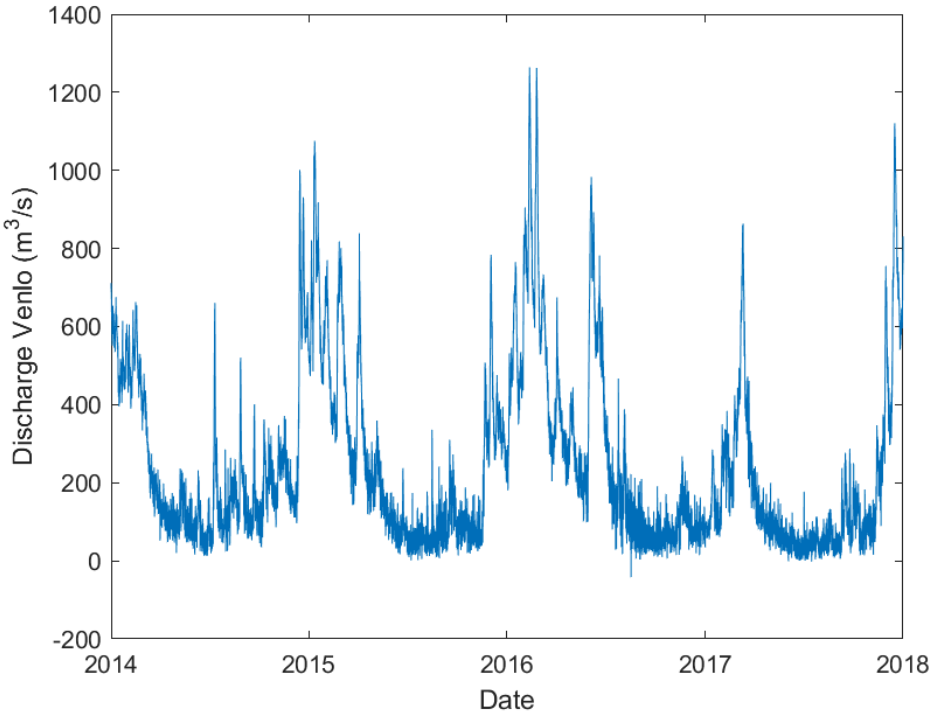

Figure 3.14 Discharge sequence at Venlo used for the discharge condition at Sambeek

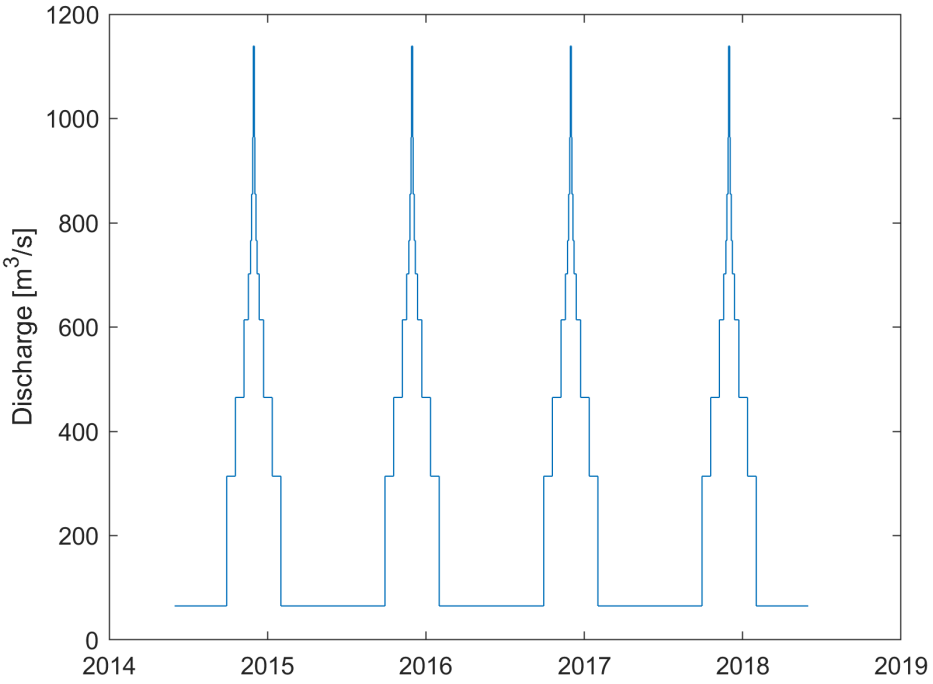

Figure 3.15 Schematic hydrograph used for the discharge condition at Sambeek

Q_e = [130.5 257.5 370.7 558.4 670.0 734.3 797.3 912.7 1014.4 1263.9].

Thirdly, by averaging and rounding the discharge levels for each period the following representative discharges are found Q_l = [65 194 314 465 614 702 766 855 964 1139].

Finally, different morphological factors were applied to the different periods. The SMT approach allows for a strong reduction in the computational time as different morphological acceleration factors can be used, depending on the discharge, the actual time needed to compute the bed level development can be significantly reduced. Table 3.1 shows an overview of the imposed morphological factors[1]. During the low flow period the bed level changes are considered to be small, and therefore larger MORFAC can be used. At the peak discharges a smaller MORFAC is used.

The resulting discharge hydrograph used in the simulation is shown in Figure 3.16.

[1] For the 65 m^3/s discharge level the morphological factor is much higher than the other discharges, but there is no composition or bed update during this time, it has been included to ensure that the morphological time frame is easier to process.

Discharge [m^3/s]	MORFAC
65	1440
194	40
314	40
465	40
614	20
702	20
766	10
855	10
964	5
1139	5
1400	1
1500	1
1600	1
1700	1
1900	1
2100	1
2200	1
2300	1
2400	1
2500	1
2700	1

Table 3.1 Overview of morphological factor per discharge.

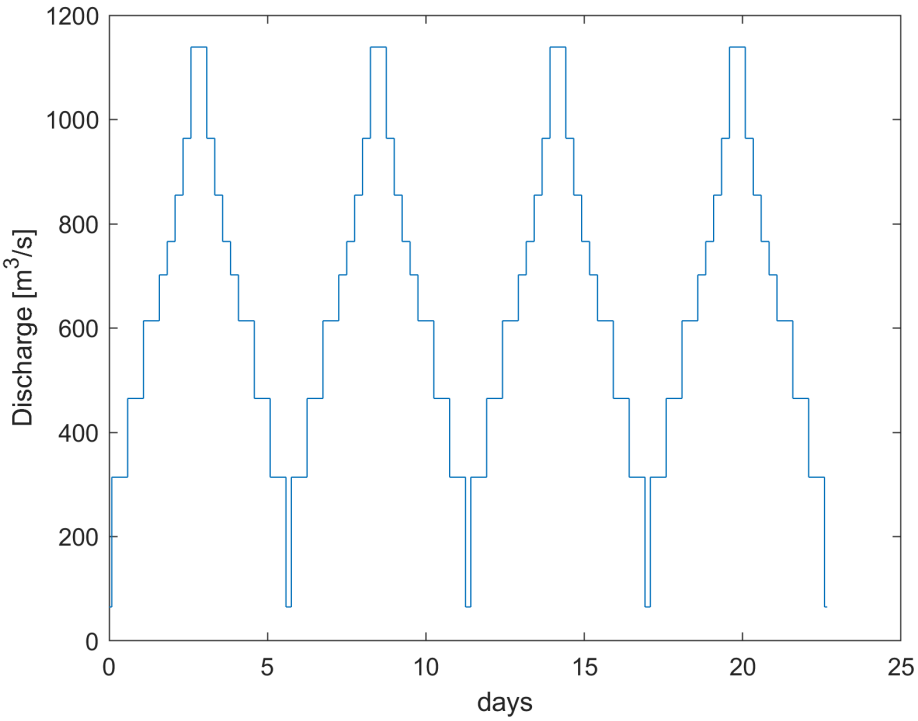

Figure 3.16 Schematic hydrograph used for the discharge condition at Sambeek

3.7 Sediment properties

Frings (2022) has updated the sediment properties of the old measurement campaign (1981-1983) and analysed the new (2020). The analysis by Frings (2022) describes the top layer content and the 10 km rolling average along the channel. For the 2020 information the width averaged values are shown in Figure 3.17. The sediment classes of the top layer have been updated according to this new data, and the subsurface layers are based on the information the model by Berends *et al.* (2020) (based on earlier work by Sloff and Barneveld (1996); Sloff and Stolker (2000); Berkhout (2003); De Jong (2005)). In addition the gravel-sand boundary of 2mm was added to the sediment classes (cf. Table 3.2). The sediment under-layers are imposed starting at the current bed level as the zero reference. As there may have been significant bed level degradation since the original data, it is a good point to investigate the effect of this choice in the model. This is left as a recommendation for further research.

Sediment fraction	Minimum diameter [m]	Maximum diameter [m]	Classification
Sediment1	8.00e-05	1.25e-04	sand
Sediment2	1.25e-04	2.50e-04	sand
Sediment3	2.50e-04	1.00e-03	sand
Sediment4	1.00e-03	2.00e-03	sand
Sediment5	2.00e-03	4.00e-03	gravel
Sediment6	4.00e-03	8.00e-03	gravel
Sediment7	8.00e-03	1.60e-02	gravel
Sediment8	1.60e-02	3.15e-02	gravel
Sediment9	3.15e-02	6.30e-02	gravel
Sediment10	6.30e-02	1.00e-01	gravel
Sediment11	1.00e-01	2.00e-01	gravel

Table 3.2 Overview of sediment fraction classes.

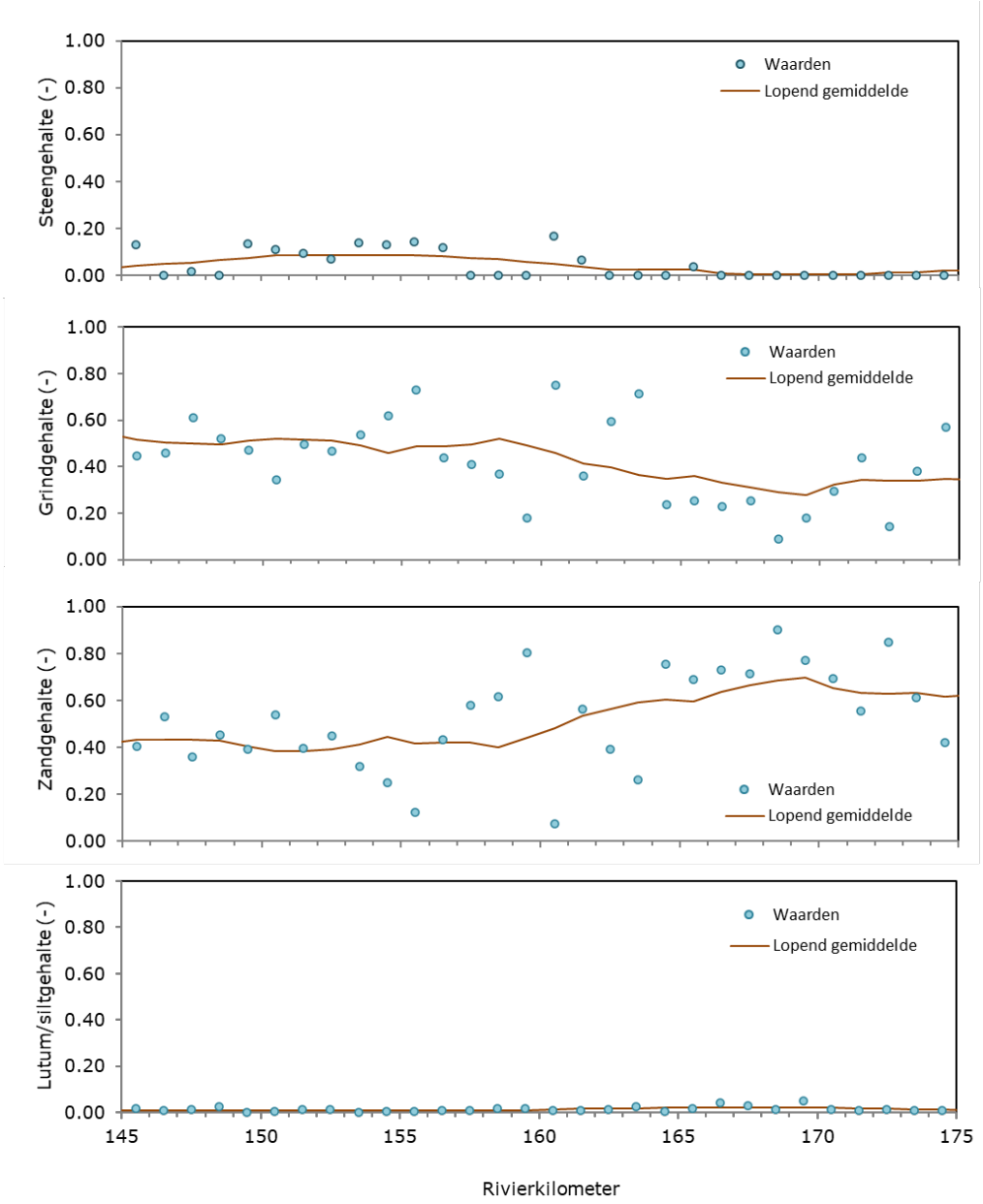

Figure 3.17 Sediment diameters based on Frings (2022). From top to bottom: stone fraction, gravel fraction, sand fraction and silt fraction.

3.8 Sediment availability

Ottevanger *et al.* (2021) analysed the bed level variation in 2018, 2019 and 2020 and combined this with known locations of fixed layers. An example is shown in Figure 3.18. An overview of the full reach is shown in Appendix D In this approach it was determined that the bed level near Mook (rkm 165) behaved as a semi-fixed layer as there was only minor bed level variation. Later RWS-ZN (Siebolt Folkertsma) confirmed that there is in fact bed protection present at this location.

Figure 3.18 Bed level classification from Ottevanger *et al.* (2021)

This information was used to prescribe the sediment availability in the model. It was assumed that there is 8 m of available sediment in general (matching the value as used by Berends *et al.* (2020)). At bank zones the initial sediment thickness is assumed to be zero, thereby matching the current approach in the DVR models. Sediment from the banks could be imposed similar to Van der Mark *et al.* (2011). At semi-fixed layer locations, the thickness could be adjusted between fully available sediment (8 m) up to a fixed layer (0 m). The simulation showing the best calibration result used fully available sediment at these locations.

4 Hydrodynamic validation and application

The current chapter presents validation of the D-HYDRO model with the flood wave of July 2021. The current validation is used to understand how the hydrodynamics contribute to the morphodynamic result, and not as a step to improve the hydrodynamic model.

During the flood, AquaVision performed measurements of the water level slope and the velocities (Eelkema, 2021). Eelkema (2021) estimate the discharge between Sambeek and Grave at 1450 and 2100 m^3/s for the 16th and 18th of July 2021, respectively. Van der Veen and Agtersloot (2021) performed an analysis of the peak discharges during the flood event. Moreover, using WAQUA they computed the hydrodynamics of the flood, which compared well for discharges at Venlo (cf. Figure 4.1). Given that the signal takes in the order of half a day to reach Sambeek from Venlo cf. Appendix B.1.5 in ENW (2021), the estimates of (Eelkema, 2021) and the values found in Van der Veen and Agtersloot (2021) can be considered similar.

In the following sections, water level slope and velocity measurements are compared. Subsequently, the model results are analysed for the discharge division between the main channel and the floodplains.

4.1 Water level slope measurements

For the 16th of July 2021, three moderate flood discharge levels were run using the Baseline j19 geometry, namely 1400, 1500 and 1600 m^3/s and a downstream water level of 7.60 m (based on the measured value, but extrapolated because the boundary lies further downstream in the model than the measurement.).

Three discharges were used, because the simulations ran using a constant discharge, rather than the dynamic discharge which happened in reality. The results are shown in Figure 4.2. The comparison shows that the discharge 1400 m^3/s is closest to the measured signal. Two clear sections are visible in the figures (rkm 147 - 165, and rkm 165-175). The results clearly show two different slopes. Just downstream of 165 the water level shows a slight dip to the narrowing at the bridge in the three model runs and in the measurements. At the downstream boundary the water level in the model is too high.

The results for the 18th of July are shown in Figure 4.3. In this case, high discharges of 2200, 2300 and 2400 m^3/s and a downstream water level of 9.60 m (based on the measured values) were imposed in the simulation. Reasons for using three discharges are similar in this case as for the moderate discharge computations. The simulation with a high discharge of 2400 m^3/s showed the best comparison to the measured water level slope.

All in all, the comparison for both days shows a reasonable agreement to the measurements. In principle, it would be possible to adjust the boundary water level, calibrate roughness, introduce a time varying discharge and water level signal to improve the comparison even further, but that would be exceeding the point of the comparison. A further and more detailed comparison of the flood wave to the D-HYDRO model has been done in the project of SITO-PS MAD09a Hydraulica schematisaties zoet (Van der Deijl, 2022).

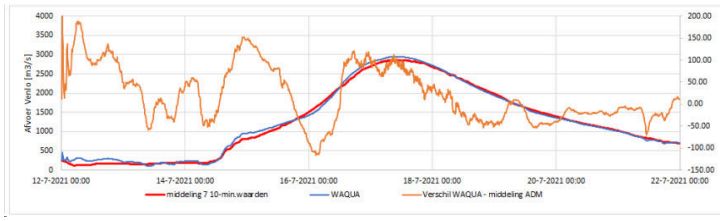

Figure 4.1 Discharge at Venlo from measurement station and WAQUA computation by Van der Veen and Agtersloot (2021).

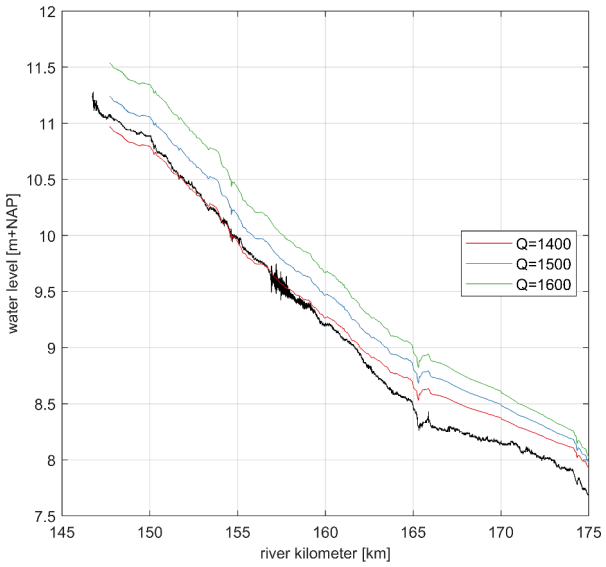

Figure 4.2 Water level slope comparison for 16-7-2021. The black line is the measured value.

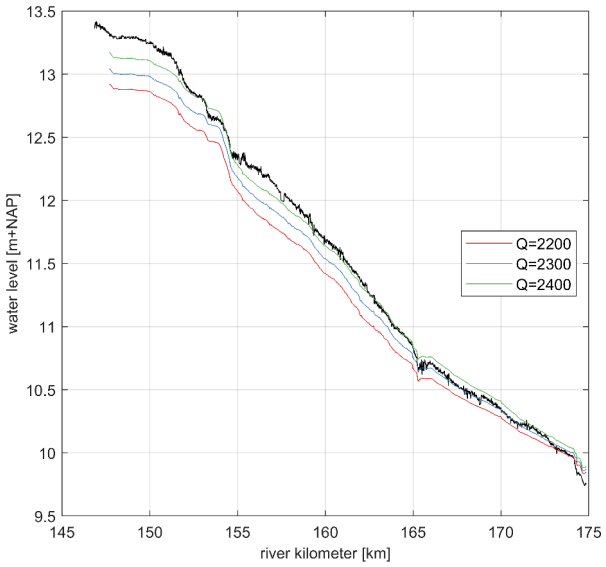

Figure 4.3 Water level slope comparison for 18-7-2021. The black line is the measured value.

4.2 Velocity measurements

Besides the water level slope measurements (Eelkema, 2021) also performed velocity measurements using ADCP. These were taken at the same days as the water level slope measurements. Subsequently the data were analysed by Arjan Sieben (personal communication, 25-03-2022 and 29-4-2022). The resulting figures below show the overall comparison for the different measurement sections for both measurement days. The measurements were averaged over the length of the ADCP measurements (cf. Figure 4.4). For this reason only width-averaged values are shown.

The underlying figures can be found in the Appendix C.1 and C.2.

Figure 4.5 shows the comparison of the different velocity fields aggregated over the cross-sections in the streamwise direction for the 16th of July. The coloured lines indicate the model results for varying discharge (similar to the water level slope comparison). The black line denotes the measurement result. At each measurement result a standard deviation up and down has been included to show the spread of the data.

For the 16th of July the flow depth is reasonably matched in the reach river kilometre 147 to 164. In the reach from 165 to 175 the model shows larger water depths than from measurements. The streamwise velocity is overestimated by 0.2 m/s on average along the entire model. The transverse velocity is within the range of variation of the measurements. The specific discharge is also somewhat overestimated by the model, but for the lowest discharge, the model result fits within the measurement variation.

The model results on the 18th of July are compared to the measurements in Figure 4.6. The flow depth shows good agreement in the upstream reach (rkm 147-164). Downstream of this reach the water depth is over predicted by the model. The streamwise velocity is within the range of the measurement variation. The cross-section averaged transverse velocity oscillates around the zero value. The specific discharge is well approximated by the model, except between rkm 147-155.

The overall impression after comparison to the measurements is that the model overestimates the flow velocity at the 1400-1500 discharge level. This could be an important conclusion for the morphodynamic calibration, where sediment transport parameters may have to be adjusted based on the overestimation of the streamwise velocity. Other than that scripts to process the measurements and the model results can be reused if new insights to the model roughness are available in the future.

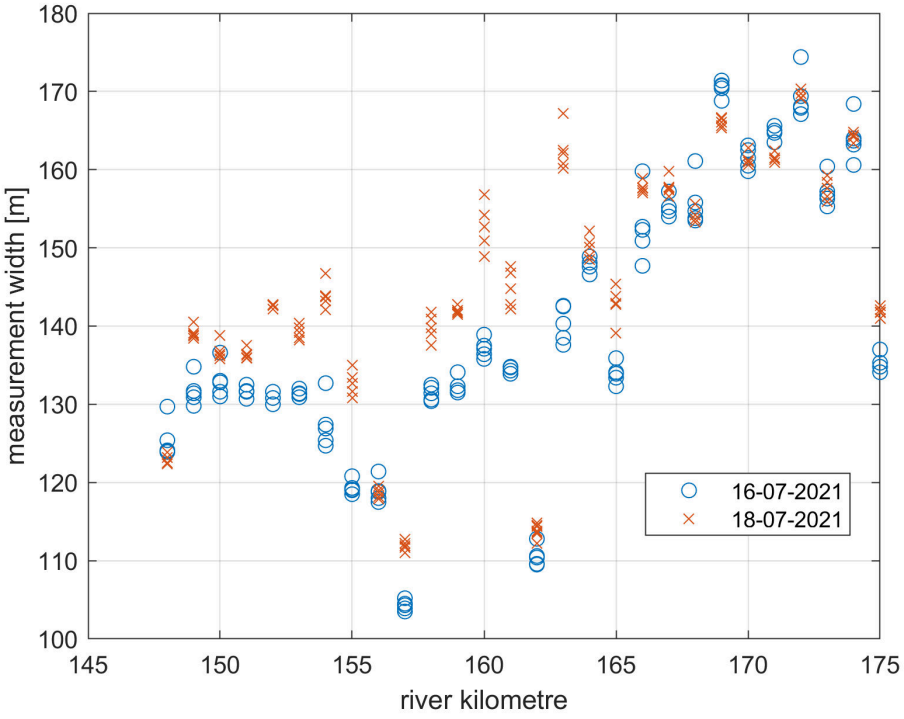

Figure 4.4 Width of ADCP measuring cross-sections

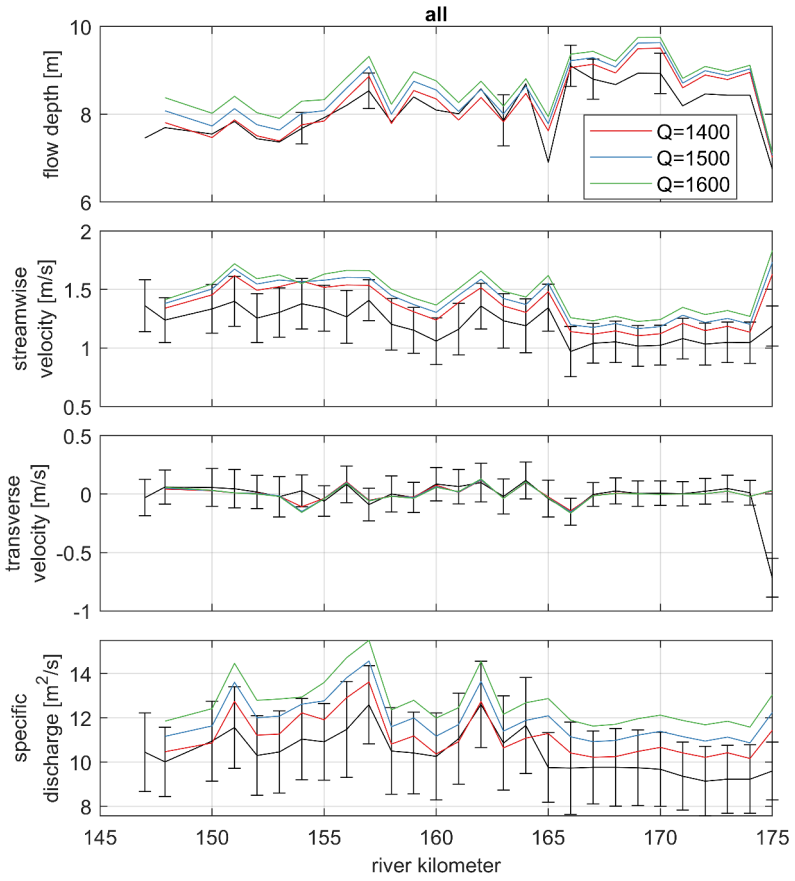

Figure 4.5 Depth averaged velocity comparison for 16-7-2021 along Sambeek Grave reach. The black line indicates the value from measurements. The whiskers correspond to a standard deviation above and below the average.

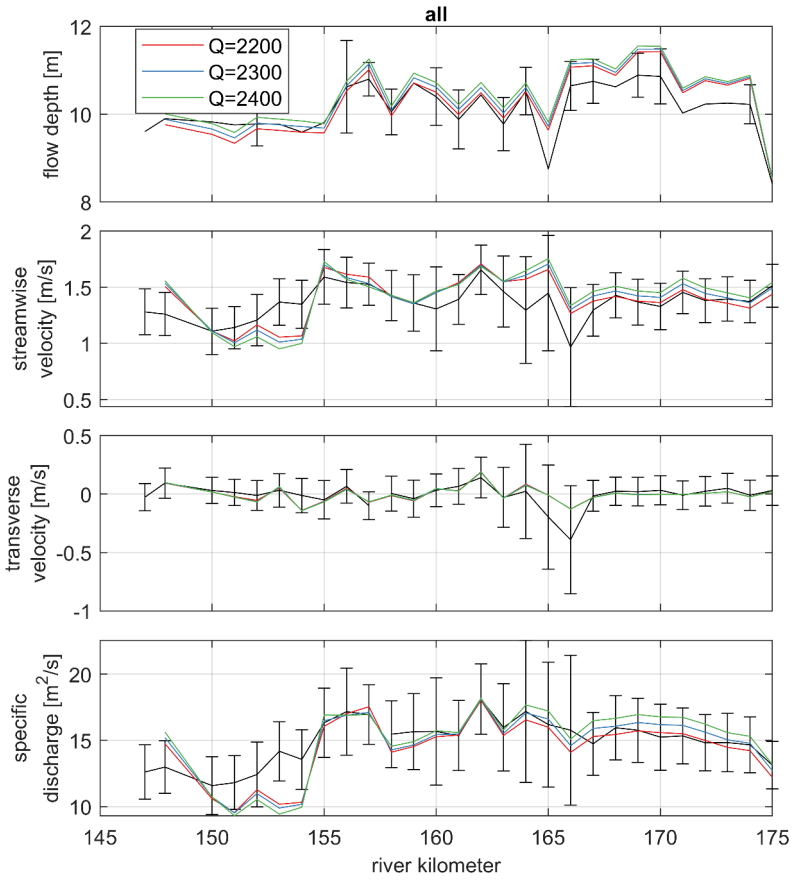

Figure 4.6 Depth averaged velocity comparison for 18-7-2021 along Sambeek Grave reach. The black line indicates the value from measurements. The whiskers correspond to a standard deviation above and below the average.

4.3 Distribution of main channel / floodplain discharge

Having compared the model results to the measurements, a next set of post processing of the simulations results was done to retrieve the discharge in the main channel versus what is flowing through the floodplain. Figure 4.7 and Figure 4.8 show the result for 1400 m^3/s and 2400 m^3/s, respectively. The other discharge levels (1500,1600 and 2200 and 2300) show similar patterns and are therefore not reported. At a discharge up till 1400 m^3/s the flow is almost entirely passing through the main channel. At a discharge of 2400 m^3/s at rkm 150 roughly 50% of the discharge is flowing in the main channel, and this gradually increases to rkm 170 (90%). Just upstream of the weir Grave the flow tends to flow over the right bank more.

The spatial pattern of the velocity magnitude is shown in Figure 4.9. This shows that indeed there is flow over the right flood plain. The discharge, however, is dominated by the deeper and faster flowing main channel section near the Grave weir.

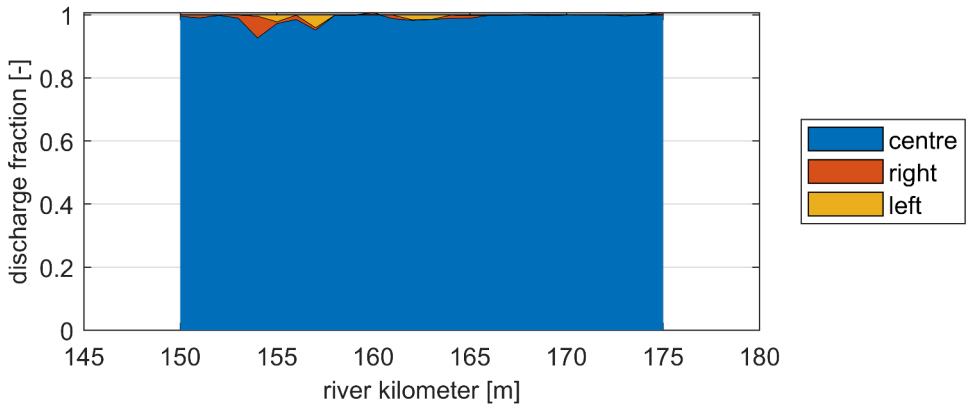

Figure 4.7 Discharge division for a discharge of 1400 m^3/s. Left and right correspond to the left and right floodplain, centre corresponds to the main channel.

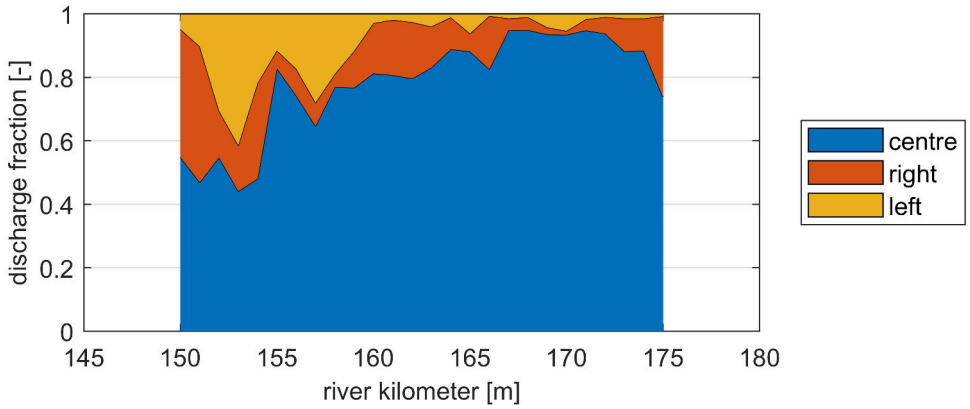

Figure 4.8 Discharge division for a discharge of 2400 m^3/s. Left and right correspond to the left and right floodplain, centre corresponds to the main channel.

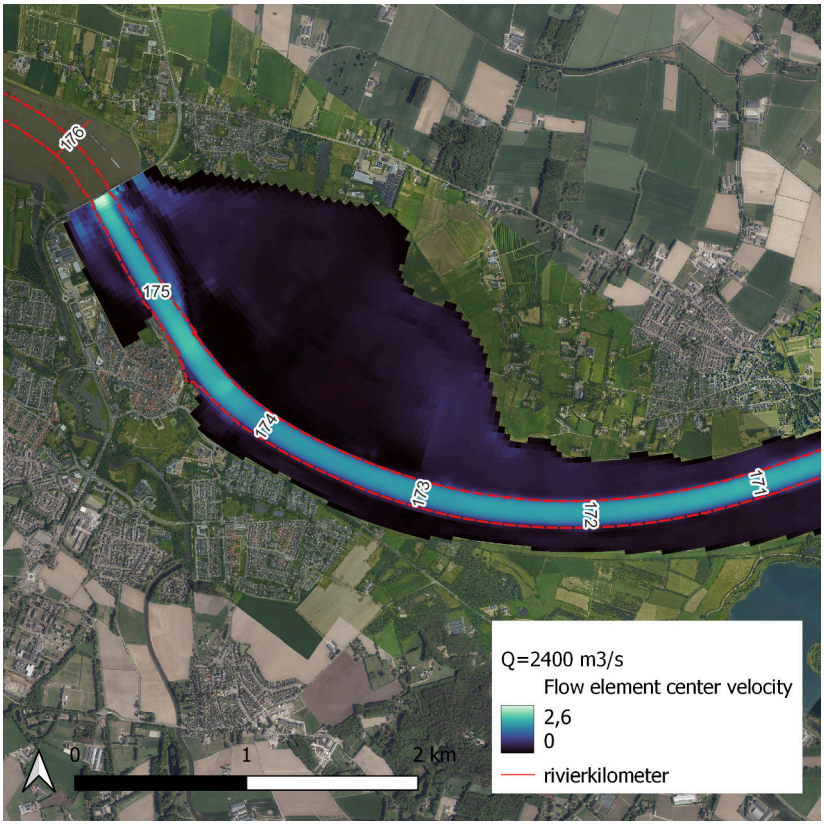

Figure 4.9 Velocity field for a discharge of 2400 m^3/s. The red dashed lines indicate the main channel extent.

4.4 Conclusion

Two different hydrodynamic validations were performed, namely a comparison with water level slope measurements and with velocity measurements. Lastly an application was performed to find out the discharge division between main channel and floodplain.

All in all the validation showed that there was an acceptable agreement with measured values to continue with the morphological simulations. It will be interesting to see which model improvements have been implemented during the detailed validation study of Van der Deijl (2022).

The streamwise change in flow division is interesting to consider for determining zones of local morphological change. Another interesting point is that for the 2014-2018 morphological simulation the flow is almost fully confined to the main channel section.

5 Morphodynamic calibration

The current chapter focusses on the morphodynamic calibration of the Meuse submodel between Sambeek and Grave. Before starting the calibration, the observed bed level changes are discussed. The calibration follows the following approach: Firstly, an order of magnitude of the sediment transport is evaluated by computing the offline sediment transport over a fixed bed. Sediment transport is evaluated for different combinations of parameters in the transport formula as well as the configuration for hiding and exposure (Section 5.3). This leads to four different combinations of parameters in the transport and hiding and exposure formulas which are evaluated in morphodynamic simulations (Section 5.4). In addition, different transport and bed level statistics were computed (Section 5.5 and Section 5.6). Different sensitivity computations have been carried out as well, to understand the influence of different model inputs (see Appendix A), such as the thickness of partially mobile areas, active sediment width, secondary flow and roughness. Finally, an investigation into the development of three trenches was performed (Section 5.7).

5.1 Observed trends between 2014 and 2018

Figure 3.1 shows the observed bed level development in the reach between Sambeek and Grave. The difference with respect to 2014 is shown in Figure 5.1. This shows that the bed level upstream of rkm 157 is relatively constant over time. At rkm 157 the filling of the summerbed lowering is visible. Upstream of the bridge at Mook (rkm 165) there is large sedimentation. Downstream of the bridge there is also sedimentation. From rkm 170 till 174 there is erosion.

The infilling of the summerbed lowering at 157 can be explained by the lowering in the transport across the jump in bed level.

The sedimentation upstream of the bridge is probably caused by a lowering in the sediment carrying capacity of the flow due to deceleration upstream of the bridge (c.f. Figure 4.2)

The sedimentation downstream of the bridge is probably also caused by a jump in the sediment transport caused by the slowing down of the velocity. This can be seen in Figure 4.5.

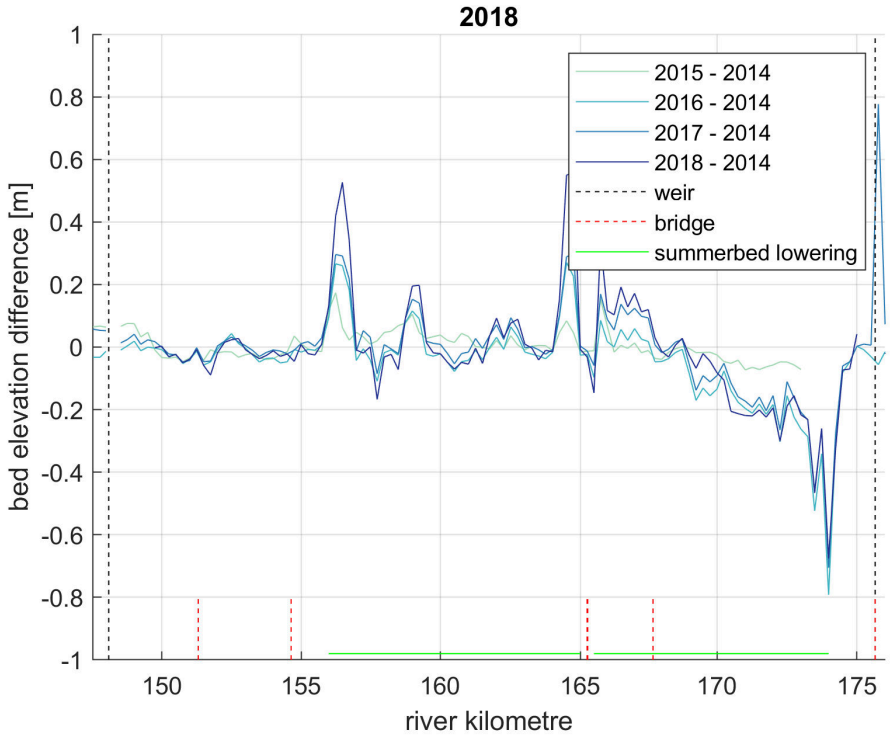

Figure 5.1 Bed level development averaged over the main channel (L3R3) compared to 2014 Meijer (2020a,b)

5.2 Discharge-dependent parameter investigation

The simulation management tool runs sequential steady state simulations with a constant discharge. This enables the use of discharge-dependent inputs and parameters such as morphological factors, which help to reduce to simulation time (Yossef *et al.*, 2008). The hydraulic and morphodynamic parameters are presented to gain insight into the different parameters at different discharges.

The hydraulic parameters which are investigated are the water level, water depth, depth-averaged velocity, roughness, and bed shear stress. Finally, the morphodynamic parameters of geometric mean grain size and computed sediment transport using a fixed bed condition are also presented.

Figure 5.2 shows the water level along the reach as a function of the discharge. The result shows that the water level for the discharges (up to 1139 m^3/s) do not show a good convergence. For these low to moderate discharges the water level around Mook (rkm 165) should be at 7.91 m + N.A.P. as this is used as a set-point for the weir operation at Grave. This implies that the Q-h boundary at Grave based on the *betrekkingslijnen* at Grave does not give accurate results for the water level (c.f. Figure 5.3). Although probably not crucial for the morphodynamic simulations, it is important that this is updated in a next version of the model and software.

The water depth is shown in Figure 5.4. It clearly shows the locations of the summer bed lowering and the shallow zones near the bridge at Mook and the weir at Grave.

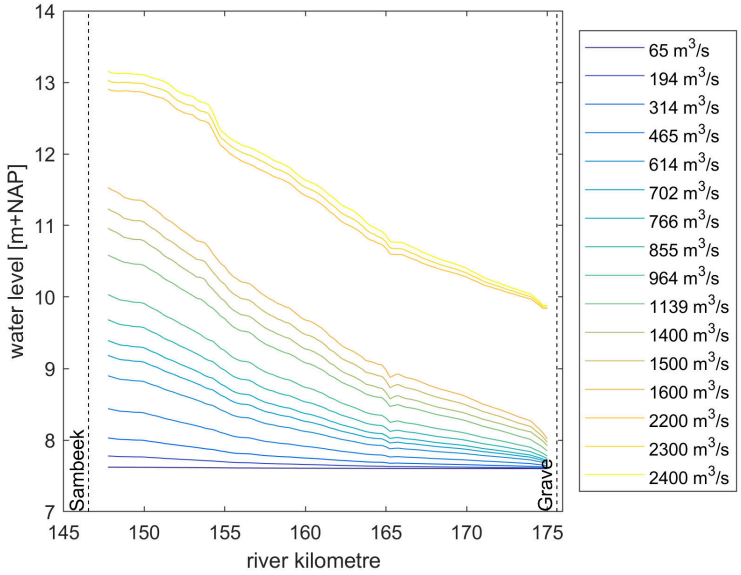

Figure 5.2 Steady computed water levels for different discharges.

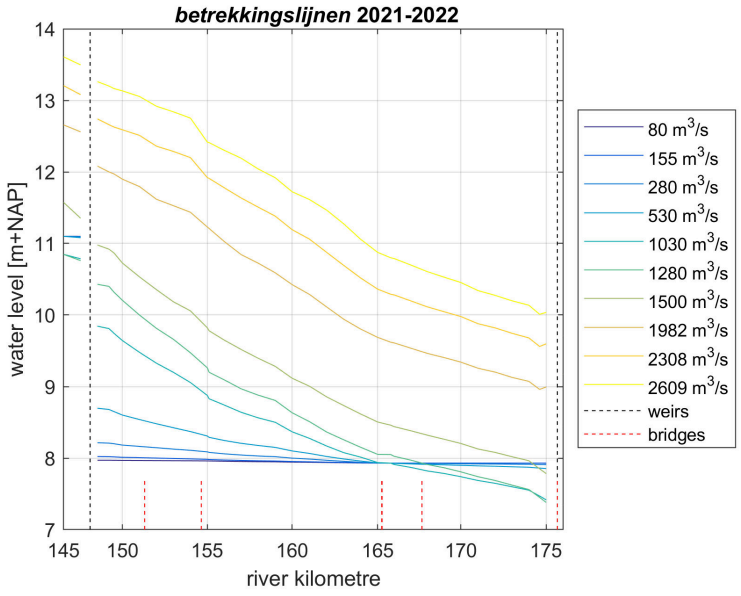

Figure 5.3 Water levels from *betrekkingslijnen* for different discharges.

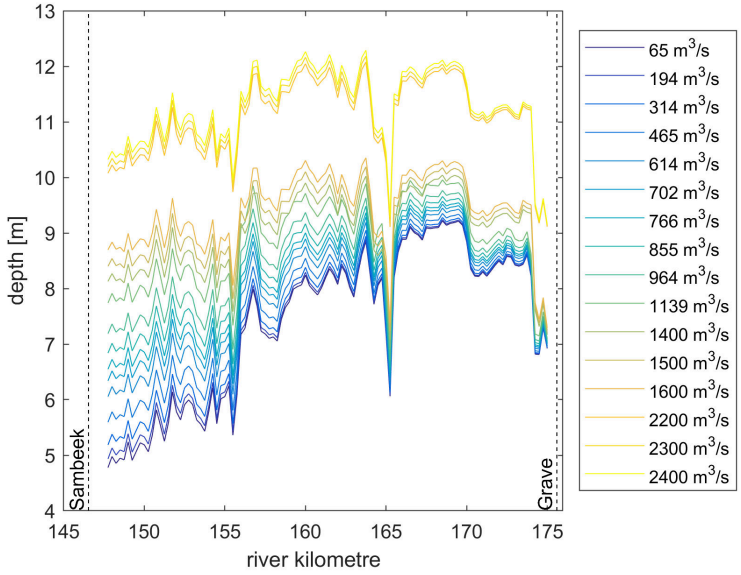

Figure 5.4 Water depth for different discharges.

The velocity magnitude averaged over L3-R3 polygons (as defined by Meijer (2020b)) is shown in Figure 5.5. This shows a slight negative gradient in the streamwise direction for the low discharges. For the high discharges the flow velocity shows a drop in the reach until rkm 153. This is caused by flood plain inundation (cf. Figure 4.8).

In Figure 5.6 the roughness of the model is shown. This shows a roughly constant Chézy value for a discharge up to 1139 m^3/s. Subsequently for the mid-discharges up to 1600 m^3/s the Chézy coefficient increases leading to a lower roughness. Finally for the high discharges (above 2200 m^3/s) the Chézy coefficient decreases again, leading to a quite varying roughness. The roughness also exhibits strong jumps at two locations for the mid to high discharges. Both the summerbed lowering and the bridge may be reasons for the jumps in the calibrated roughness sections.

The roughness is prescribed using a Nikuradse roughness height computed as the simplified Van Rijn approach:

$$k = Ah^{0.3}\left[1 - e^{-Bh^{-0.3}}\right], \tag{5.1}$$

where h denotes the local water depth, and the constants $A = 0.1$ and $B = 2.5$ are defined as in the hydrodynamic model.

The resulting bed shear stress per discharge level is shown in Figure 5.7. For low discharges the bed shear stress shows a negative gradient in streamwise direction and for the high discharges the pattern it varies. Until rkm 153 the bed shear stress decreases. At rkm 155 the bed shear stress increases greatly, caused by the jump in flow velocity at the narrowing reach. The bed shear stress gradually increases towards the bridge at Mook (rkm 165). Subsequently the deeper section between 10 km and 1 km upstream of the weir at Grave has a lower bed shear stress again. At the weir the bed shear stress increases.

Finally, using the available sediment and a fixed bed, the bed load transport is computed (cf. Figure 5.8). This follows the bed shear stress pattern.

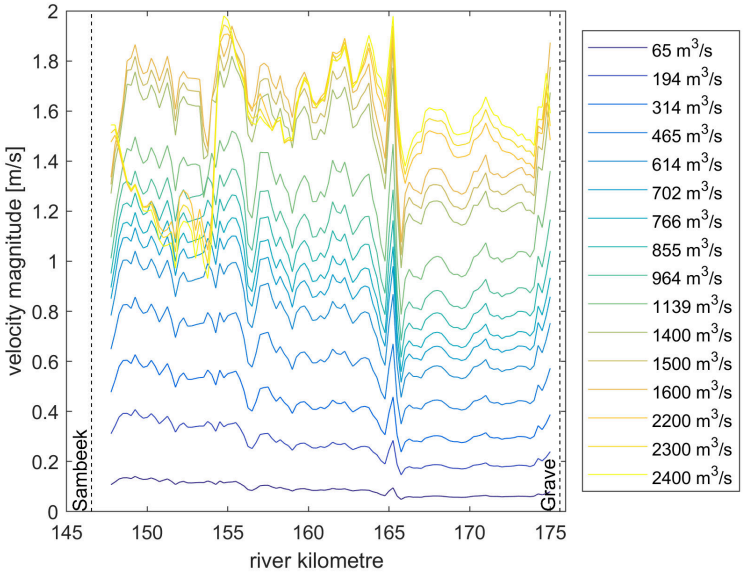

Figure 5.5 Width-averaged velocity magnitude for different discharges (L3R3).

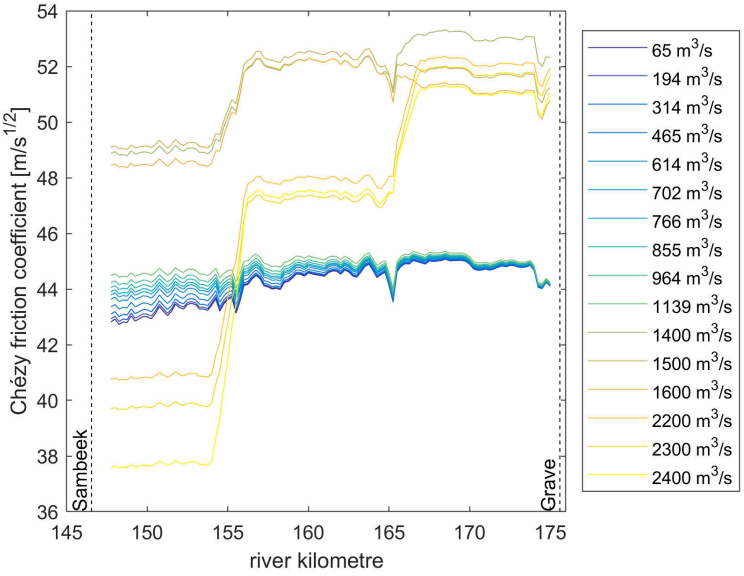

Figure 5.6 Width-averaged roughness for different discharges (L3R3).

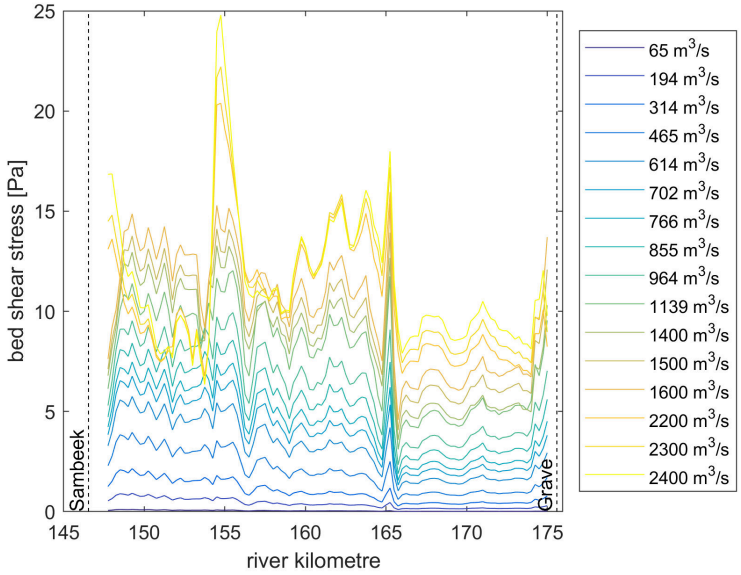

Figure 5.7 Width-averaged computed bed shear stress for different discharges (L3R3).

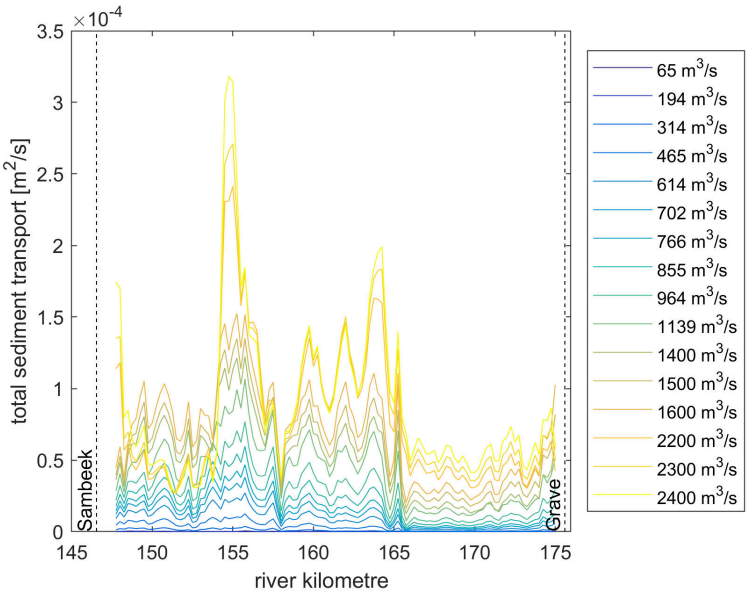

Figure 5.8 Width-averaged bed load transport capacity for different discharges (L3R3).

5.3 Offline calibration

For the calibration of the morphological simulation it is necessary to determine the transport relation. To find an initial estimate for this, we use two observations. The first is that the upstream reach is close to equilibrium as the bed level does not change. The second is the volume of deposited sediment just downstream of the summerbed lowering rkm 156-157.

To determine the sedimentation in the Figure 5.9 shows the results of the offline sediment transport calibration in which the multiplication factor A_{cal} and the influence of the hiding exposure exponent A_{SKLHE} are varied. Offline sediment transport is a computation of the sediment transport based on fixed bed level simulations, for different steady discharges, subsequently combined to form a sediment transport per year.

Based on the sedimentation in the reach (rkm 156-157) a jump in transport of 7700 m^3/year is considered. Besides this values which are 50% lower and 50% higher are also included. To place the results of the calibration in perspective the average yearly transport in the upstream reach rkm 150-155 is also included in the figure. To see the influence of the upstream variation in sediment transport (i.e. variation from the equilibrium transport) the standard deviation of the transport in the upstream section is also presented. As the bed level is fixed, the transport should be close to constant in the upstream reach, for the material to arrive in the summerbed lowering.

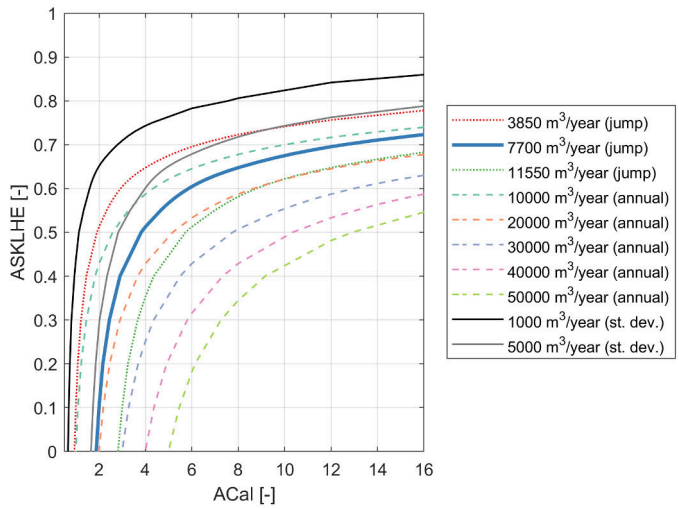

Figure 5.9 Offline sediment tranport per year [m^3/year] indicating the jump in sediment transport upstream and downstream of the summerbed lowering, the annual computed transport and the variation of the bed level in the steady upstream reach.

The results show that choosing parameters that are appropriate for a sedimentation volume of 7700 m^3/year results in an average yearly transport between 10 000 and 20 000 m^3/year between rkm 150 and 155. The variation in the upstream transport amounts to more than 5000 m^3/year. This indicates that the computed transport is not in equilibrium for this reach. A 50% smaller and 50% larger sedimentation volume are included in Figure 5.9 to get an impression of the spread of the transport depending in on a 50% range of uncertainty in the determined sedimentation volume. For the next steps in the investigation we will consider the 7700 m^3/year sedimentation as the starting point. Depending on the outcome of the calibration runs, this choice can be revisited.

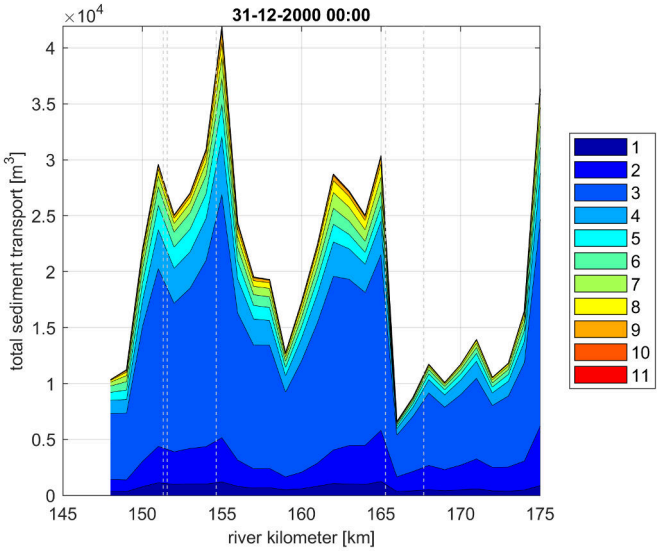

Figure 5.10 Longitudinal profile of A_{cal}=8 and A_{SKLHE}=0.65. The numbers indicate the sediment fraction, where 1 is fine and 11 is coarse sediment.

An example of the total transport per year is shown in Figure 5.10. Note that there is a difference in the computed transport in Figure 5.9 versus Figure 5.10. This difference needs to be clarified, but it is likely related to the improvements of the offline sediment transport computation.

5.4 Online calibration

Based on the results in Figure 5.9, four combinations of parameter values are selected for simulation including bed level updating. These are presented in Table 5.1.

Simulation	A_{cal} [-]	A_{SKLHE} [-]
D1	4	0.5
D2	8	0.65
D3	16	0.72
D4	2	0.0

Table 5.1 Overview of chosen settings from the offline calibration.

These simulations include a bed level lowering of 5 cm/year, which is based on the analysis by Meijer (2020a,b).

The bed level development of the four simulations D1-D4 is shown in Figure 5.11. All four simulations show a bed level which is constantly sloping in the upstream reach rkm 150 - 155. D2 and D3 show the best agreement with the measured bed level. At the summerbed lowering D2 and D3 also show the best results. At the downstream boundary the model does not predict the bed level change from measurements. As the D2 simulation is closest to the original transport formula of Meyer-Peter and Müller (1948) we continue with this simulation as the best calibrated result.

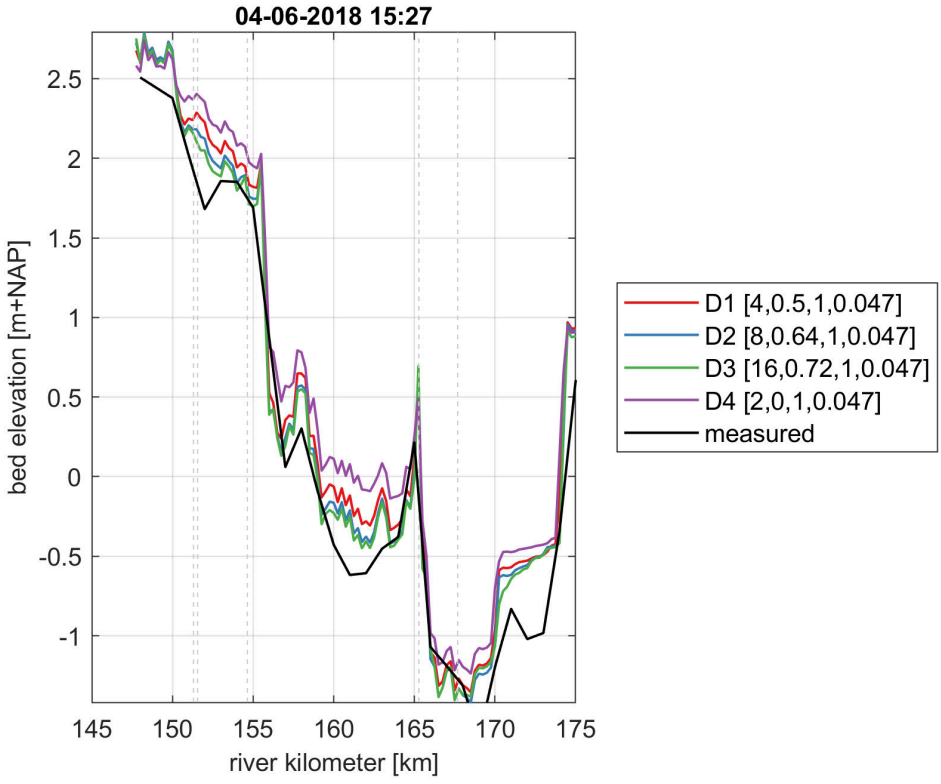

Figure 5.11 Bed level between July 2014 and June 2018

The simulated bed level development shows quite some variation compared to the measurements Figure 5.12. This can be attributed to the difference in resolution at which the model results and measurements are plotted (250 m vs. 1 km). The other reason is that due to the numerical approximation of the bed levels and the fact that the model has modelling choices which could differ from reality, the bed level in the model takes some time to adjust to the numerical solution. In the relative comparison the simulation D2 and D3 show the best result, except for the section between 170 and 175, where the model predicts sedimentation, whereas the measurements show a decreasing bed level. The reason for this difference is not directly apparent.

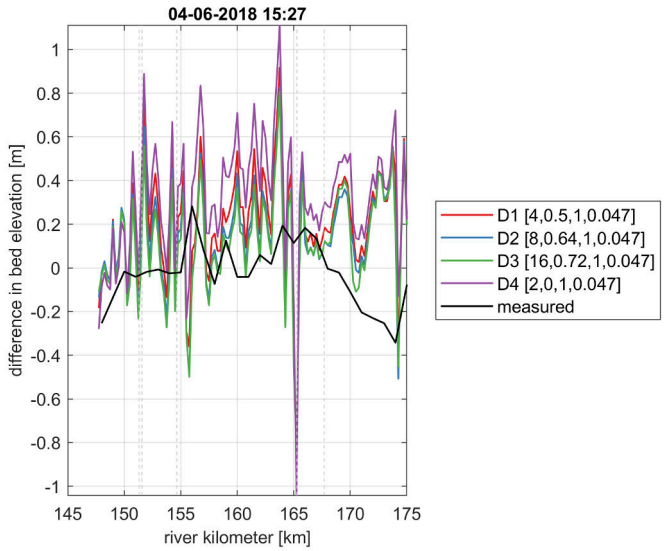

Figure 5.12 Bed level difference with respect to July 2014

5.5 Temporal-average and temporal-variation of spatial bed level variations

Sieben (2022a) derived different characteristics of the bed level development to be used for the calibration of the model. These characteristics are expected to be indicative of the bed level dynamics. Figure 5.13 shows the temporal-average of the spatial variation in bed levels based on selected years (black line). This line is indicative of bed level jumps (e.g. start of summerbed lowering) and the presence of migrating bed forms, and the latter is indicative of sediment transport.

Figure 5.14 shows the computed average transport, which pattern can be compared to the pattern of the temporal-average of the spatial variation in bed levels (black line in Figure 5.13). For ease of comparison this line has been included in Figure 5.14 (also as a black line).

The simulation upstream section (rkm 145-155), whereas the temporal average of the bed level variations (TABLV) is average in that reach. In rkm 150 and 155 the computed transport is higher than average, and the TABLV is average in the reach. The region coincides with the bend cut-off near Boxmeer. Possibly the bed is fixed here as the subsurface includes clay (RWS, Directie Limburg, 1979), or coarser material (Tolman, 1987). The transports are larger than average between rkm 155 and rkm 164, and the TABLV shows a large value at 155 and average values between 156 and 164. At rkm 165 (at the bridge of Mook) the transport shows a sharp drop whereas the TABLV shows a strong spike. From rkm 166-169 the transport and TABLV show lower than average values which correspond to the deeper section of the summerbed lowering. At rkm 170 the transport increases and so does the TABLV. From rkm 171 to 176 the total transport is average and the TABLV is smaller than average.

There is quite a bit of difference in the transport and TABLV patterns. Possible explanations could be that the computed transport in the reach is too high, underlying assumptions for the comparison do not hold everywhere, that the bed level is influenced by maintenance dredging, or that the statistics have been made over different periods. The period of the simulation is between 2014-2018, whereas the TABLV is averaged over multiple years.

The orange line in Figure 5.13 shows the temporal-variation of the spatial variation in bed level. This is somewhat harder to interpret, but the lack of variation in the orange line implies that the dynamic behaviour of bed forms is constant or not present. Sieben (2022b) argues that as the bed levels are from periods in time with very varying hydrographs in between the measurements, low values of the parameters are indicative of fixed structures or zones with low dynamics. He further argues that low dynamics over a length of 250 m implies that the transport of bed material is very low over the years.

A similar analysis for the orange line is done for the computed temporal-variation in the bed level variation based on the simulations between 2014-2018 and as computed by Sieben (2022b) over years 1994-1995 2000-2001, 2004-2005 2009-2010, 2015 and 2019 (cf. Figure 5.15). The temporal variation in the upstream and downstream sections is larger in the model simulations compared to the pattern from measurements. In the downstream reach (rkm 165 - 170) the pattern is similar, however in this part of the domain the model showed differences in the bed level development. Apparently the variation shows good agreement, while the average bed level trend does not. The differences could possibly be explained by differences in the periods chosen for the analysis, differences between the modelled and measured bed levels, difference in the horizontal resolution between the model (roughly 20 m x 20 m), versus the raster data (1 m x 1 m), and possibly the influence of maintenance dredging.

In Figure 5.14 it is seen that the temporal-average of the spatial variation in the models is captured at rkm 154.75, 155.75, 164, 165.25, 170 and 174. The first location corresponds to the crossing of the N264, the second and third to the start and end of the most upstream summerbed lowering. The location around 165.25 is due to the shallow fixed zone from 165 until the bridge at Mook, which transitions in to a new summerbed lowering. The last part of the lowering which is somewhat shallower starts at rkm 170 and ends at rkm 174. Between these spikes which are accurately captured by the model, more variation is visible in the measurements than from the model. This is likely caused by the difference in the horizontal resolution between the model (roughly 20 m x 20 m), versus the raster data (1 m x 1 m).

The temporal-variation of the spatial variation in bed levels over 250 m polygons is shown in Figure 5.15

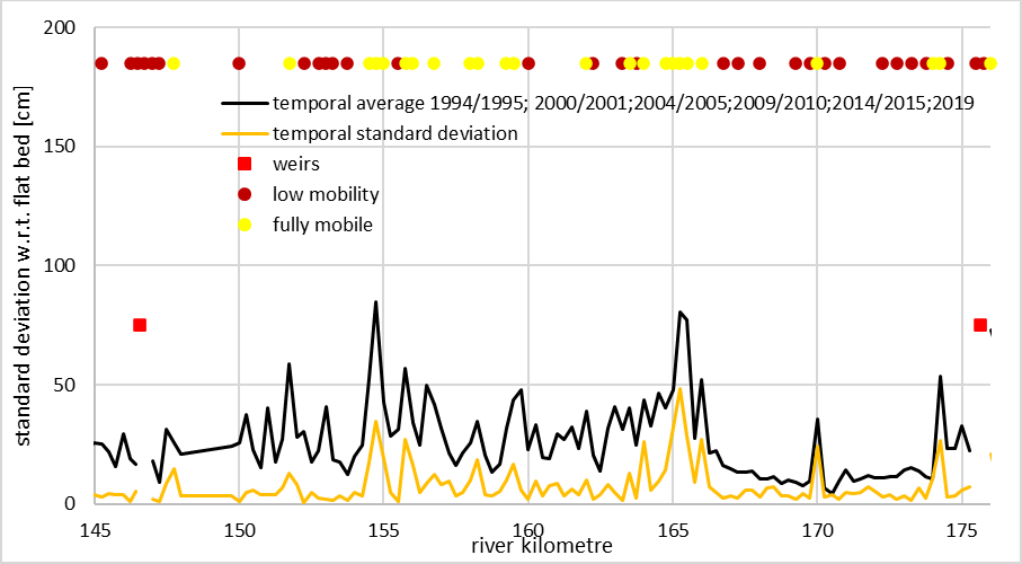

Figure 5.13 Average and standard deviation of the bed level variation (adapted from Sieben (2021))

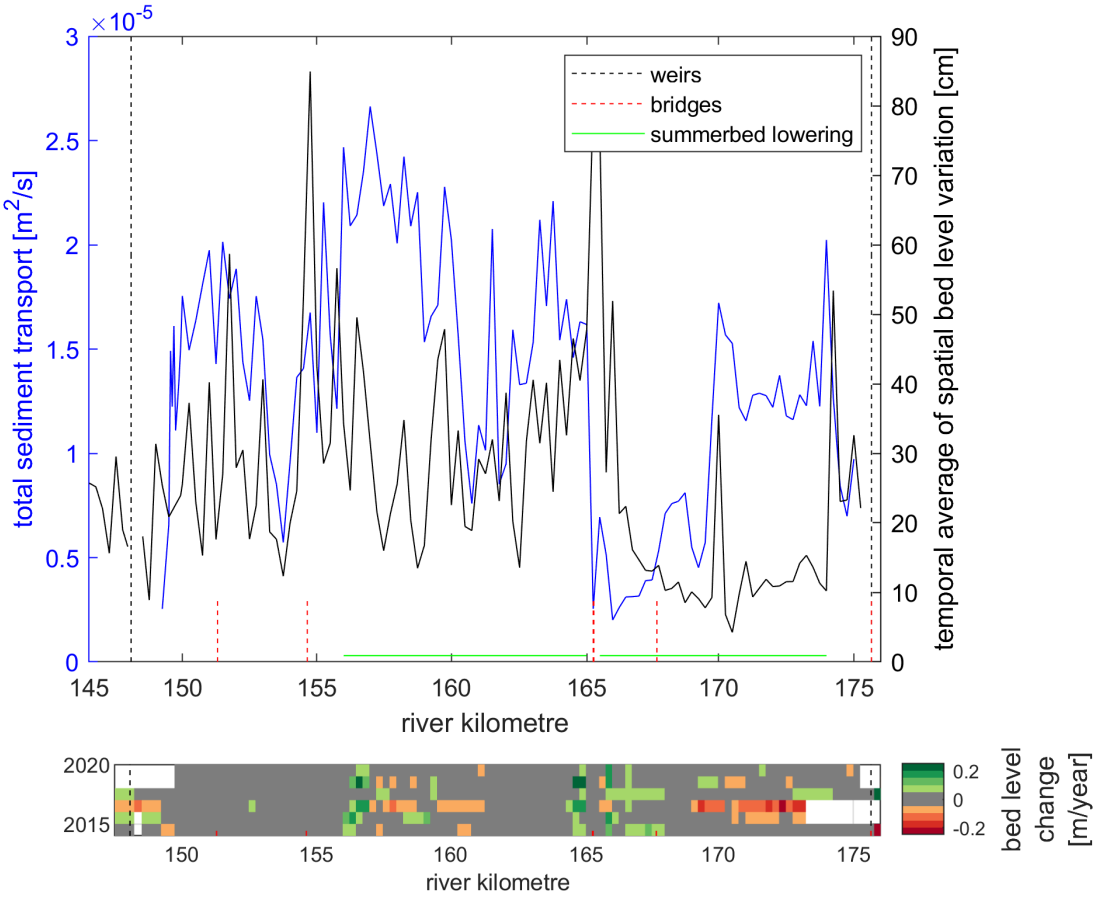

Figure 5.14 Temporal-average of the average sediment transport in L1R1 by computation (between 1-6-2014 and 1-6-2018, blue line) and temporal average of bed level variations based on 1994-1995 2000-2001, 2004-2005, 2009-2010, 2015 and 2019 (black line). The bottom panel shows the bed level change between subsequent years. The values bewtween -5 and 5 cm/year are shown as grey, indicating the possible presence of a fixed layer.

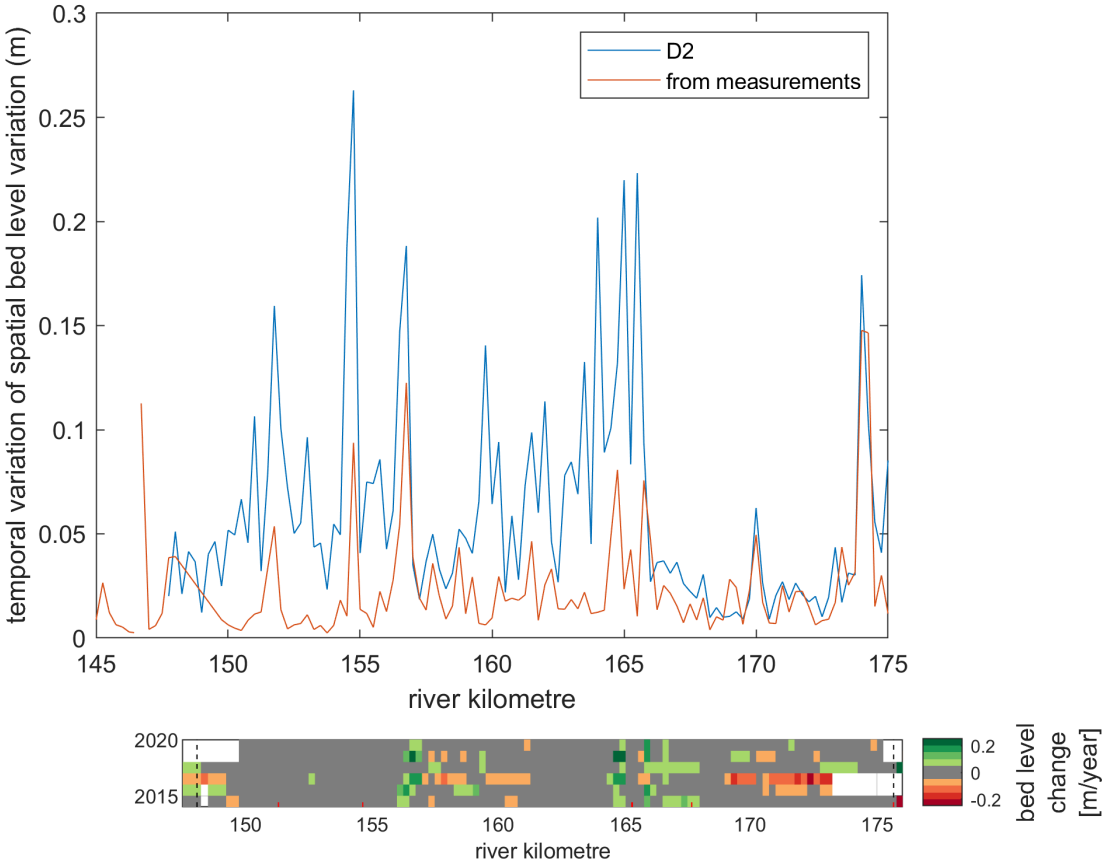

Figure 5.15 Temporal-standard deviation of the spatial bed level variation in L1R1 by computation. The bottom panel shows the bed level change between subsequent years. The values bewtween -5 and 5 cm/year are shown as grey, indicating the possible presence of a fixed layer.

5.6 Displacement speed of bed level variations

Sieben (2022a) proposes a computation for displacement speeds of the bed level as the standard deviation in the bed level change divided by the standard deviation in bed level gradient:

$$c = \sqrt{\frac{\left(\overline{\frac{\partial \tilde{z}}{\partial t}} - \overline{\overline{\frac{\partial \tilde{z}}{\partial t}}}\right)^2}{\left(\overline{\frac{\partial \tilde{z}}{\partial s}} - \overline{\overline{\frac{\partial \tilde{z}}{\partial s}}}\right)^2}}, \tag{5.2}$$

where $\tilde{z}$ is the bed level in m + N.A.P averaged over the river kilometer and between the L3 and R3 polygons as defined by Meijer (2020a,b). t denotes the time in years, s is the distance along the channel in kilometers.

The displacement speeds are derived for the period between 2014 and 2018, and plotted alongside the values derived by Sieben (2022a). The results show a similar order of magnitude except for a spike at rkm 160. In the model the standard deviation of the bed level slope is small at this location, and this may indicate some difference in the modelled bed level slope evolution compared to the measured bed level slope evolution.

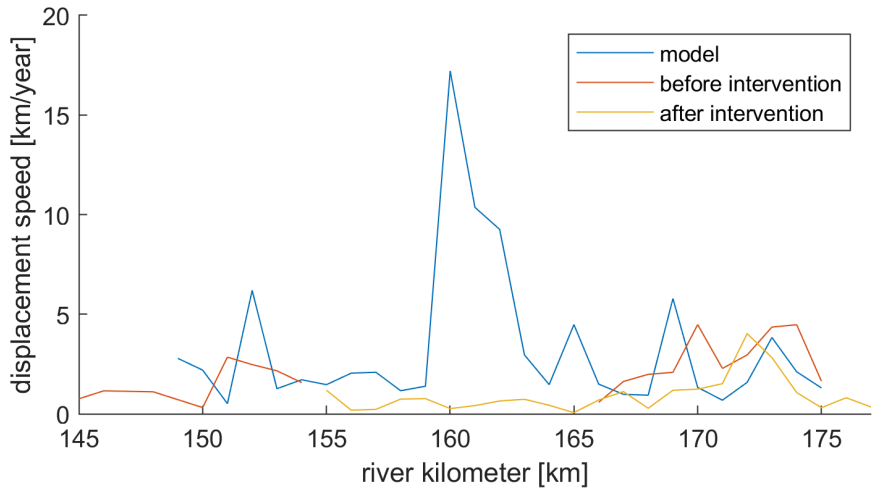

Figure 5.16 Displacement speeds of the bed level determined from model, and from data (before and after the summerbed lowering) by Sieben (2022a))

5.7 Trench development

To test the model, the development of a set of trenches was studied using the calibrated model. In the 2014 bed level three trenches with a length of approximately 250 m were added to the simulation (cf. Figure 5.17). The result relative to the reference simulation is shown in Figure 5.18. The result shows that besides downstream propagation of the trench, there is also infilling of the trench from upstream. This behaviour is different from the theoretical propagation of trench plots which are typically shown, because there is a critical threshold of motion for the sediment. The fact that zones far away from the trenches are not influenced is a positive result, which suggests that the model can be used to study effects of measures.

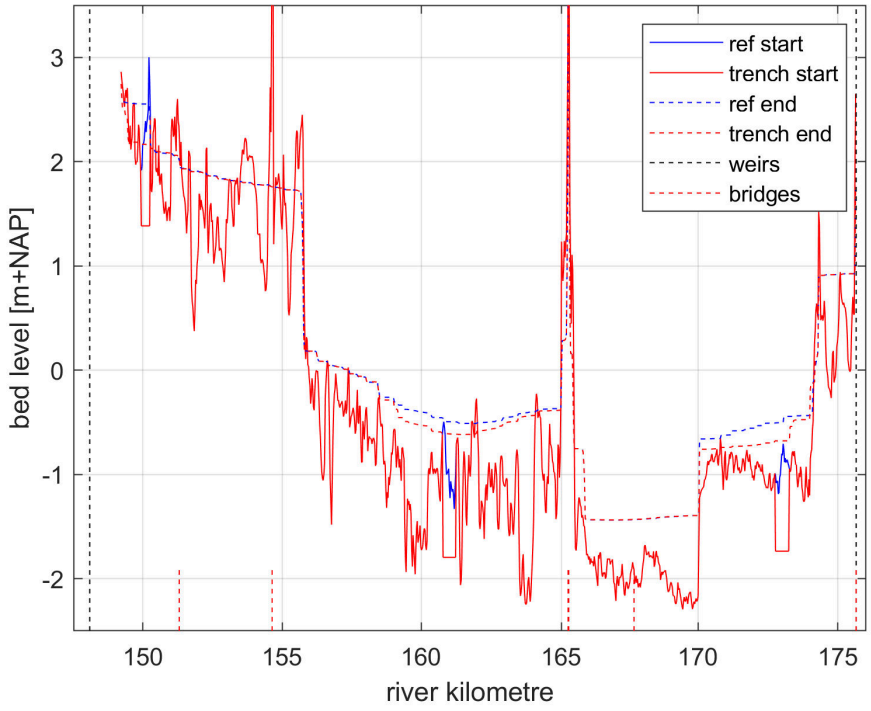

Figure 5.17 Initial imposed trenches development (relative to the simulation without the trenches)

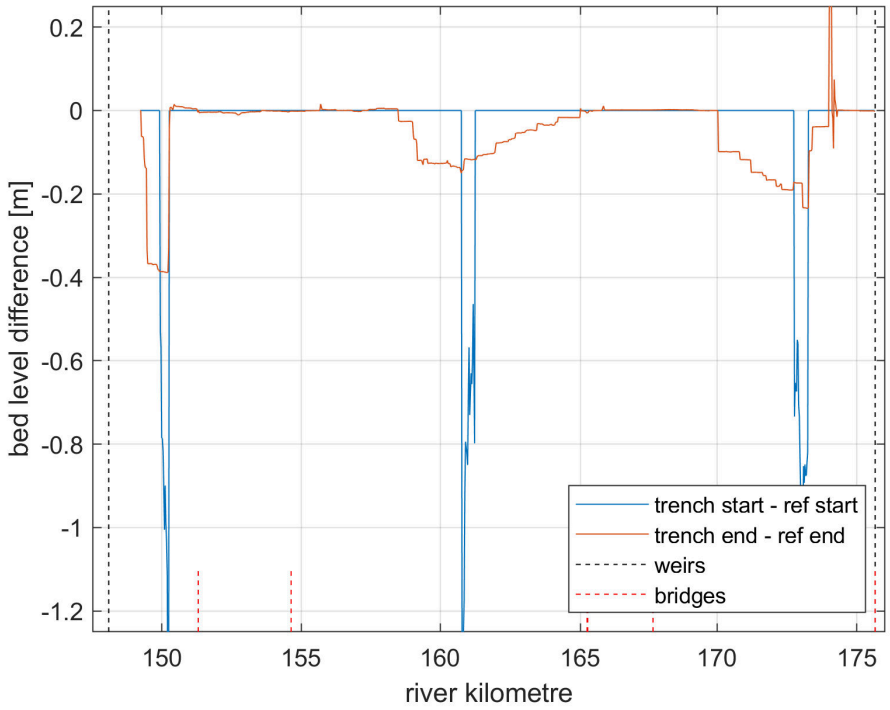

Figure 5.18 Trench development (relative to the simulation without the trenches)

The result for the upstream trench (relative to the simulation without a trench) is shown in Figure 5.19. The behavior is consistent with the imposed measure.

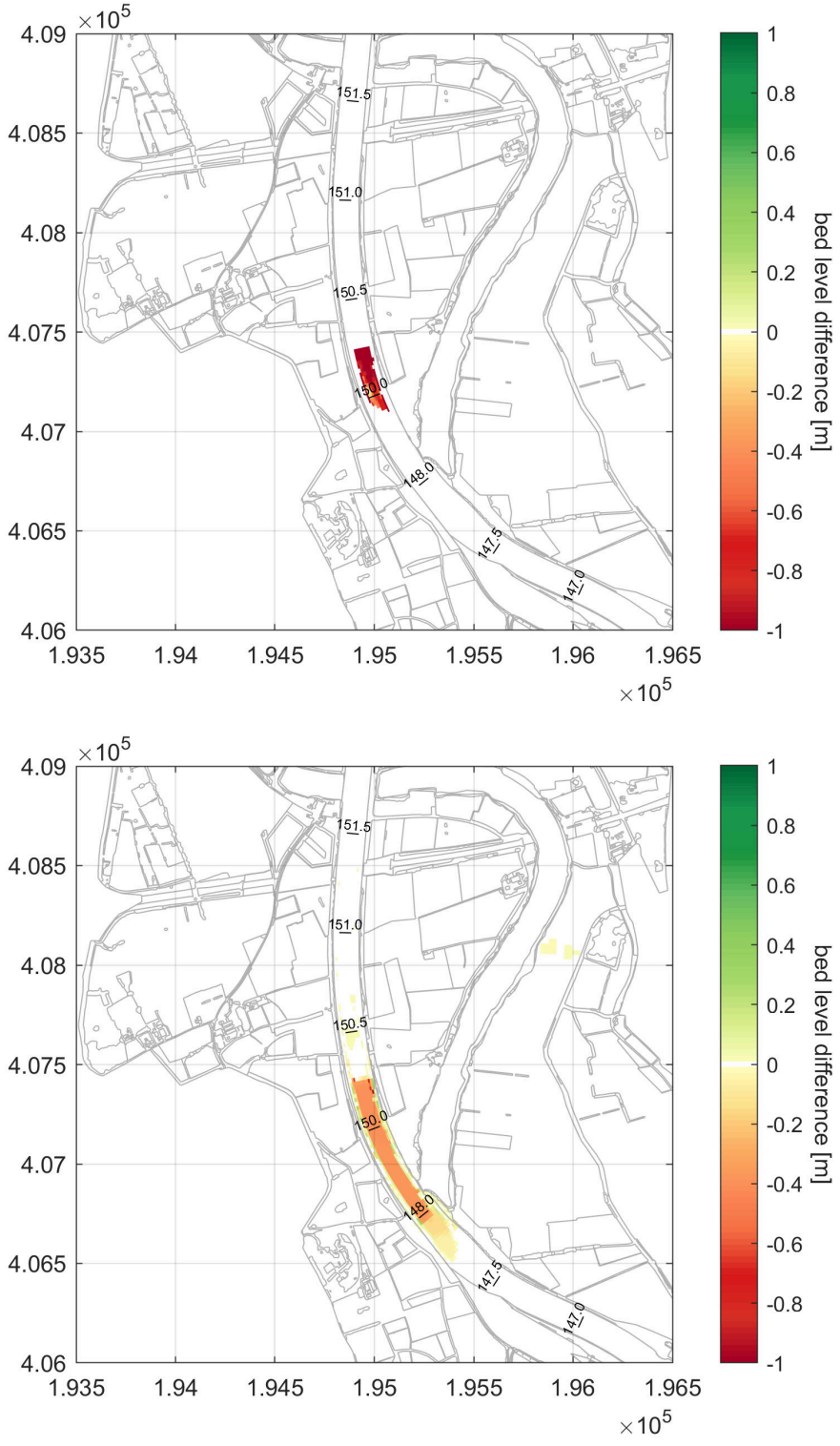

Figure 5.19 Initial (top) and trench development after 4 years (bottom)

6 Discussion

In developing the model, several features have been applied which require further research.

6.1 Improvement of the hydraulic settings of the model

The Sambeek-Grave model has boundary conditions which do not match the steering water level at Mook. This implies that the downstream Q-h boundary condition based on the betrekkingslijnen at Grave does not give accurate results for the water level. This should be updated in a new update of the model and the software. Currently simulations are being setup including the weir operation at Grave. Possibly, the results of this model can be used to set the downstream boundary.

6.2 Dredging maintenance, eroding banks, and time of bed level measurements

At some parts along the reach between rkm 168-174 the bed level measurements seem to suggest that dredging maintenance took place (cf. Appendix B) . This information is not included in the model yet, as the dredging operation is not known yet.

The role of sediment from the eroding banks is assumed to be of minor importance in the overall average bed level development. This should however be verified in the future.

Furthermore, the exact time of the bed level measurements is sometimes unclear, which forms a bottleneck in determining the ground truth which can be used for the calibration.

6.3 Locations with limited bed level change

A key point in morphodynamic modelling of the Maas River is dealing with locations in which the bed appears to be fixed. The banks of the river, for instance, are protected at some locations and erosion under normal circumstances cannot occur. Along the main channel there are areas showing no changes in bed elevation which can be due to a strong armouring of the bed. It could also be due to timing of the measurements, preventing to capture a dynamic behaviour around a mean constant value. It was decided in discussion with *Rijkswaterstaat* to model the areas in which the bed appears to be fixed as a “lack of sediment” (cf. A.1).

This option consists of removing the sediment in the initial condition at the cells in which the bed level is considered to be fixed. Hence, the bed cannot erode below the initial limited thickness of sediment, although sedimentation can occur. As a consequence of the modelling choice, the sediment transport rate over the fixed areas is initially small. This is because the sediment transport capacity computed by the sediment transport relation of choice is reduced as a function of thickness of sediment (initially small) relative to the alluvial threshold (an input parameter set equal to the active layer thickness) (Struiksma, 1999; Chavarrías *et al.*, 2022). Upstream sediment entering the fixed area will be deposited there, as the output is reduced due to the limited thickness, and deposition will continue until the thickness of alluvial sediment is enough to transport the sediment that enters from upstream.

While this approach yields a fit-for-purpose model, it is limited in several respects. For instance, the bed level could be showing no temporal changes because normal flow prevails in that area for all flow conditions while there is sediment being transported. If there are no longitudinal gradients in flow properties, there will be no longitudinal gradients in sediment transport which implies that there will be no temporal changes in bed level. Initially setting the thickness of sediment to a small value will give the right solution (i.e., no bed level change) but for the wrong reasons. Also, a depositional wave will form at the upstream end of the fixed area and an erosional wave will be generated at the downstream end, which are not realistic if flow is normal.

This example highlights that eliminating or reducing the thickness of sediment in the areas where no bed level changes are observed may not be the right solution for all cases. It is important to understand what physical processes cause that no bed level changes are observed in each zone independently and we recommend to conduct such study for improving the modelling exercise.

Other options rather than setting the initial sediment thickness to a small value are available that limit bed level development. If, for instance, bed level changes are limited because the bed surface is coarse and the sediment rather immobile, the coarse sediment can be modelled as such using the standard mixed-size sediment approach (i.e., the active-layer model (Hirano, 1971)). This approach also has limitations. If sediment in the immobile region is much coarser than the rest, it will “trap” the other sediment due to the hiding-exposure effect. Fine sediment will be unable to be transported on a bed where the mean grain size is much coarser, hence accumulating. A specific hiding-exposure relation should be developed that can deal with cases in which sediment fractions with a large difference in characteristic size are modelled.

Recently, a model has been developed to reproduce formation and break-up of armour layers (Chavarrías *et al.*, 2022). This approach could help in rightly capturing periods of no bed level change while correctly modelling bed level change under the conditions in which it may occur. Nevertheless, the model is subject to limitations e.g. sediment transport must be larger than 0 (Chavarrías *et al.*, 2022).

In the current Sambeek-Grave reach, assuming full sediment availability provided good agreement with the bed level development between 2014 and 2018. This does not imply that this setting will be the best along all reaches of the Meuse. For other reaches, it is recommended to still keep this property as a possible modelling approach to yield a fit-for-purpose model.

6.4 Morphodynamic acceleration factor

A second important point of attention is the morphodynamic acceleration factor. Long term (in the order of years) two-dimensional morphodynamic simulation of long river stretches (tens of kilometres) require a significant computational time. Parallelization helps decreasing the computational time but it has a limit above which more computational power does not decrease the computational time. Hence, a morphodynamic acceleration factor has been used for developing this model. The essence is that the bed level changes in one hydrodynamic time step are multiplied by a factor larger than 1. As a consequence, the modelled changes in bed level are larger than the hydrodynamic time modelled. The physical set of equations solved using a morphodynamic acceleration factor is different than the original set of equations and only for “small” factors the differences are acceptable. The larger the Froude number and the sediment transport the smaller the factor can be. While some analytical approximations can be derived for the upper bound of the morphodynamic acceleration factor under some idealized conditions, a comparison of one case with no morphodynamic acceleration factor is required to provide evidence that the negative effects are small. This point has not been studied in detail and requires further exploration.

6.5 Steady discharge

An optimal use of the morphodynamic acceleration factor is obtained when applied in combination with a set of steady-state flow discharges. This is what is done when using the Simulation Management Tool (SMT). The hydrograph is discretized into a set of constant (i.e., steady) discharges, which allows to apply different morphodynamic factors per discharge. Intrinsic to this approach is the fact that the dynamics of a flood wave cannot be modelled. The discharge for each step in the schematized hydrograph using the SMT is the same throughout the entire domain while during a flood wave the peak discharge at each location along a river changes due to flood wave attenuation.

As a consequence, only if flood attenuation is acceptable given the flood and domain properties, the results of the SMT are acceptable. The longer is the domain and the steeper is the hydrograph, the less acceptable is the assumption of negligible flood wave attenuation. Whether it can be applied to the particular case under consideration should be carefully studied. The inclusion of discharge extraction in constant discharge simulations was investigated in the SITO-PS model schematisations project Fujisaki *et al.* (2022). Conclusions of this model may be useful for the setup of the morphodynamic model of the Meuse.

6.6 Spin-up

The initial flow condition in a hydrodynamic simulation rarely “matches” the initial data (i.e., bed level, friction parameters, fixed weirs, flow in structures, etcetera). For instance, the initial velocity may be 0 and the water level constant everywhere in the domain while the bed is sloping. At the beginning of such a run the solution is not of interest and a certain period of time called “spin-up” time is needed for the solution to adapt to the data. In the spin-up period, the simulation is run under constant boundary conditions until the solution reaches steady state.

An initial fast morphodynamic development is also often observed. One is tempted to apply the same principle as for hydrodynamic simulations and let the simulation spin-up for a period of time before considering the results to be of interest. The idea behind this practice is that the initial bed elevation and composition “need to adapt” to the model solution.

To our knowledge, no detail study of the concept of morphodynamic spin-up with clear definitions for its application is available. In analogy to the hydrodynamic spin-up concept, one could consider to run a morphodynamic simulation using a constant forcing until steady state is reached. In general, this is not reasonable because it assumes that the river is initially under equilibrium conditions, which does not need to be the case. A variation of this approach by forcing with a periodic boundary condition until a dynamic-steady state is reached is equally unreasonable if there is no knowledge about the river’s equilibrium state. For instance, running such a spin-up period for modelling the Waal River would imply not modelling the ongoing long-term bed degradation.

One can run a shorter spin-up period not until a steady state is reached but until “large” changes are not observed. This is common practice but lacks substantial argumentation. There is no definition of what “large” is and it remains expert knowledge. The key problem in applying this approach is that the behaviour one intends to model (e.g., long-term bed degradation, filling of a trench) is superimposed to the behaviour one considers noise. Spinning up the noise is combined with spinning up a part of the physical solution. Moreover, a spin-up of the solution may hide model limitations (Section 6.3).

One solution is to manually filter the noise that it is acknowledged to not form part of the solution reproduced by the model. For instance, a depth-averaged model does not resolve bedforms and these should be filtered from the initial condition. Similarly, large changes in grain size distribution over a limited distance are intrinsic to the variability observed that occurs in a river and the limitations of the measurement procedures. These differences are noise not reproduced by the model that should be filtered. Filtering of the initial data requires also expert knowledge, but it is thought to be less subjective than spin-up of morphodynamic simulations. We recommend to further study how to best filter model input data for morphodynamic purposes.

For the follow-up of the model, we consider two methods to filter the bed level. The first is running the model based on the filtered data of Meijer (2020a,b), Besides that it may be necessary to allow some change for filtering the initial adaptation of the bed level. In the old DVR model this spin-up time was set to 5 years but in the Meuse the time may need to be much longer, due to the lower transport rates. The impact of this choice should be made visible so that it is understood what the implications of the initial conditions are on the final result for different type of studies.

6.7 Upstream morphodynamic boundary condition

Setting the appropriate morphodynamic boundary condition is particularly difficult in morphodynamic simulations given the usual lack of data or quality of it. Ideally one would impose the sediment entering the model for varying flow discharge. Unfortunately, little is known about the amount of sediment passing the weir at Sambeek. Given that the bed level has not changed considerably, the alternative followed here has been to impose a fixed bed. In this case the amount of sediment entering the domain is computed by the model to guarantee the observed change in bed elevation at the upstream end. In case of mixed-size sediment a boundary condition needs to be imposed for each size fraction. As with the bed level, a constant composition has been imposed.

A detailed study of the sediment passing the weir is recommended. We foresee that during low flow most of the sediment is trapped and does not pass the weir, in essence causing degradation downstream from the weir. During high flows the weir is open and it may not cause a significant impact on the sediment transport. During medium flows, the fine fractions may be able to pass while the coarse fractions are retained, causing a change in composition.

In the current calibrated simulations, a bed level trend based on historical information is imposed and this gives improved results compared to the 2022 model results. As in the previous section, the implications of this choice should be made clear.

7 Conclusions

In the current report, a pilot morphological model for the Sambeek-Grave reach was set up.

The hydrodynamic part of the model (assuming a fixed bed level) agreed reasonably with the water level slope and the velocity measurements. The distribution of the main channel discharge looked plausible, but could not be verified directly. Analysing the water levels as function of the discharges showed that the steering water levels at Mook were not satisfied for the low steering discharges. It is recommended to look at the behaviour for the full scale Meuse model including real time control of the weir, as well as the discharge extraction technique to deal with flood attenuation, as used in SITO-PS Modelschematisaties (personal communication, Anke Becker).

The morphodynamic development was analysed based on measurements. Based on discharge dependent simulations under a fixed bed condition, an estimate of the yearly sediment transport was generated to align with sedimentation in the summerbed lowering.

Subsequently, the influence of sediment availability and composition on the sediment transport was assessed. Including a fully available sediment layer in the upstream part of the model showed a proper passage of sediment along the reach rkm 150-155. This behaviour appeared to give a better response than imposing a fixed layer at this location.

The current calibration, including fully available sediment at the identified partially mobile zones, and a bed level degradation as an upstream boundary produced reasonable results. As the calibration period consisted of relatively low discharges it is recommended to perform a validation run checking the changes after the July 2021 flood.

8 Outlook

The current best calibration of the Sambeek Grave model still shows reasonable agreement in most of the Sambeek-Grave reach, with exception of the section just upstream of weir Grave. In this section, erosion was found in the measurements, whereas the model showed a slight sedimentation.

The following recommendations are given to further improve the current calibration.

1. The bed level dynamics of the current time frame (2014-2018) may be too small, resulting in an uncertain calibration.

We recommend to consider a different time frame which has larger dynamic behaviour, for instance the flood wave of 2021, provided that the measured bed levels are accurate enough to compare bed level development.

2. It is not certain how accurate the measured bed level data are for the current calibration time frame. Currently it was assumed that the bed level measurements are recorded in the summer period. Sometimes, however, the bed level data could include data from a previous measurement campaign. It would be recommended to verify the data sets and the time at which they were recorded.

3. In addition dredging activity is not yet included in the model. Is this information available and accurate enough to be included in the model?

4. The current bed level developments are done without considering the relative transport of sand and gravel, during low and high flows. It would be very useful to know the transport of fine sediment fractions in relation to the coarse fractions during low and high flows. Any information regarding this could be worthwhile to include in the model setup.

5. The role of flood attenuation is currently not considered. An approach using a dynamic wave and a time-varying MorFac may provide different insights to the morphodynamic changes in the reach Sambeek-Grave.

6. Besides the current calibration, which is based on largely 1D parameters, it is recommended to also look at two dimensional charateristics (river-axis (L1-R1), left and right side of the main channel (L1-L3, R1-R3) and transverse bed level effects ((L1-L3) - (R1-R3))).

References

Berends, K., R. Daggenvoorde and K. Sloff, 2020. *Morphological models for IRM: Meuse 1D*. Tech. Rep. 11203684-015-ZWS-0016, Deltares and HKV.

Berkhout, W. A., 2003. *Modelling of large-scale morphological processes in sand-gravel rivers. Analytical and numerical analysis of graded morphological processes in the River Meuse*. Master's thesis, Universiteit Twente.

Chavarrias, V., 2021. *Differences between parallel and sequential simulations*. Tech. rep., Deltares, the Netherlands. Presentation.

Chavarrias, V. and W. Ottevanger, 2022. *Modelling study of the sediment transport along the Meuse River during the flood wave of 2021*. Memo 11208012-013-ZWS-0001, Deltares, Delft, the Netherlands.

Chavarrías, V., W. Ottevanger, K. Sloff and E. Mosselman, 2022. "Modelling morphodynamic development in the presence of immobile sediment." *Geomorphology* 410: 108290. DOI: https://doi.org/10.1016/j.geomorph.2022.108290, ISSN 0169-555X, URL https://www.sciencedirect.com/science/article/pii/S0169555X22001830.

Chrzanowski, C. and T. Buijse, 2019. *Factsheets monitoring en ontwikkeling Maasoevers 2008 – 2017*. Bijlage bij rapport, Deltares, Delft.

Chrzanowski, C., M. Weeber, G. Geerling, T. Buijse, M. Dorenbosch and B. Peters, 2019. *Achtergrondrapport 'Natuurvriendelijke oevers langs de Maas: toestand en trend na 10 jaar ontwikkeling'*. rapport, Deltares, Bureau Drift and Bureau Waardenburg.

van der Deijl, E., 2022. *Validatie hoogwater Maas juli 2021*. Tech. Rep. 11208053-002-ZWS-0006, Deltares, Delft, the Netherlands.

Eelkema, M., 2021. *Afvoermetingen Hoogwater Maas & Waal*. Tech. Rep. AV200163 juli 2021 v1 definitief, Aqua Vision B.V.

ENW, 2021. *Hoogwater 2021 Feiten en Duiding*. Rapport, Expertise Netwerk Waterveiligheid.

Frings, R., 2022. *De bodemsamenstelling van de Maas in 1983 en 2020*. Tech. Rep. only data - report to follow, Rijkswaterstaat.

Fujisaki, A., R. Agtersloot and A. Becker, 2022. *B&O-modellen en deelmodellen Maas.* Tech. Rep. 11208053-002-ZWS-0005, Deltares, Delft, the Netherlands.

Hirano, M., 1971. "River bed degradation with armoring." *Proc. Jpn. Soc. Civ. Eng.* 195: 55–65. DOI: 10.2208/jscej1969.1971.195_55.

de Jong, J., 2021. *Ontwikkeling zesde-generatie Maas-model: Modelbouw, kalibratie en validatie*. Tech. Rep. 11200569-003-ZWS-0014, Deltares, Delft, the Netherlands.

de Jong, W., 2005. *Onzekerheidsanalyse bodemverandering Grensmaas: Een onderzoek naar de onzekerheid in de met SOBEK-graded gemodelleerde bodemverandering van de Grensmaas ten gevolge van de variatie in de afvoer.* rapport R0002/R/WDJ/Nij, Royal Haskoning.

Kuypers, J. .-. and M. v. Osch, 1853. "Kaart der provincie Noordbrabant." Schaal 1:200.000.

Lely, C. W., 1926. *De Verbetering van de Maas voor Groote Afvoeren*. Tech. rep., Rijkswaterstaat.

van der Mark, C. F., R. A. M. van der Sligte, A. Becker, E. Mosselman and H. J. Verheij, 2011. *Morfologische effectstudie KRW-maatregelen IJssel*. rapport 147 p., Deltares, Delft.

Meijer, D. G., 2020a. *Kennis- en data-inventarisatie voor bodemhoogteanalyses Maas; Systeemrapportage morfologie Maas: Analyserapport (fase 2)*. Tech. Rep. 117.01-02, RiQuest.

Meijer, D. G., 2020b. *Kennis- en data-inventarisatie voor bodemhoogteanalyses Maas; Systeemrapportage morfologie Maas: Overzichtsrapport (fase 1)*. Tech. Rep. 117.01-02, RiQuest.

Meyer-Peter, E. and R. Müller, 1948. "Formulas for bed-load transport." In *Proc. 2nd IAHR World Congress, 6–9 June, Stockholm, Sweden*, pages 39–64.

Ottevanger, W., 2021. *Morphological model for the River Meuse: Case Study for the reach Sambeek-Grave*. Tech. Rep. 11206793-014-ZWS-0004, Deltares, Delft, the Netherlands.

Ottevanger, W., 2023. *D-Morphology: Implementation of a separate roughness field for morphodynamics*. Memo 11209261-002-ZWS-0002, Deltares, Delft, the Netherlands.

Ottevanger, W. and V. Chavarrias, 2022a. *Morphological model for the River Meuse: Case Study for the reach Lixhe-Keizersveer*. Tech. Rep. 11208033-002-ZWS-0005, Deltares, Delft, the Netherlands.

Ottevanger, W. and V. Chavarrias, 2022b. *Morphological model for the River Meuse: Case Study for the reach Sambeek-Grave*. Tech. Rep. 11208033-002-ZWS-0003, Deltares, Delft, the Netherlands.

Ottevanger, W., V. Chavarrias, M. Busnelli, A. Omer and C. Eijsberg, 2024a. *Morphodynamic model of the Meuse River*. Tech. Rep. 11209261-002-ZWS-0006, Deltares, the Netherlands.

Ottevanger, W., V. Chavarrias, S. Giri and E. van der Deijl, 2021. *Morphological model for the River Meuse: Model setup, input visualisation, and future steps*. Tech Rep. 11206792-003-ZWS-0002, Deltares, Delft, the Netherlands.

Ottevanger, W., V. Chavarrias and A. Omer, 2024b. *Morphological model for the River Meuse: Case Study for the reach Sambeek-Grave*. Tech. Rep. 11209261-002-ZWS-0008, Deltares, Delft, the Netherlands.

Ottevanger, W., E. Verschelling and S. Giri, 2020. *Initiële modelbouw morfologisch model voor de Maas*. Tech Rep. concept 11205234-003-ZWS-0001, Deltares, Delft, the Netherlands.

Rijkswaterstaat and Deltares, 2022. *Factsheet zesde generatie Modelschematisaties D-FLOW FM 2D Maas*. Tech. rep., Rijkswaterstaat.

Rijkswaterstaat Zuid Nederland, 2019. "Betrekkingslijnen Maas 2019-2020."

van Rijn, L. C., 1984. "Sediment Transport, Part III: Bed forms and Alluvial Roughness." *J. Hydraul. Eng.* 110 (12): 1733–1754. DOI: 10.1061/(ASCE)0733-9429(1984)110:12(1733).

RWS, Directie Limburg, 1979. “Waterloopkundige aspecten in het winterbed van de Maas, samenhangend met de bochtafsnijding Boxmeer en rijksweg 77.”

Sieben, A., 2021. *Korte verkenning relatie C_d*. Note 2021, Rijkswaterstaat.

Sieben, A., 2022a. *Notitie update kentallen lokale 1D bodemdynamiek Maas*. Tech. rep., Rijkswaterstaat.

Sieben, A., 2022b. *Perspectief Maas 2022*. Note 28-1-2022, Rijkswaterstaat.

Sieben, A., 2023. *Bepaling standaardset afvoeren DFAST-MI*. Note 31-08-2023, Rijkswaterstaat.

Sloff, C. J. and H. J. Barneveld, 1996. *Morfologisch model Zandmaas : MAASMOR 1995*. rapport Deltares, WL Delft Hydraulics, Delft.

Sloff, C. J. and C. Stolker, 2000. *Calibratie SOBEK-Gegradeerd Zandmaas: voorbereiding voor morfologische berekeningen OTB*. Tech. Rep. Q2589, Delft Hydraulics Laboratory, Delft, the Netherlands.

Spruyt, A. and W. Ottevanger, 2019. *Plan van aanpak morfologisch model Maas*. rapport, Deltares, Delft.

Struiksma, N., 1999. “Mathematical modelling of bedload transport over non-erodible layers.” In *Proceedings of the 1st IAHR symposium on River, Coastal, and Estuarine Morphodynamics, Genova, Italy*, pages 89–98.

Tolman, F., 1987. *Bochtafsnijding in de Maas bij Boxmeer*. Master’s thesis, Delft University of Technology.

Veen, R. van der and R. C. Agtersloot, 2021. *Topafvoeren hoogwater Maas juli 2021*. Tech. Rep. versie 2.0 d.d. 16-12-2021, Rura-Arnhem and AHA BV.

Yossef, M. F. M., H. R. A. Jagers, S. van Vuren and A. Sieben, 2008. “Innovative techniques in modelling large-scale river morphology.” In M. Altinakar, M. A. Kokpinar, İsmail Aydin, Şevket Cokgor and S. Kirgoz, eds., *Procedings of the 4th International Conference on Fluvial Hydraulics (River Flow), 3-5 September, Cesme, Izmir, Turkey*. Kubaba Congress Department and Travel Services, Ankara, Turkey.

A Morphodynamic sensitivity computations

Simulations in this section are based on results in which the calibration has not yet been updated to the current approach.

A.1 Modelling partially mobile sediment regions

In Ottevanger *et al.* (2021) different regions were identified with limited bed level changes. These regions could be indicative of a constant sediment transport or a consequence of limited availability of sediment in the vertical. In this section different models are setup comparing the influence of the choice in the thickness of sediment availability on the bed level changes. The initial sediment thickness is shown in Figure A.1.1. The "full" includes a 1 m sediment layer over the full model with composition of Frings (2022), and a 9.75 m thickness below in the main channel based on Berends *et al.* (2020). In "main 1 m", the sediment is specified solely in the main channel. The 1 m relates to thickness according to the composition as in "full". The "main 0.25 m" includes this layer with 0.25 thickness. The "fixed ..." have limited sediment availabilty in the vertical at the semi-fixed layer locations (between rkm 148 and 155, and locally at rkm 165 at the railway bridge at Mook). The asterisk (*) indicates the region of the fixed layer has been extended up to the upstream boundary of the model at Sambeek.

The resulting bed level changes are shown in Figure A.1.2. First considering the upstream reach up to rkm 155 we see the following bed level development.

Assuming full available sediment thickness leads to sedimentation in the upstream reach. The pattern of the simulations including only sediment in the main channel "main 1 m" and "main 0.25 m" shows a similar trend, with more erosion in rkm 155. Adding fixed layer sections, leads to sedimentation in the section upstream of rkm 150. When extending the fixed layer section "fixed 0.25 m (*)" up to the model boundary, the upstream boundary and the reach show hardly any change.

Considering the start of the summerbed lowering at rkm 156-157 the measurements show a clear sedimentation pattern (cf. measured trends in Figure 3.1). This is overestimated by "full", "main .." and underestimated by the "fixed .." simulations. This seems to lead to a situation in which either the upstream condition or the downstream condition is satisfied, and the solution we seek for has to satisfy both.

We continue with "fixed 0.25 m (*)" as it captures the upstream behaviour well, but we realise that the result is still intermediate as the overall pattern is not well described in the rest of the reach.

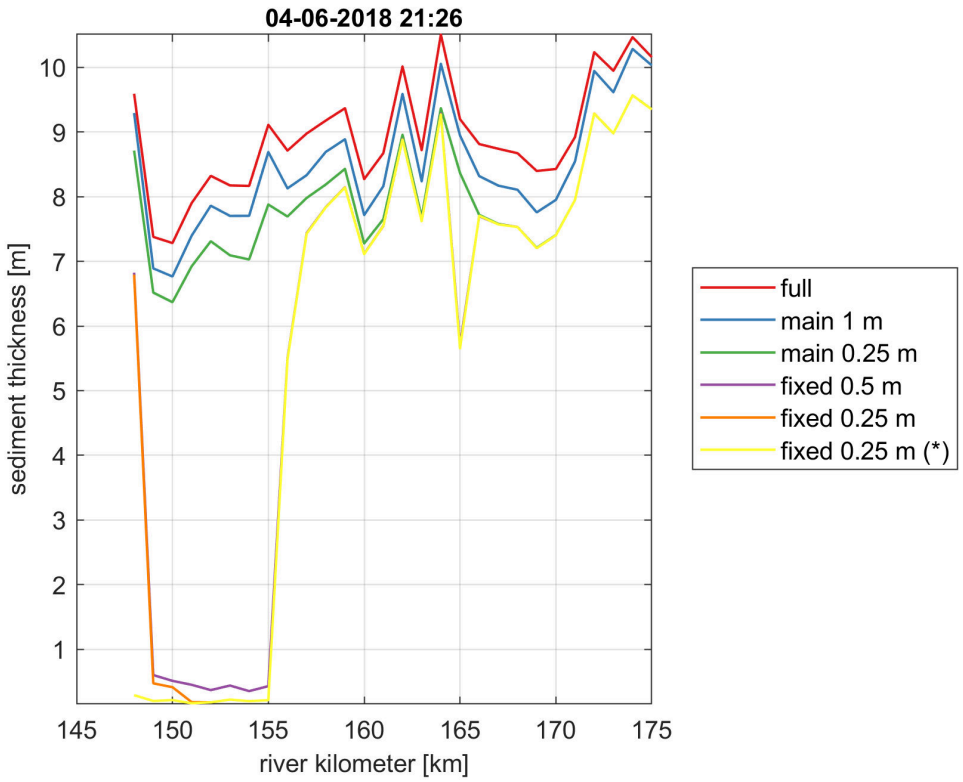

Figure A.1.1 Sediment thickness averaged per river-kilometre between L3 and R3.

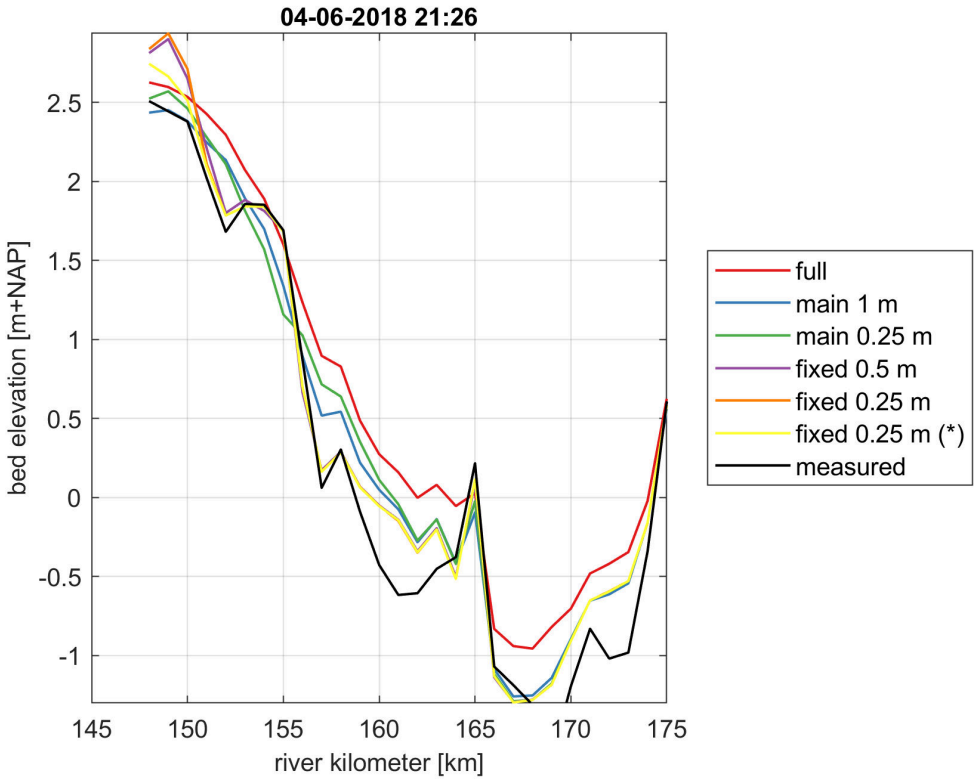

a)

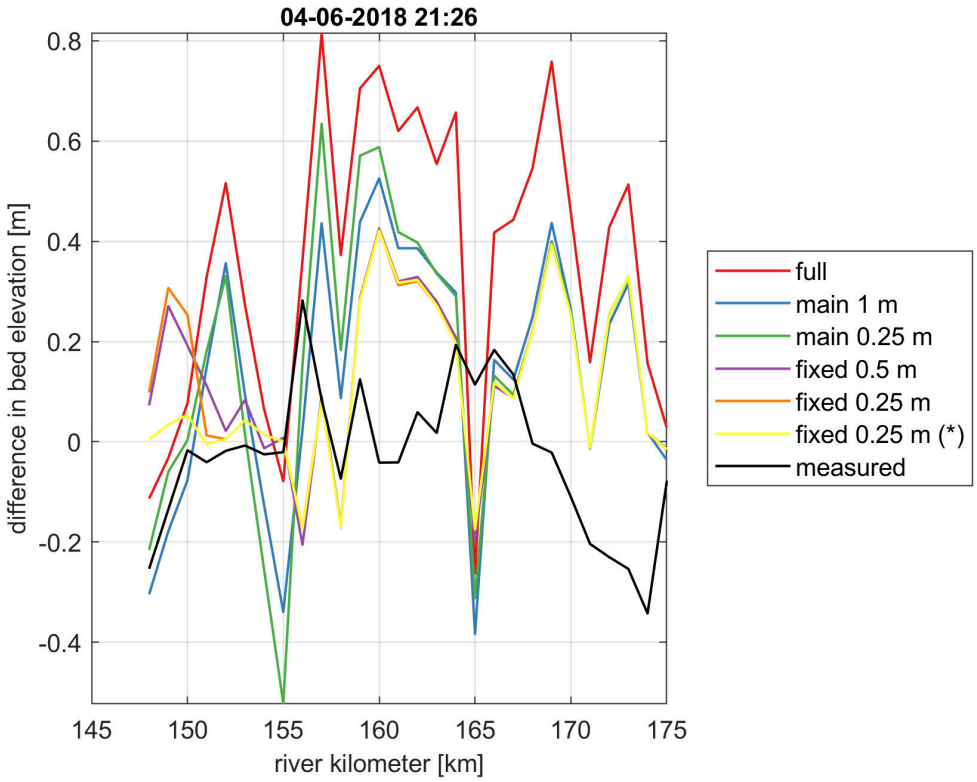

b)

Figure A.1.2 Bed level development for varying sediment thickness a) in 2018, and b) difference with the initial bed level (2014).

A.2 Effect of bed level averaging method

Two methods related to the schematization of the bed level in the model were assessed. The first is the approach from Baseline[1], which uses the grid cell value from the TIN by pinpointing the cell centre value, and is overwritten by the downstream summer bed lowering which was missing in the Baseline schematisation. The second approach overwrites the bed level by grid cell averaged values, wherever the yearly multi-beam measurement covers 80 % or more in the grid cell.

Figure A.2.3a) shows that the average bed level is somewhat higher in certain regions when using an averaging method. The final erosion and sedimentation patterns are not affected a lot (cf. Figure A.2.3b). This implies that the bed level averaging method is sufficiently described by the pinpointing method in the current schematisation.

[1] https://iplo.nl/thema/water/applicaties-modellen/watermanagementmodellen/baseline/

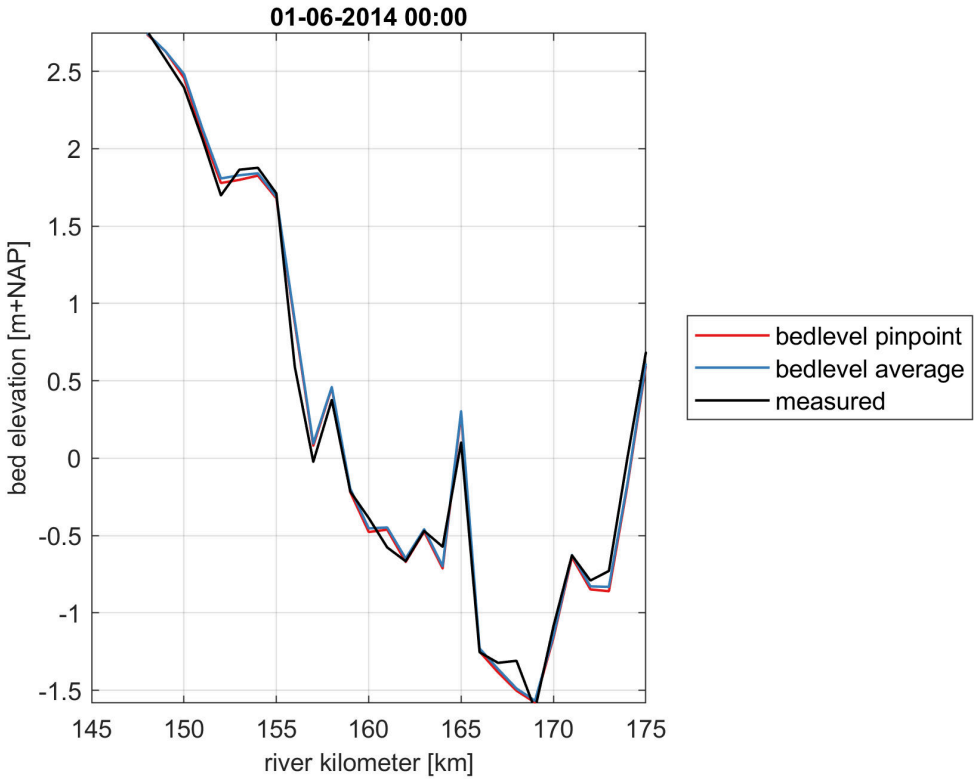

a)

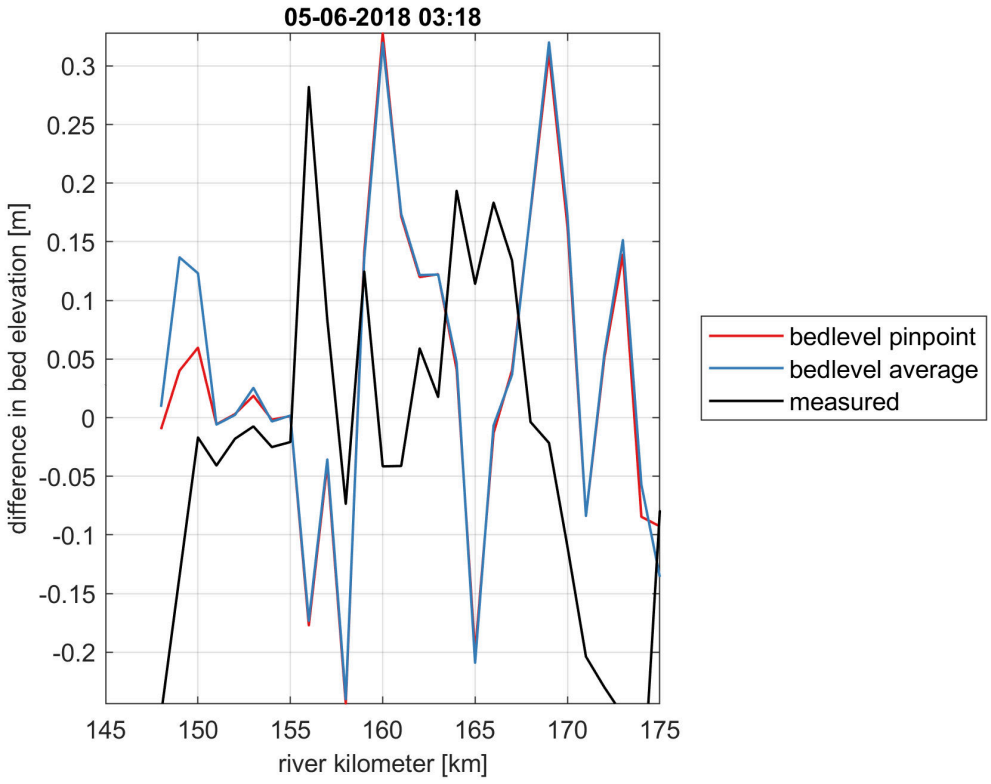

b)

Figure A.2.3 Initial bed level development for varying bed level interpolation a) in 2014, and b) difference with the initial bed level (2018 - 2014).

A.3 Effect of secondary flow correction on the bed load transport

To check the influence of the secondary flow on the bed load transport correction, three different simulations are considered. The factor which weights the distribution of the secondary flow was varied between 0.25, 0.0 and 0.5, and the resulting bed levels are shown in Figure A.3.4. This shows that the computed effect of the secondary flow is minimal in the Sambeek - Grave reach.

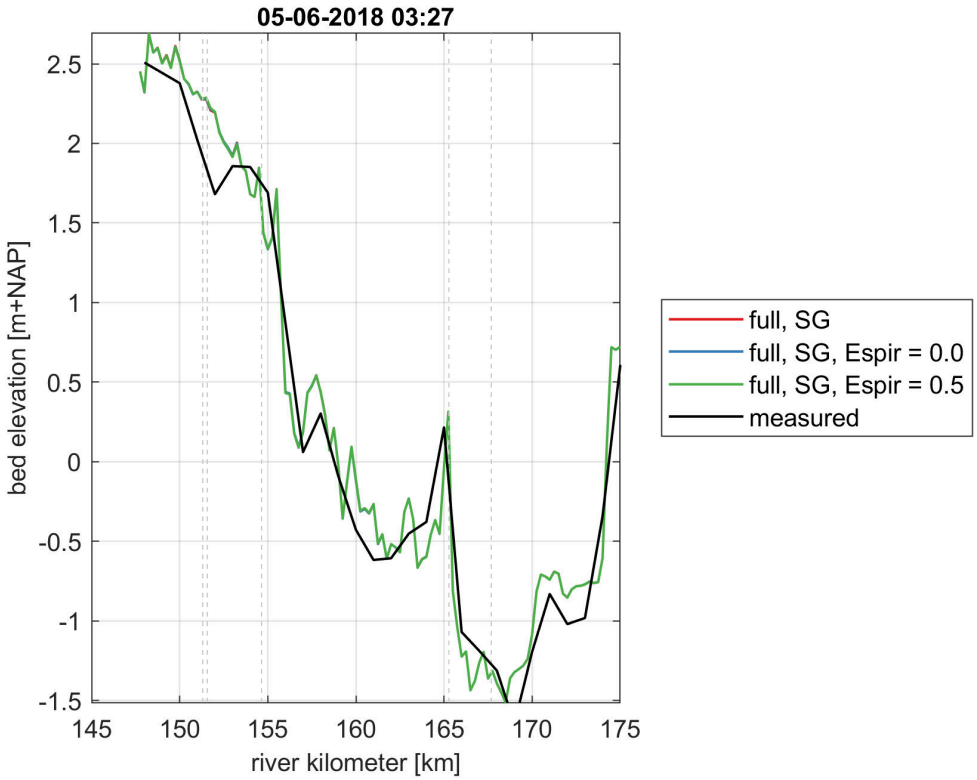

a)

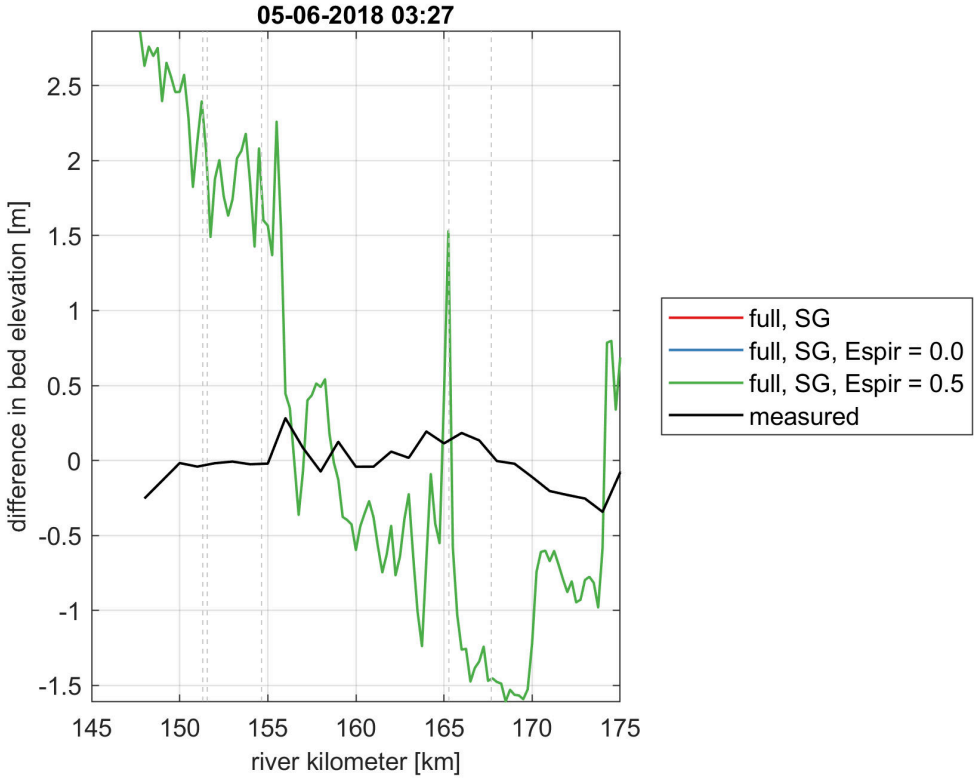

b)

Figure A.3.4 Initial bed level development for varying influence of the secondary flow bed load transport correction. a) in 2014, and b) difference with the initial bed level (2018 - 2014).

A.4 Effect of roughness in the transport computation

The roughness distribution seems to have a strange step-wise transition in the stream-wise direction. This roughness has been calibrated on water levels, yet it is unclear if this roughness description fits the sediment transport as well. The current roughness follows a simplified van Rijn relation, which possibly does not hold in the current reach.

This year, a method was proposed to introduce a separate roughness definition for the computation of the sediment transport while flow computations keep using the roughness definition from the original hydrodynamic model (Ottevanger, 2023). Unfortunately, due to the current complexity of the roughness module, there was not a common ground to further increase the complexity. Therefore, this implementation was not undertaken.

As an alternative a DLL sediment transport formula was generated which passes the roughness as an additional parameter. The results were however not significantly different from the results with the original roughness definition. This lead to a new iteration of the sediment transport calibration this year. The results shown in Figure A.4.5 and Figure A.4.6 confirm that there is little effect on the bed level development when using the adjusted formula.

Simulation	Label	Roughness [$m^{1/2}/s$]
D2	General formula	Roughness from simulation
R2	General formula through DLL (constant Chezy)	44

Table A.1 Overview of chosen settings for the effect of roughness choice.

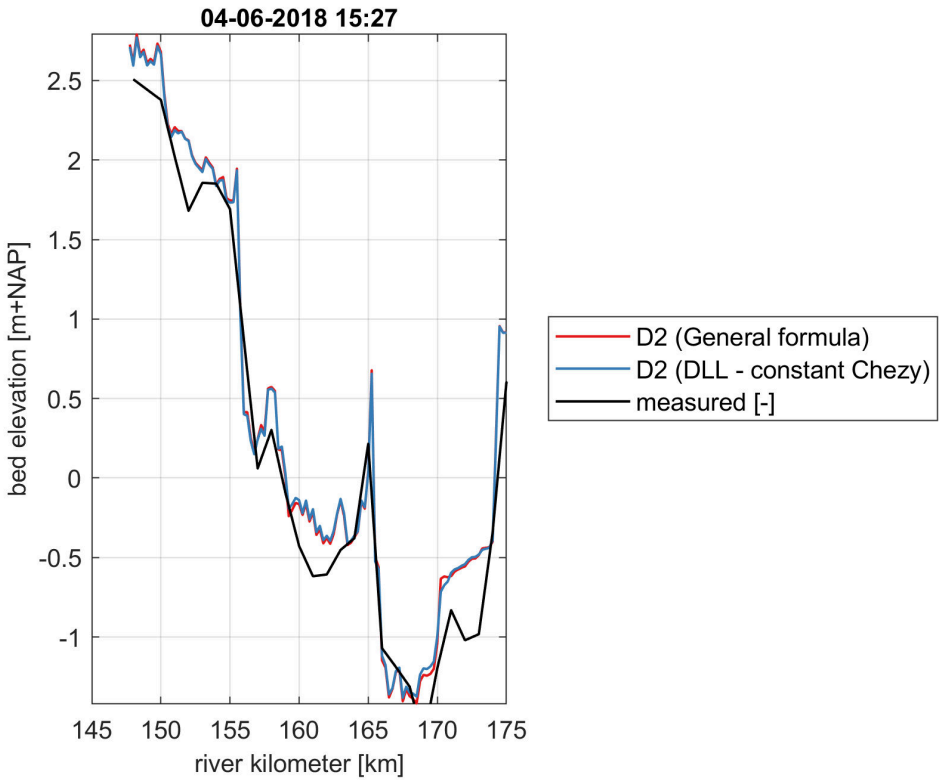

Figure A.4.5 Bed level development for the different roughness simulations

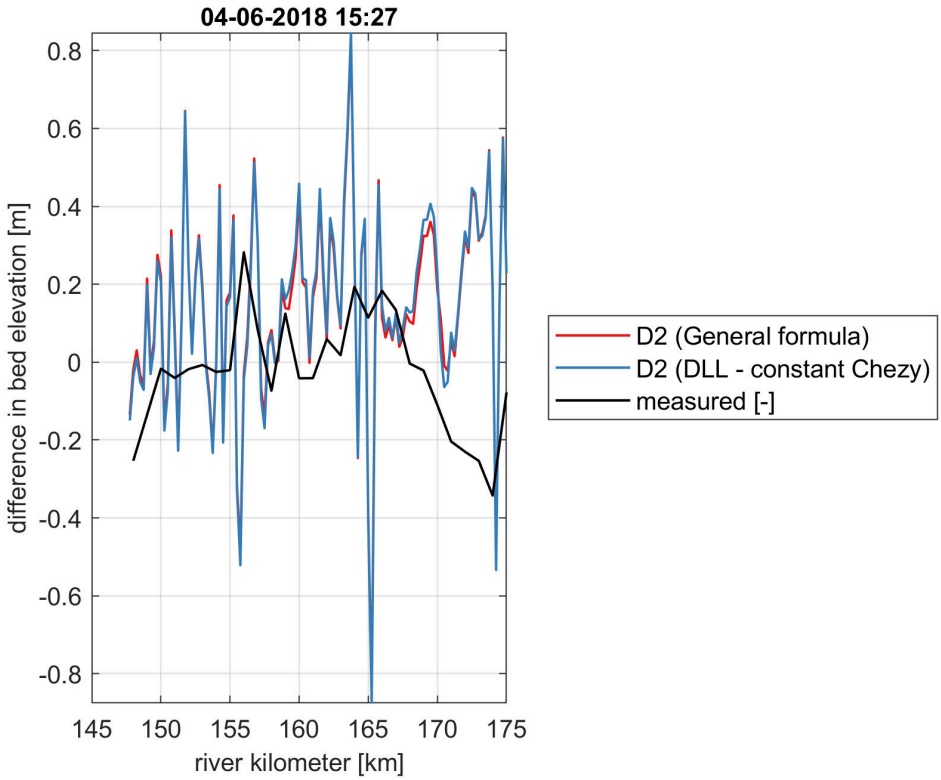

Figure A.4.6 Bed level difference for the different roughness simulations with respect to the initial bed level

B Observed trends between 2014 and 2019

In addition to the large scale trends, we describe the trends per river kilometre in the reach between 2014 and 2019.

147 Downstream of weir Sambeek, a scour hole is present, just off centre to the right. This scour hole has deepened by more than 2 metres. Locally, downstream of the scour hole sedimentation is visible. The main channel shows a few patches of sedimentation and erosion, but nothing large. To the left side, near the sluice gates, sedimentation is visible and it appears that local exit channels of the right lock have been dredged.
148 The confluence of the lock passage and the main channel show sedimentation. At the right side of the channel the connection to the former maas channel “Oude Maas” shows some sedimentation. Just downstream of the connection to the Oude Maas, is a local zone with removed bank protection. Between 5 to 10 metres of bank erosion is visible over a length of 1,5 km. Close to the bank, this does not appear as sedimentation, possibly due to the measurement extent. Strikingly, in the main channel a narrow band of sedimentation is visible. This may be related with the locally widened reach at the eroded bank.
150 Just downstream of 150 there is a local shallow zone visible. This could possibly be burried infrastructure such as a pipe or cable.
151 A deeper reach just upstream with a shallow zone towards the left side of the channel. Locally some streaks of erosion show, possibly due to shipping?
152 At the connection to the Oude Maas, a local scour exists. The entrance to the Oude Maas shows sedimentation. In the main channel at that location erosion occurs. At the left bank a nature friendly bank is present with local bank erosion of up to 10 m. Its length is roughly 400 m. In the main channel a streamwise line of sedimentation is present. At the right bank a “strang” is present, and some deposition is visible.
153 Both banks show a nature friendly bank. The left has a length of around 300 m, and the right is approximately 100 m. Bank erosion of up to 10 m is visible. A local streamwise oriented patch of sedimentation is present. Along the right bank deposition is shown. The confluence with the Oude Maas shows some sedimentation. At 153.5 a harbour is visible, with pronounced sedimentation and erosion, which could be linked to shipping vessels, making the turn into the harbour.
154 At the left bank upstream of 154 is an eroding bank, with erosion distance of 10-15 m, with a length of 560 m. Some sedimentation is visible in the centre of the channel, but also local patches of erosion. Upstream of 154, these are two local scour areas, with sharp interfaces in the bed. Mid channel at 154 a local shallow zone shows some erosion. At the right bank an eroding bank is present with a length of 450 m, with local bank erosion of up to 10 m. Along the banks erosion and deposition is visible.
155 Upstream of 155, there is a bridge crossing the channel. Just downstream of the bridge pier there is erosion and subsequently deposition. Further downstream a local patch of erosion is also visible. At 155, there are patches of erosion and deposition
156 Just upstream of 156, marks the start of the summerbed lowering. A large sedimentation trend is visible downstream of 156. Local erosion is visible near the sides of the summerbed lowering. Possible adaptation of the slopes to the created lowering.
157 Along the left bank erosion at the toe of the groynes. Strikingly, these weirs do not show on satellite images. It appears that they are either inundated on satellite images, or that the top part has been removed? Just downstream of 157 the Niers enters the Meuse. Here erosion is visible, probably due to the increase in discharge.

158 Upstream of 158, marks a pool labelled “Boral Nedusa Baksteen Milsbeek”, suggesting a location where sediment (clay?) is extracted to create bricks. Along the left bank the shape suggests ongoing bank erosion over a length of 700 m. This shows as local sedimentation and erosion patterns along the left bank. In the main channel the summerbed lowering seems to have eroded/excavated a bit more?
159 Large sedimentation in deepend part of the channel. Slight erosion along the banks, particularly the left bank.
160 Downstream of 159 until past 162, weirs are present at the right bank. These do not show large erosion or sedimentation patterns until rkm 162. The main section of the summerbed lowering downstream of 162 shows erosion. At the left bank some small bed level change patches are visible (maybe banks?, local slope failure of the summerbed lowering?)
161 Up till 161 erosion is visible in the main channel. This is a zone where the channel is locally deeper in the main channel, which could form a bottle neck, thereby increasing flow velocities and resulting in erosion. Just downstream of 161 there is widening leading to sedimentation. Next there is a shallower section, which erodes somewhat, and subsequently a deeper pool which leads to sedimentation.
162 Along the left interface of the summerbed lowering, erosion is visible. Along the inner bend sedimentation is visible.
163 Upstream of 162, a scour hole is visible just downstream of the first weir on the left bank. The weirs along the left bank are present until 164. Upstream in the main section there is sedimentation. A local contraction is visible at 163, and also some erosion. Downstream of 163, there are patches of erosion and sedimentation.
164 Until 164 the summerbed lowering is pronounced showing patchy erosion and sedimentation. Along the right bank weirs are present. Downstream of 164 the connection to the Mookerplas is present, this shows some erosion locally (run-off? shipping?). Downstream of 164, the river turns to the west, and sedimentation along the point bar is visible.
165 Upstream of 165 the point bar sedimentation is visible. At 165, two small harbours are present, showing sedimentation at the entrance. For a distance of around 200 m from 165 until past the bridge, there is hardly any bed level change. This appears to be a fixed layer of some sort. Downstream of the “fixed” bed level, erosion is visible
166 Upstream of 166, the entrance to the Maas-Waalkanaal is present. This local widening leads to sedimentation at the inner bend. Along the side of the interface between the main channel and the canal, erosion of the underwater banks is present. Downstream of 166 sedimentation is visible.
167 All along the left bank sedimentation is visible, along the inner bend and at the entrance to the Cuijk harbours. The right side of the channel shows little change.
168 Continuous sedimentation is seen along the left bank. Just downstream of 168 two patches of local scour are visible in the centre of the channel.
169 The upstream part shows little change. Downstream of 169, erosion (dredging?) is visible in the main channel.
170 The erosion (dredging?) continues until 170 where there is a shallow layer with no bed level change. Downstream of this area, there is again erosion (dredging?).
171 Erosion (dredging?) of the main channel?
172 Erosion (dredging?) of the main channel?
173 Erosion (dredging?) of the main channel?
174 Erosion (dredging?) of the main channel until just downstream of 174, subsequently a shallow section (pipe / tunnel ?)

175 Erosion (dredging?) near the bifurcation to the lock entrance at Grave. Sedimentation and erosion in track like form in the lock entrance part. Local erosion in the main channel near the weir Grave. Little bed level change just upstream of the weir Grave. Downstream of the weir a deep pool is present. Recent reparation works to the bed protection downstream of the weir are visible. Strong bank erosion, following the incident of the ship collision at Grave.

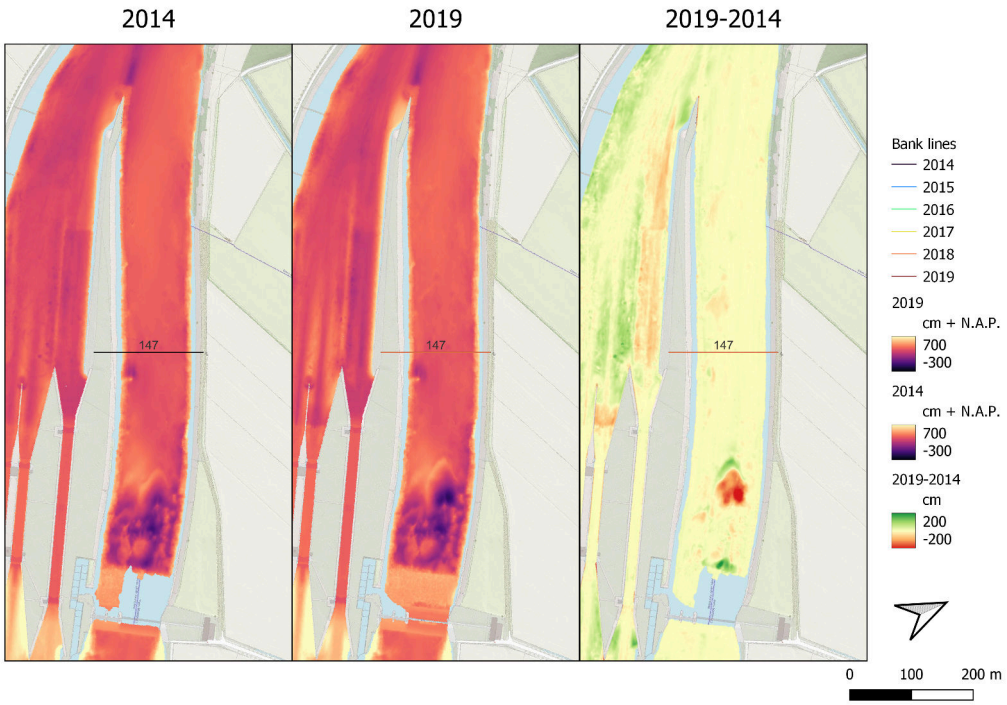

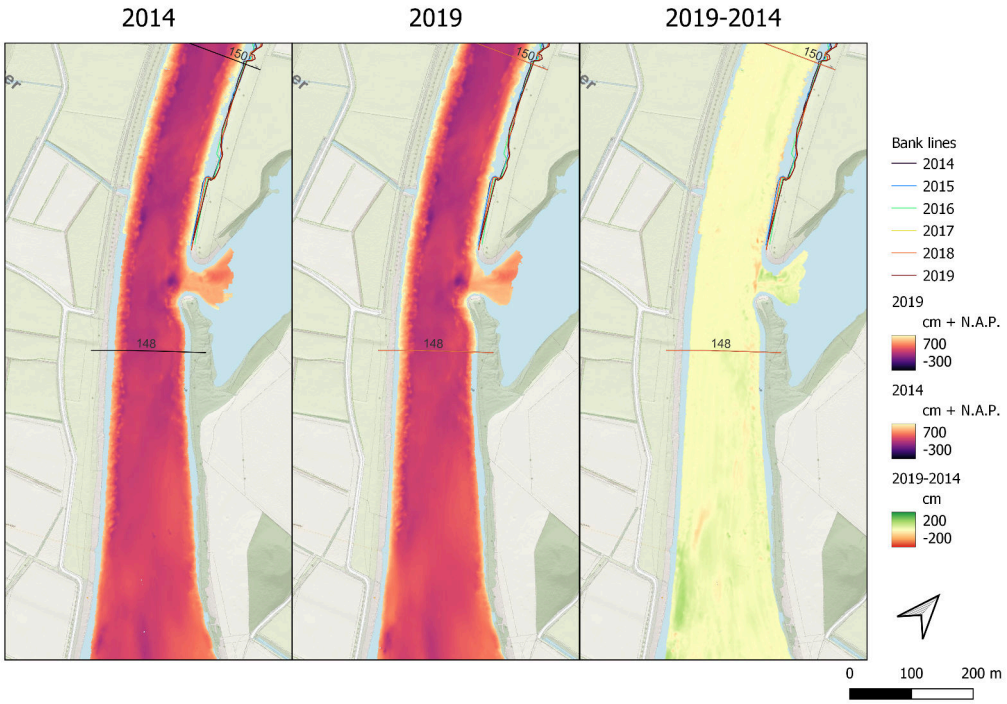

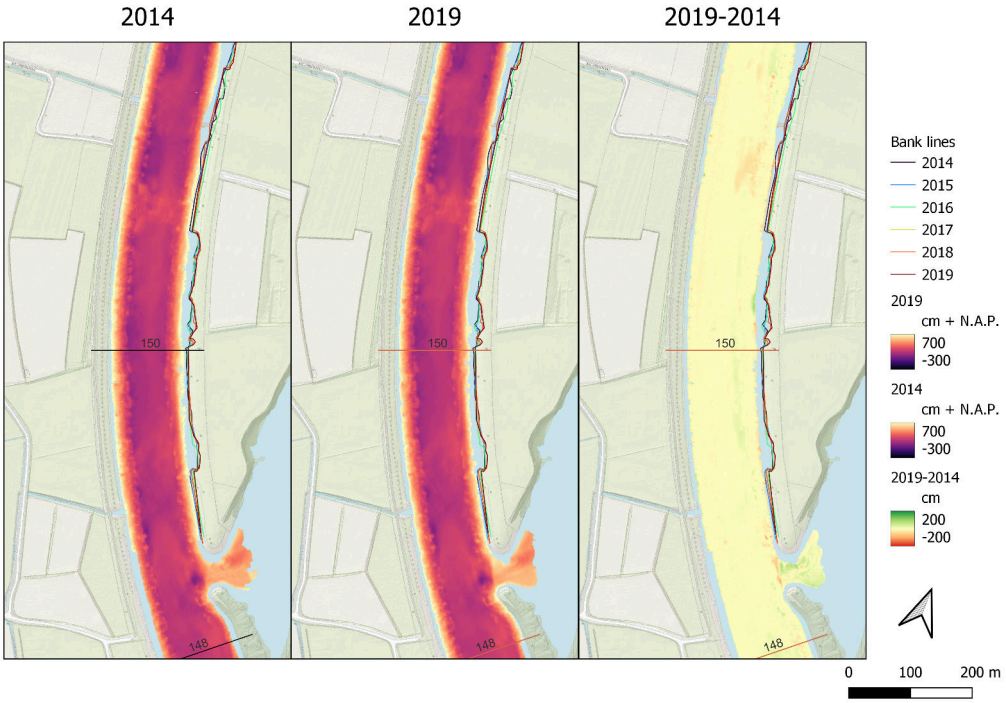
2014
2019
2019-2014
150
148
Bank lines
2014
2015
2016
2017
2018
2019
2019
cm + N.A.P.
700
-300
2014
cm + N.A.P.
700
-300
2019-2014
cm
200
-200
0
100
200 m

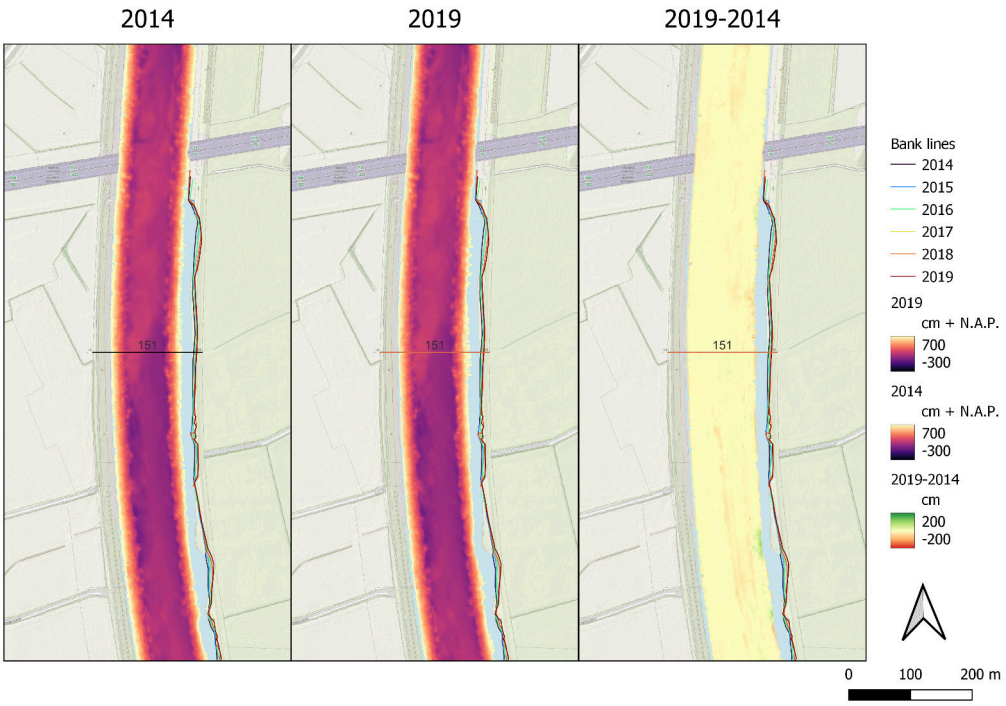
2014
2019
2019-2014
151
Bank lines
2014
2015
2016
2017
2018
2019
2019
cm + N.A.P.
700
-300
2014
cm + N.A.P.
700
-300
2019-2014
cm
200
-200
0
100
200 m

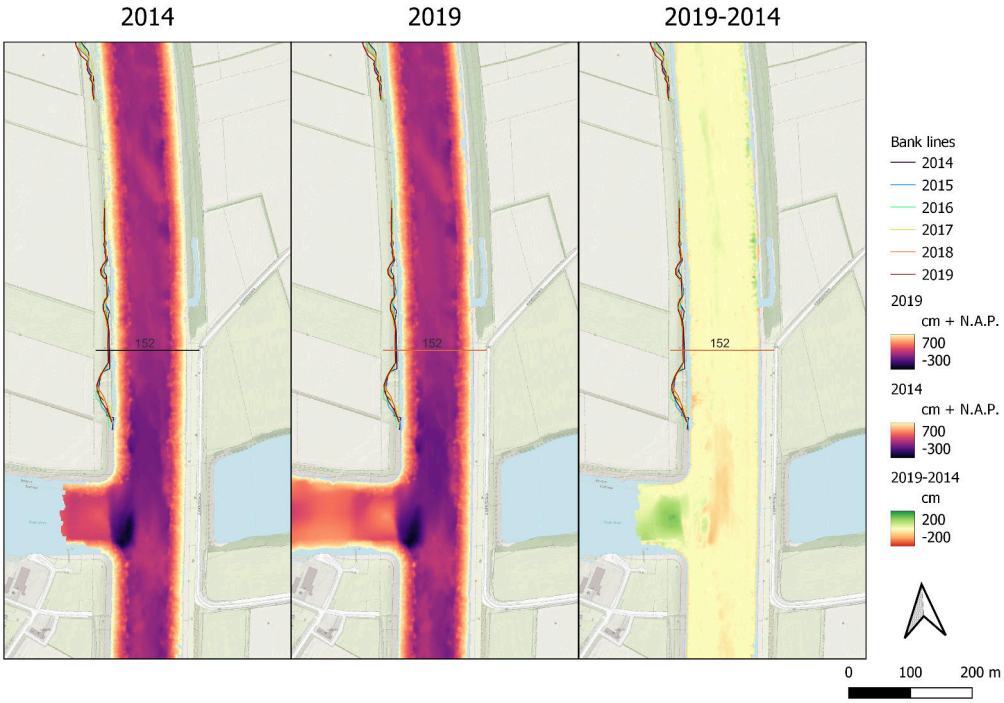
2014
2019
2019-2014
152
Bank lines
2014
2015
2016
2017
2018
2019
2019
cm + N.A.P.
700
-300
2014
cm + N.A.P.
700
-300
2019-2014
cm
200
-200
0
100
200 m

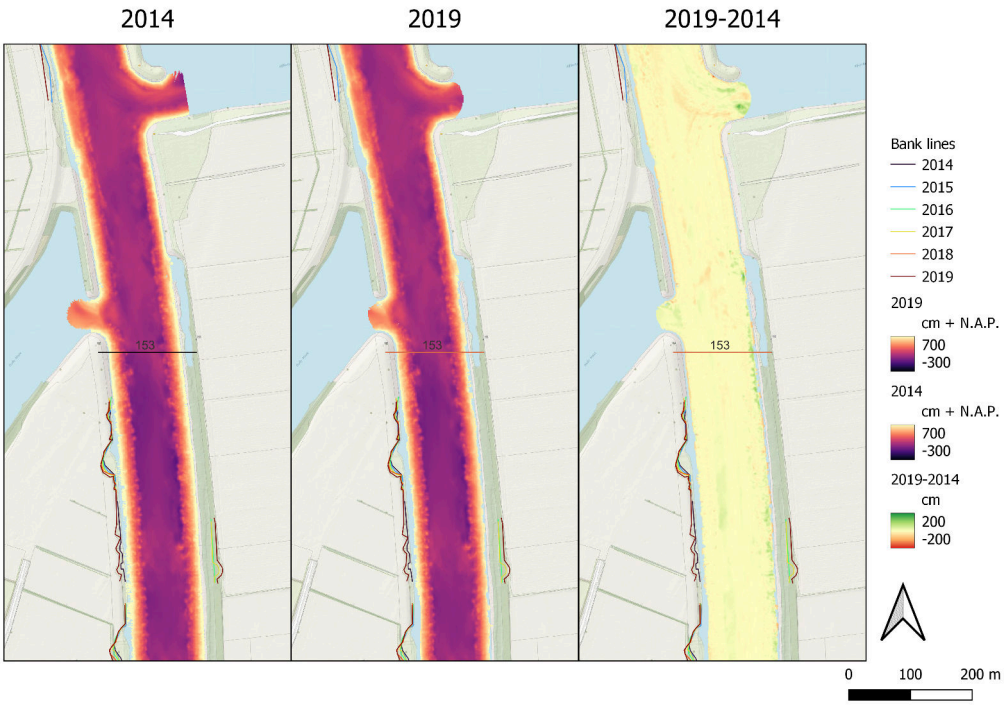
2014
2019
2019-2014
153
Bank lines
2014
2015
2016
2017
2018
2019
2019
cm + N.A.P.
700
-300
2014
cm + N.A.P.
700
-300
2019-2014
cm
200
-200
0
100
200 m

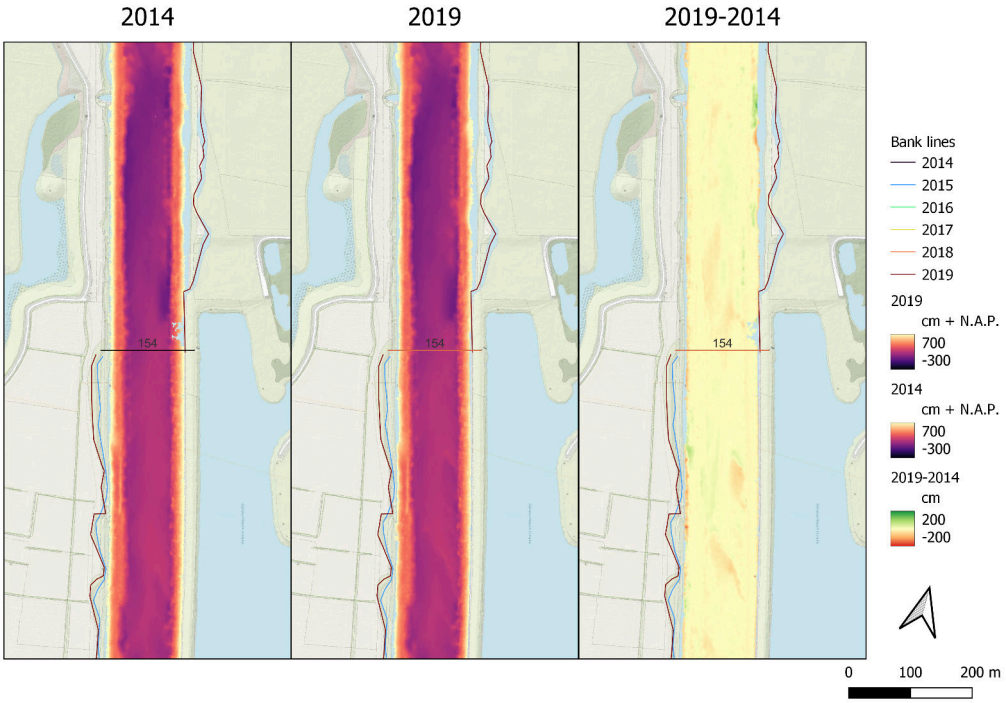
2014
2019
2019-2014
154
154
154
Bank lines
2014
2015
2016
2017
2018
2019
2019
cm + N.A.P.
700
-300
2014
cm + N.A.P.
700
-300
2019-2014
cm
200
-200
0
100
200 m

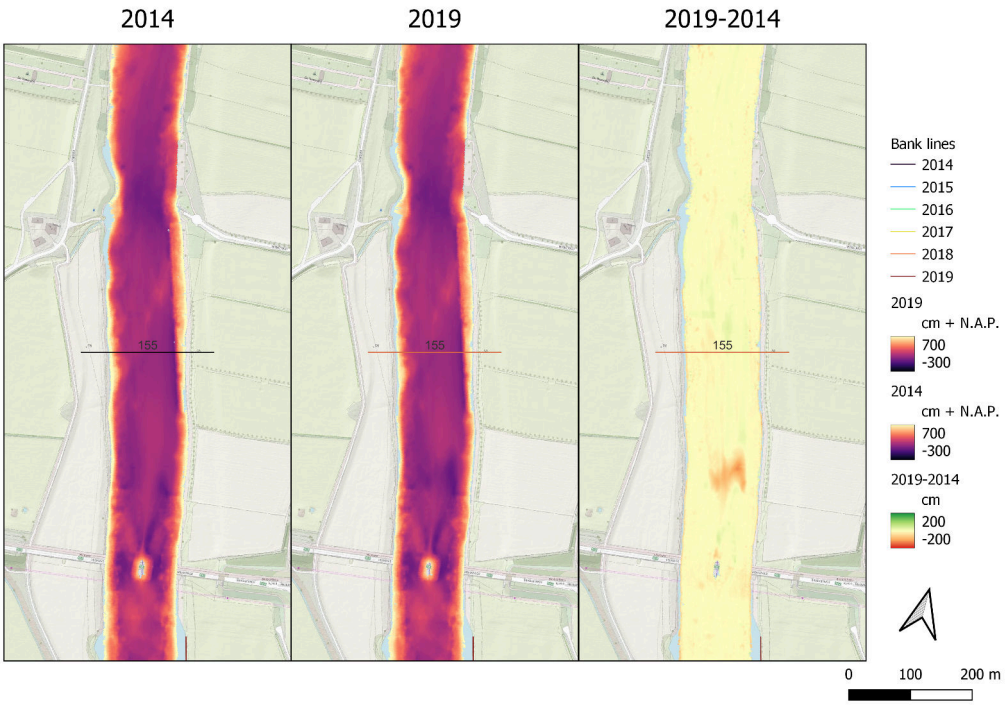
2014
2019
2019-2014
155
155
155
Bank lines
2014
2015
2016
2017
2018
2019
2019
cm + N.A.P.
700
-300
2014
cm + N.A.P.
700
-300
2019-2014
cm
200
-200
0
100
200 m

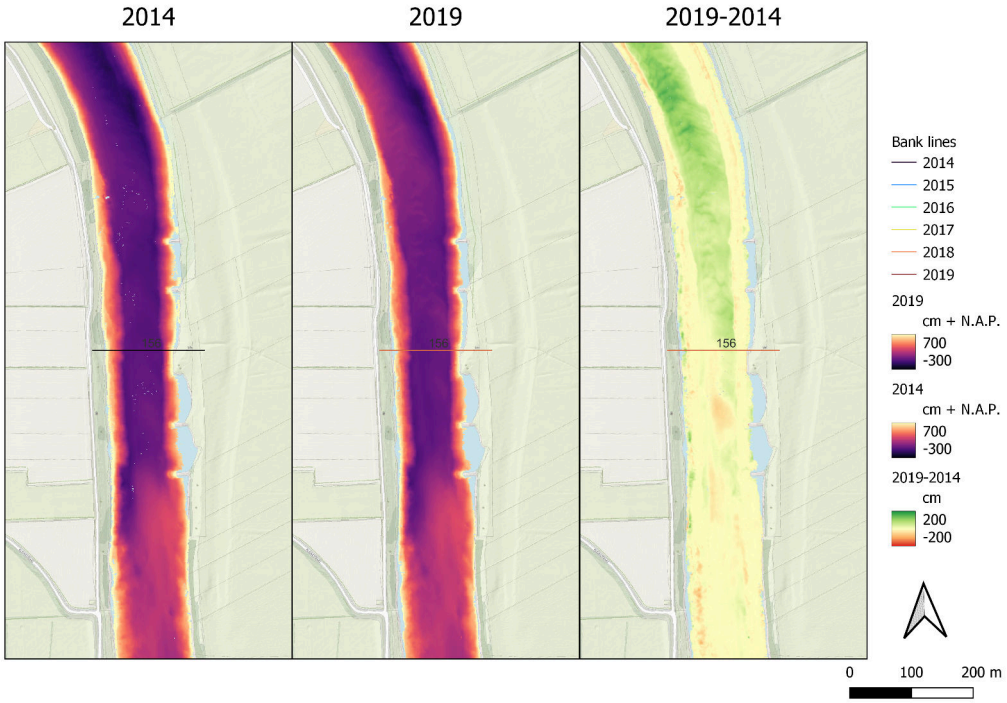
2014
2019
2019-2014
156
156
156
Bank lines
2014
2015
2016
2017
2018
2019
2019
cm + N.A.P.
700
-300
2014
cm + N.A.P.
700
-300
2019-2014
cm
200
-200
0
100
200 m

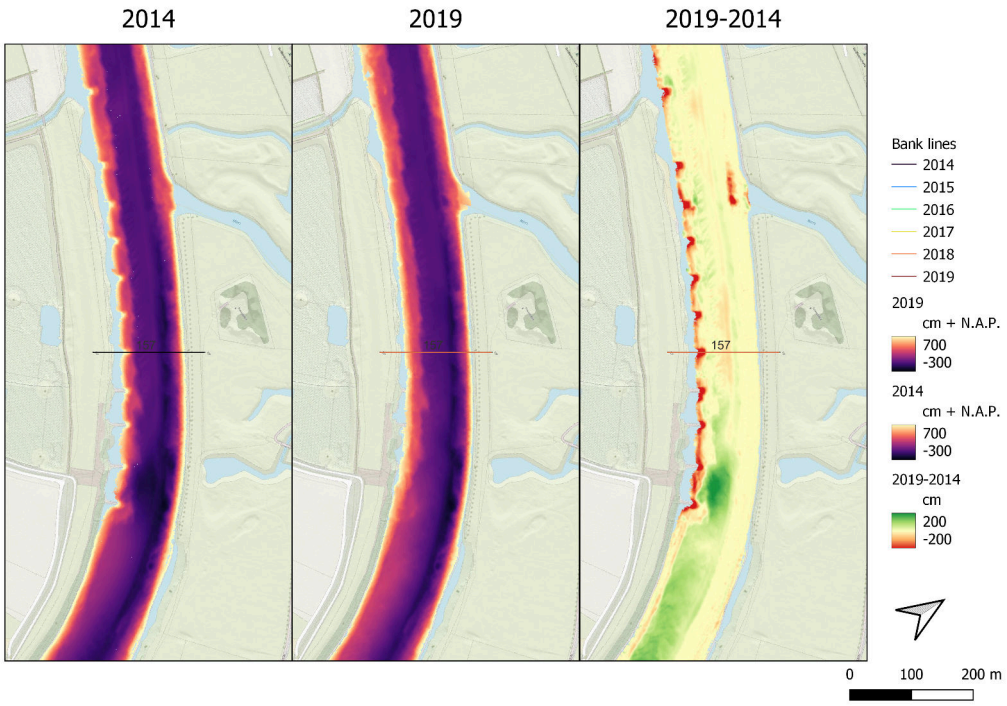
2014
2019
2019-2014
157
157
157
Bank lines
2014
2015
2016
2017
2018
2019
2019
cm + N.A.P.
700
-300
2014
cm + N.A.P.
700
-300
2019-2014
cm
200
-200
0
100
200 m

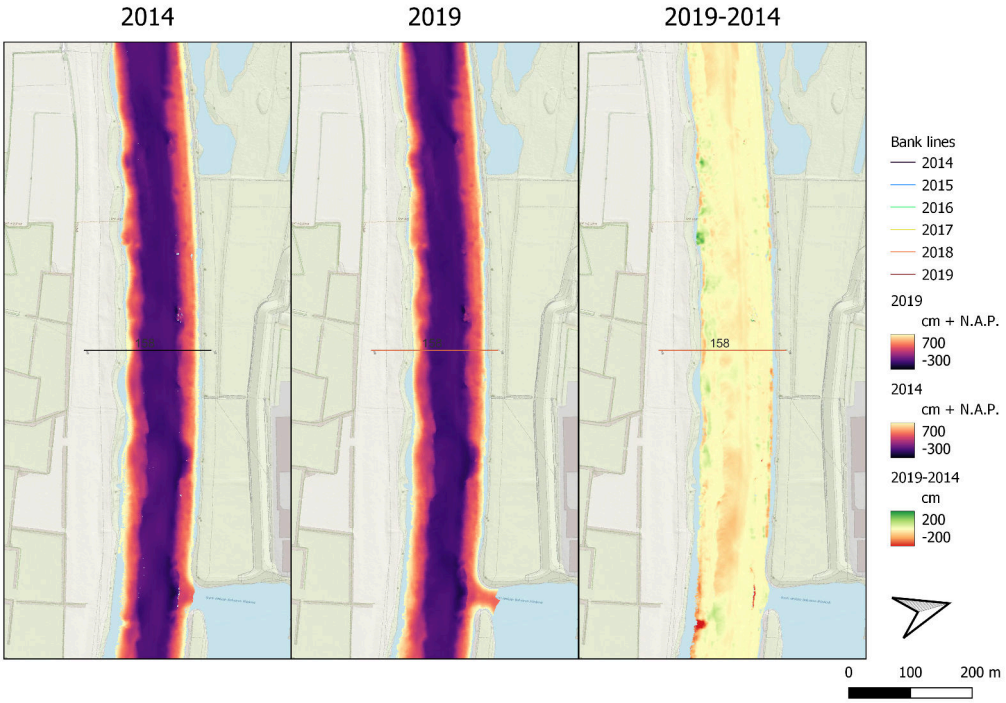
2014
2019
2019-2014
158
Bank lines
2014
2015
2016
2017
2018
2019
2019
cm + N.A.P.
700
-300
2014
cm + N.A.P.
700
-300
2019-2014
cm
200
-200
0
100
200 m

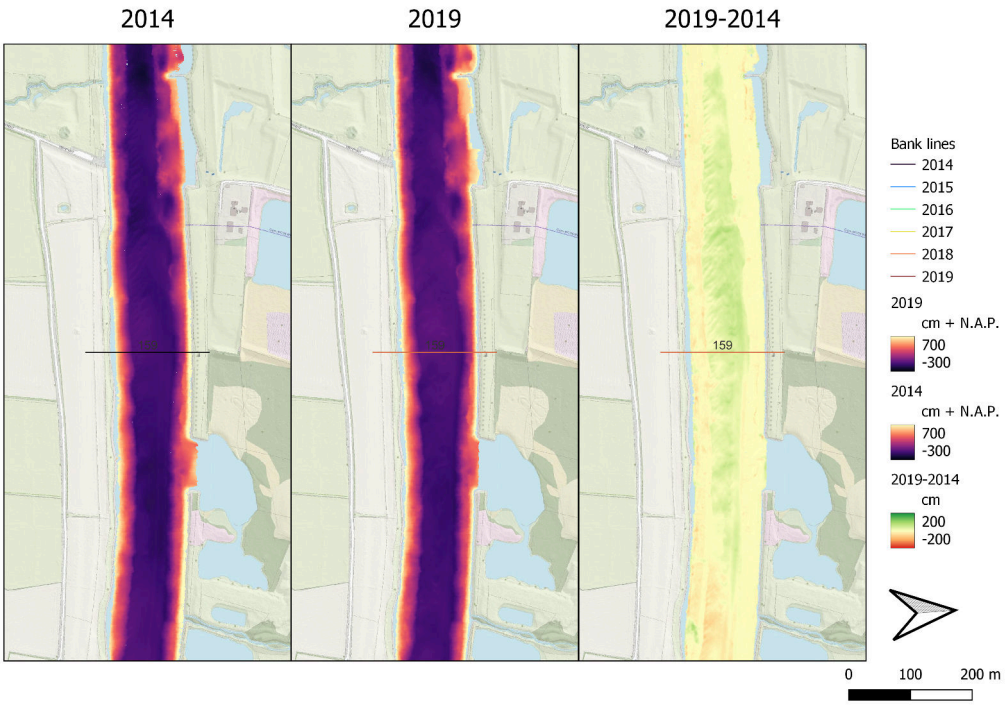
2014
2019
2019-2014
159
Bank lines
2014
2015
2016
2017
2018
2019
2019
cm + N.A.P.
700
-300
2014
cm + N.A.P.
700
-300
2019-2014
cm
200
-200
0
100
200 m

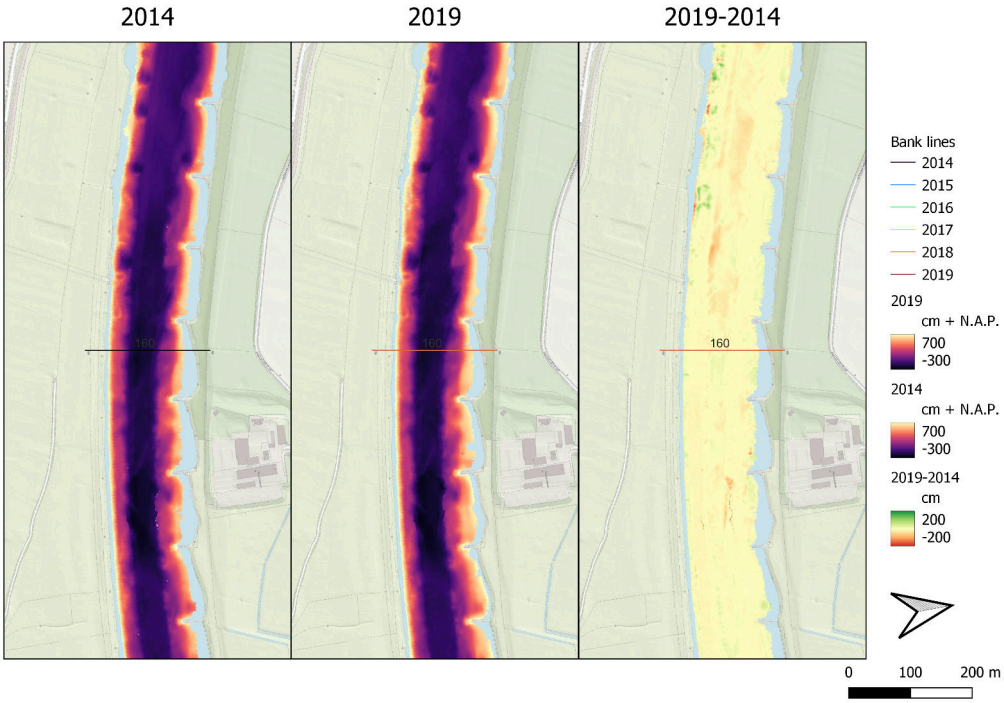
2014
2019
2019-2014
160
160
160
Bank lines
2014
2015
2016
2017
2018
2019
2019
cm + N.A.P.
700
-300
2014
cm + N.A.P.
700
-300
2019-2014
cm
200
-200
0
100
200 m

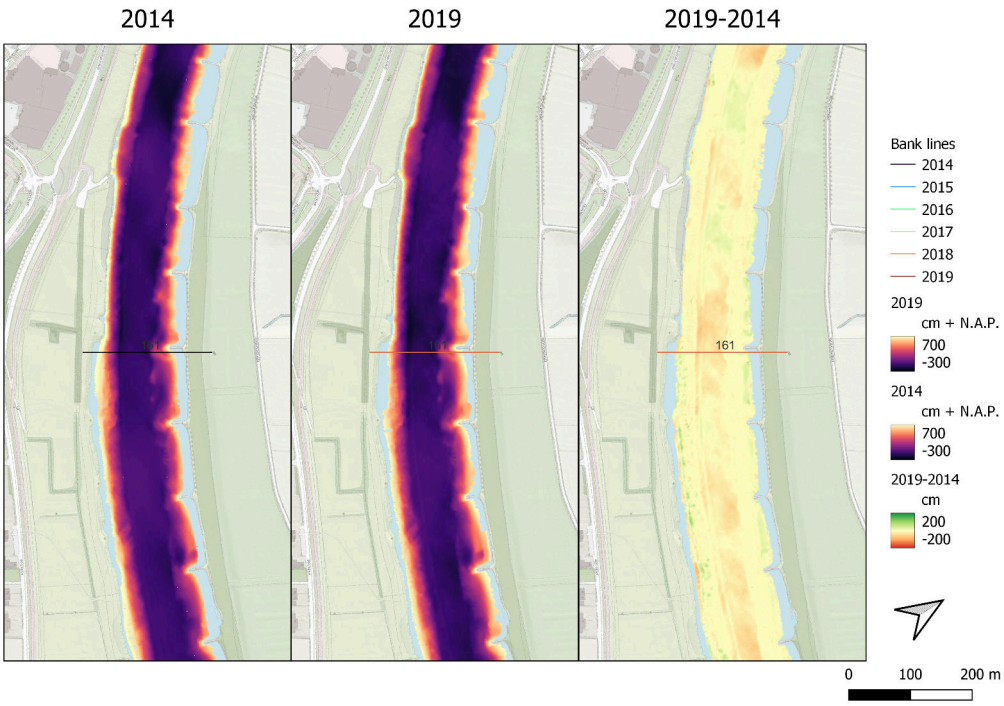
2014
2019
2019-2014
161
161
161
Bank lines
2014
2015
2016
2017
2018
2019
2019
cm + N.A.P.
700
-300
2014
cm + N.A.P.
700
-300
2019-2014
cm
200
-200
0
100
200 m

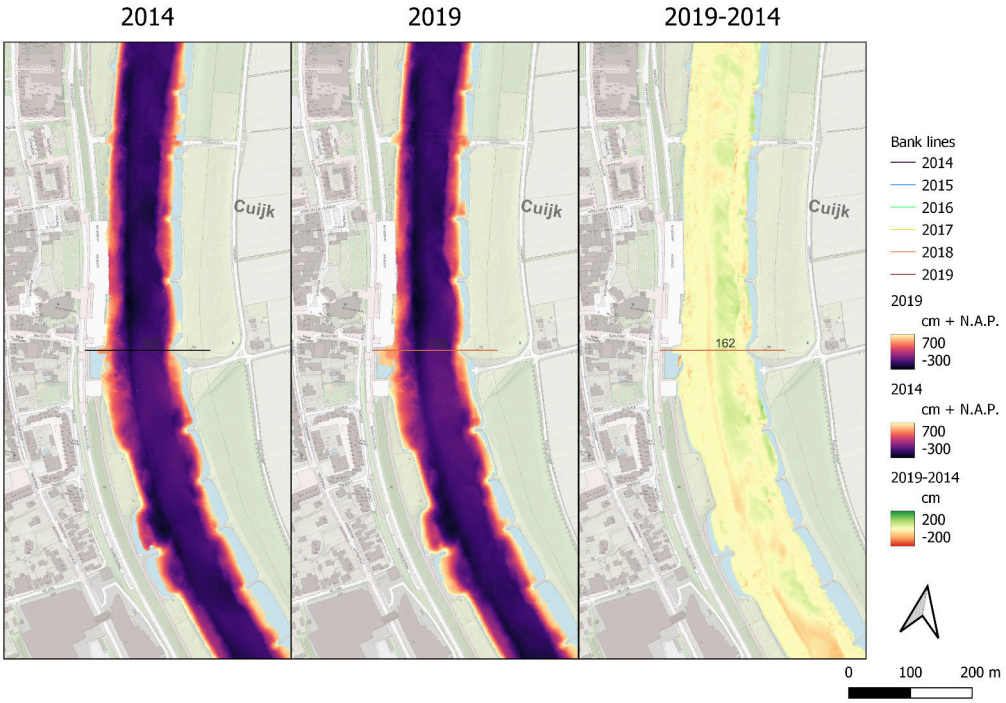
2014
2019
2019-2014
Cuijk
Cuijk
Cuijk
162
162
162
Bank lines
2014
2015
2016
2017
2018
2019
2019
cm + N.A.P.
700
-300
2014
cm + N.A.P.
700
-300
2019-2014
cm
200
-200
0
100
200 m

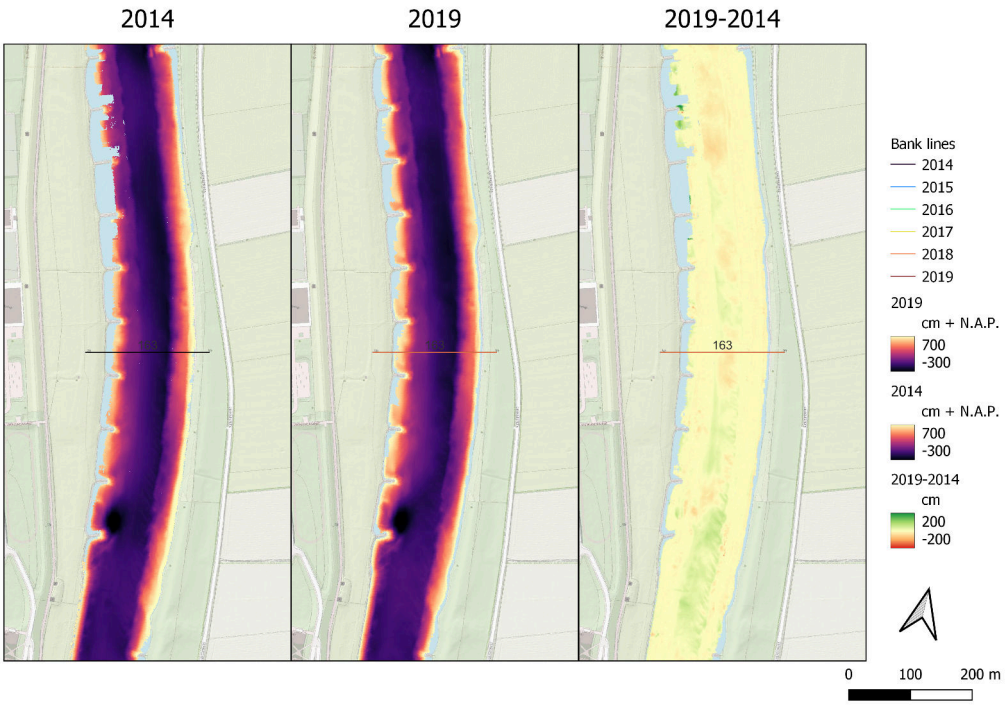
2014
2019
2019-2014
163
163
163
Bank lines
2014
2015
2016
2017
2018
2019
2019
cm + N.A.P.
700
-300
2014
cm + N.A.P.
700
-300
2019-2014
cm
200
-200
0
100
200 m

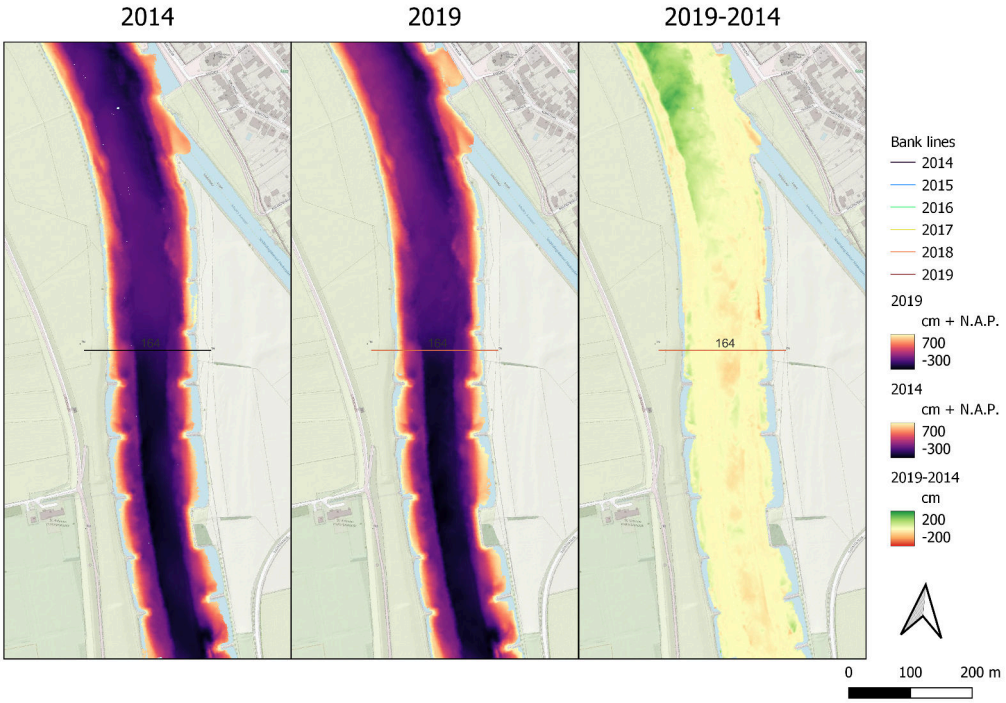
2014
2019
2019-2014
164
Bank lines
2014
2015
2016
2017
2018
2019
2019
cm + N.A.P.
700
-300
2014
cm + N.A.P.
700
-300
2019-2014
cm
200
-200
0
100
200 m

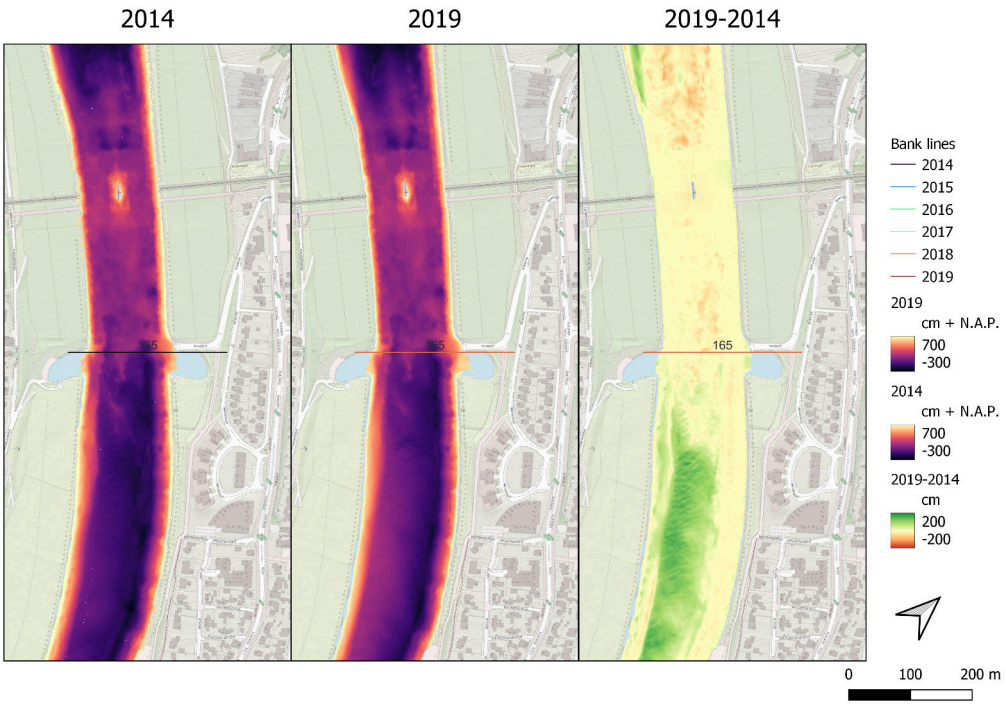
2014
2019
2019-2014
165
Bank lines
2014
2015
2016
2017
2018
2019
2019
cm + N.A.P.
700
-300
2014
cm + N.A.P.
700
-300
2019-2014
cm
200
-200
0
100
200 m

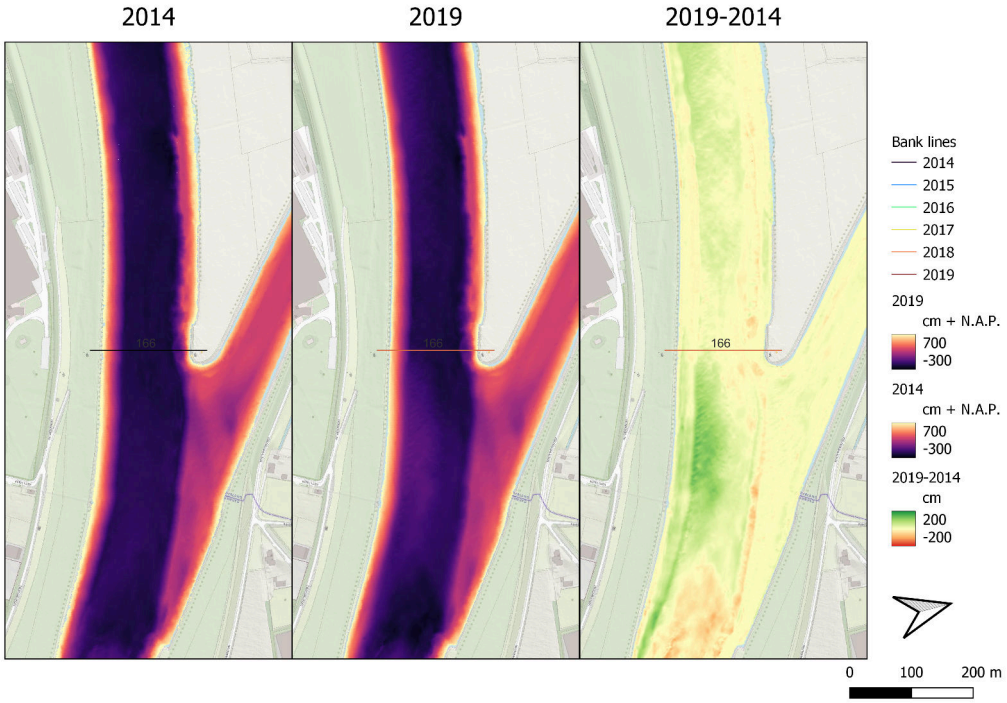
2014
2019
2019-2014
166
Bank lines
2014
2015
2016
2017
2018
2019
2019
cm + N.A.P.
700
-300
2014
cm + N.A.P.
700
-300
2019-2014
cm
200
-200
0
100
200 m

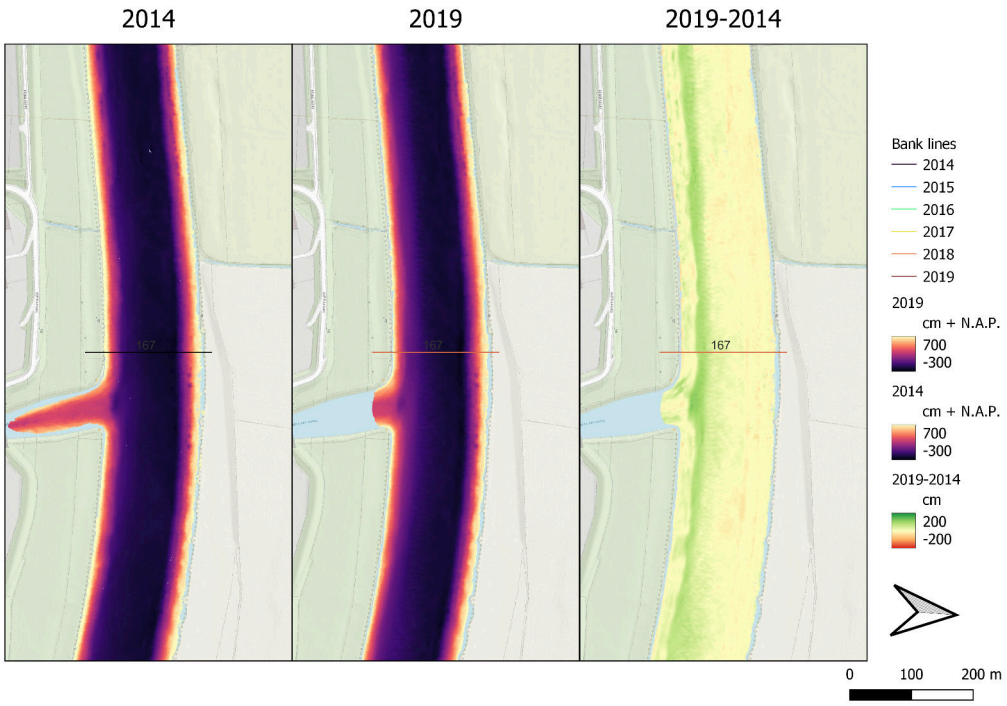
2014
2019
2019-2014
167
Bank lines
2014
2015
2016
2017
2018
2019
2019
cm + N.A.P.
700
-300
2014
cm + N.A.P.
700
-300
2019-2014
cm
200
-200
0
100
200 m

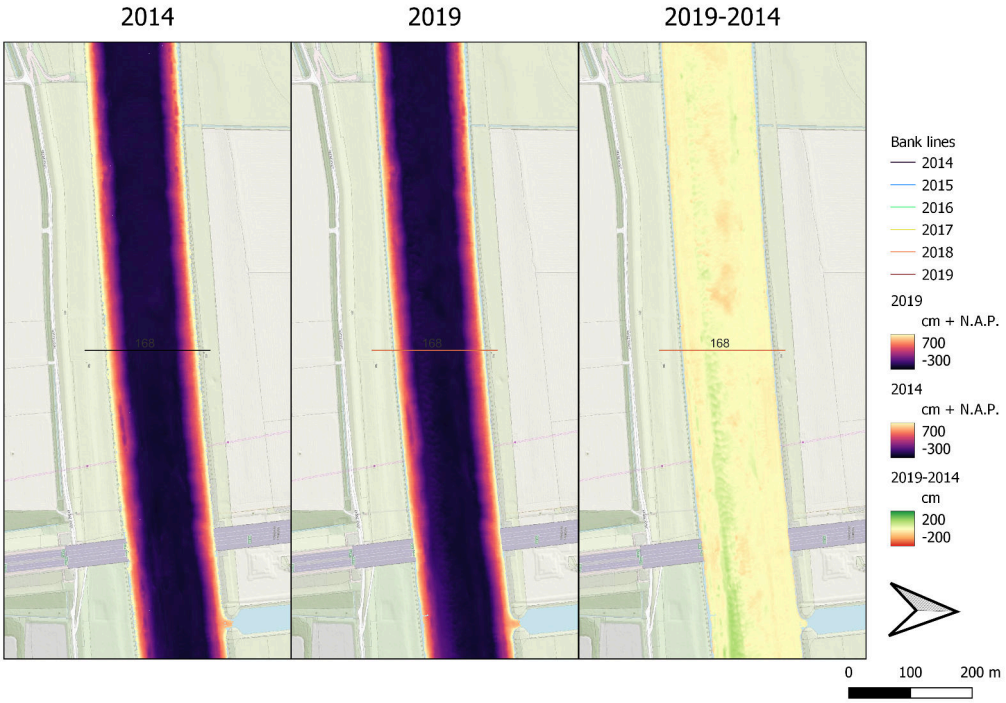
2014
2019
2019-2014
168
Bank lines
2014
2015
2016
2017
2018
2019
2019
cm + N.A.P.
700
-300
2014
cm + N.A.P.
700
-300
2019-2014
cm
200
-200
0
100
200 m

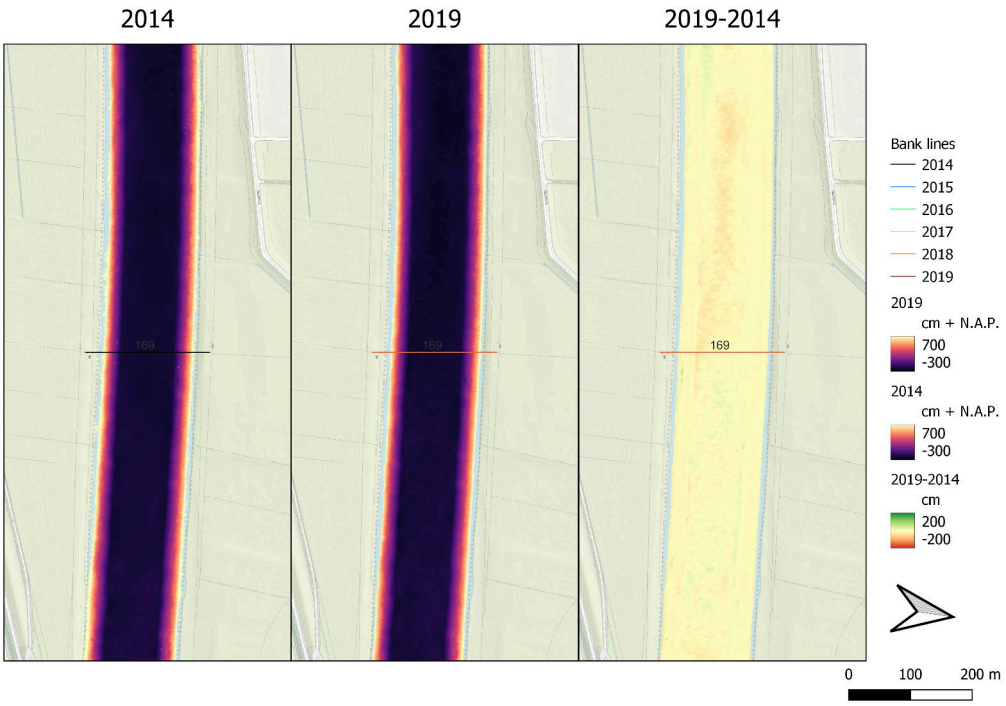
2014
2019
2019-2014
169
Bank lines
2014
2015
2016
2017
2018
2019
2019
cm + N.A.P.
700
-300
2014
cm + N.A.P.
700
-300
2019-2014
cm
200
-200
0
100
200 m

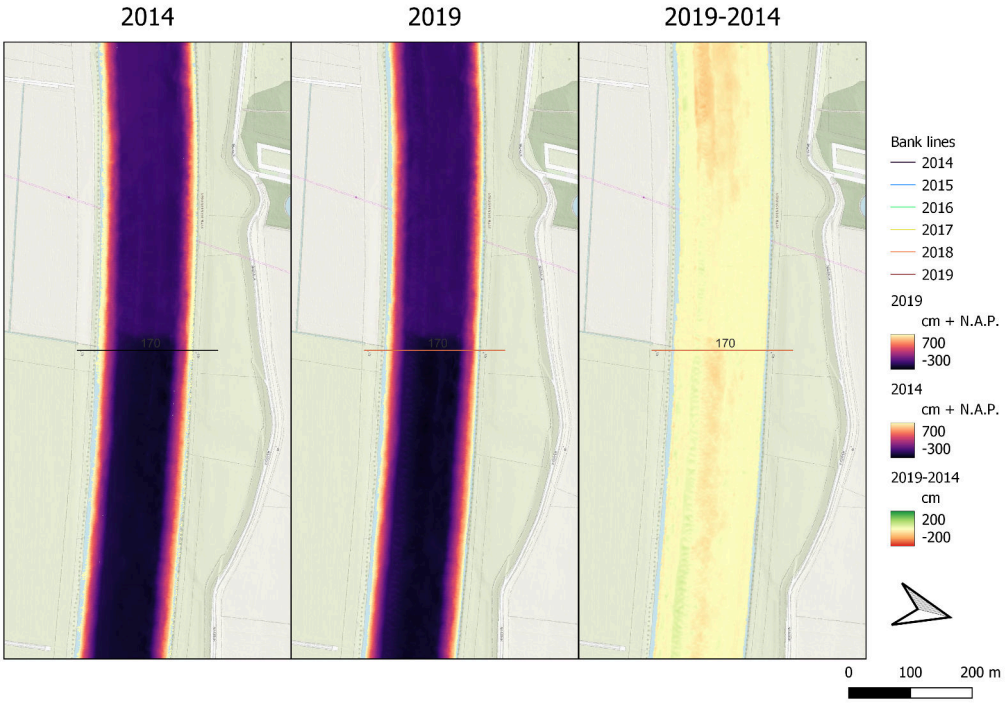
2014
2019
2019-2014
170
Bank lines
2014
2015
2016
2017
2018
2019
2019
cm + N.A.P.
700
-300
2014
cm + N.A.P.
700
-300
2019-2014
cm
200
-200
0
100
200 m

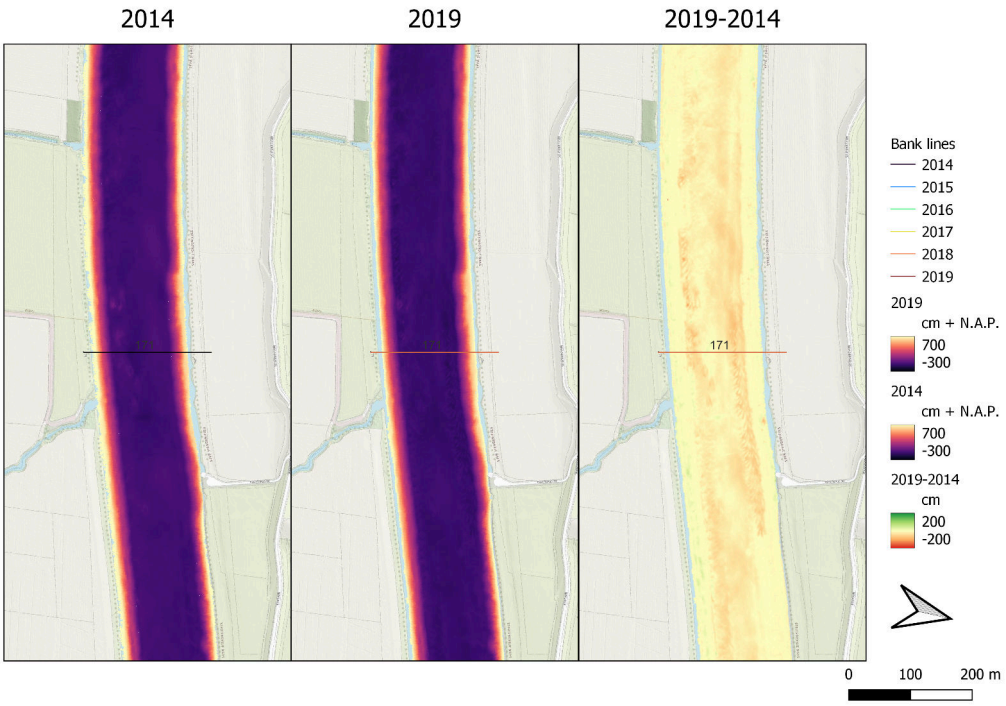
2014
2019
2019-2014
171
Bank lines
2014
2015
2016
2017
2018
2019
2019
cm + N.A.P.
700
-300
2014
cm + N.A.P.
700
-300
2019-2014
cm
200
-200
0
100
200 m

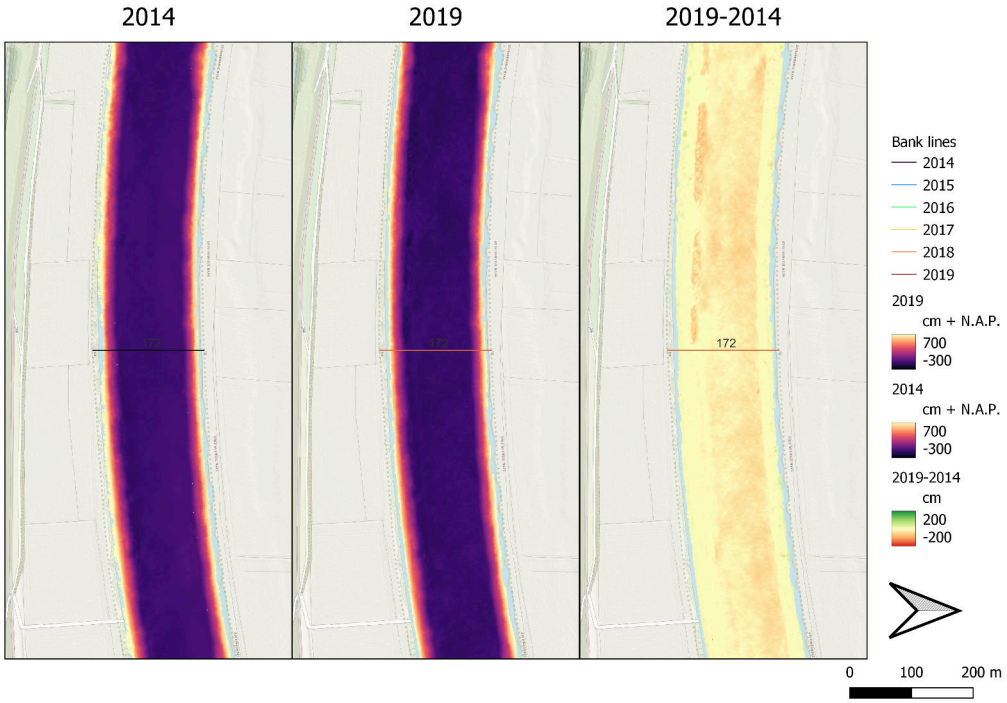
2014
2019
2019-2014
172
Bank lines
2014
2015
2016
2017
2018
2019
2019
cm + N.A.P.
700
-300
2014
cm + N.A.P.
700
-300
2019-2014
cm
200
-200
0
100
200 m

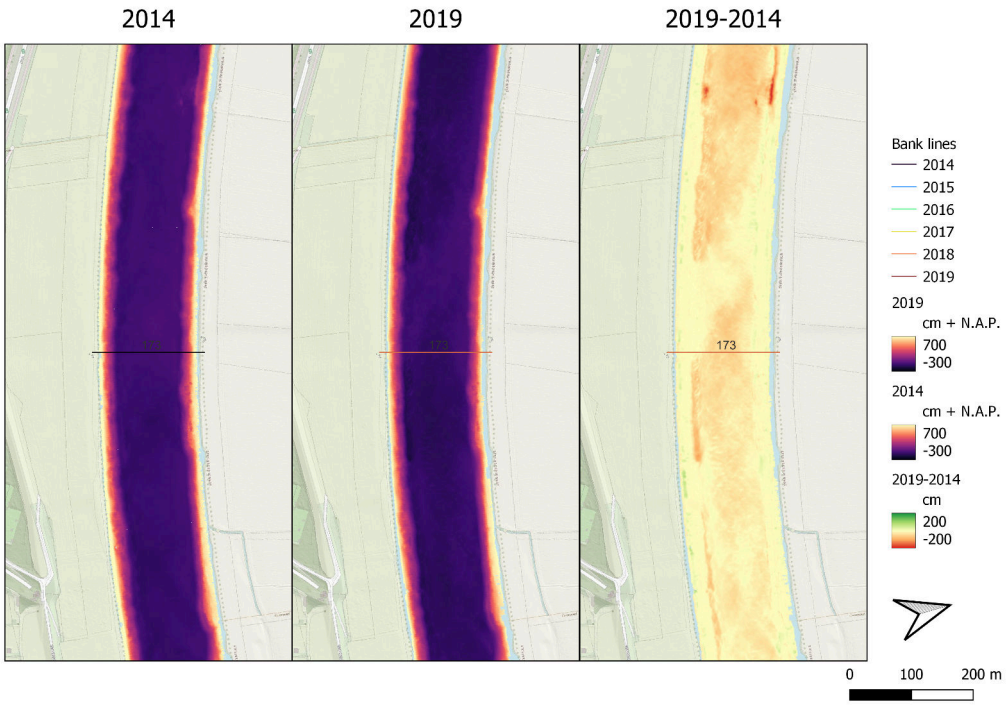
2014
2019
2019-2014
173
Bank lines
2014
2015
2016
2017
2018
2019
2019
cm + N.A.P.
700
-300
2014
cm + N.A.P.
700
-300
2019-2014
cm
200
-200
0
100
200 m

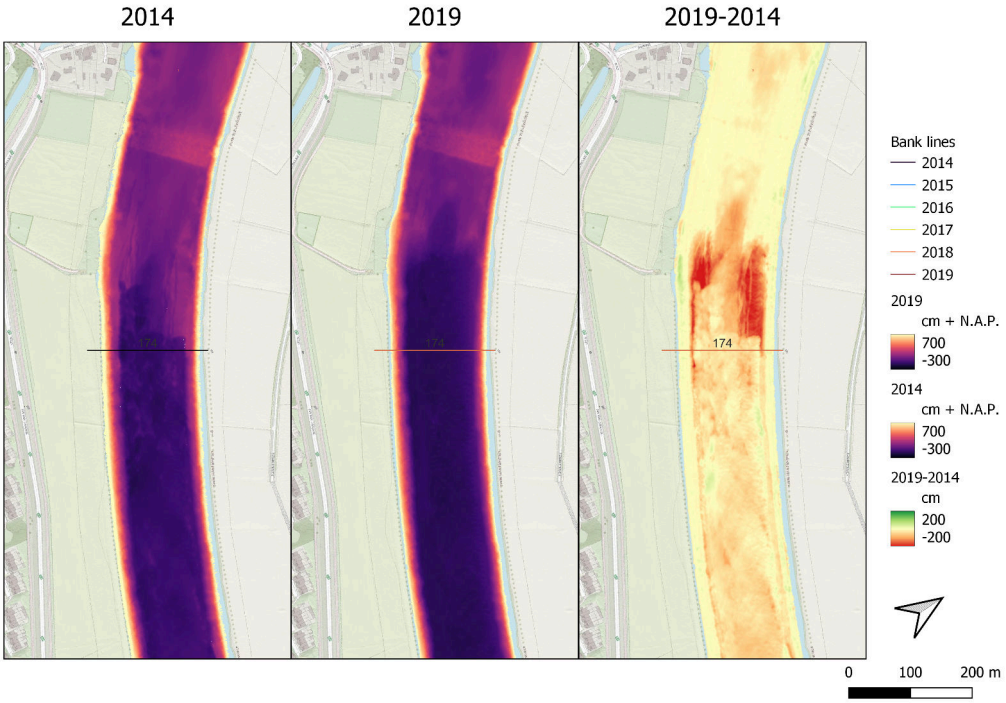
2014
2019
2019-2014
174
Bank lines
2014
2015
2016
2017
2018
2019
2019
cm + N.A.P.
700
-300
2014
cm + N.A.P.
700
-300
2019-2014
cm
200
-200
0
100
200 m

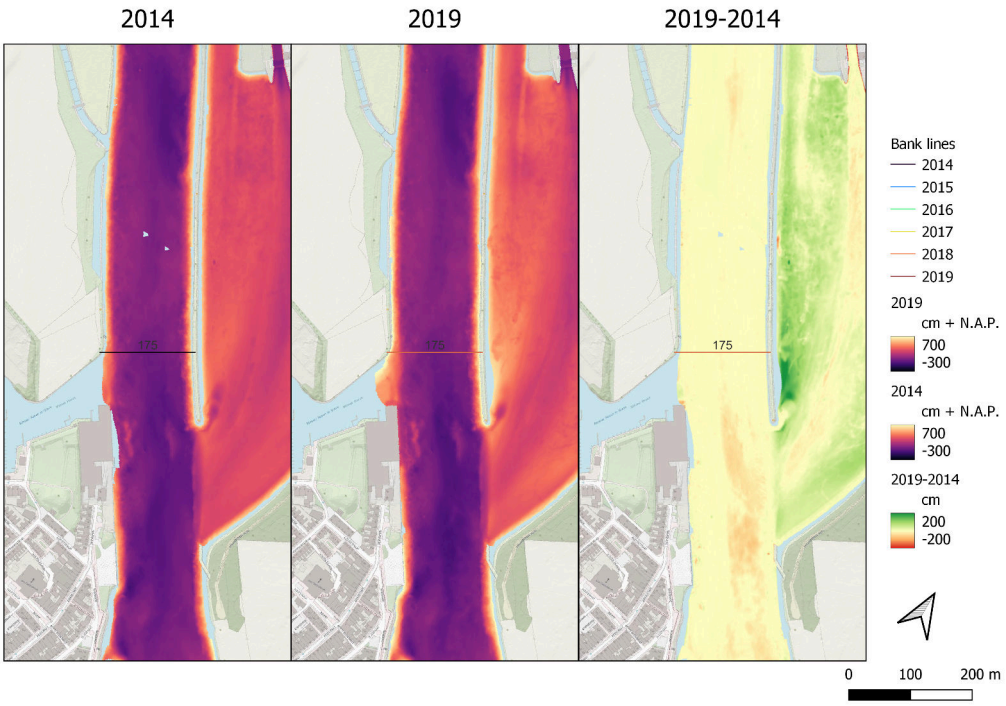
2014
2019
2019-2014
175
Bank lines
2014
2015
2016
2017
2018
2019
2019
cm + N.A.P.
700
-300
2014
cm + N.A.P.
700
-300
2019-2014
cm
200
-200
0
100
200 m

C Comparison to ADCP measurements

C.1 16-7-2021

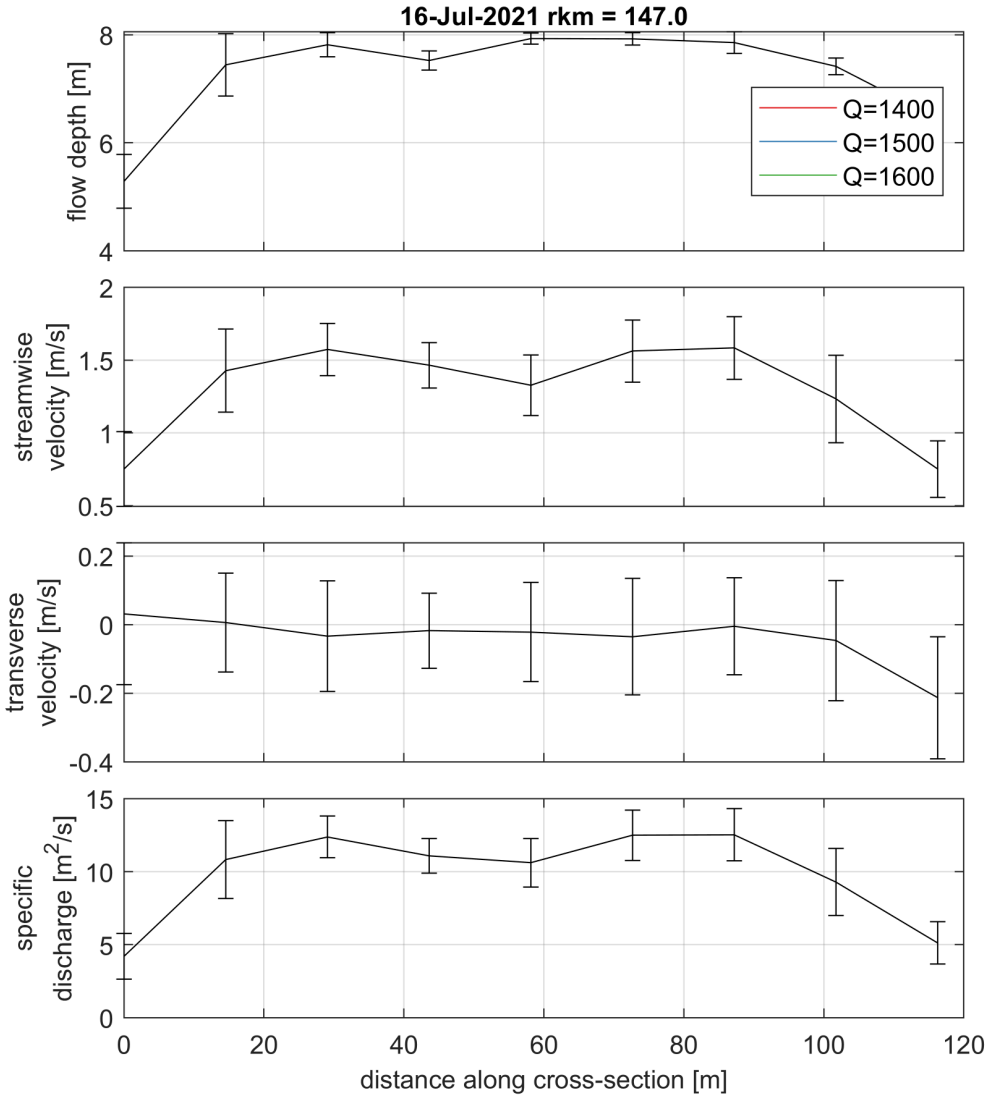

Figure C.1.1 Depth averaged velocity comparison for 16-7-2021 at river kilometre 147.0.

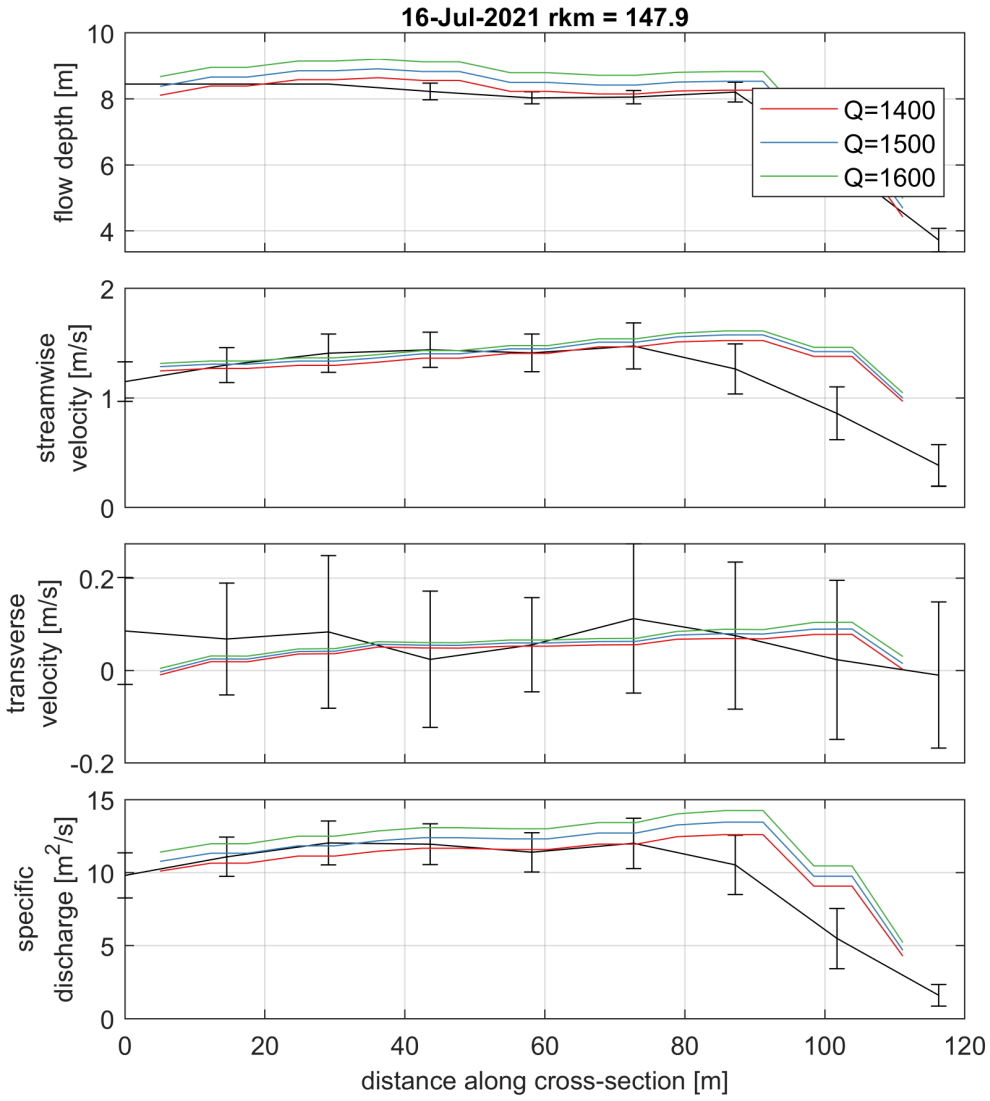

Figure C.1.2 Depth averaged velocity comparison for 16-7-2021 at river kilometre 147.9.

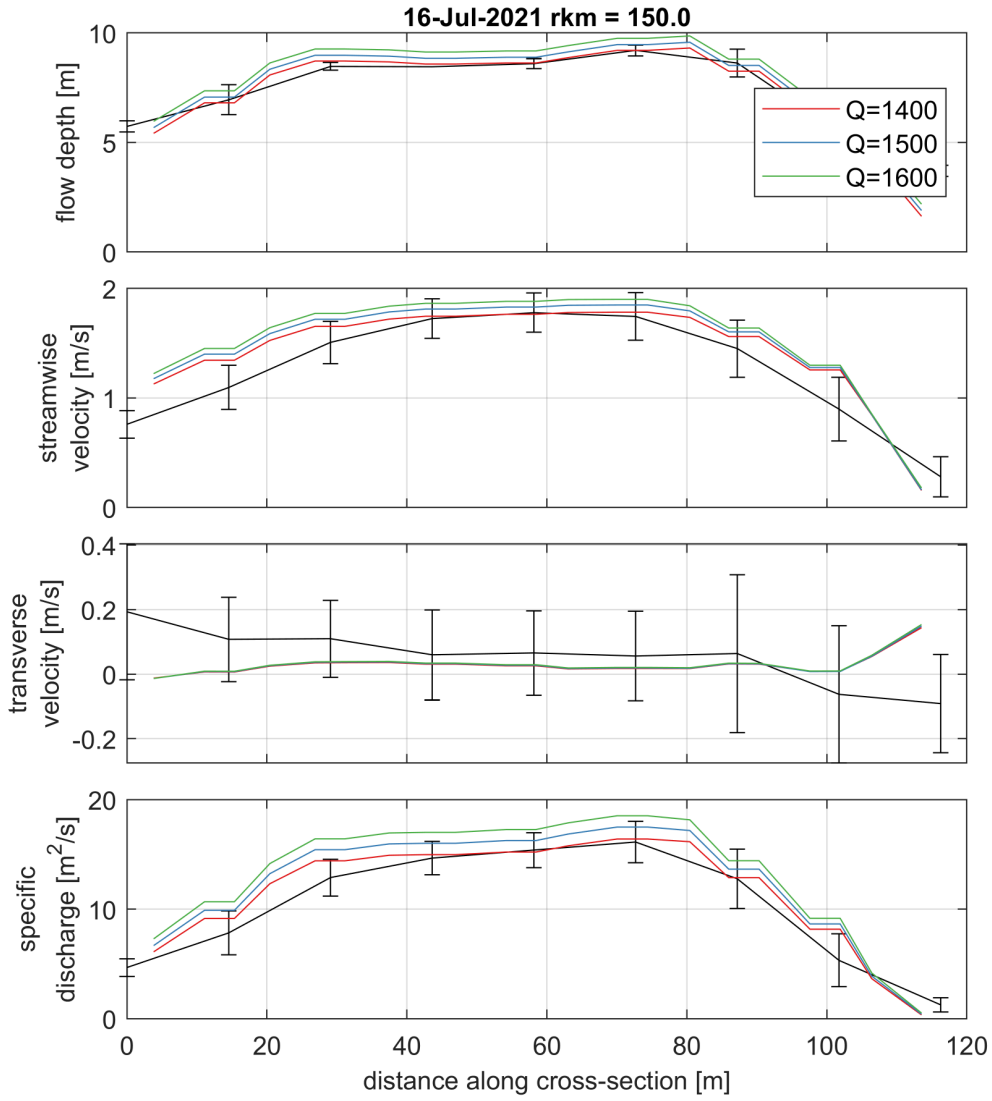

Figure C.1.3 Depth averaged velocity comparison for 16-7-2021 at river kilometre 150.0.

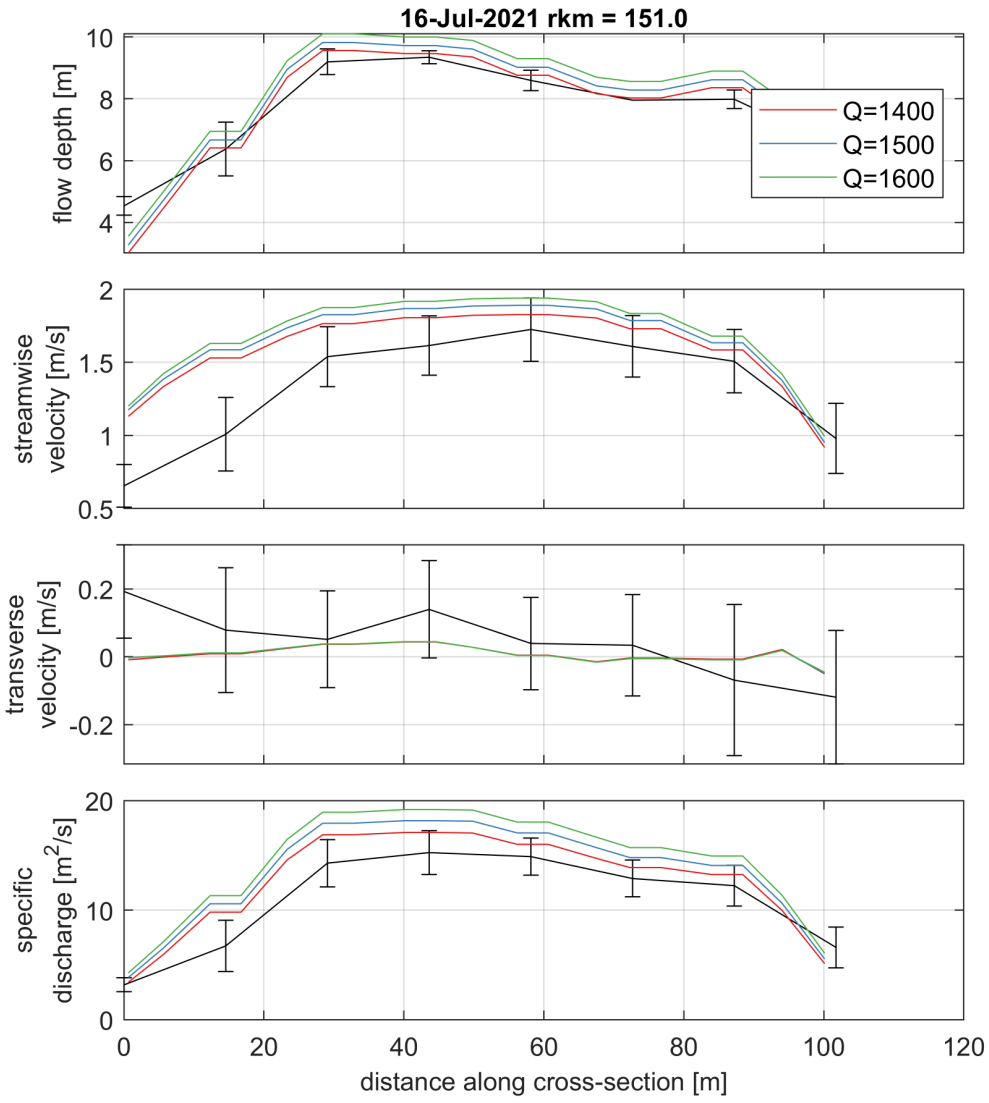

Figure C.1.4 Depth averaged velocity comparison for 16-7-2021 at river kilometre 151.0.

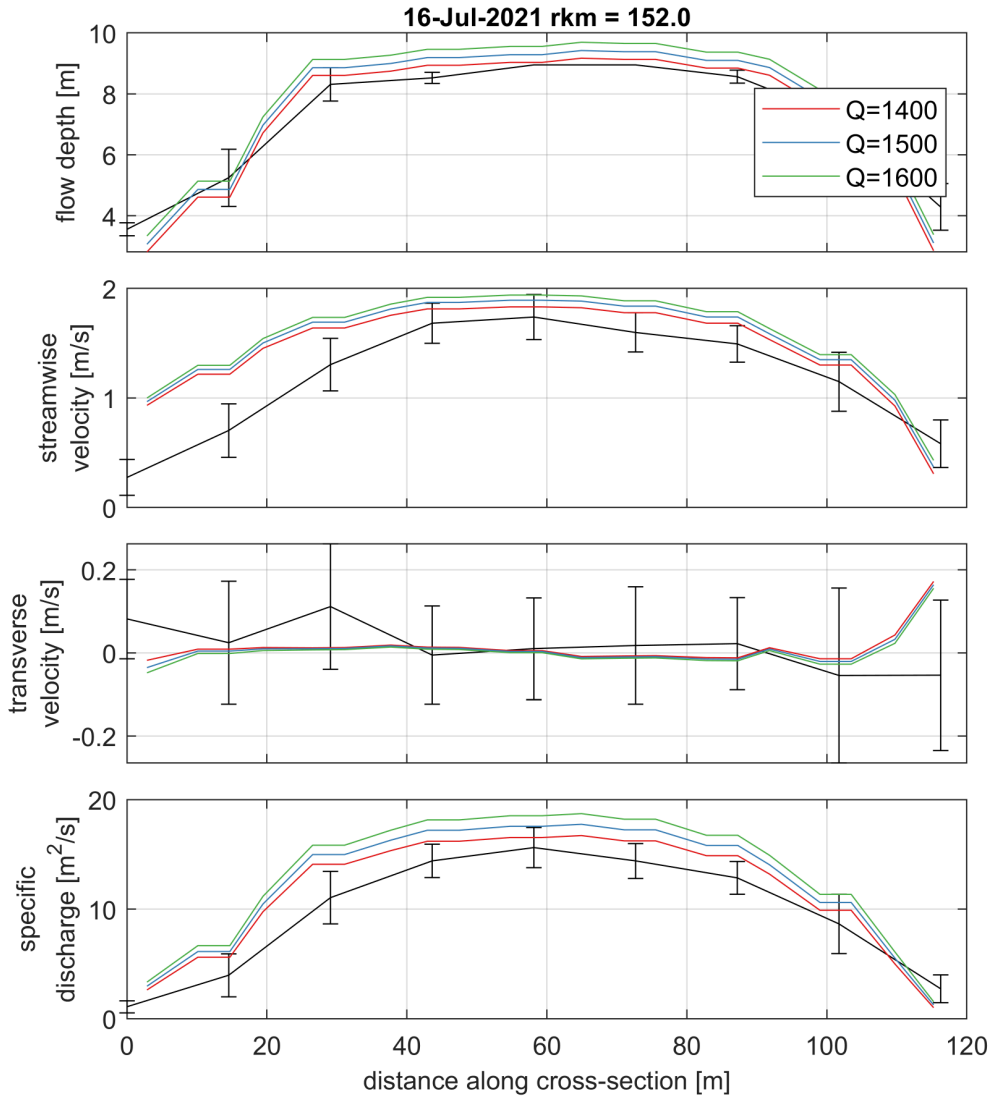

Figure C.1.5 Depth averaged velocity comparison for 16-7-2021 at river kilometre 152.0.

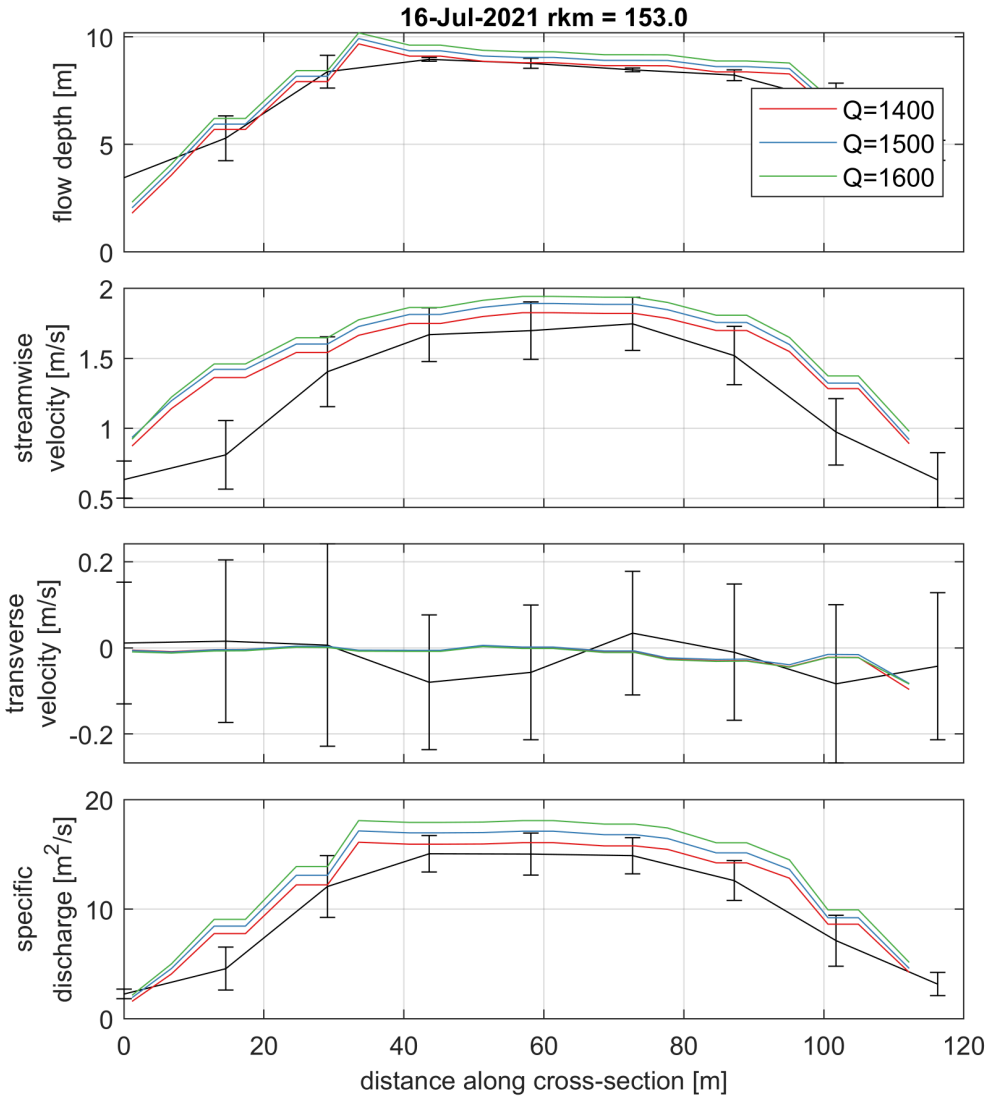

Figure C.1.6 Depth averaged velocity comparison for 16-7-2021 at river kilometre 153.0.

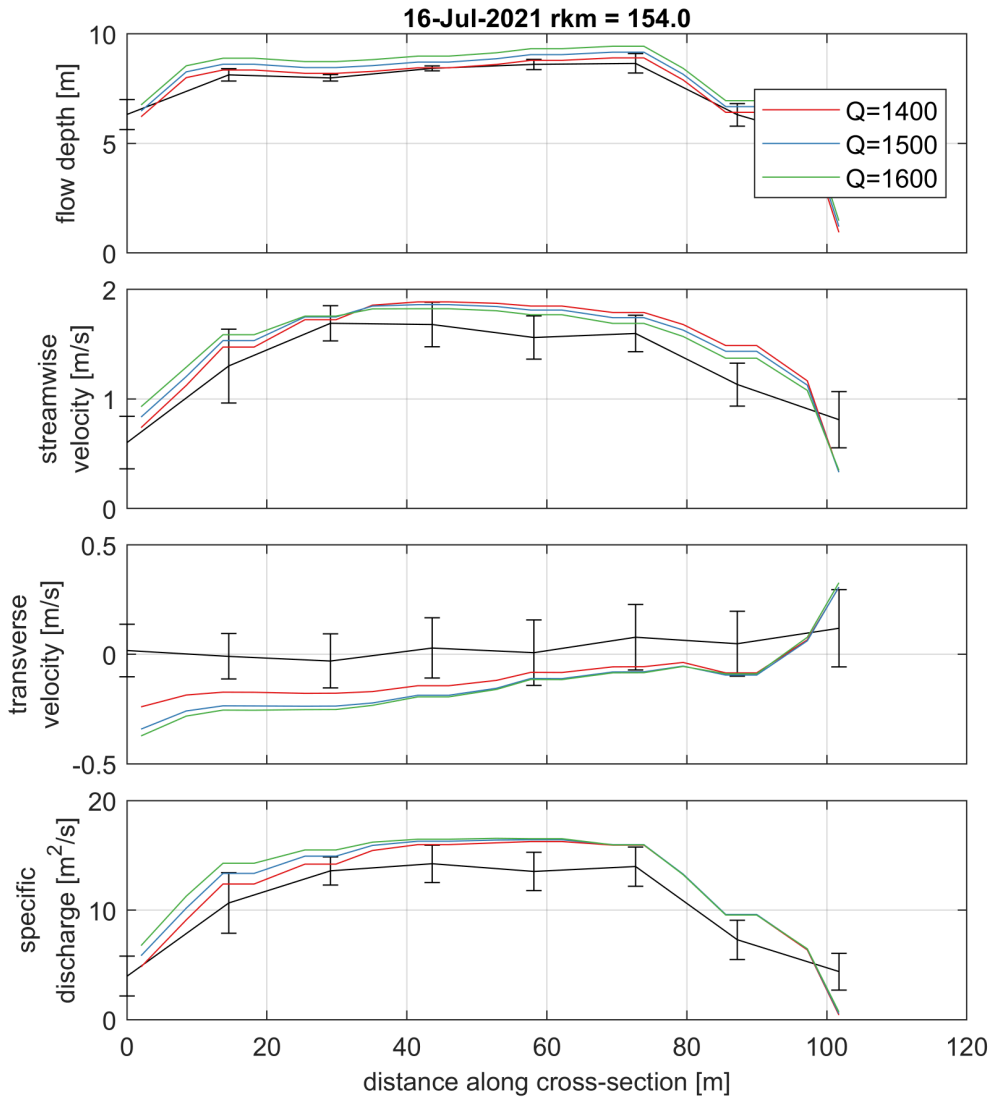

Figure C.1.7 Depth averaged velocity comparison for 16-7-2021 at river kilometre 154.0.

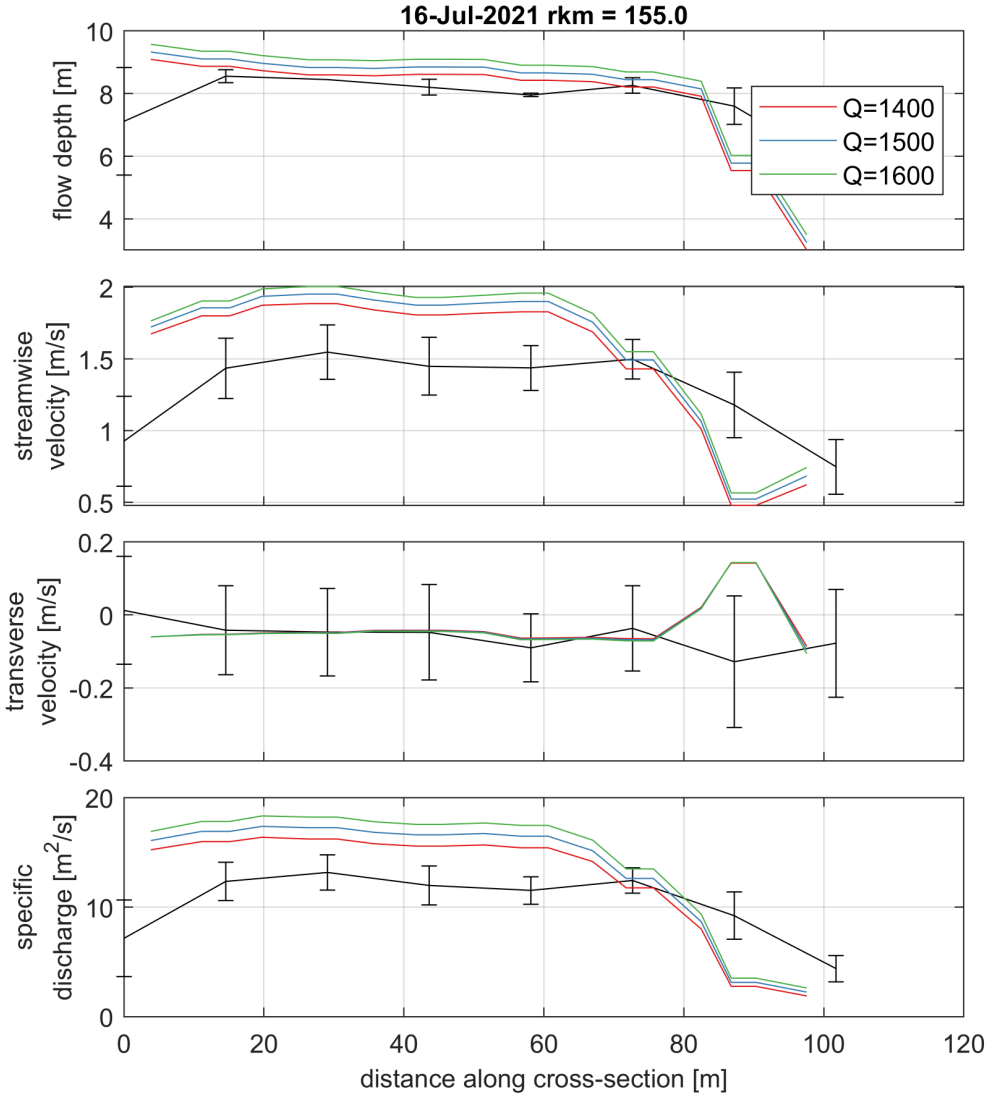

Figure C.1.8 Depth averaged velocity comparison for 16-7-2021 at river kilometre 155.0.

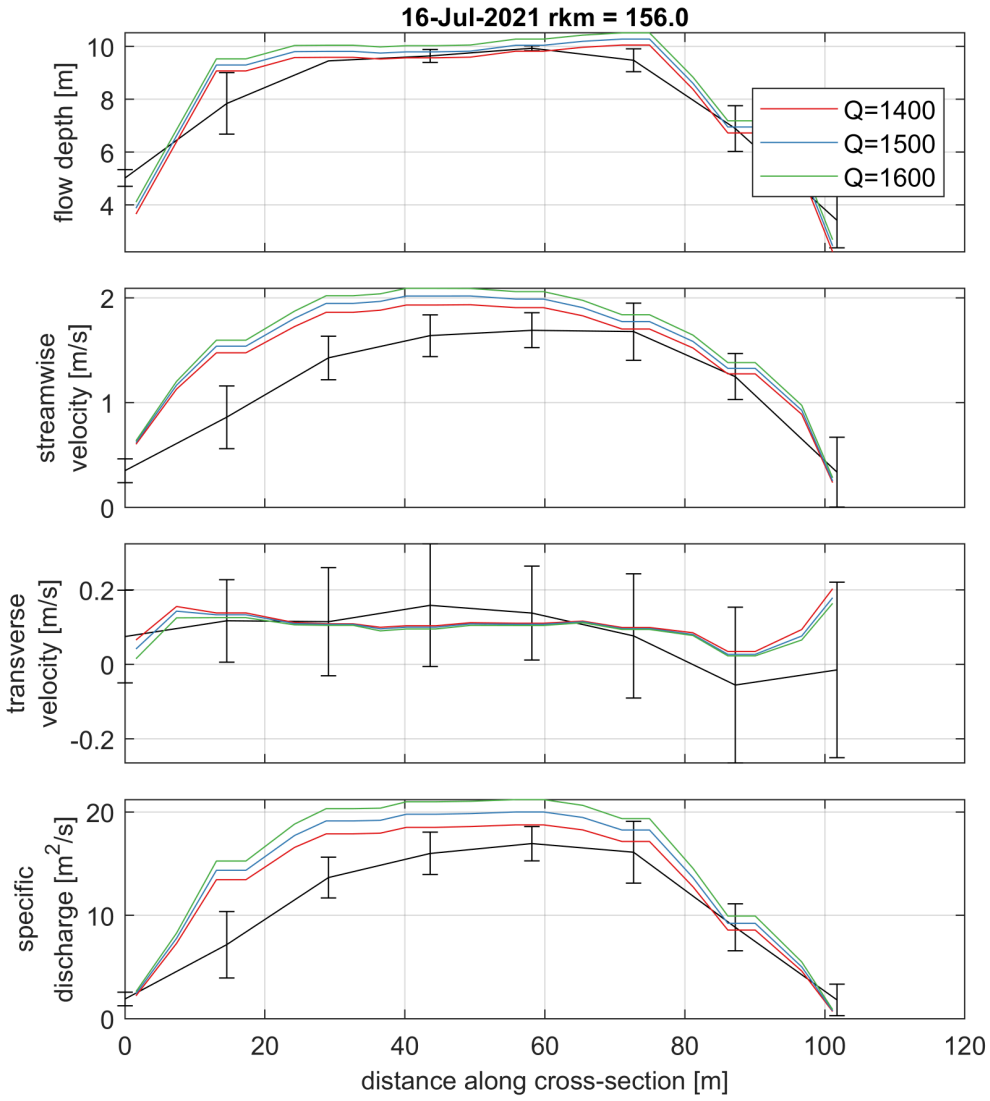

Figure C.1.9 Depth averaged velocity comparison for 16-7-2021 at river kilometre 156.0.

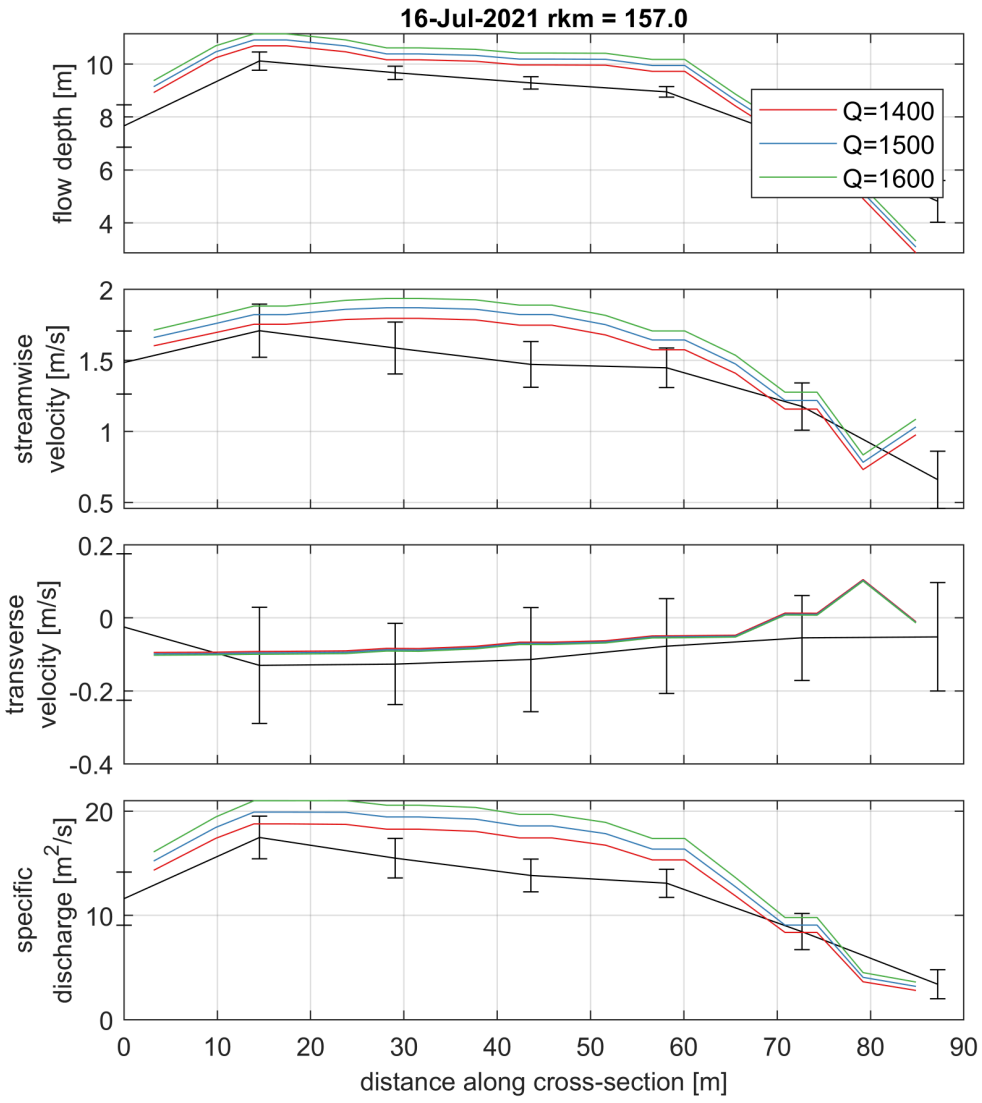

Figure C.1.10 Depth averaged velocity comparison for 16-7-2021 at river kilometre 157.0.

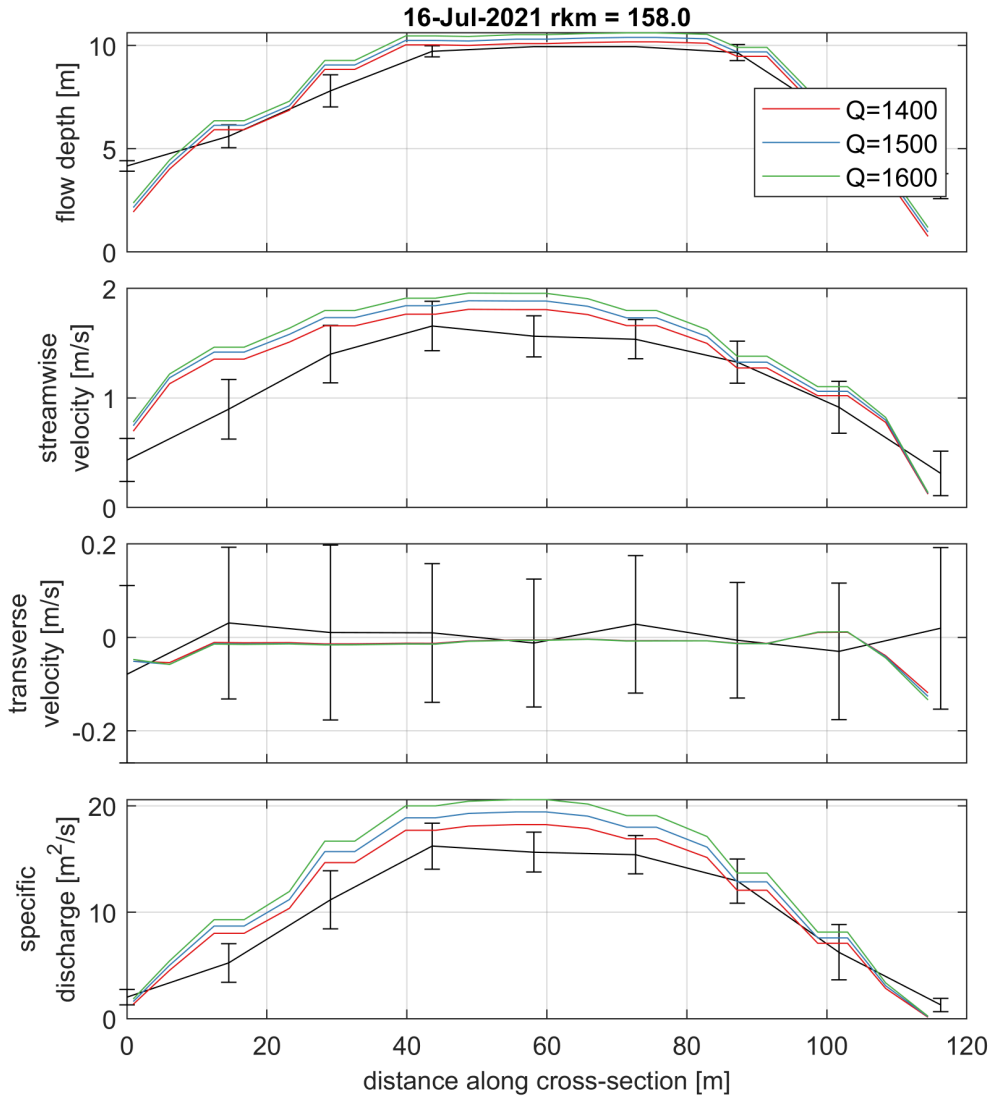

Figure C.1.11 Depth averaged velocity comparison for 16-7-2021 at river kilometre 158.0.

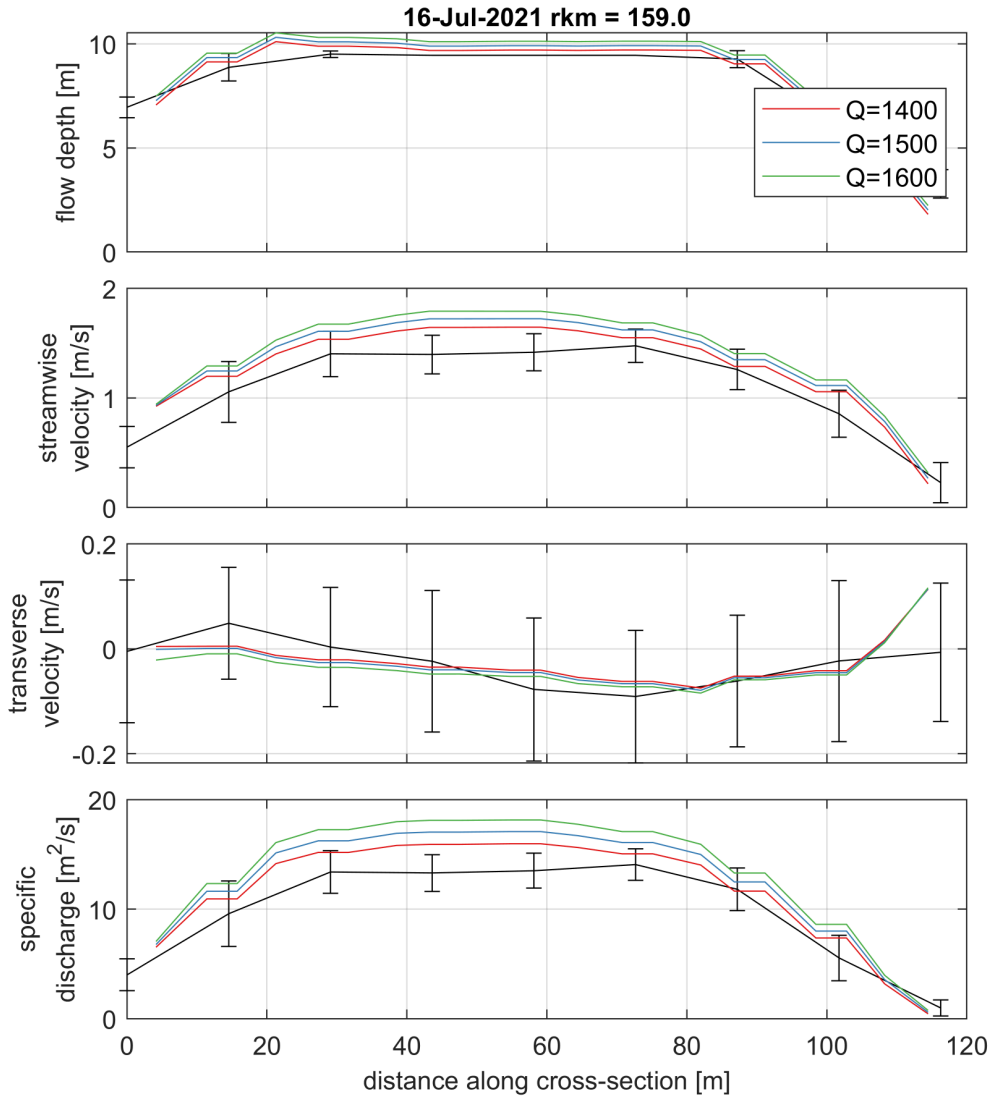

Figure C.1.12 Depth averaged velocity comparison for 16-7-2021 at river kilometre 159.0.

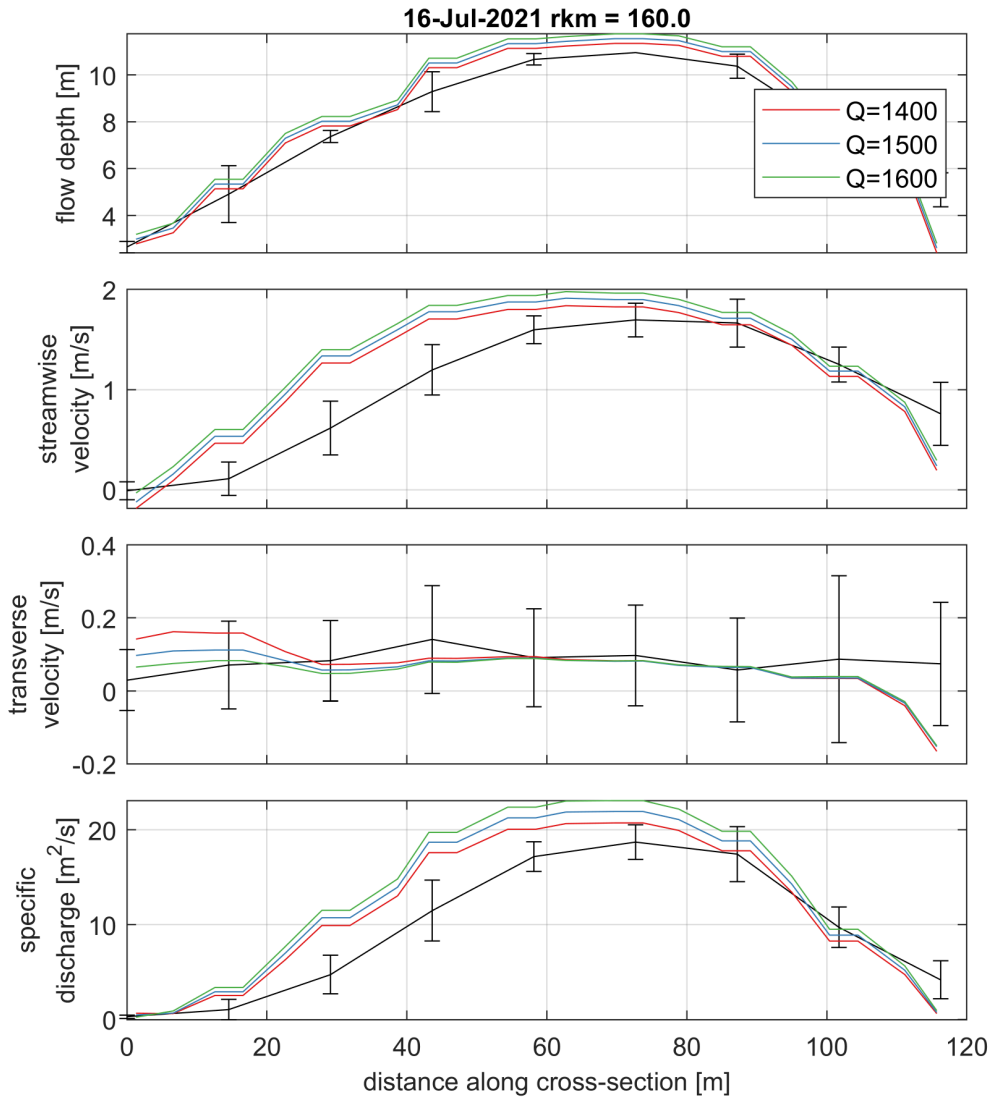

Figure C.1.13 Depth averaged velocity comparison for 16-7-2021 at river kilometre 160.0.

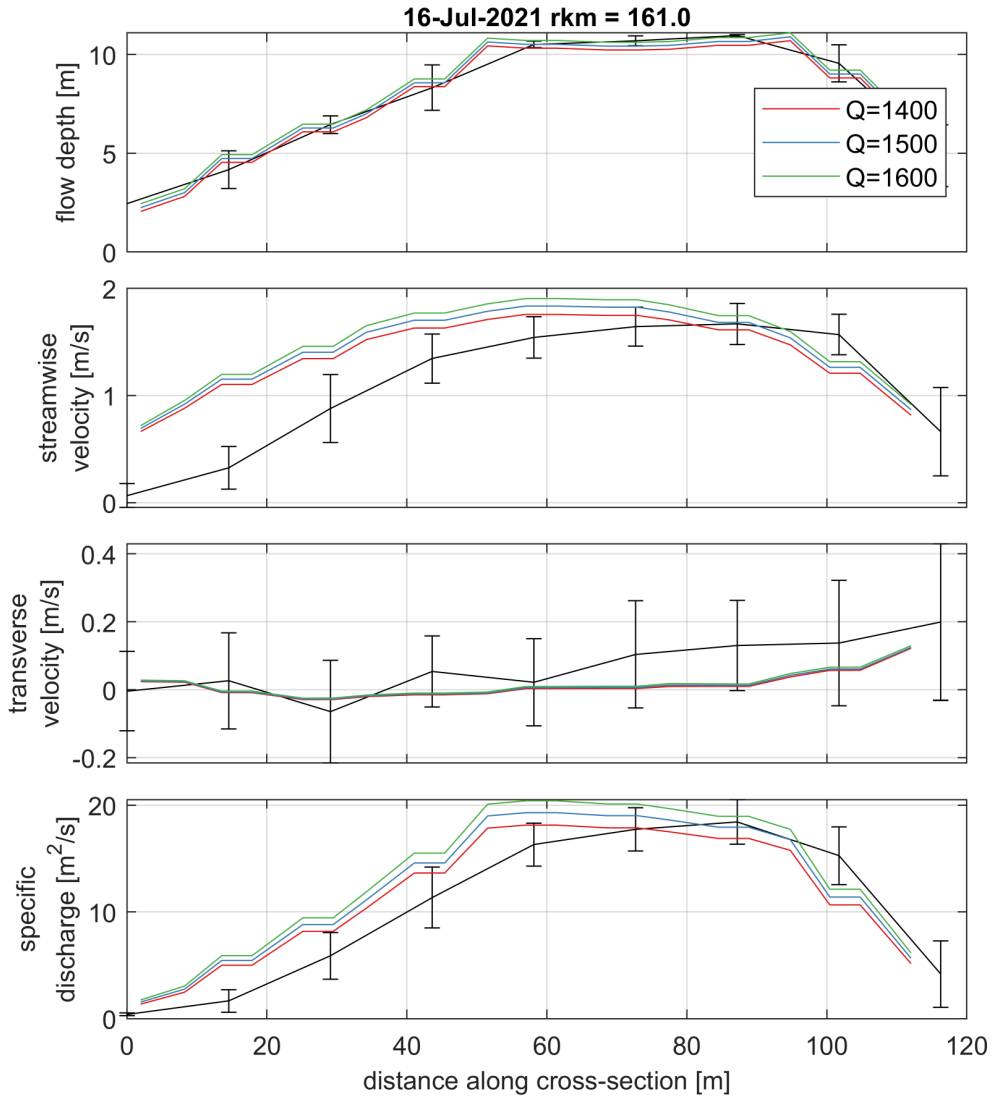

Figure C.1.14 Depth averaged velocity comparison for 16-7-2021 at river kilometre 161.0.

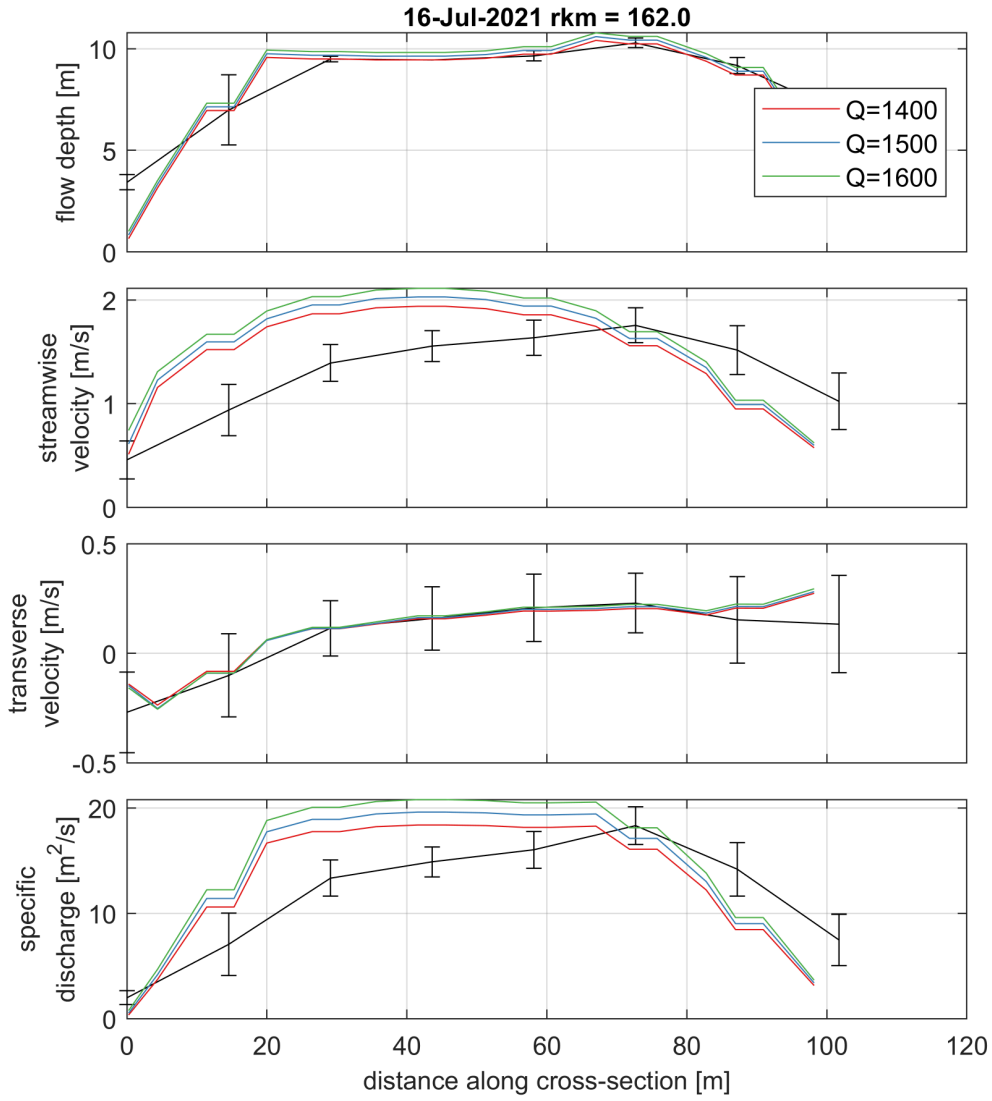

Figure C.1.15 Depth averaged velocity comparison for 16-7-2021 at river kilometre 162.0.

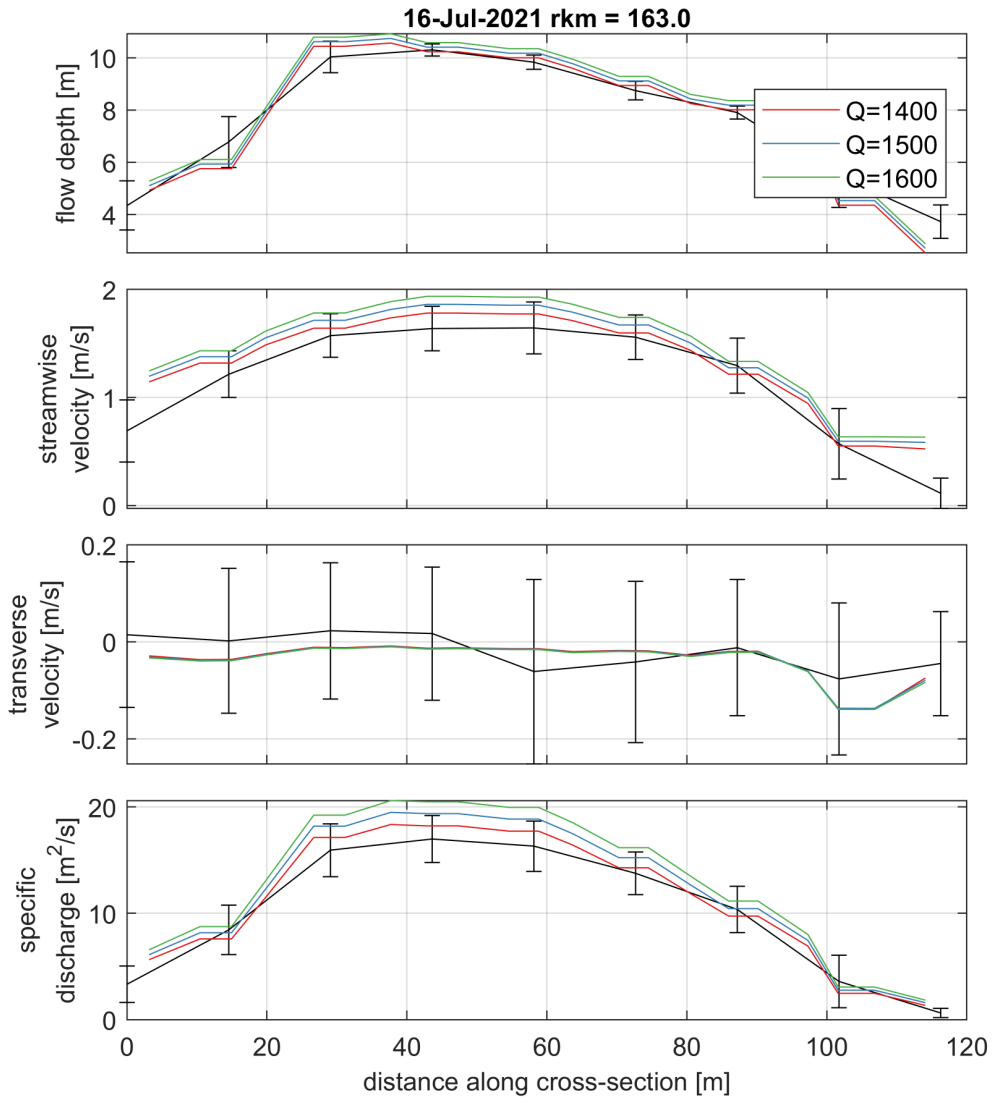

Figure C.1.16 Depth averaged velocity comparison for 16-7-2021 at river kilometre 163.0.

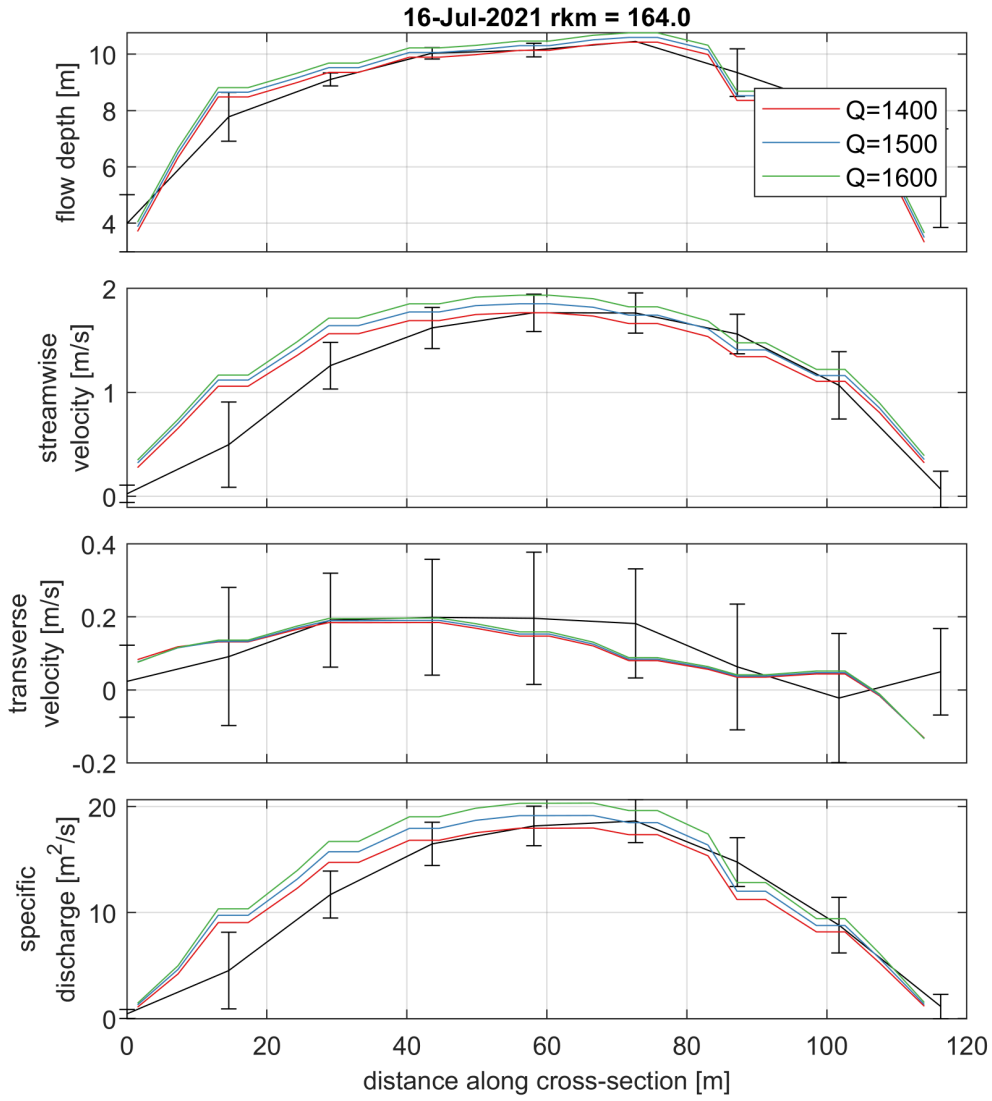

Figure C.1.17 Depth averaged velocity comparison for 16-7-2021 at river kilometre 164.0.

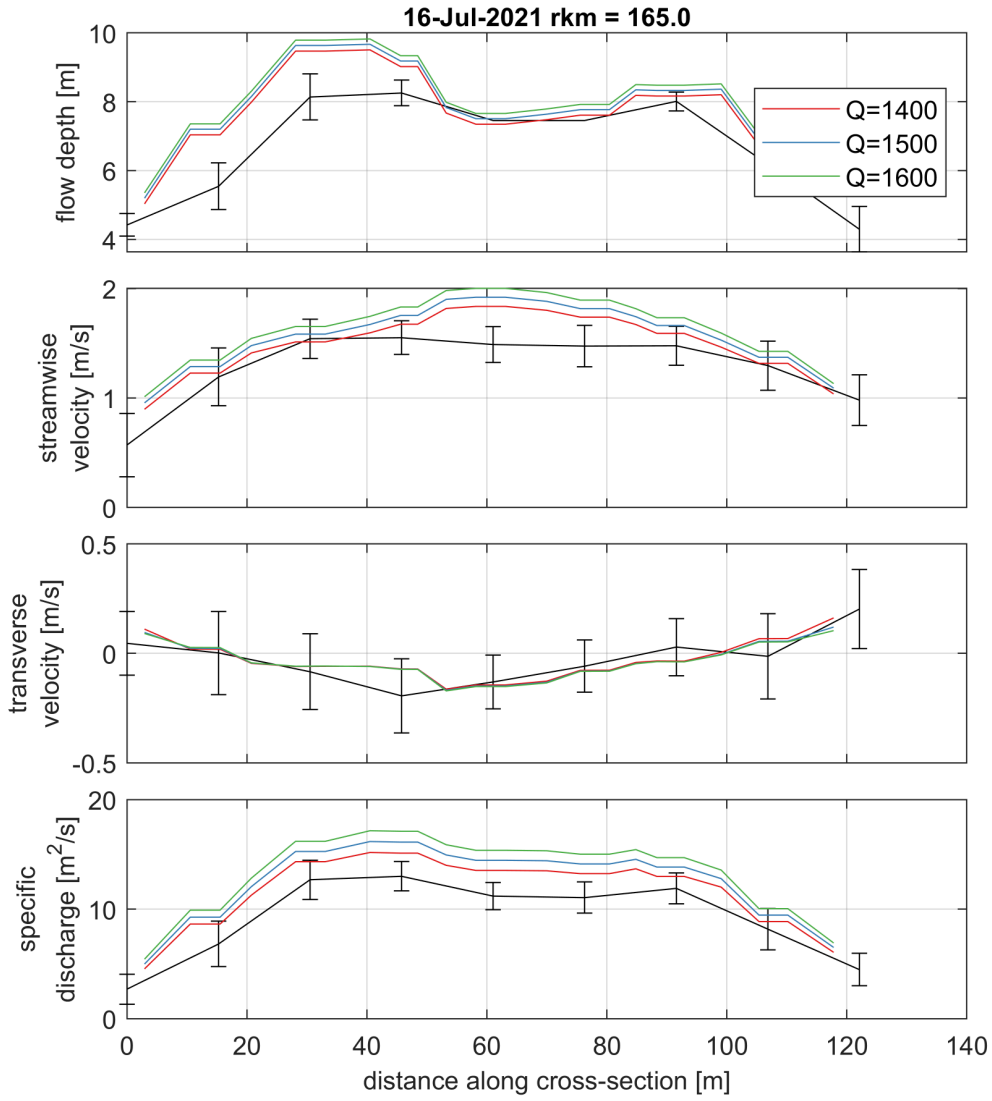

Figure C.1.18 Depth averaged velocity comparison for 16-7-2021 at river kilometre 165.0.

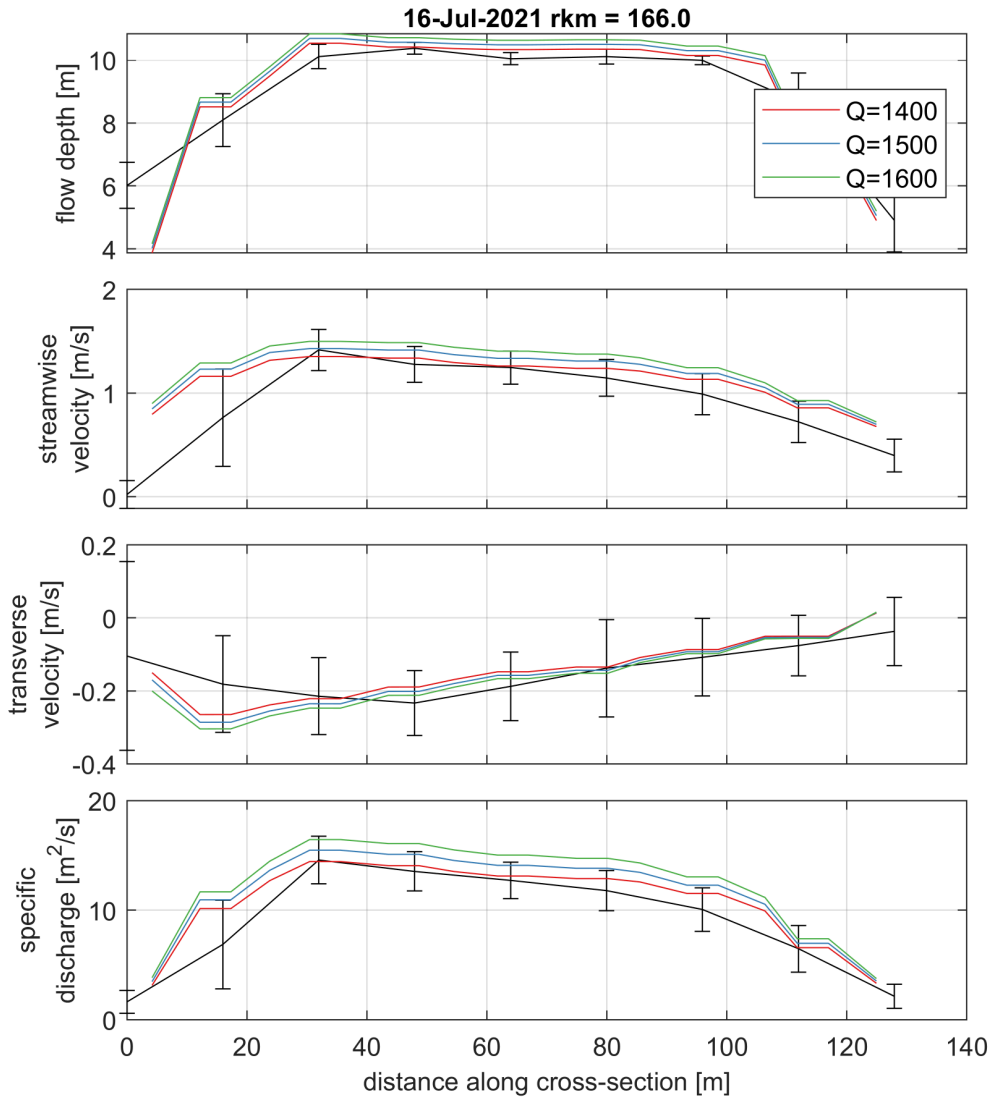

Figure C.1.19 Depth averaged velocity comparison for 16-7-2021 at river kilometre 166.0.

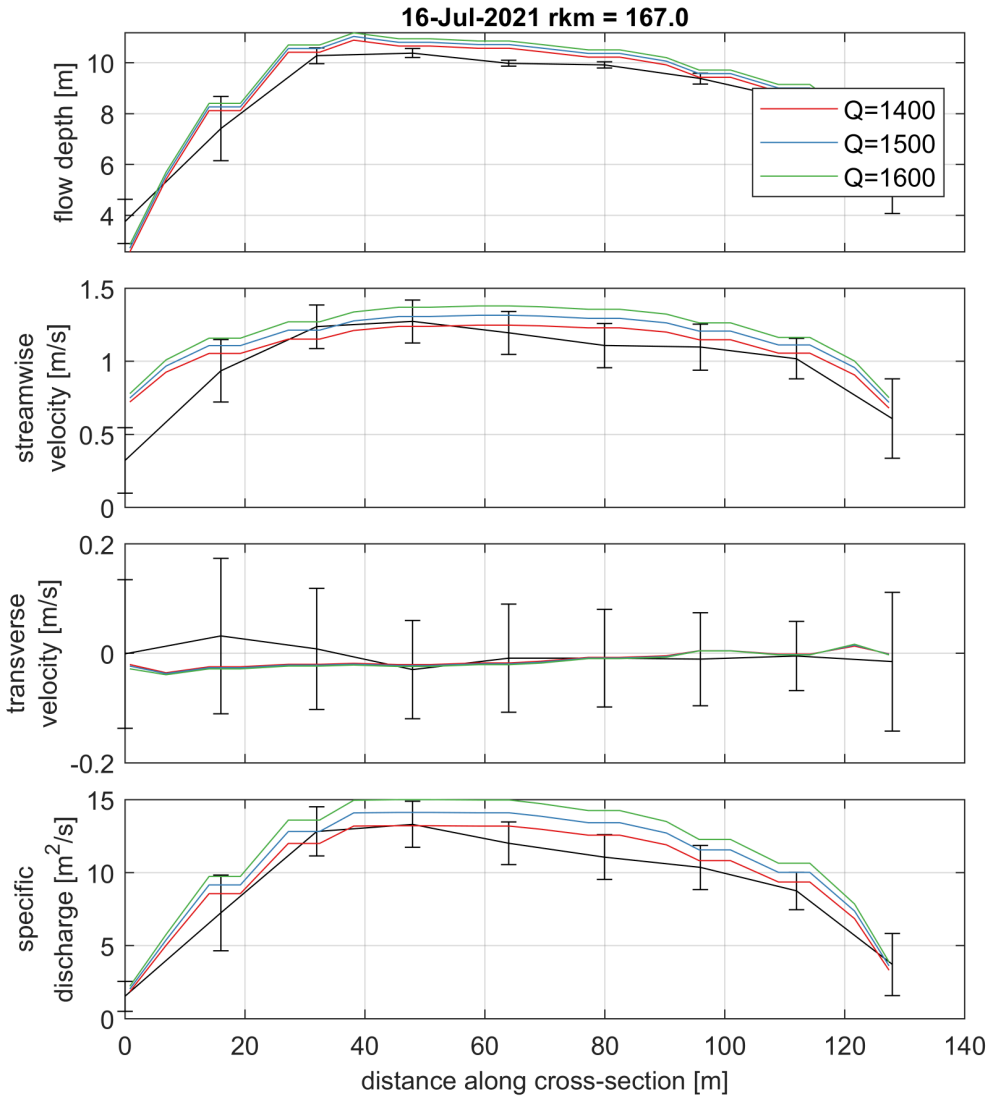

Figure C.1.20 Depth averaged velocity comparison for 16-7-2021 at river kilometre 167.0.

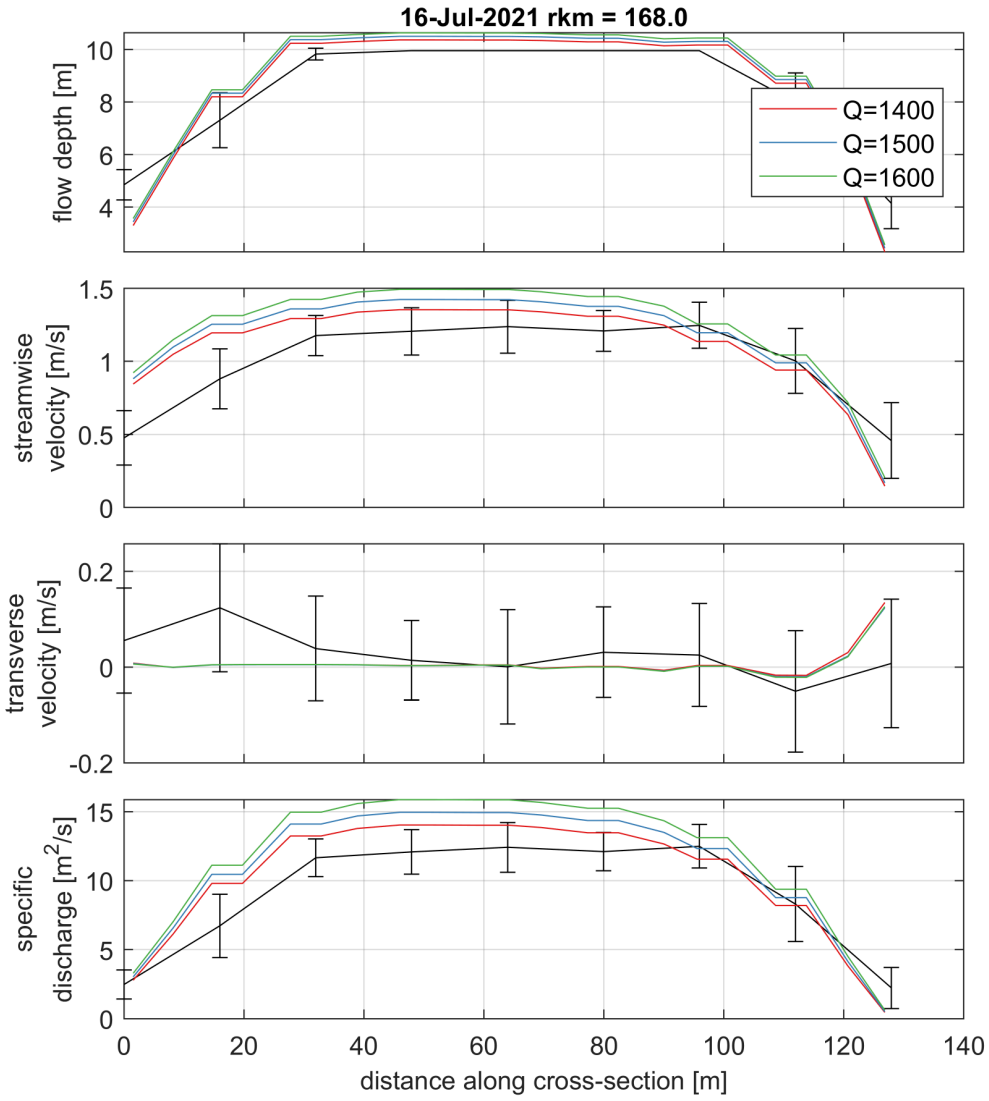

Figure C.1.21 Depth averaged velocity comparison for 16-7-2021 at river kilometre 168.0.

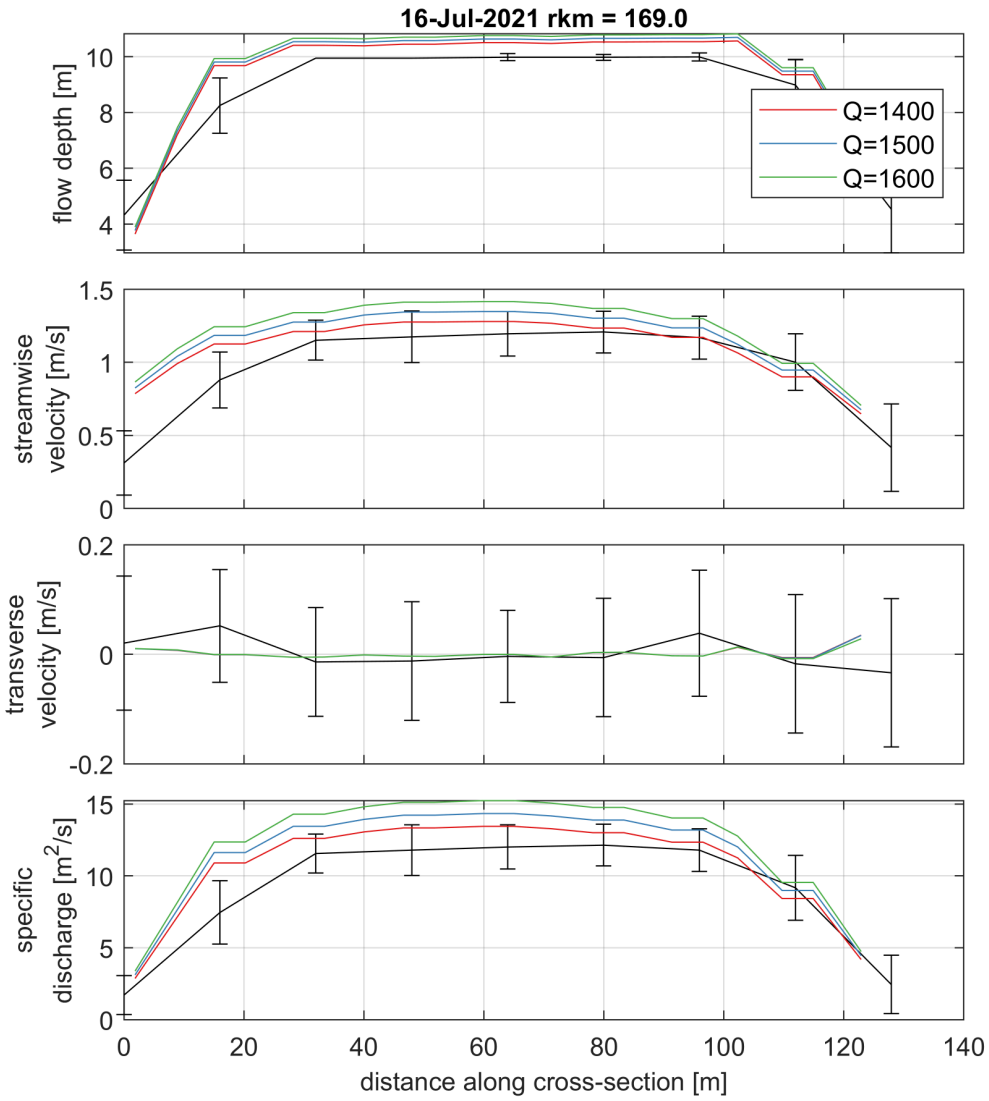

Figure C.1.22 Depth averaged velocity comparison for 16-7-2021 at river kilometre 169.0.

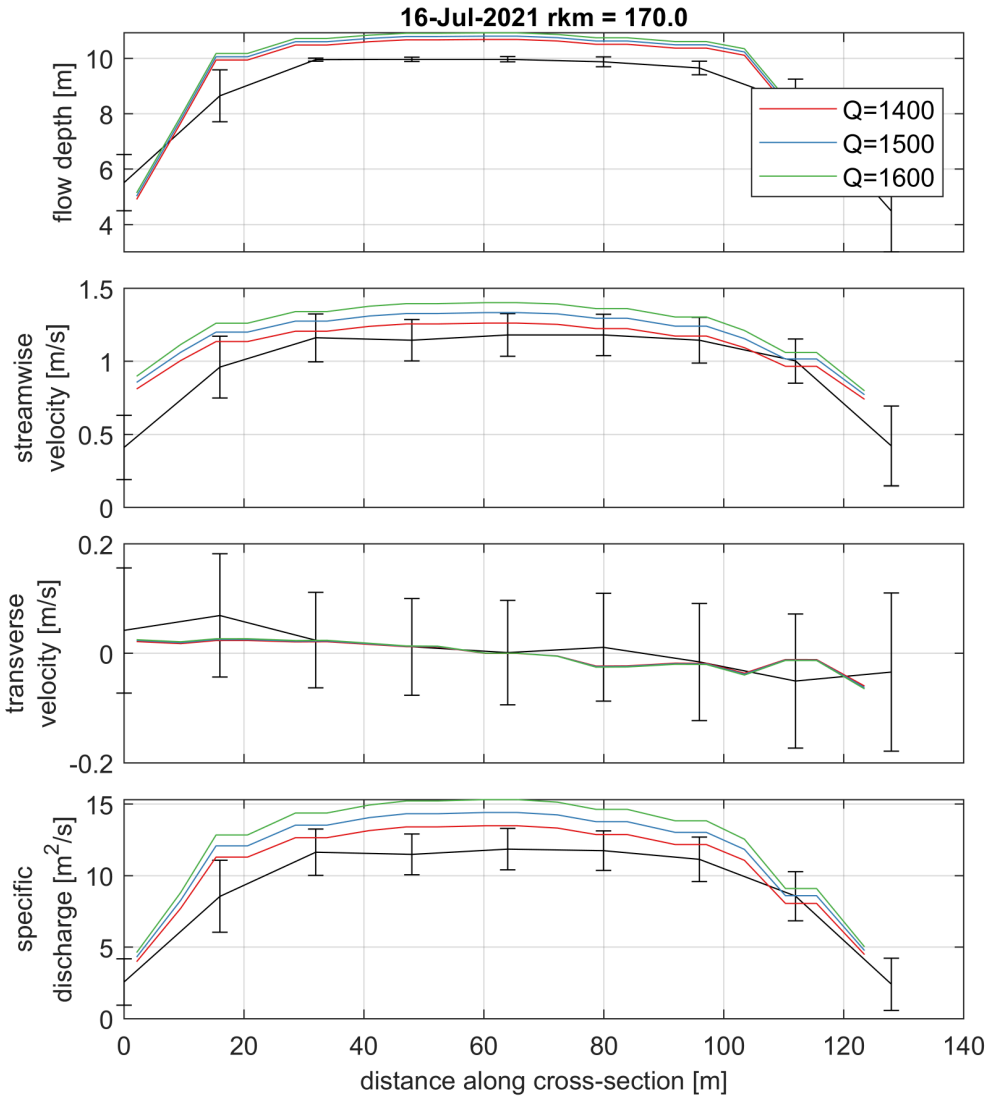

Figure C.1.23 Depth averaged velocity comparison for 16-7-2021 at river kilometre 170.0.

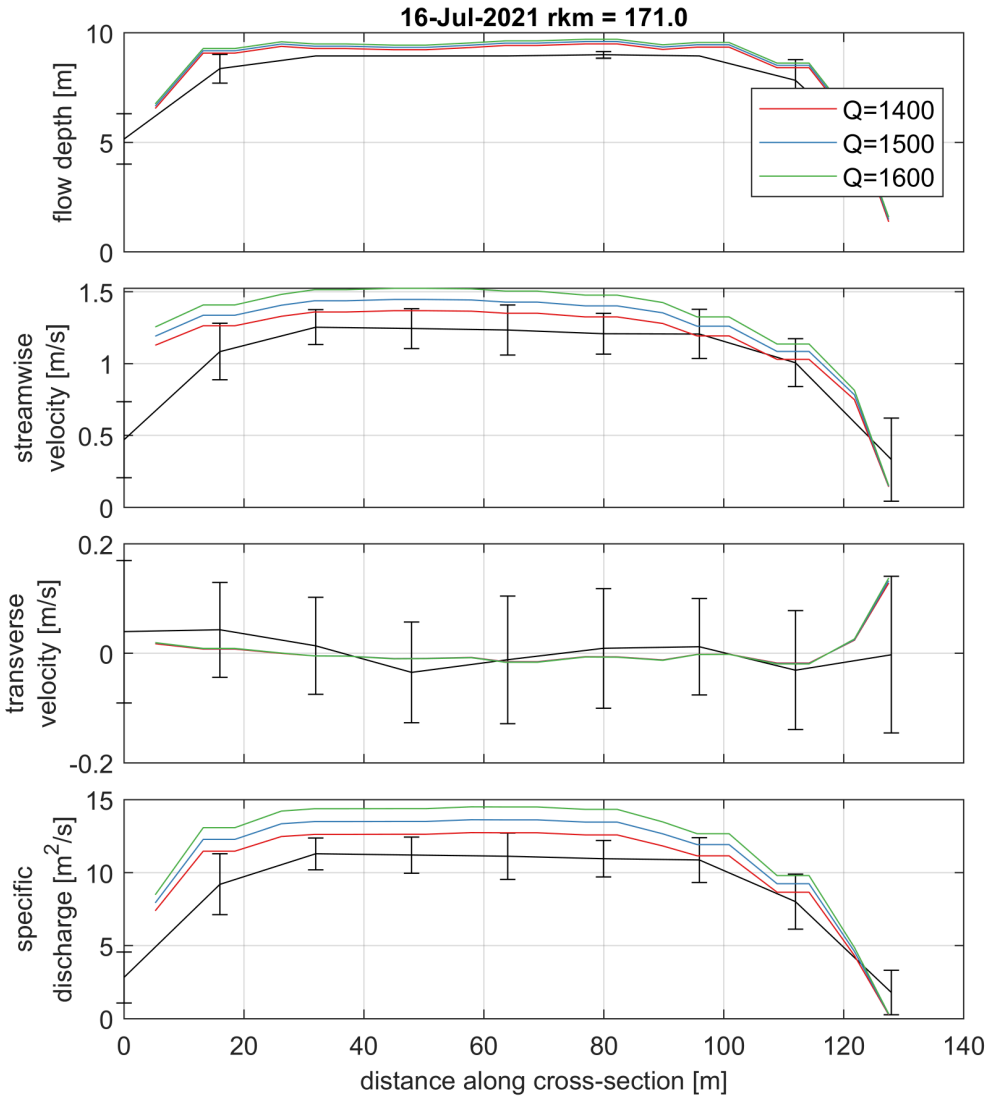

Figure C.1.24 Depth averaged velocity comparison for 16-7-2021 at river kilometre 171.0.

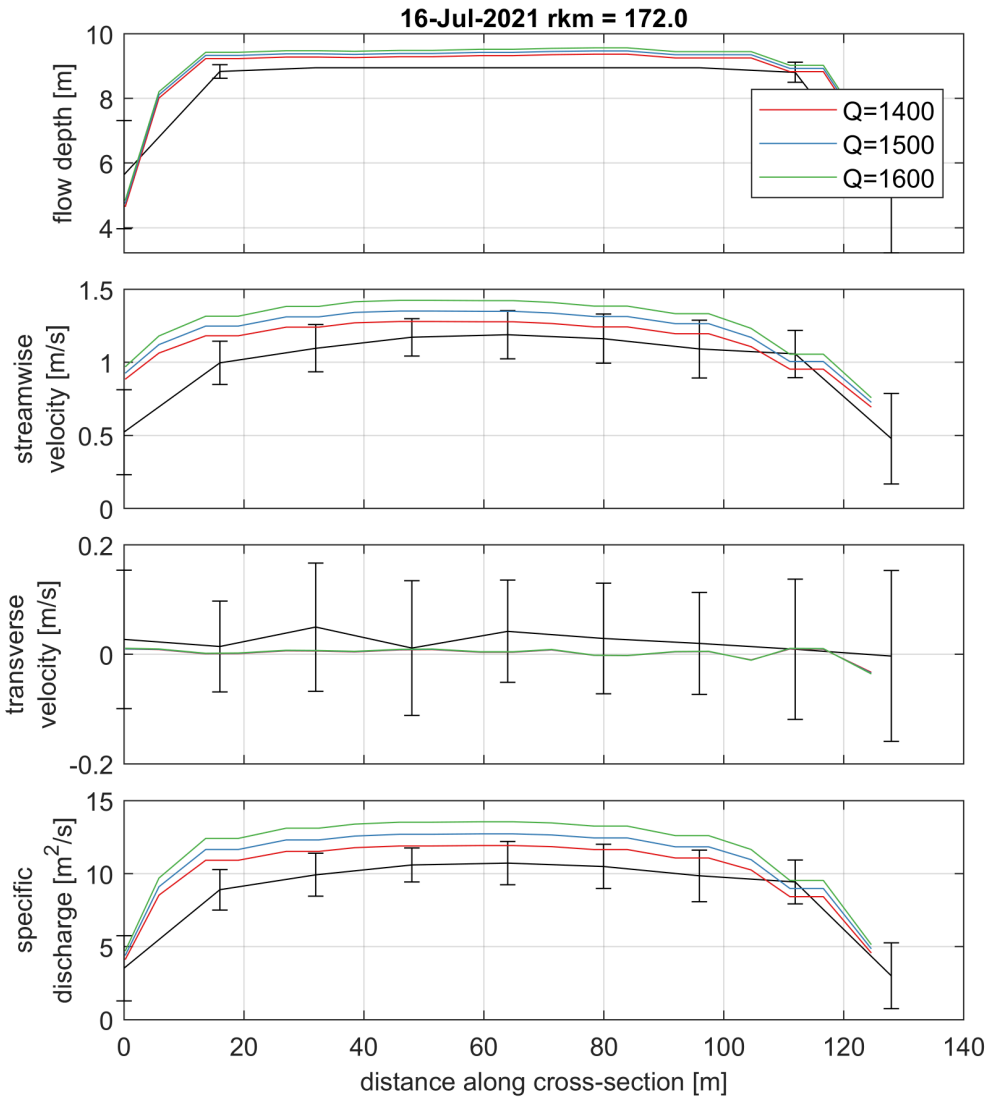

Figure C.1.25 Depth averaged velocity comparison for 16-7-2021 at river kilometre 172.0.

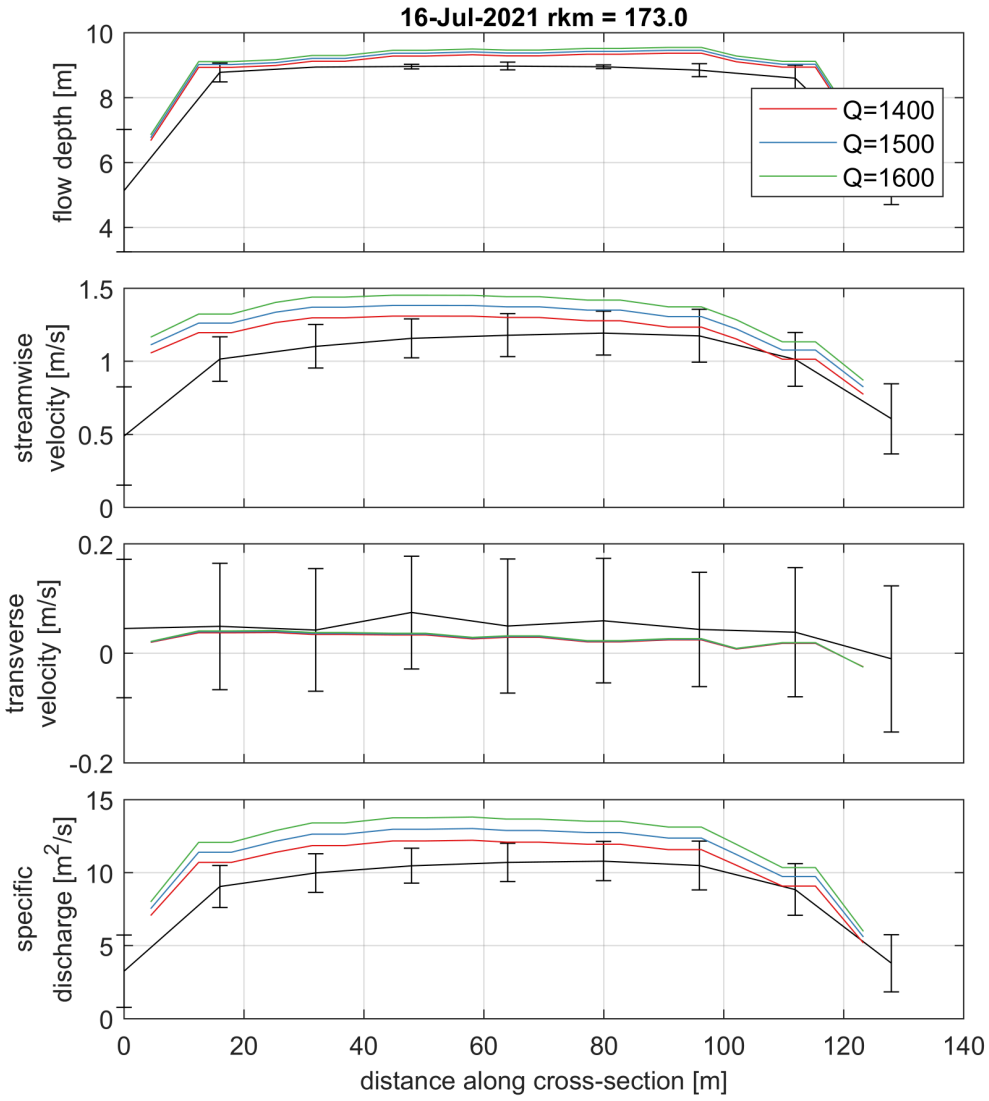

Figure C.1.26 Depth averaged velocity comparison for 16-7-2021 at river kilometre 173.0.

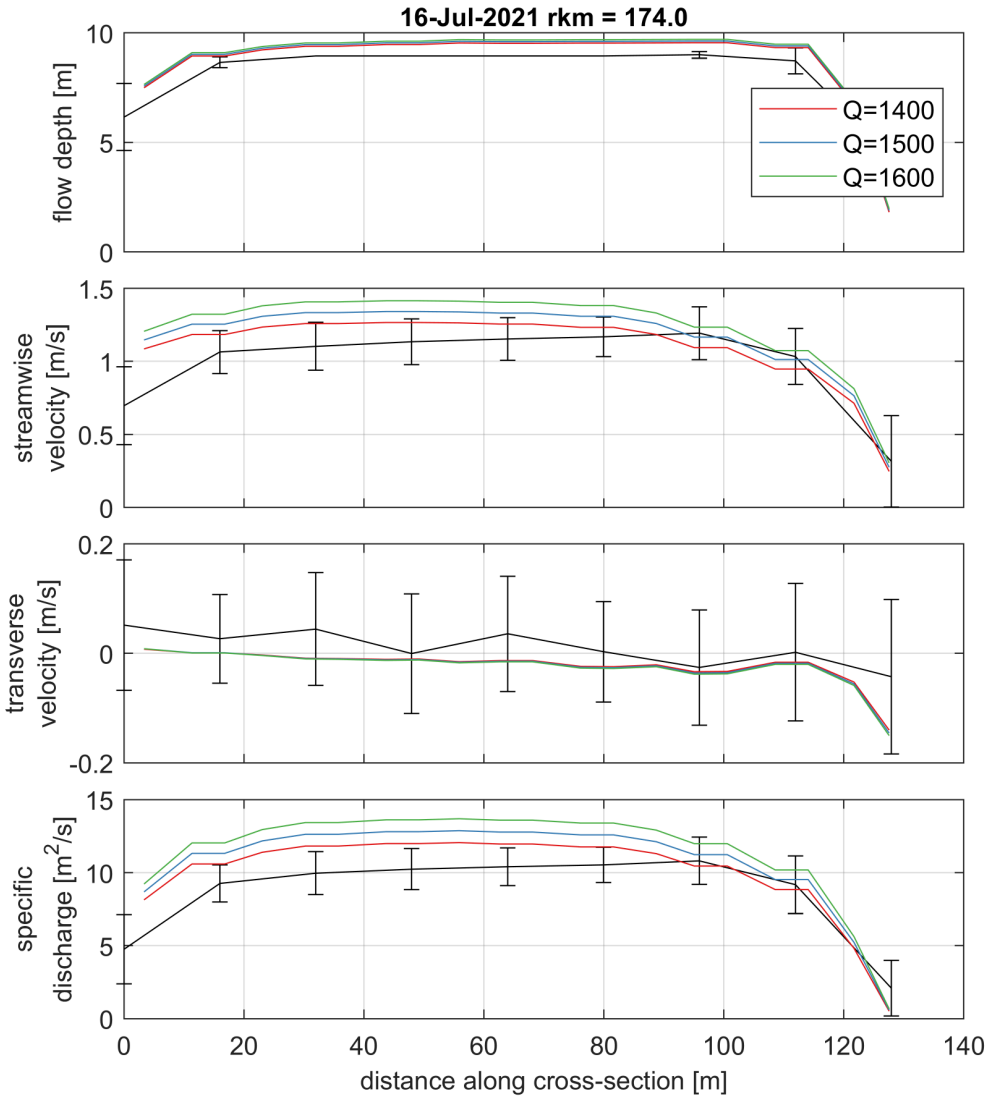

Figure C.1.27 Depth averaged velocity comparison for 16-7-2021 at river kilometre 174.0.

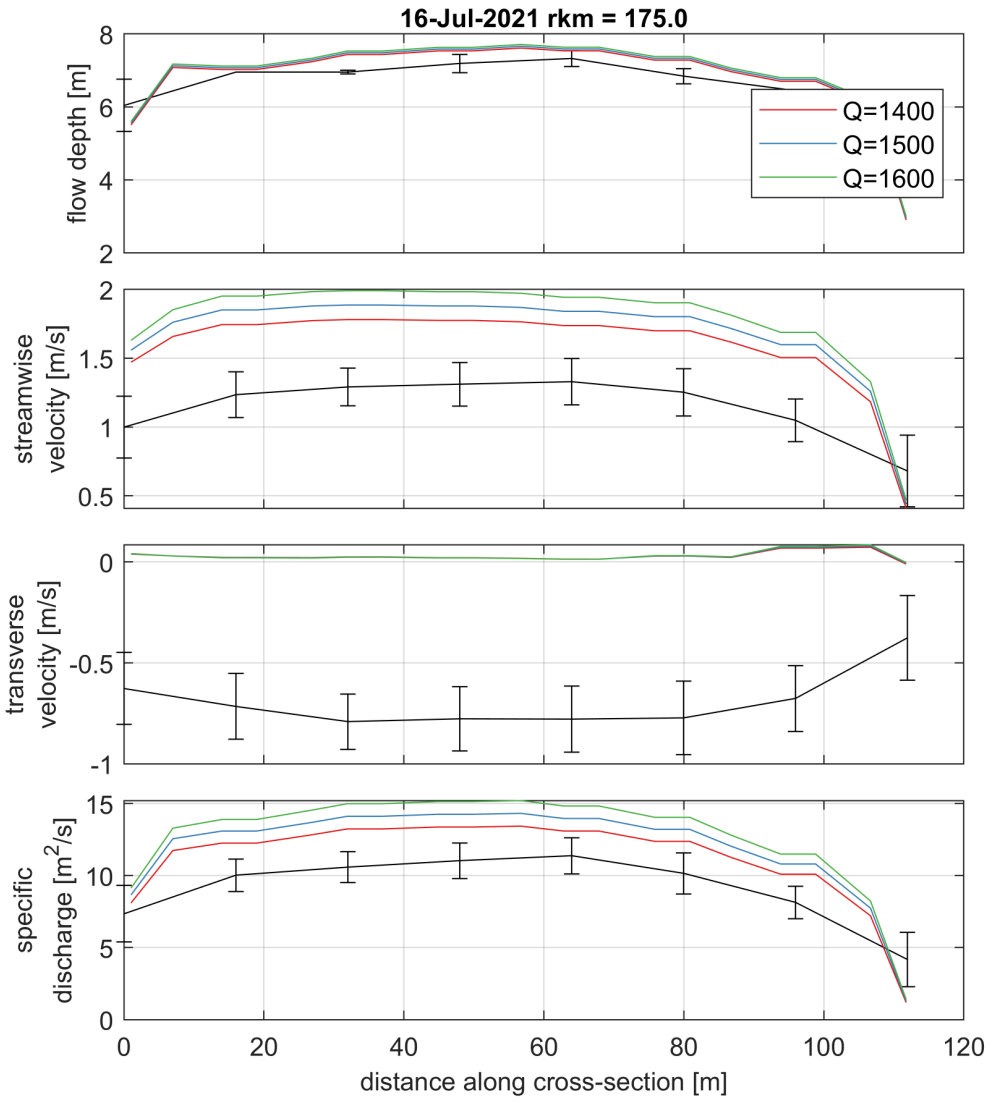

Figure C.1.28 Depth averaged velocity comparison for 16-7-2021 at river kilometre 175.0.

C.2 18-7-2021

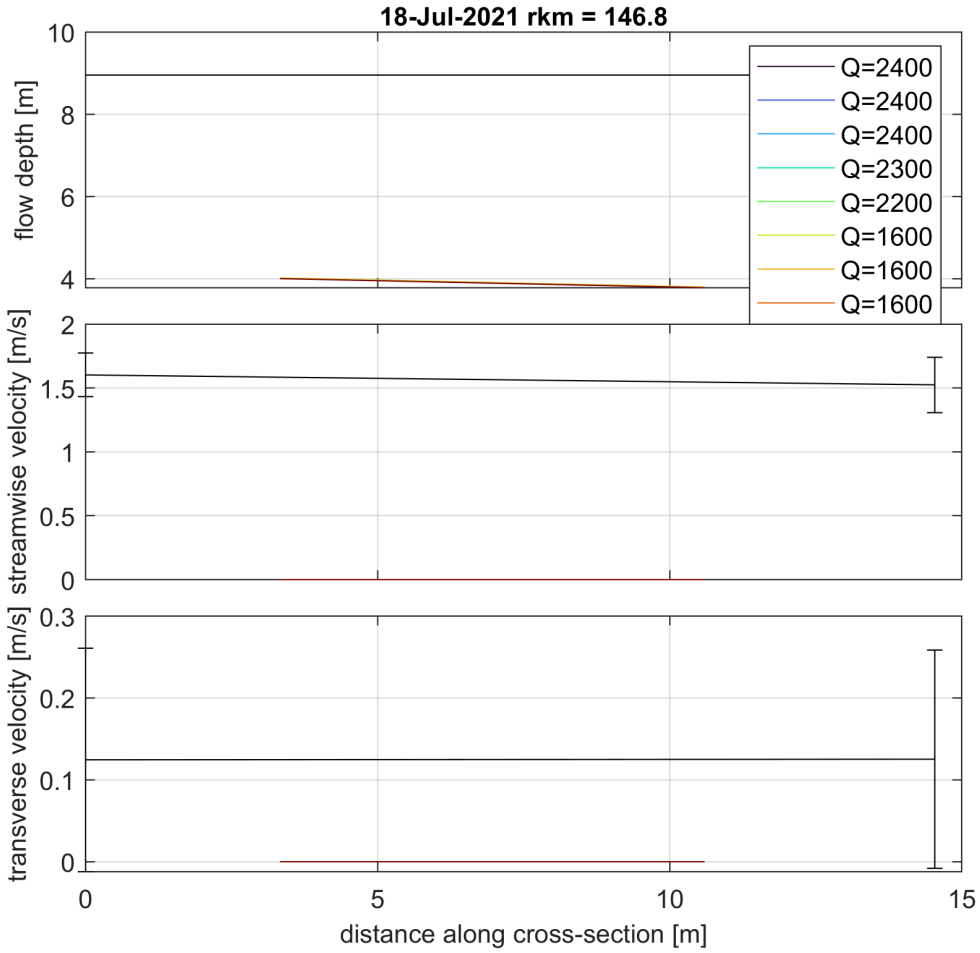

Figure C.2.29 Depth averaged velocity comparison for 18-7-2021 at river kilometre 146.8.

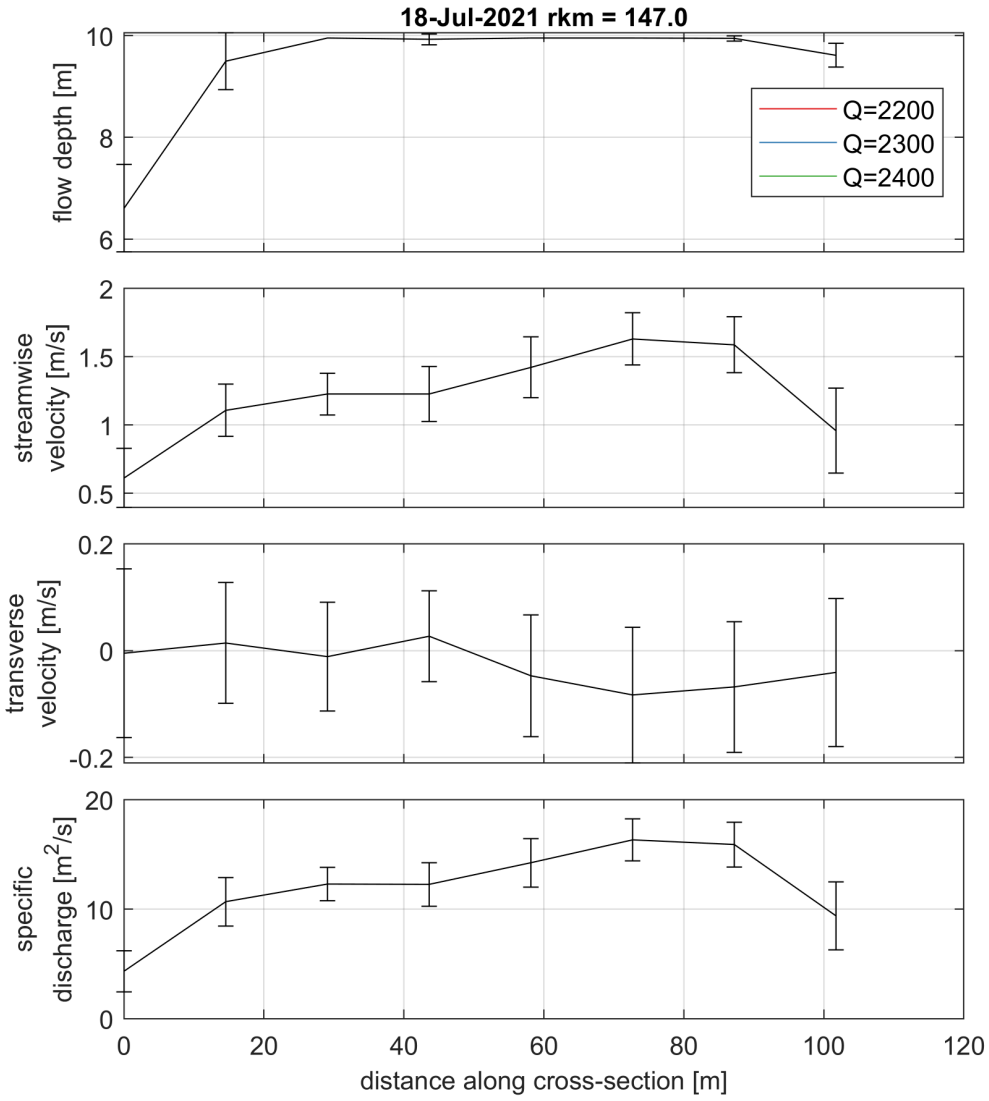

Figure C.2.30 Depth averaged velocity comparison for 18-7-2021 at river kilometre 147.0.

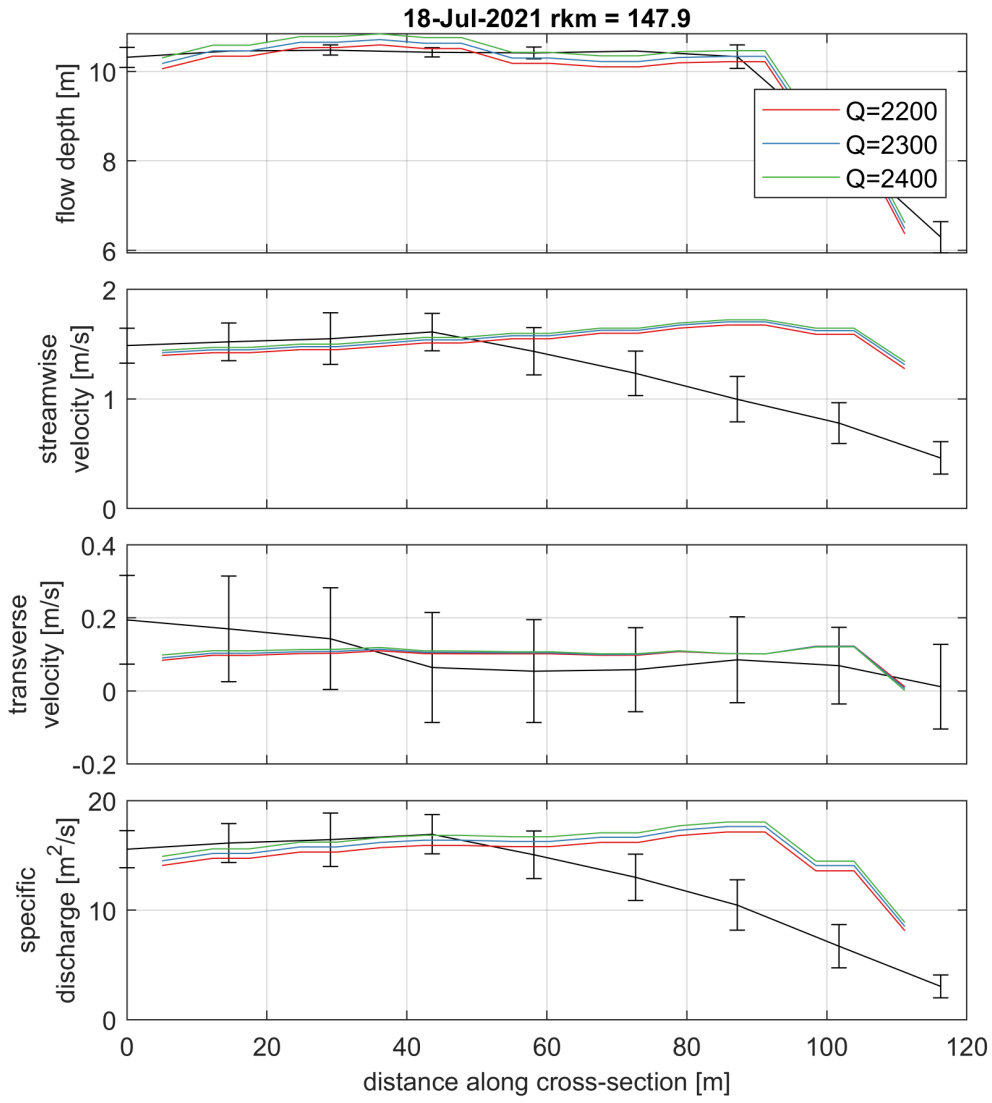

Figure C.2.31 Depth averaged velocity comparison for 18-7-2021 at river kilometre 147.9.

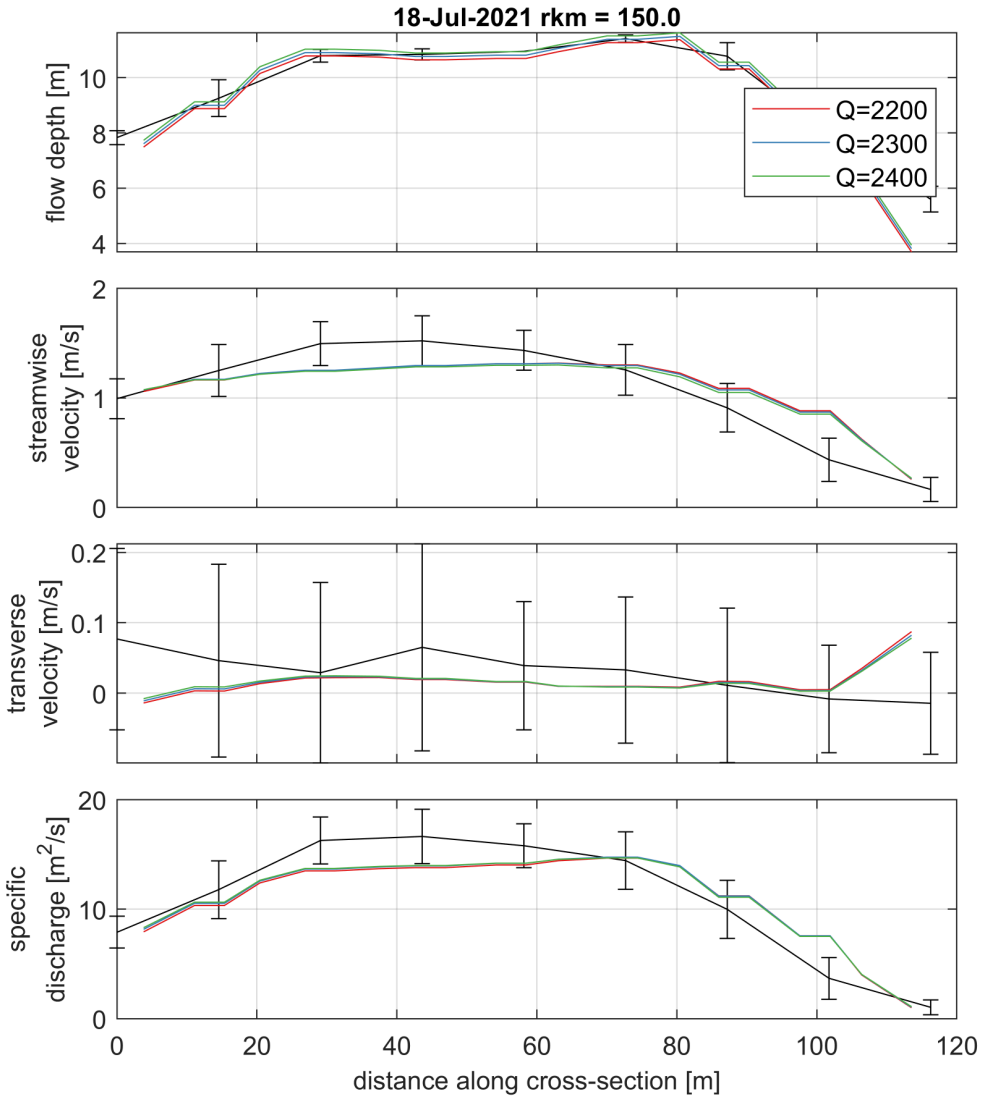

Figure C.2.32 Depth averaged velocity comparison for 18-7-2021 at river kilometre 150.0.

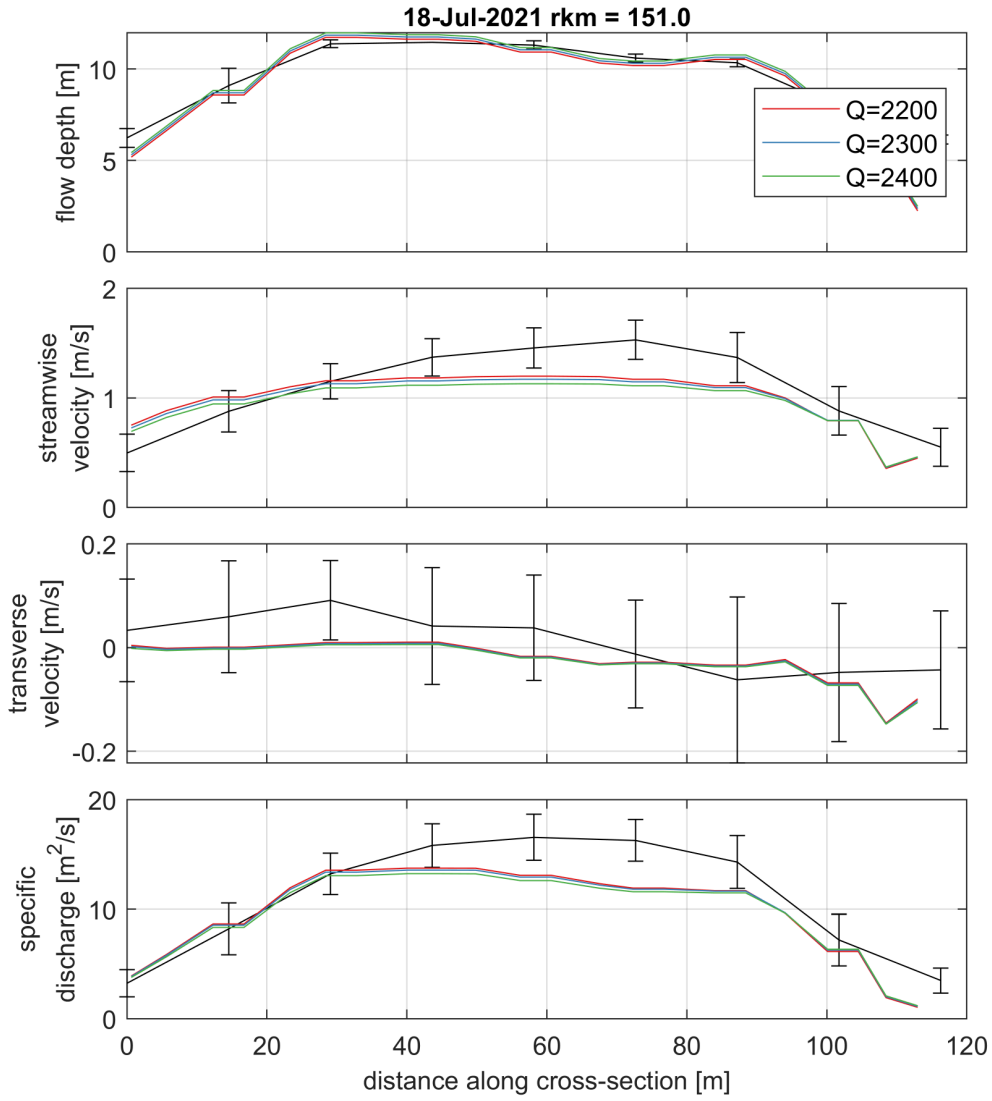

Figure C.2.33 Depth averaged velocity comparison for 18-7-2021 at river kilometre 151.0.

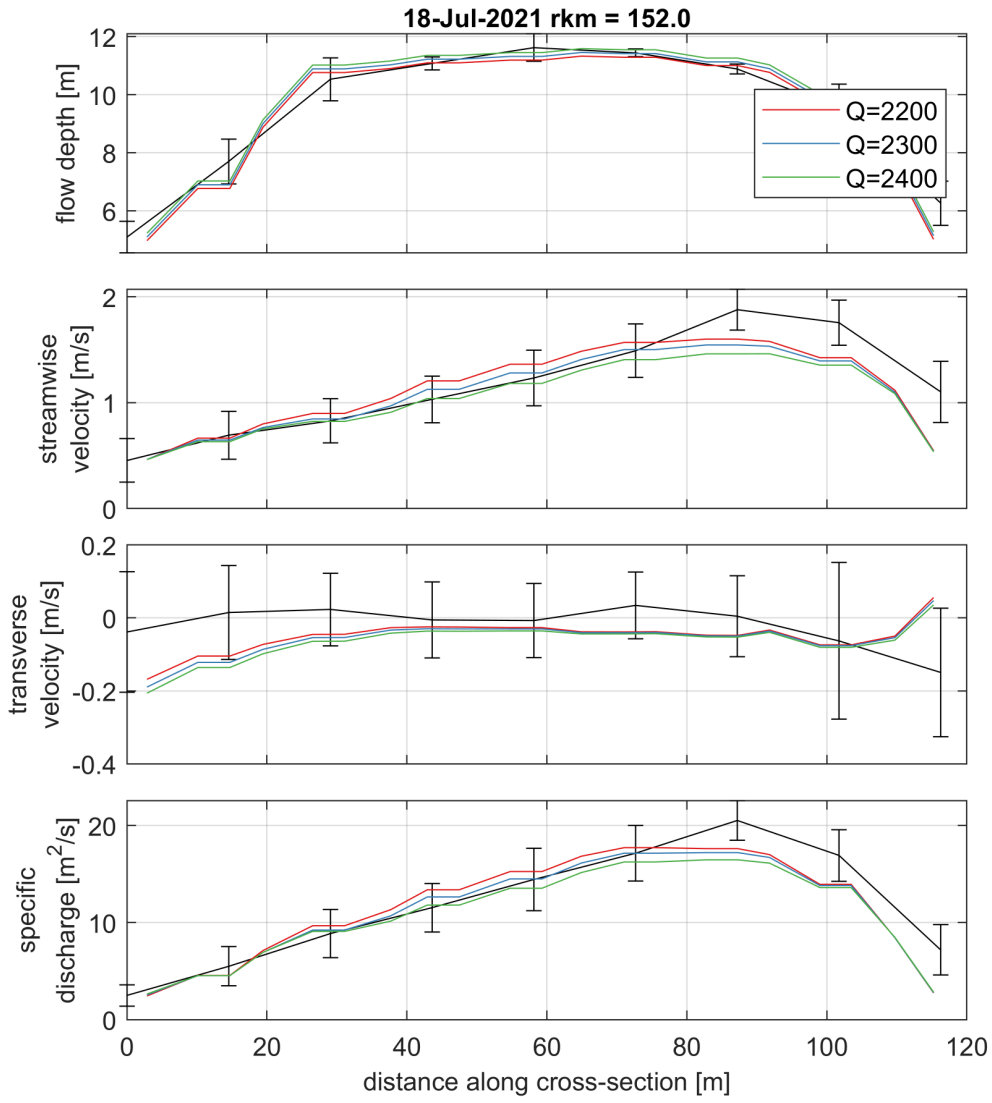

Figure C.2.34 Depth averaged velocity comparison for 18-7-2021 at river kilometre 152.0.

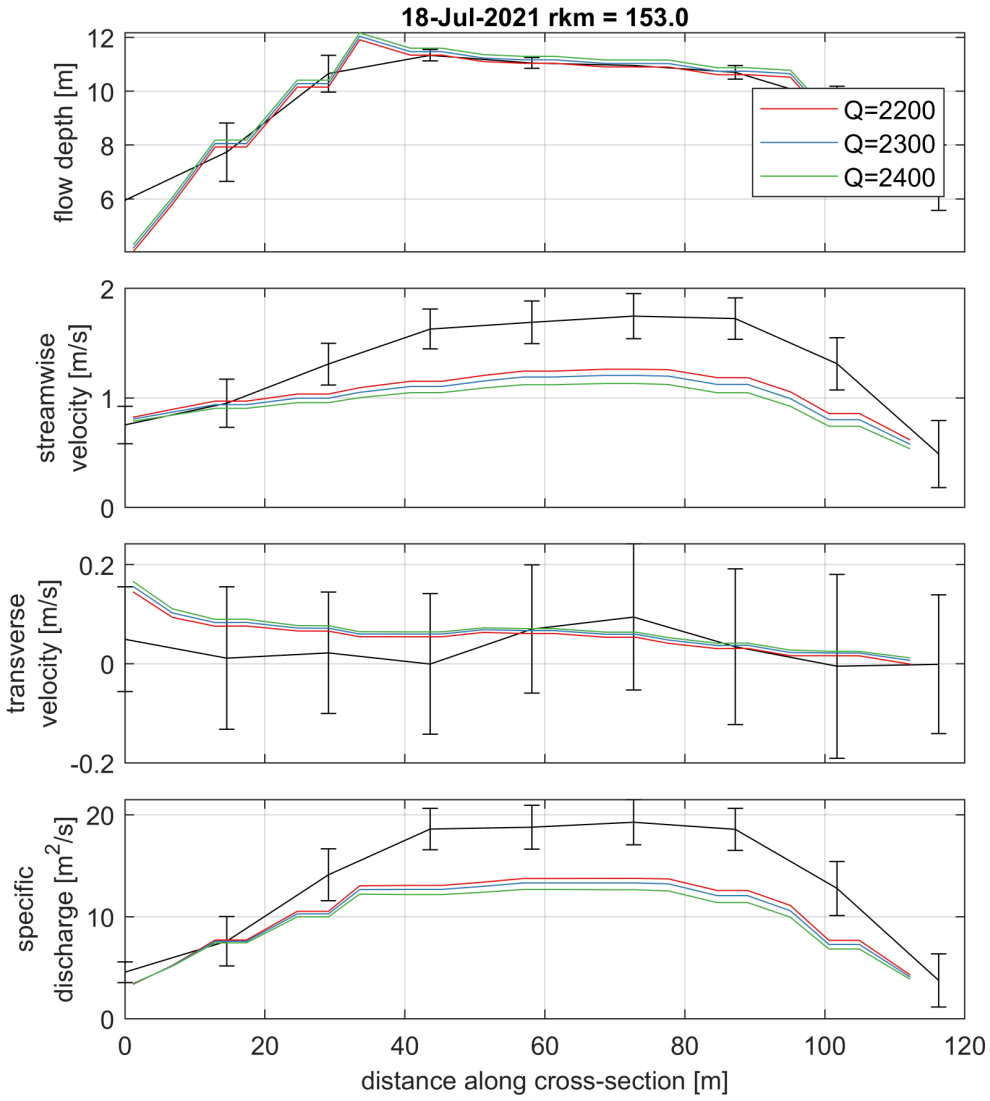

Figure C.2.35 Depth averaged velocity comparison for 18-7-2021 at river kilometre 153.0.

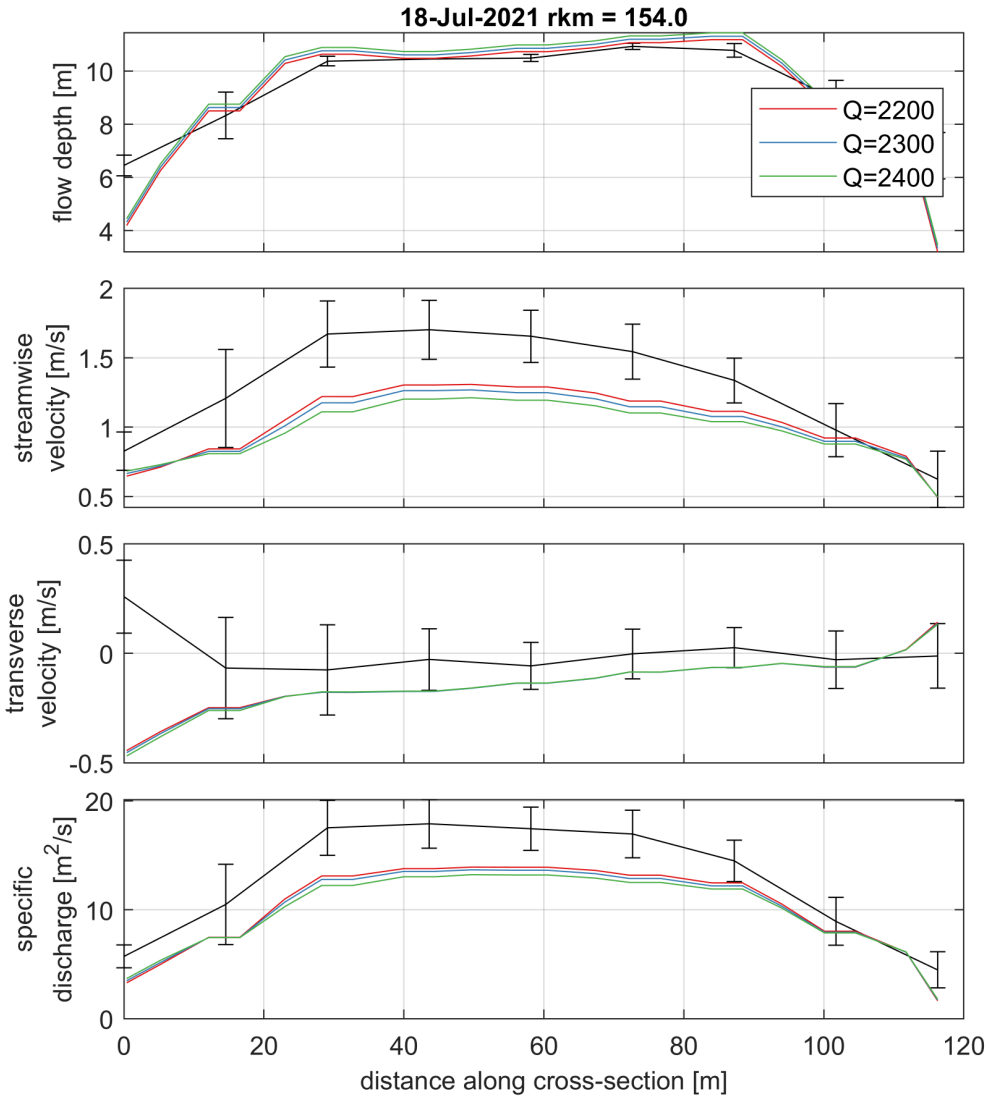

Figure C.2.36 Depth averaged velocity comparison for 18-7-2021 at river kilometre 154.0.

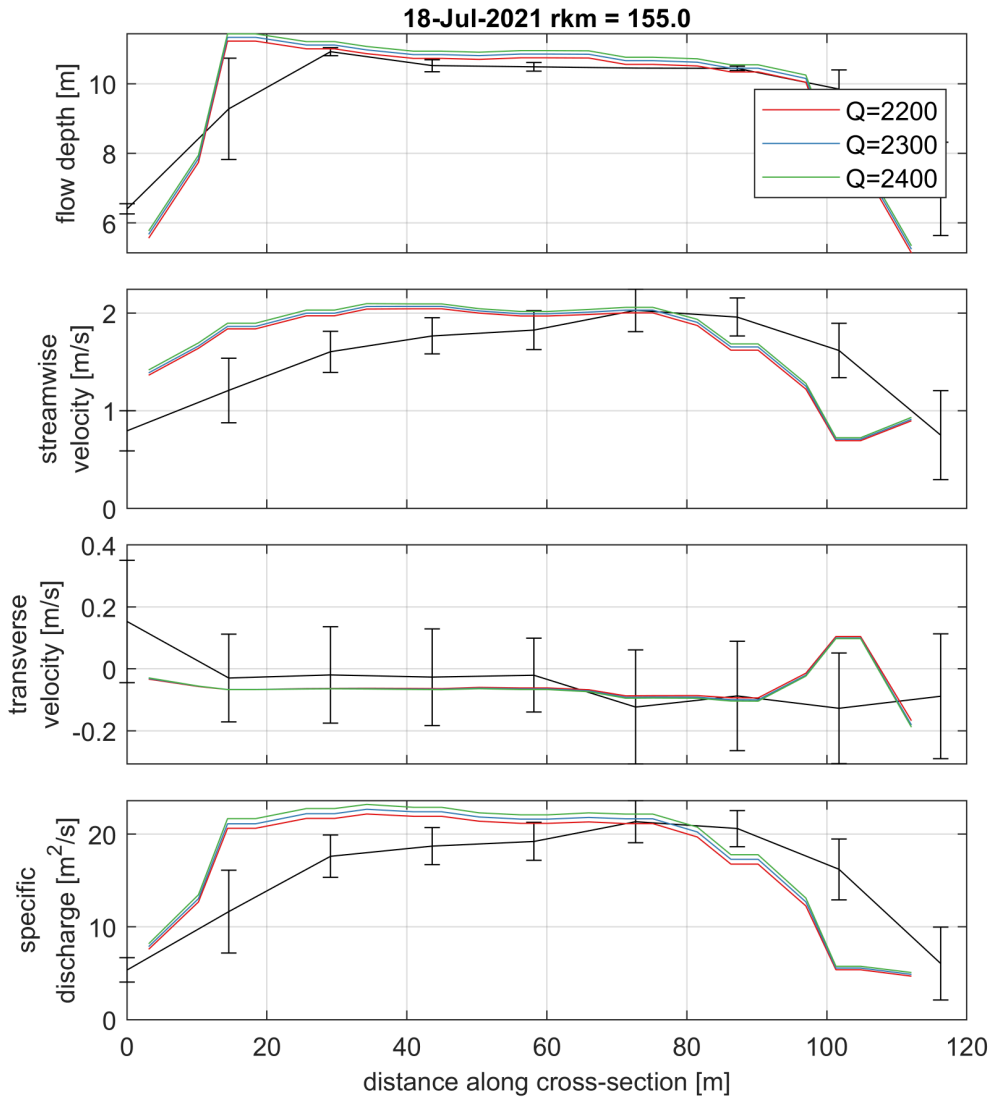

Figure C.2.37 Depth averaged velocity comparison for 18-7-2021 at river kilometre 155.0.

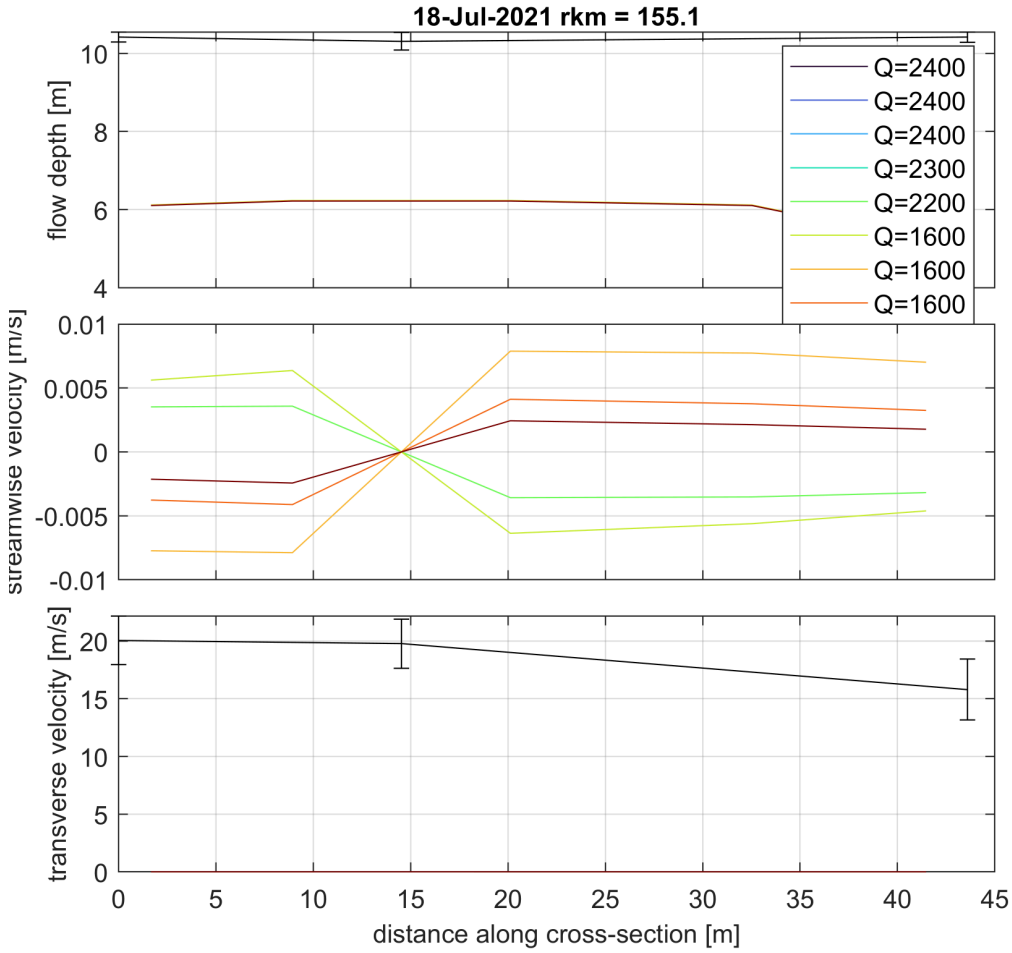

Figure C.2.38 Depth averaged velocity comparison for 18-7-2021 at river kilometre 155.1.

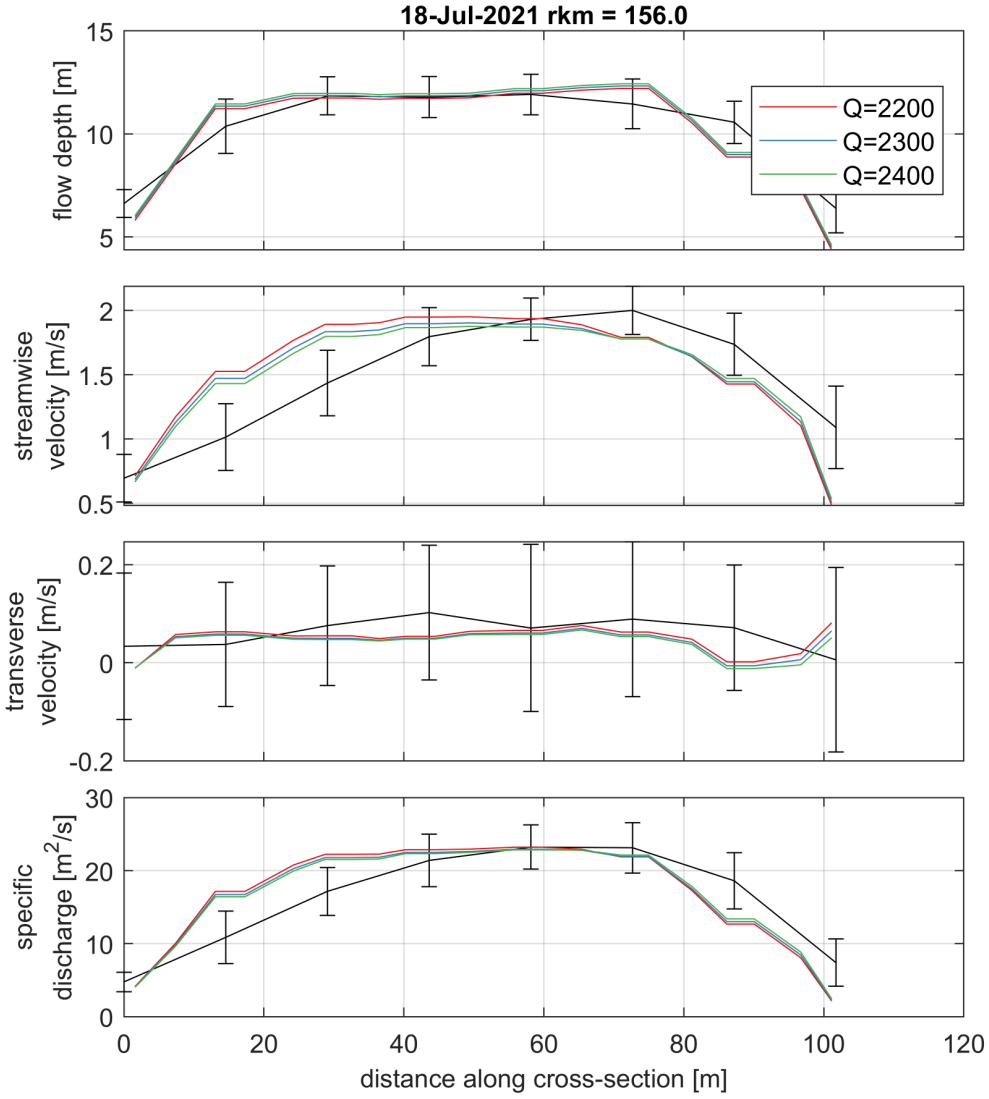

Figure C.2.39 Depth averaged velocity comparison for 18-7-2021 at river kilometre 156.0.

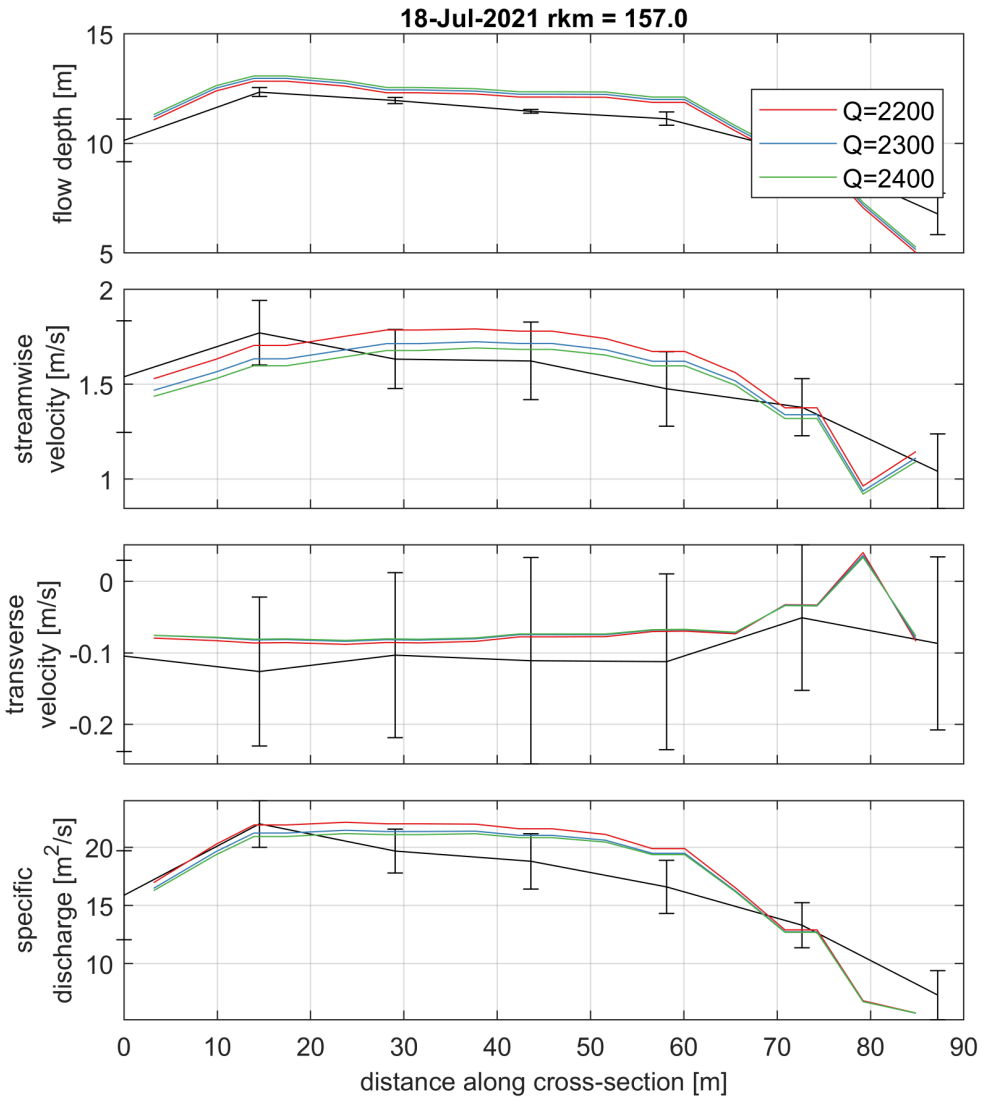

Figure C.2.40 Depth averaged velocity comparison for 18-7-2021 at river kilometre 157.0.

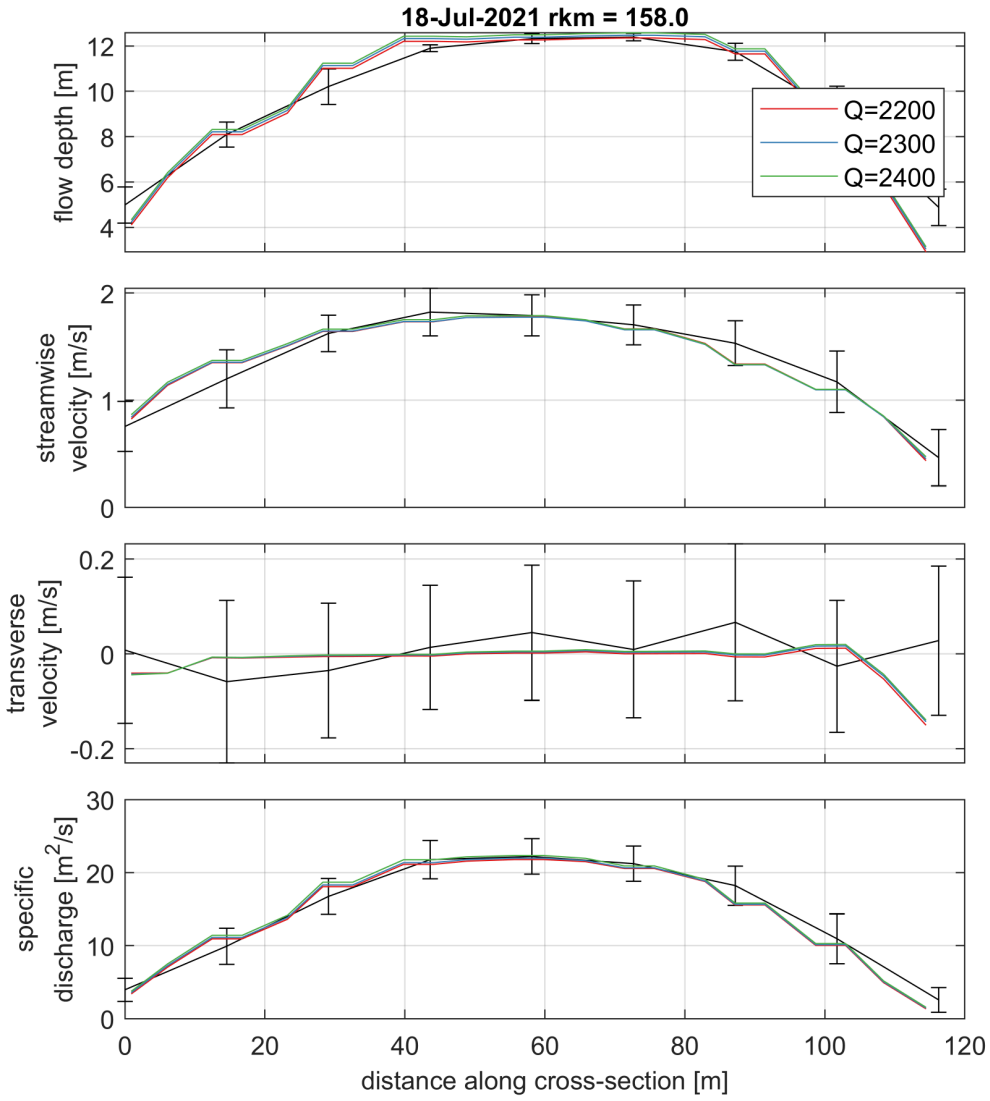

Figure C.2.41 Depth averaged velocity comparison for 18-7-2021 at river kilometre 158.0.

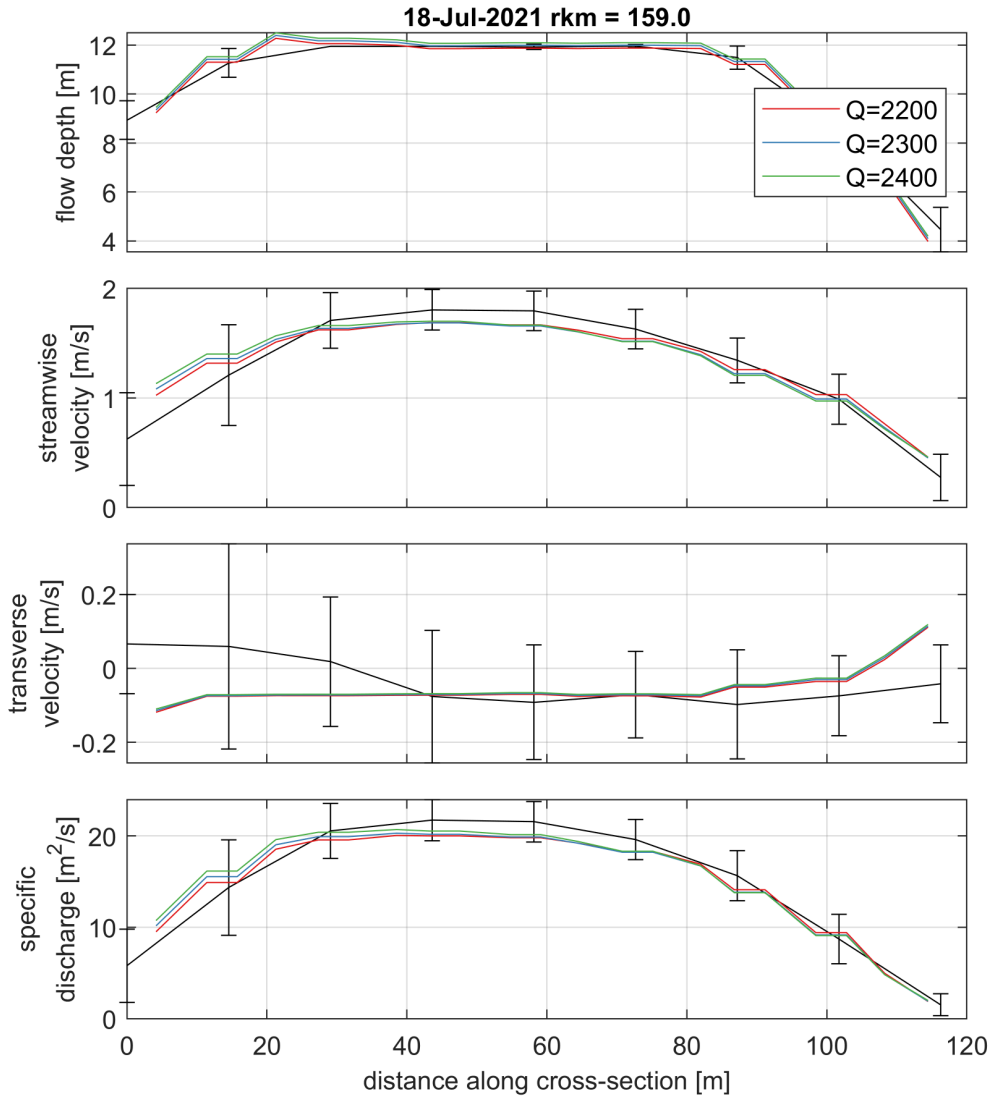

Figure C.2.42 Depth averaged velocity comparison for 18-7-2021 at river kilometre 159.0.

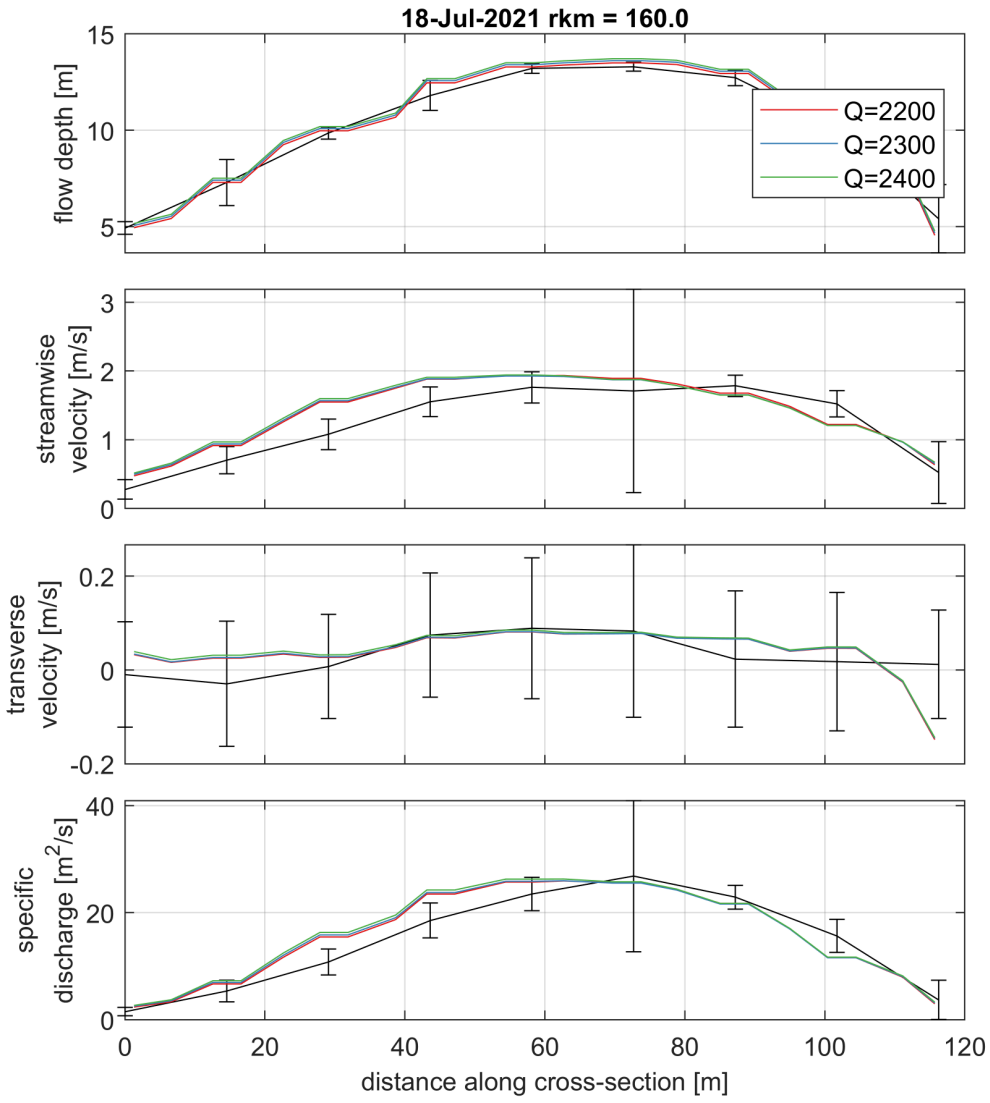

Figure C.2.43 Depth averaged velocity comparison for 18-7-2021 at river kilometre 160.0.

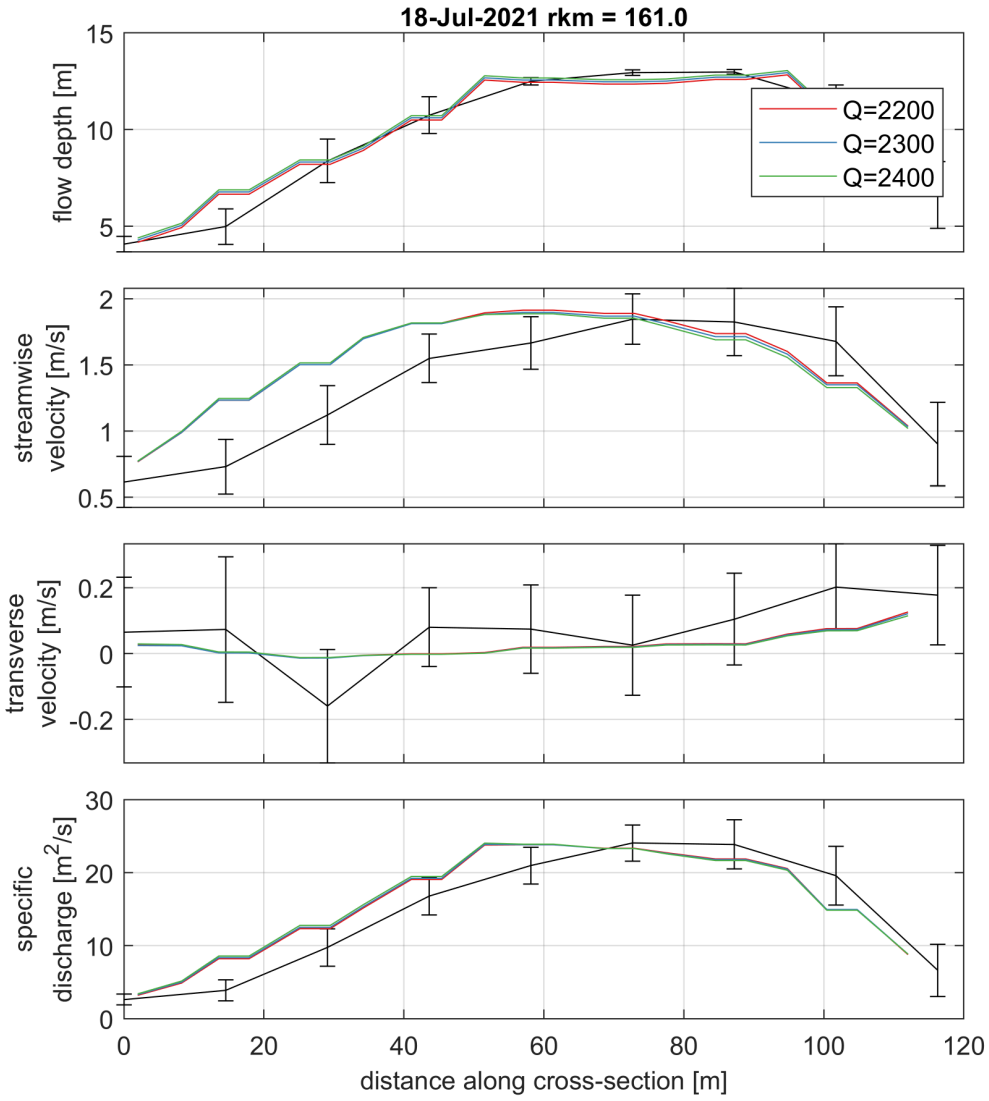

Figure C.2.44 Depth averaged velocity comparison for 18-7-2021 at river kilometre 161.0.

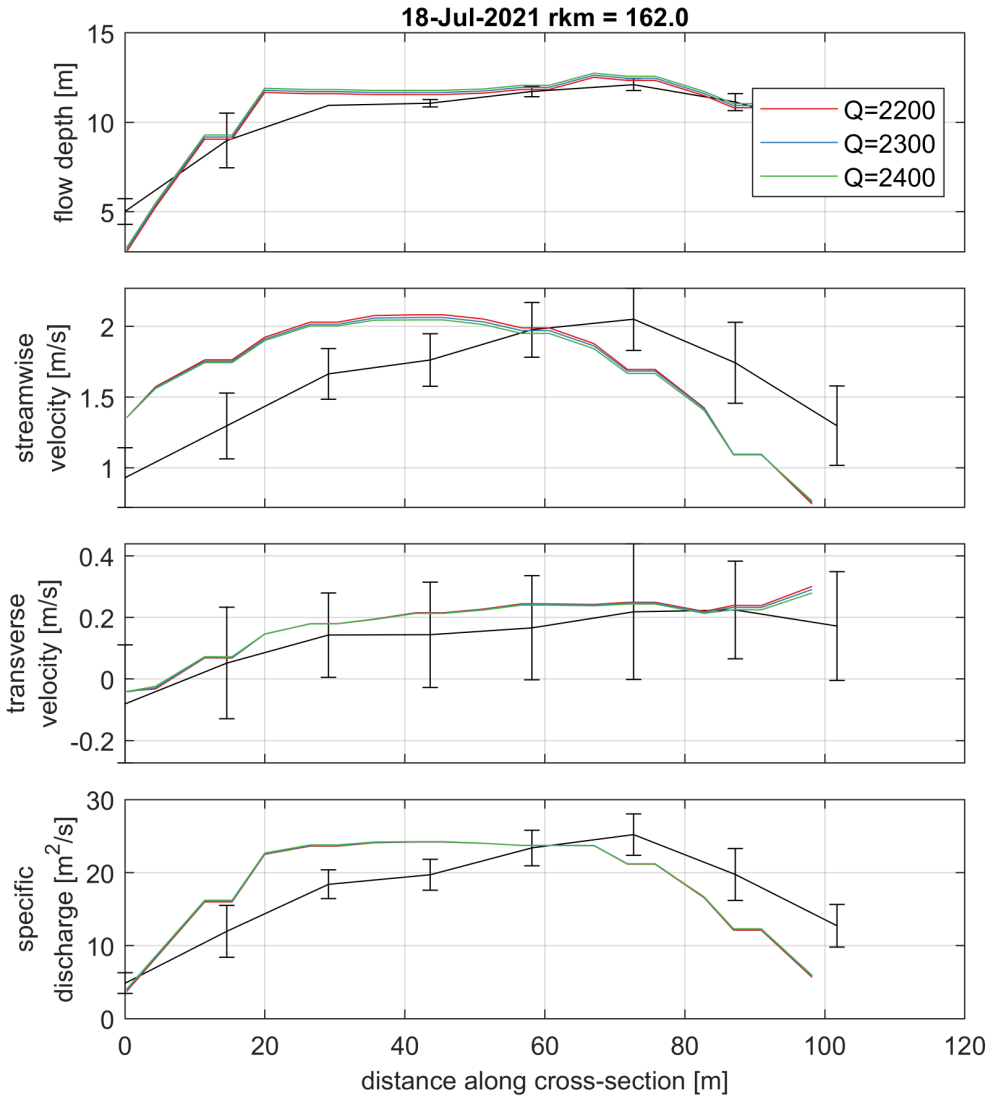

Figure C.2.45 Depth averaged velocity comparison for 18-7-2021 at river kilometre 162.0.

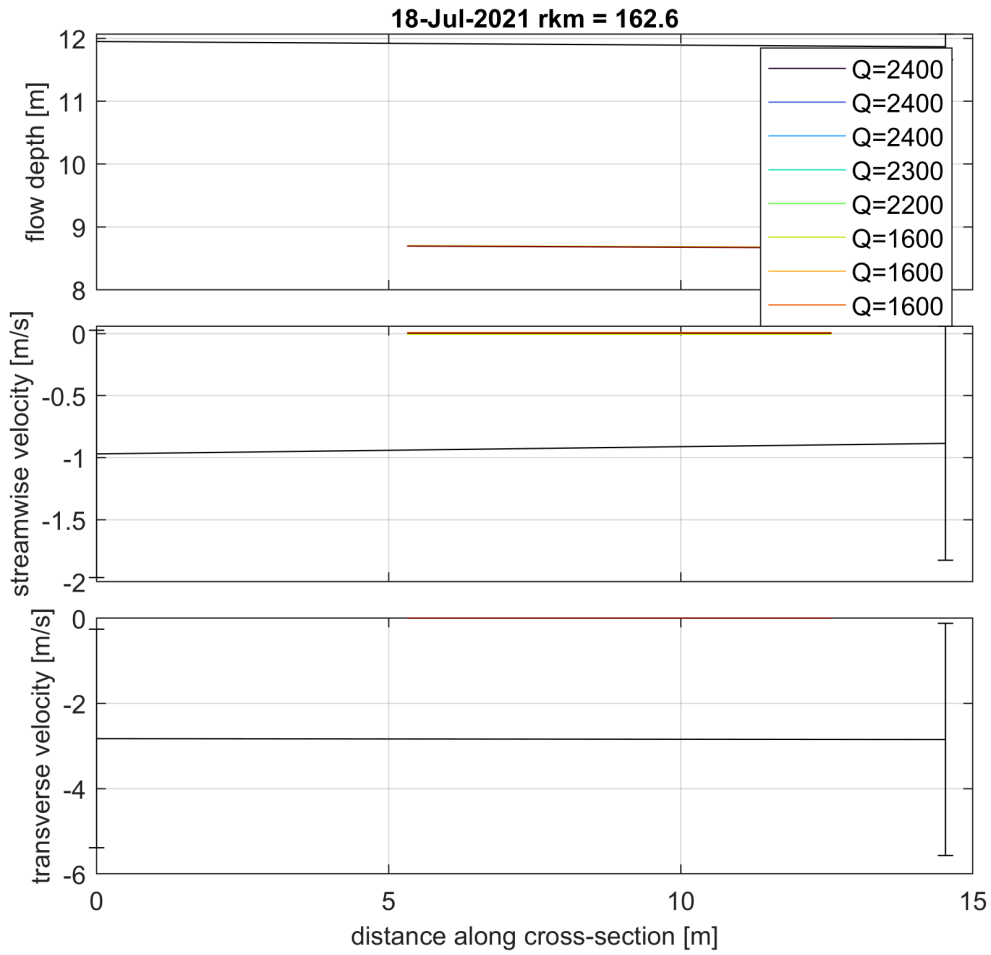

Figure C.2.46 Depth averaged velocity comparison for 18-7-2021 at river kilometre 162.6.

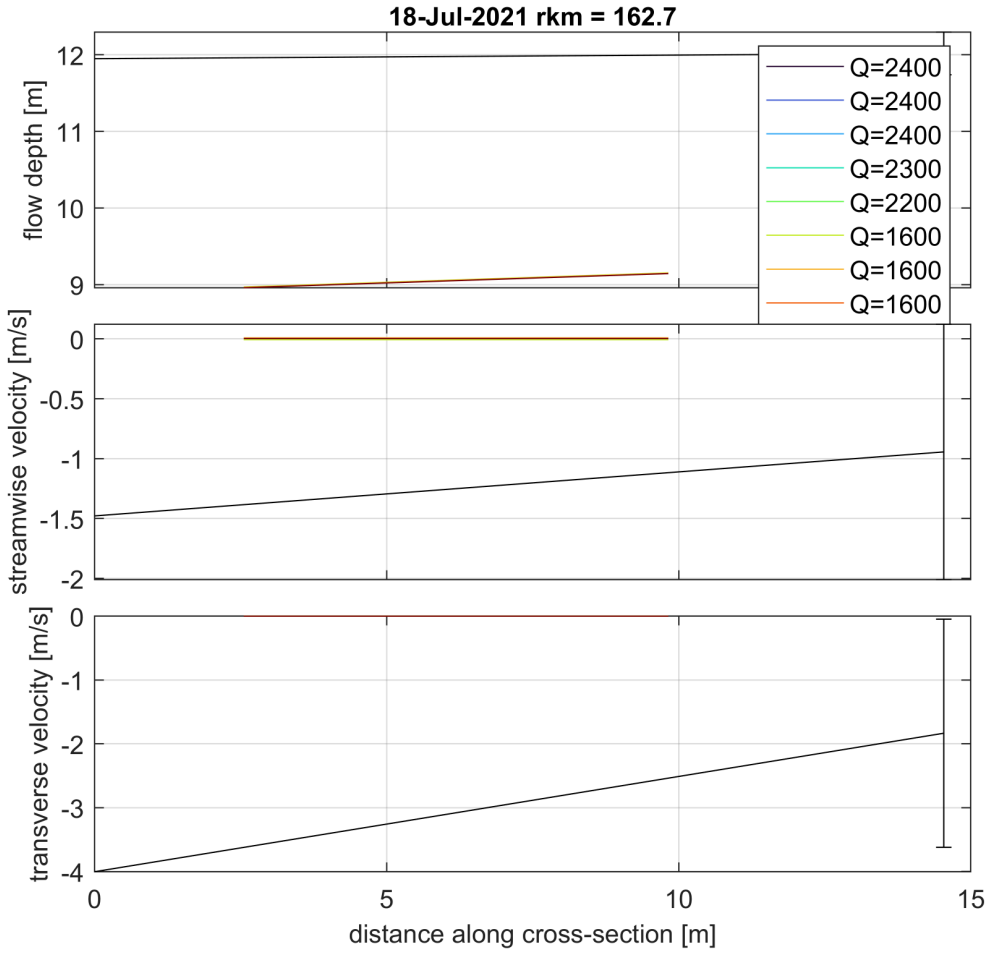

Figure C.2.47 Depth averaged velocity comparison for 18-7-2021 at river kilometre 162.7.

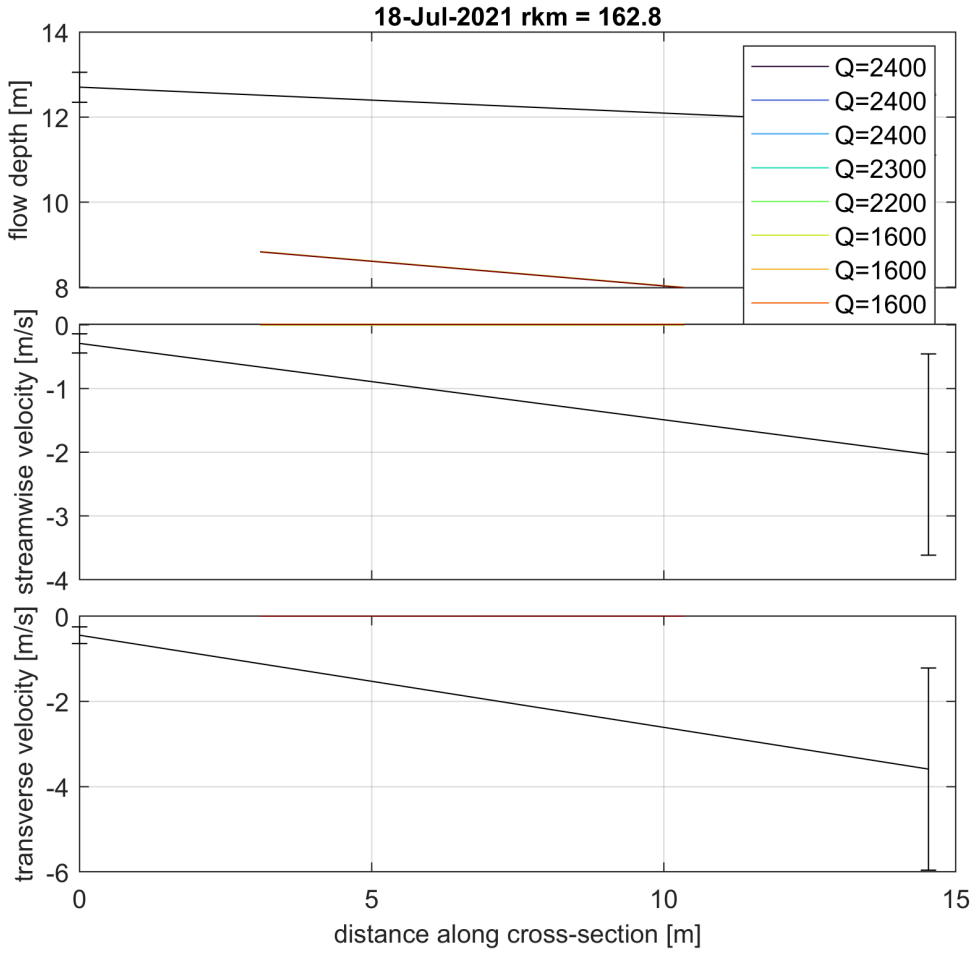

Figure C.2.48 Depth averaged velocity comparison for 18-7-2021 at river kilometre 162.8.

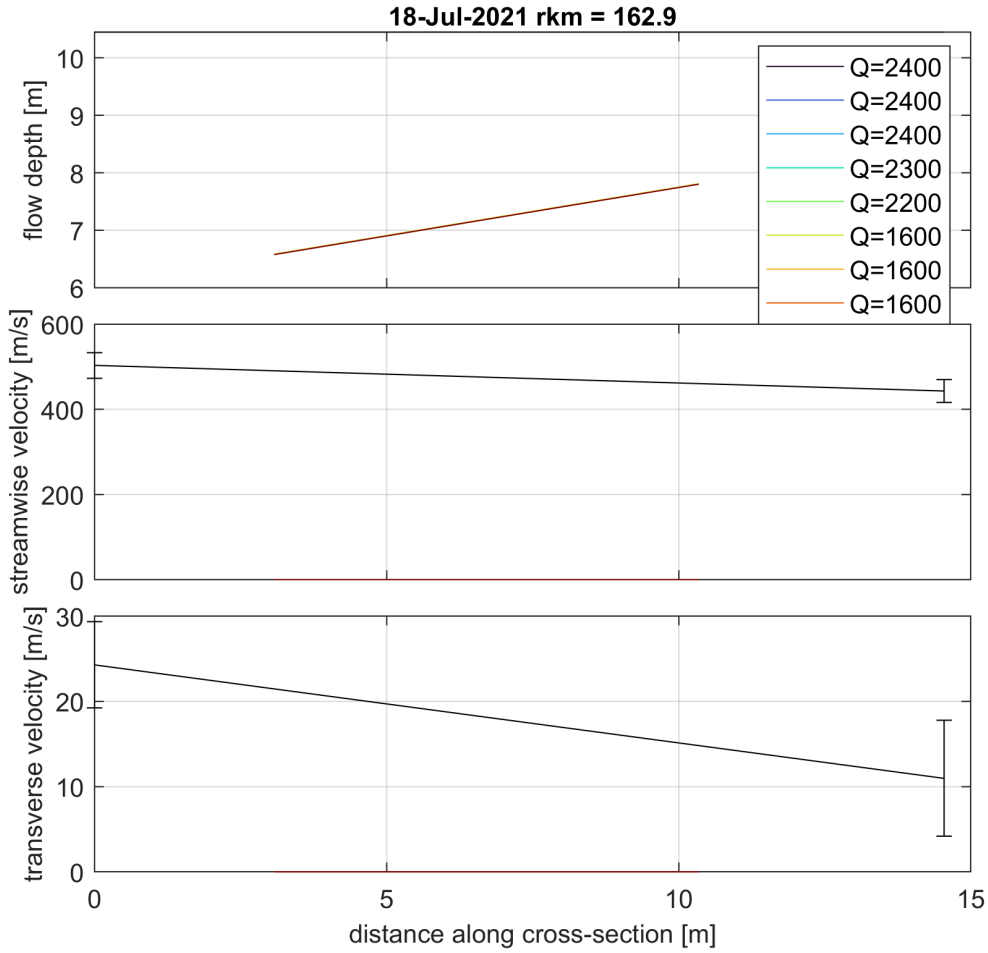

Figure C.2.49 Depth averaged velocity comparison for 18-7-2021 at river kilometre 162.9.

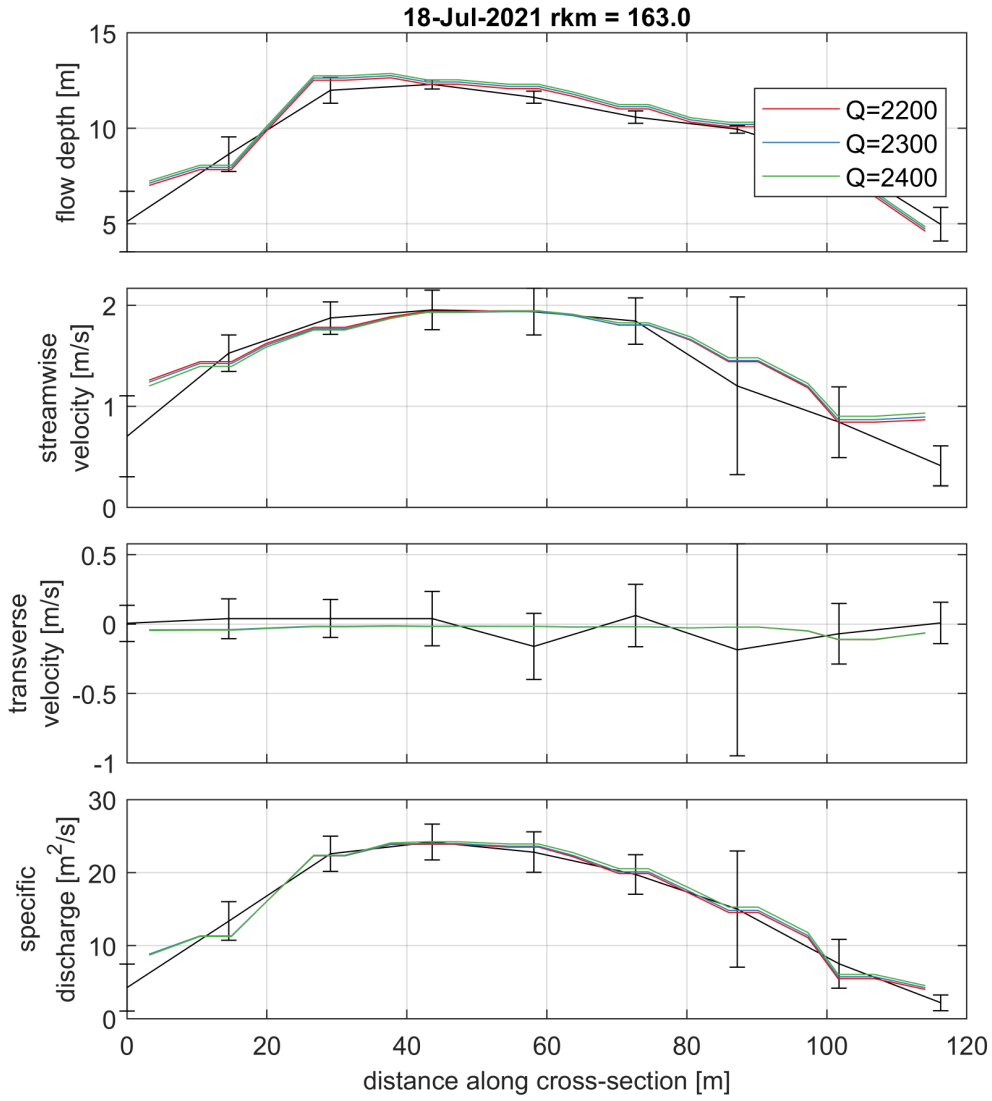

Figure C.2.50 Depth averaged velocity comparison for 18-7-2021 at river kilometre 163.0.

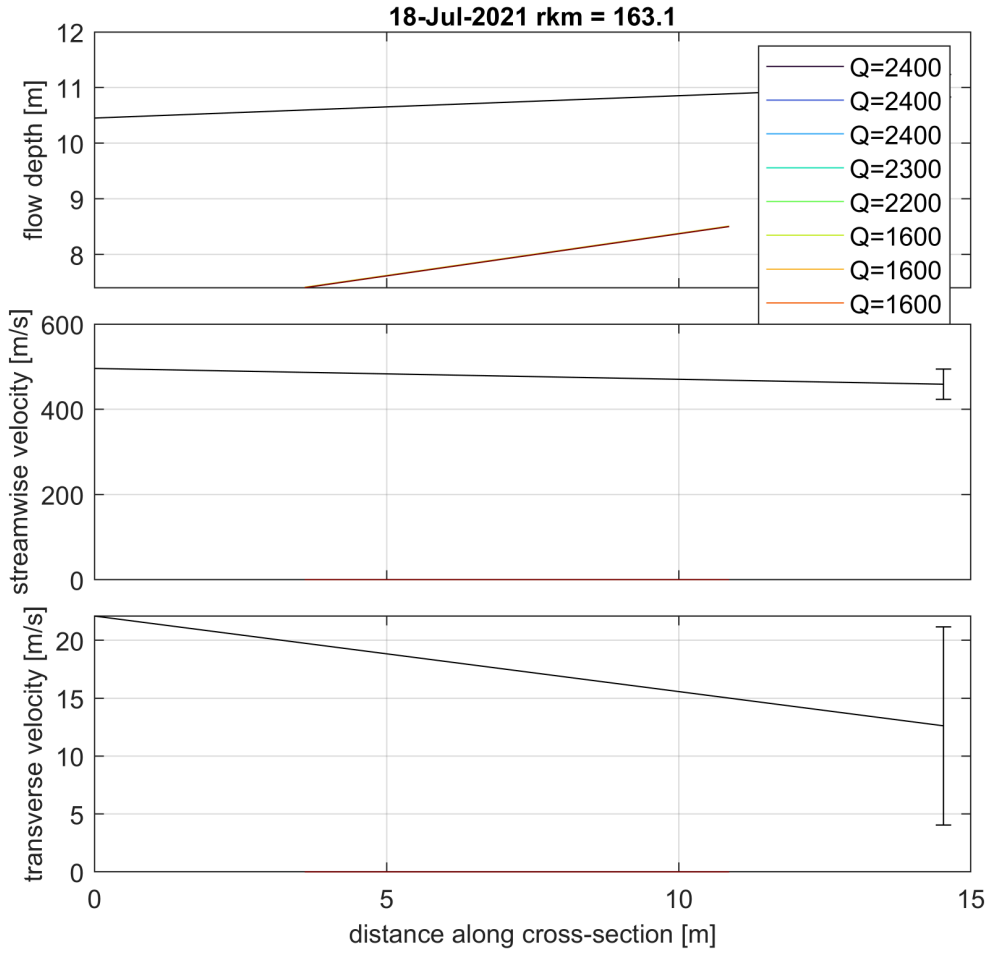

Figure C.2.51 Depth averaged velocity comparison for 18-7-2021 at river kilometre 163.1.

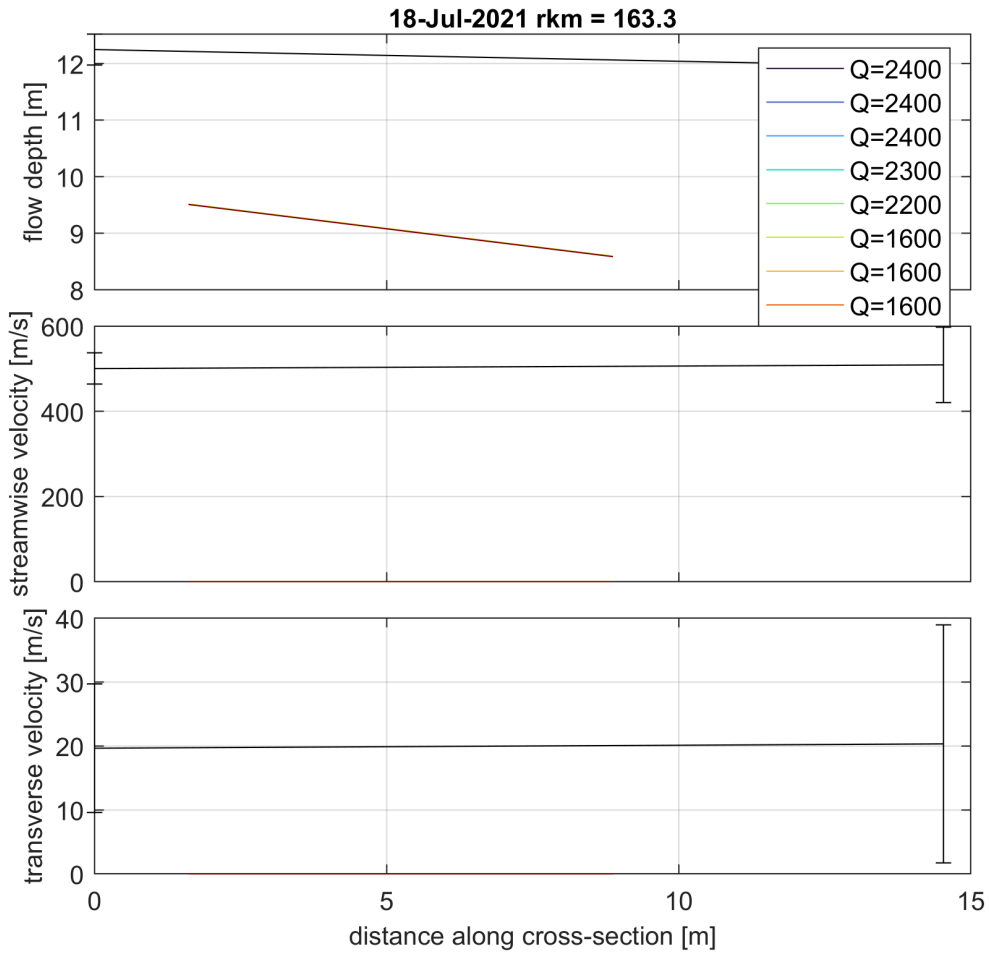

Figure C.2.52 Depth averaged velocity comparison for 18-7-2021 at river kilometre 163.3.

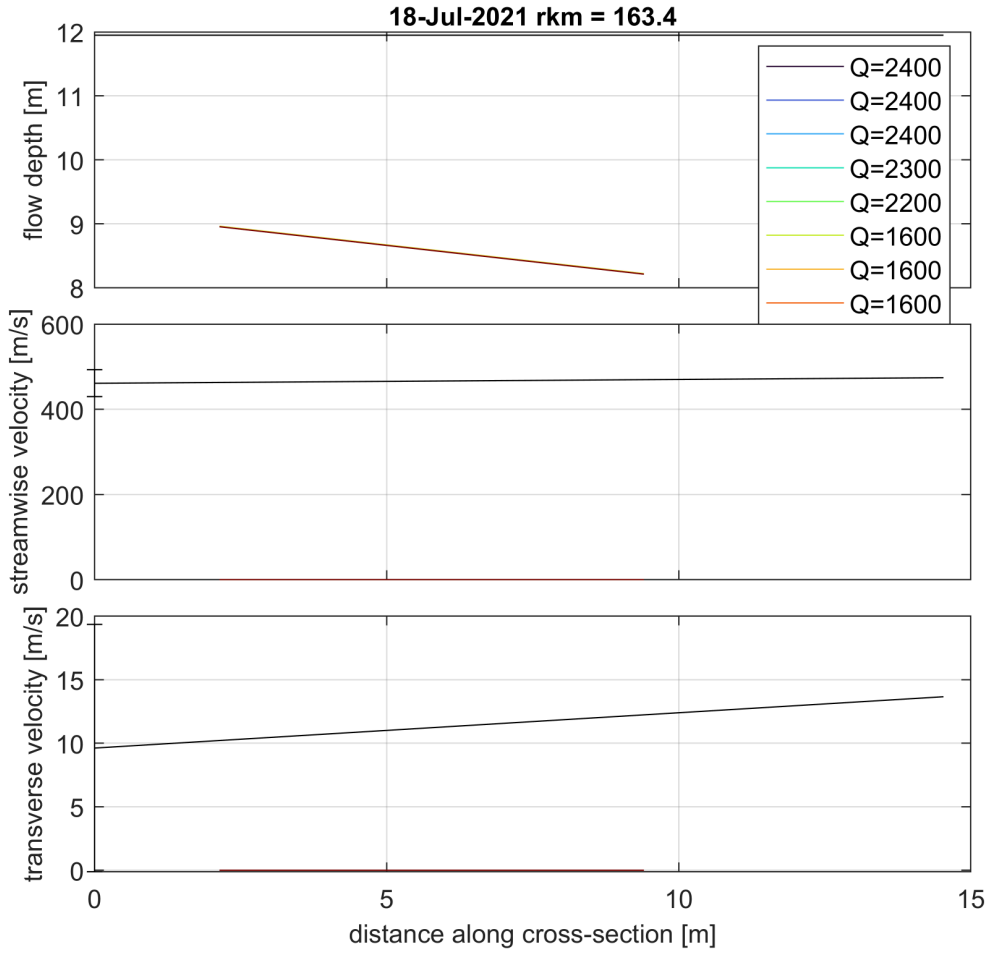

Figure C.2.53 Depth averaged velocity comparison for 18-7-2021 at river kilometre 163.4.

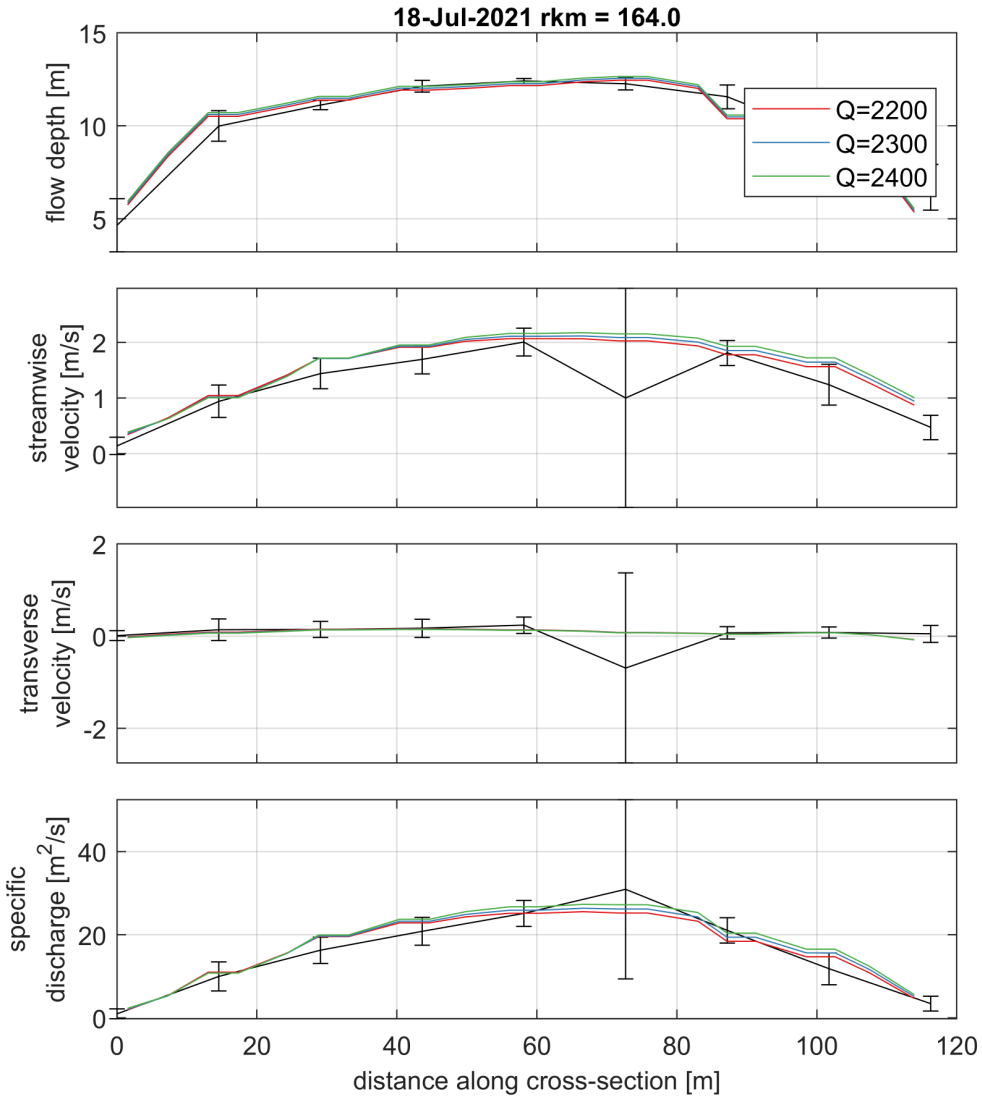

Figure C.2.54 Depth averaged velocity comparison for 18-7-2021 at river kilometre 164.0.

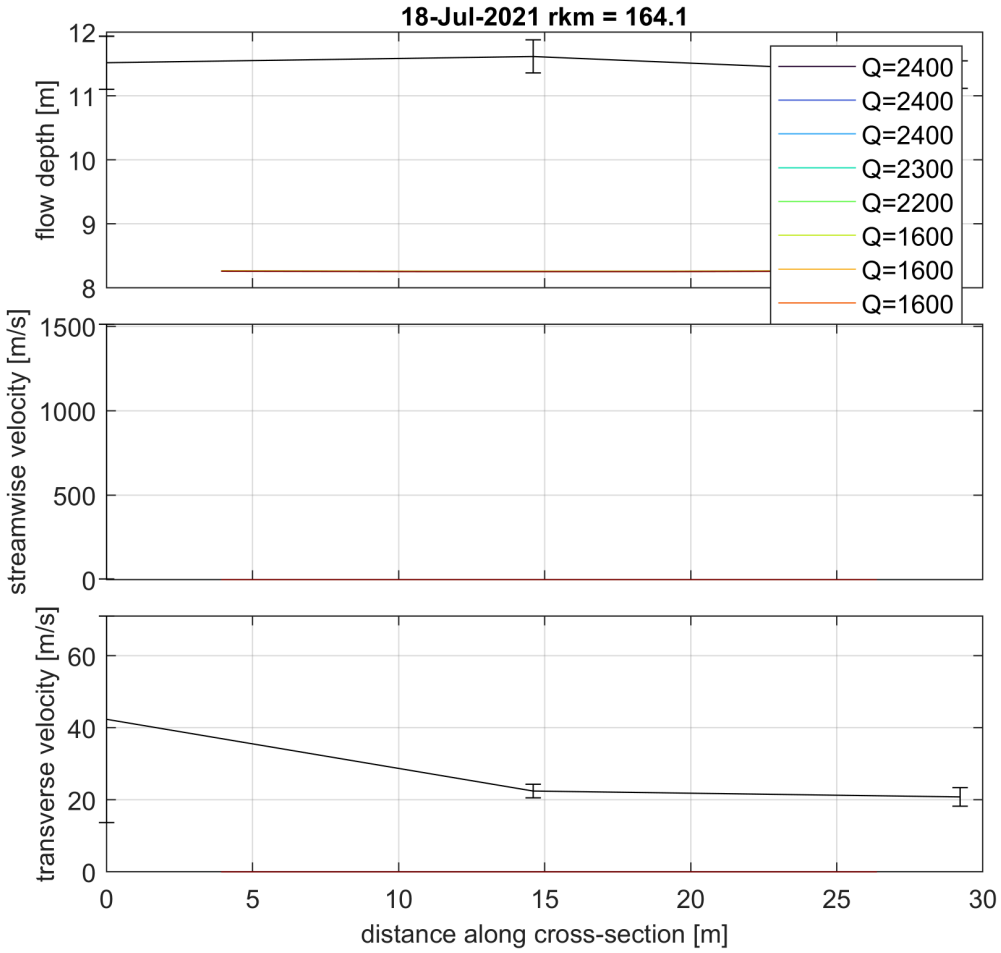

Figure C.2.55 Depth averaged velocity comparison for 18-7-2021 at river kilometre 164.1.

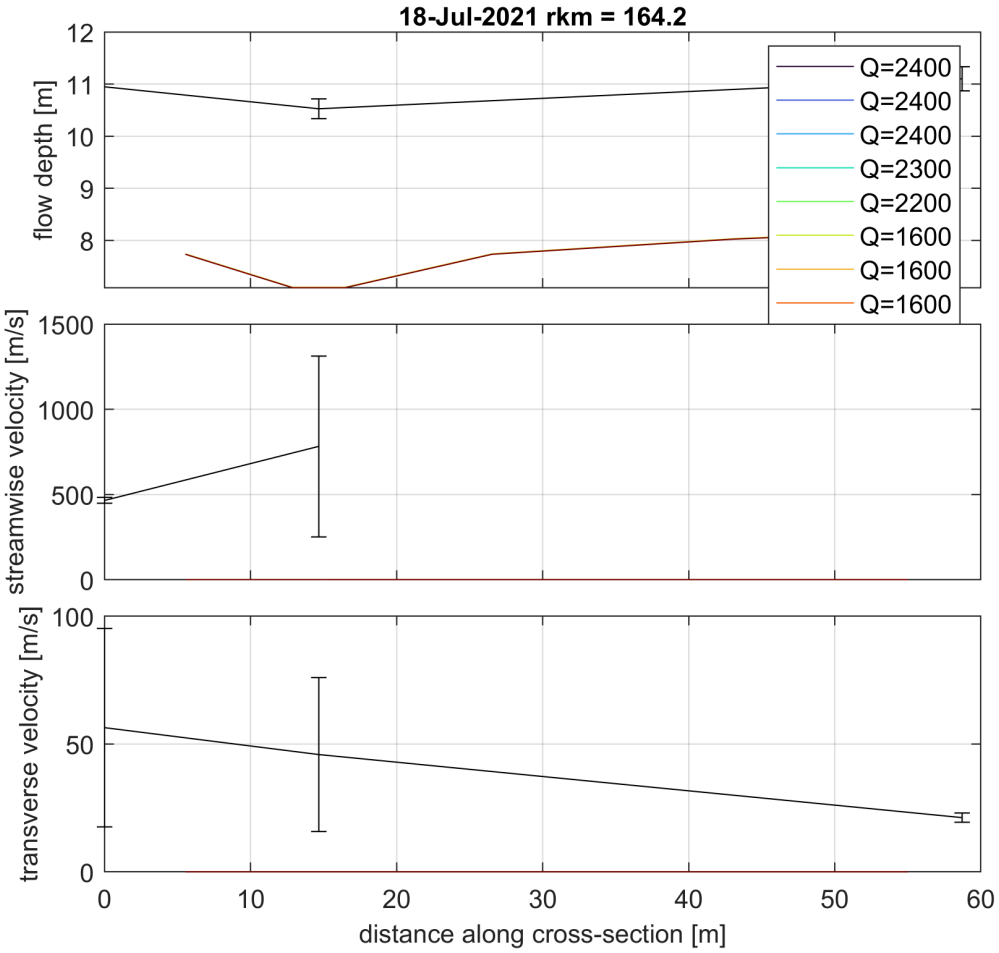

Figure C.2.56 Depth averaged velocity comparison for 18-7-2021 at river kilometre 164.2.

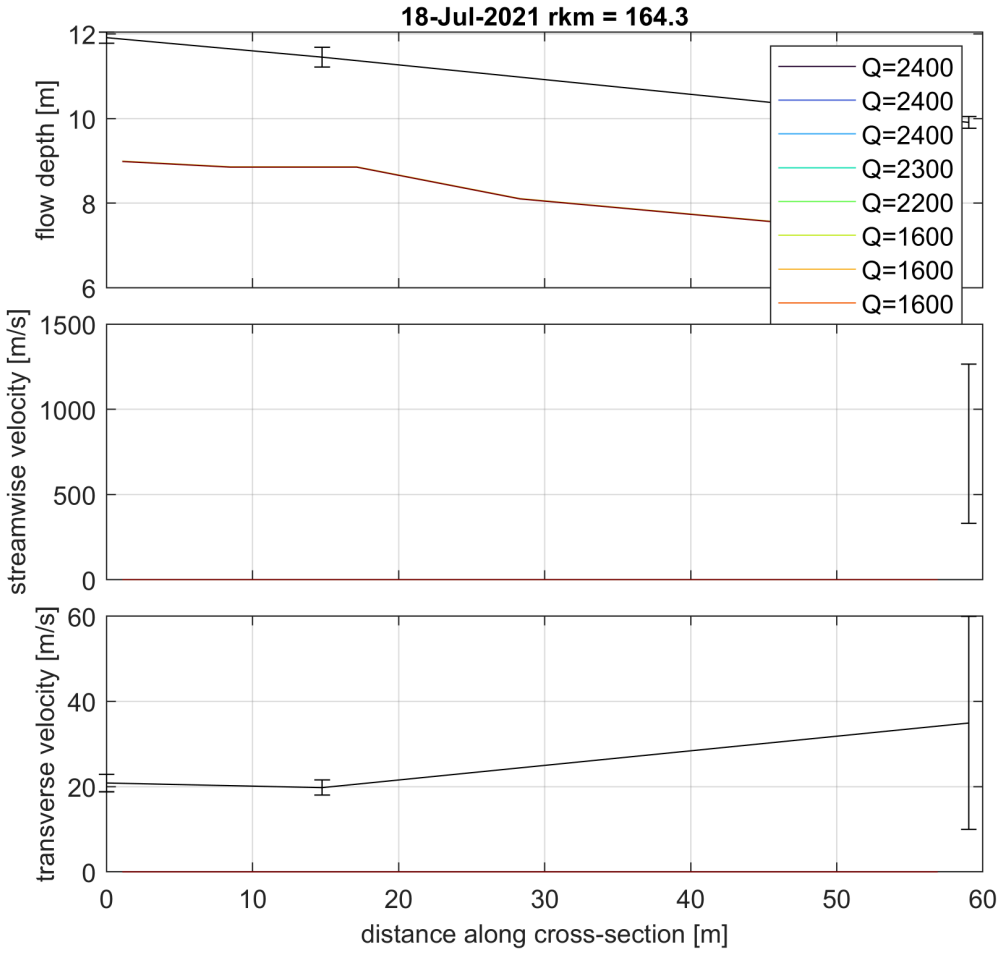

Figure C.2.57 Depth averaged velocity comparison for 18-7-2021 at river kilometre 164.3.

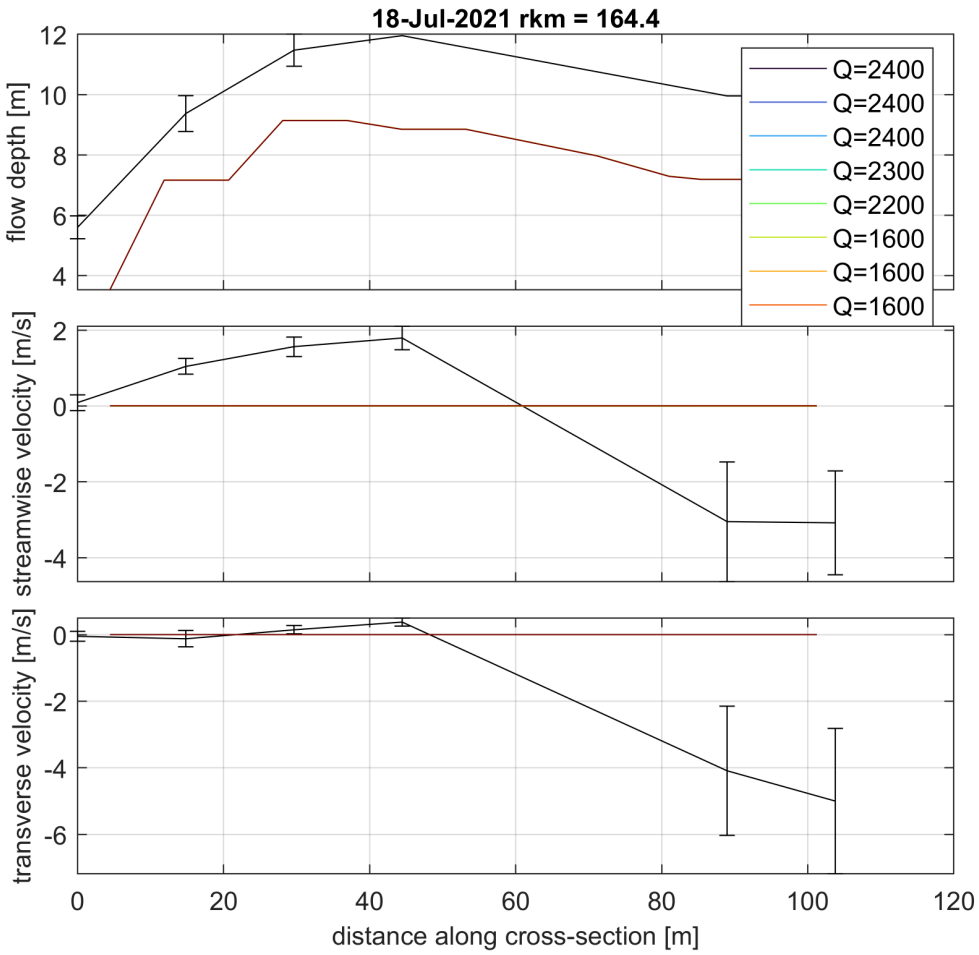

Figure C.2.58 Depth averaged velocity comparison for 18-7-2021 at river kilometre 164.4.

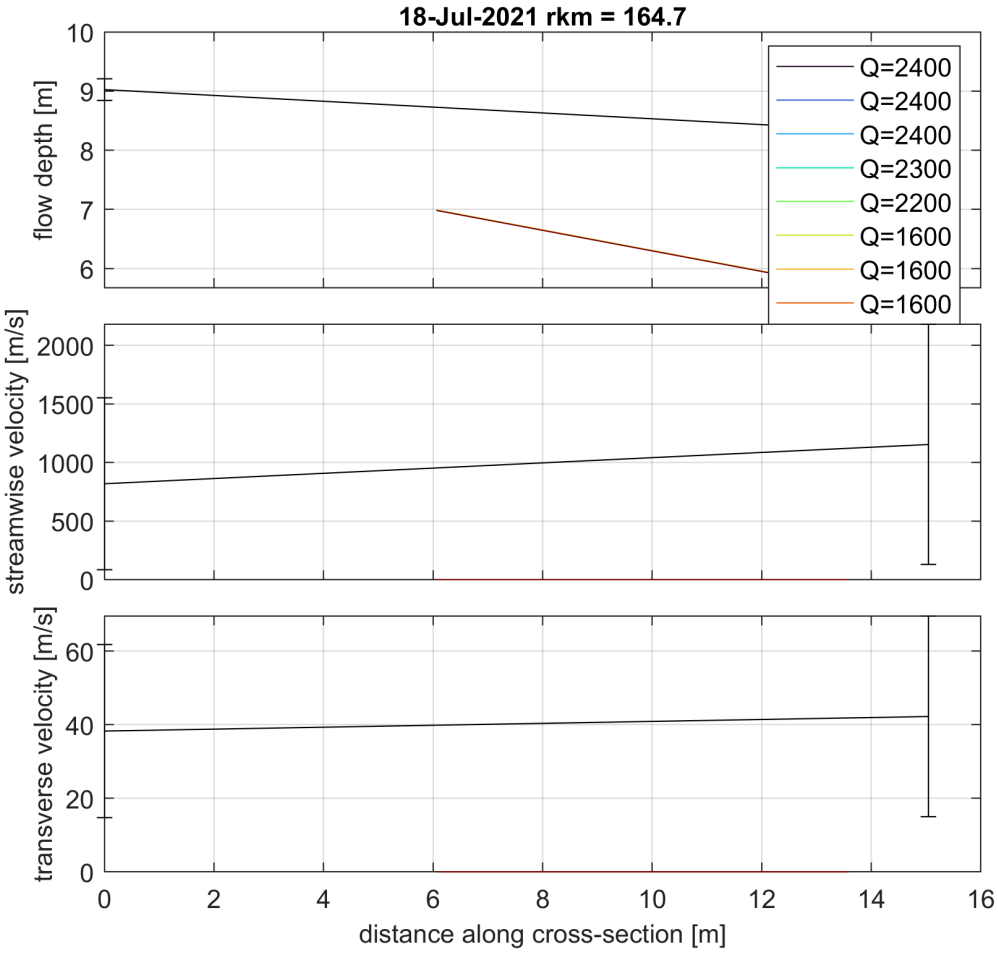

Figure C.2.59 Depth averaged velocity comparison for 18-7-2021 at river kilometre 164.7.

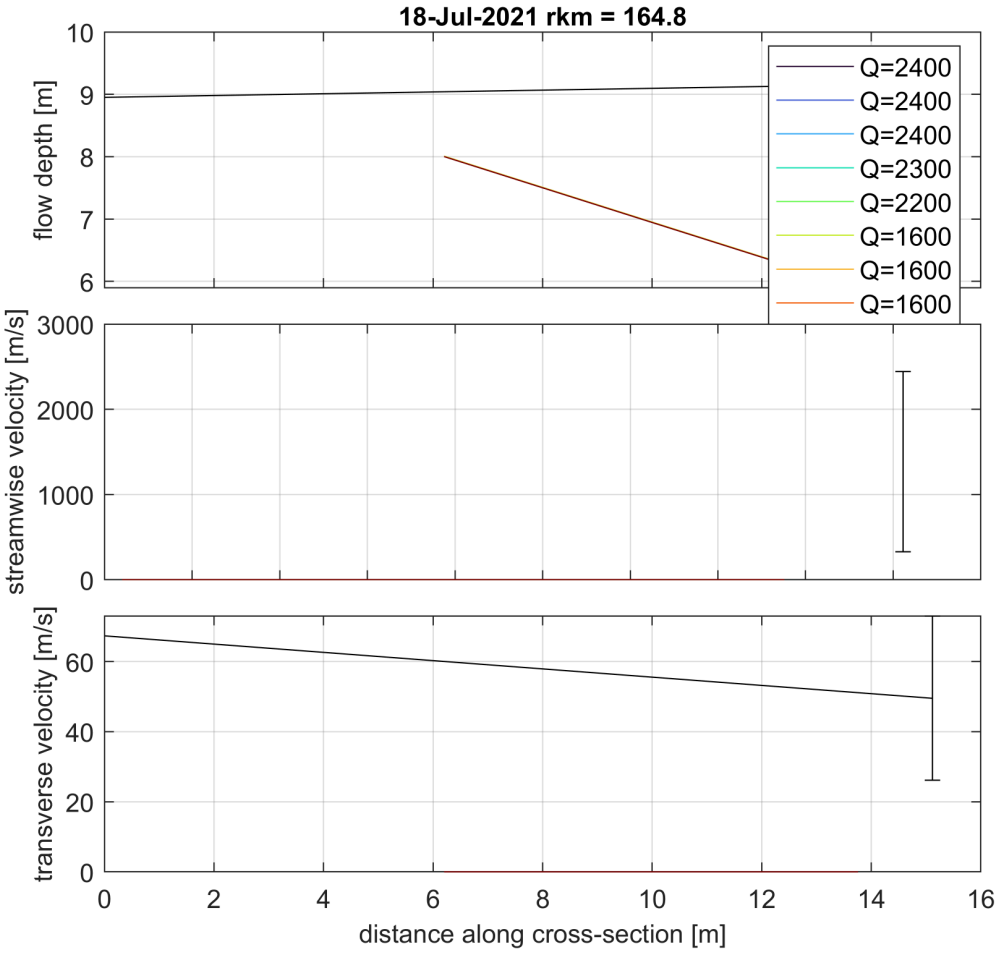

Figure C.2.60 Depth averaged velocity comparison for 18-7-2021 at river kilometre 164.8.

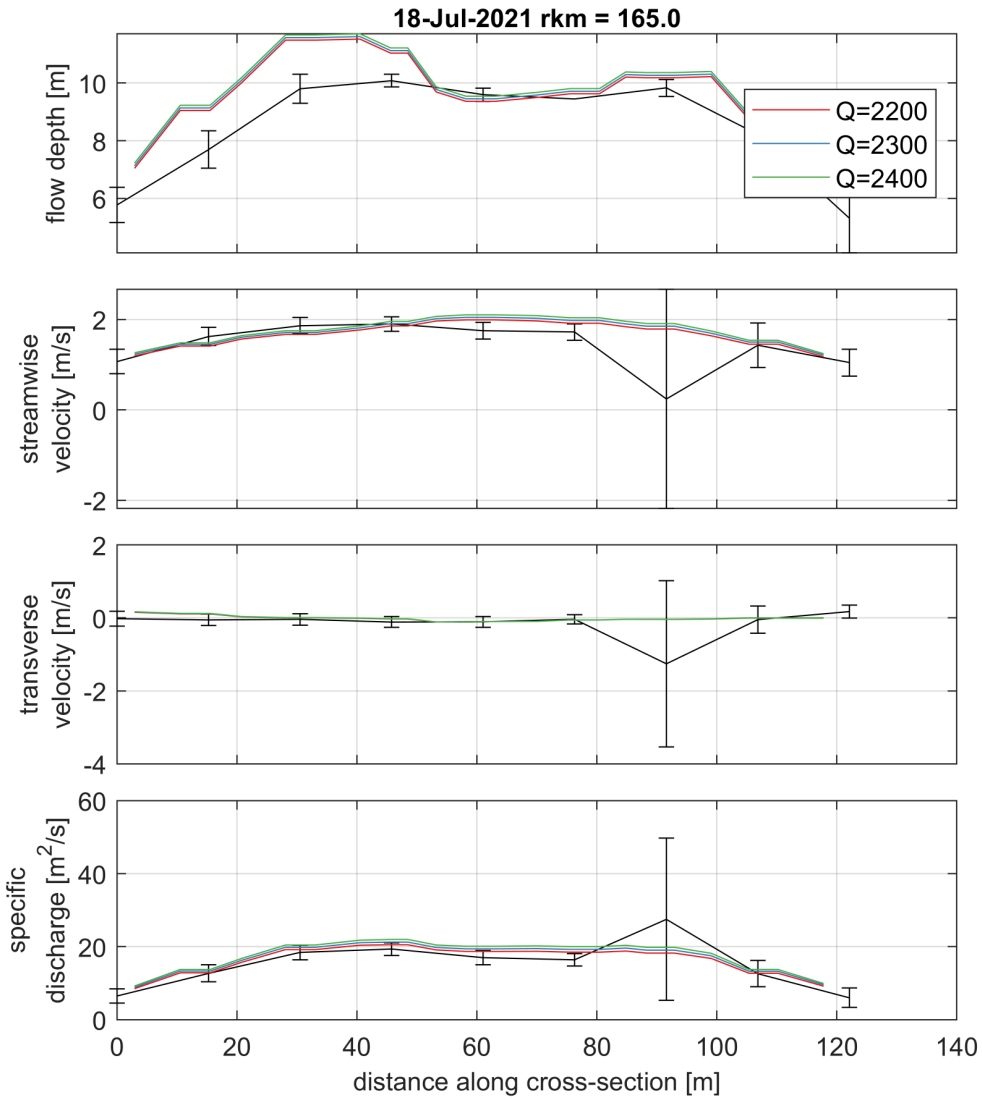

Figure C.2.61 Depth averaged velocity comparison for 18-7-2021 at river kilometre 165.0.

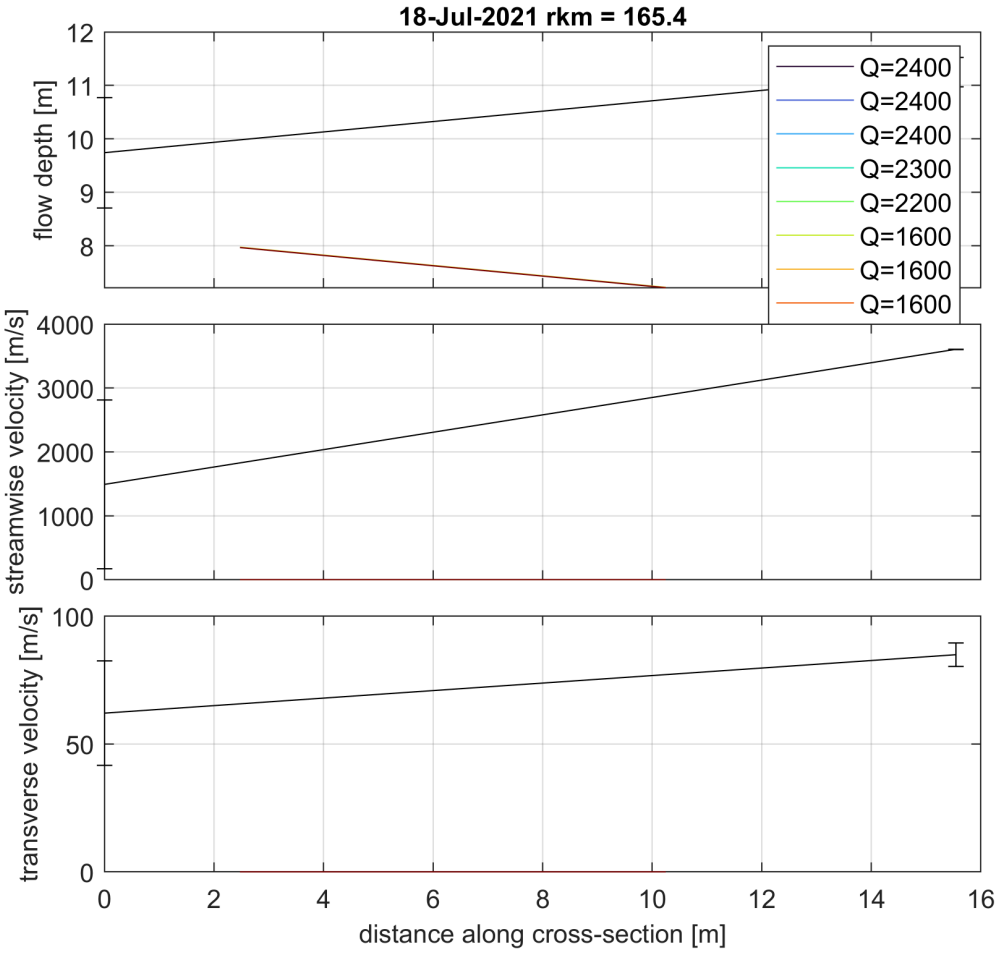

Figure C.2.62 Depth averaged velocity comparison for 18-7-2021 at river kilometre 165.4.

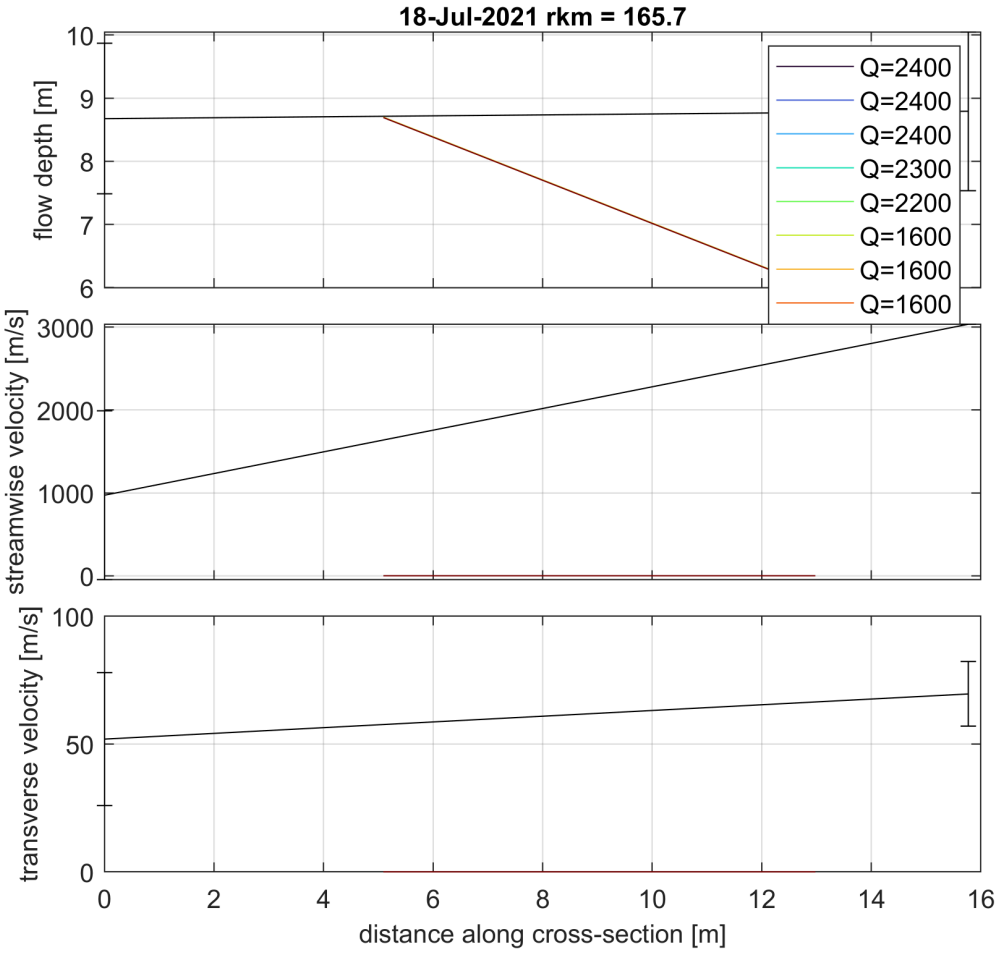

Figure C.2.63 Depth averaged velocity comparison for 18-7-2021 at river kilometre 165.7.

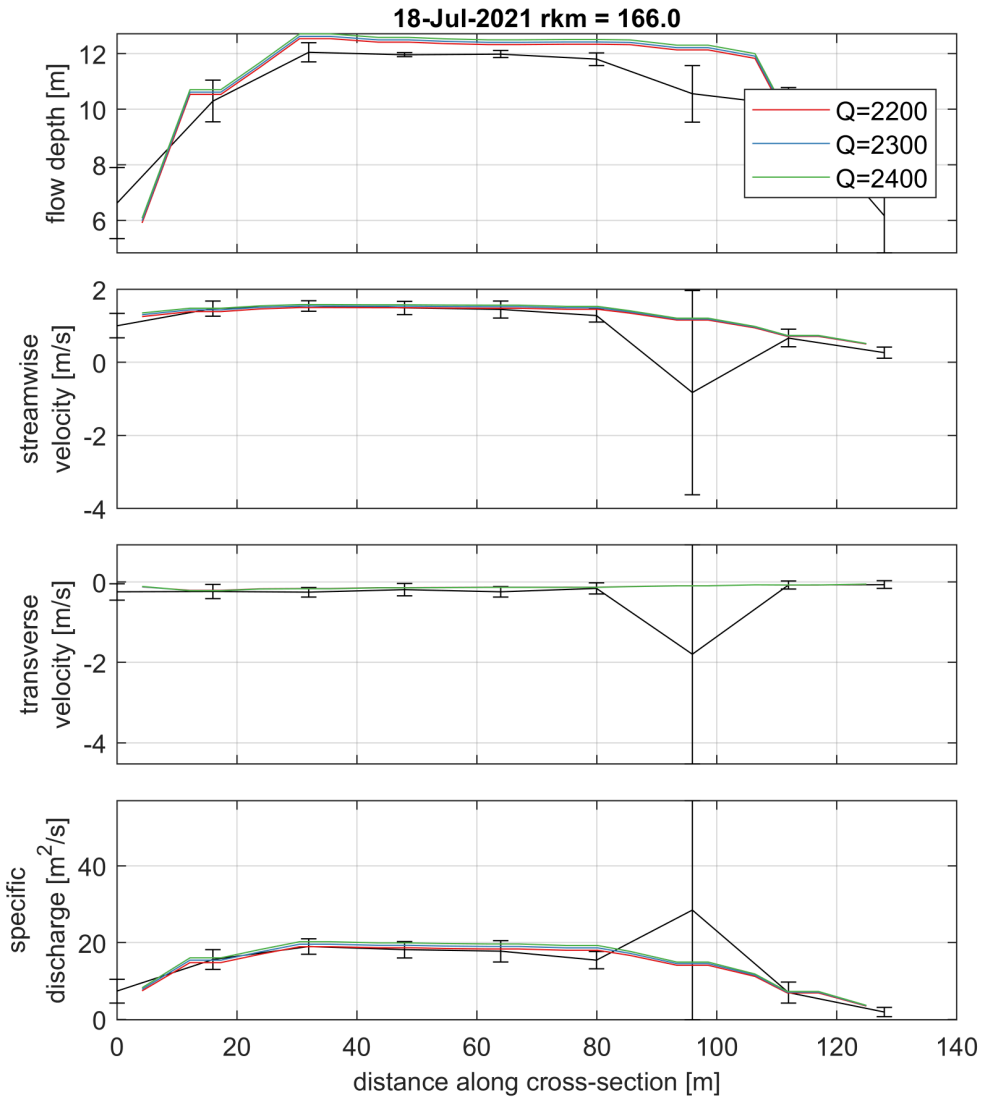

Figure C.2.64 Depth averaged velocity comparison for 18-7-2021 at river kilometre 166.0.

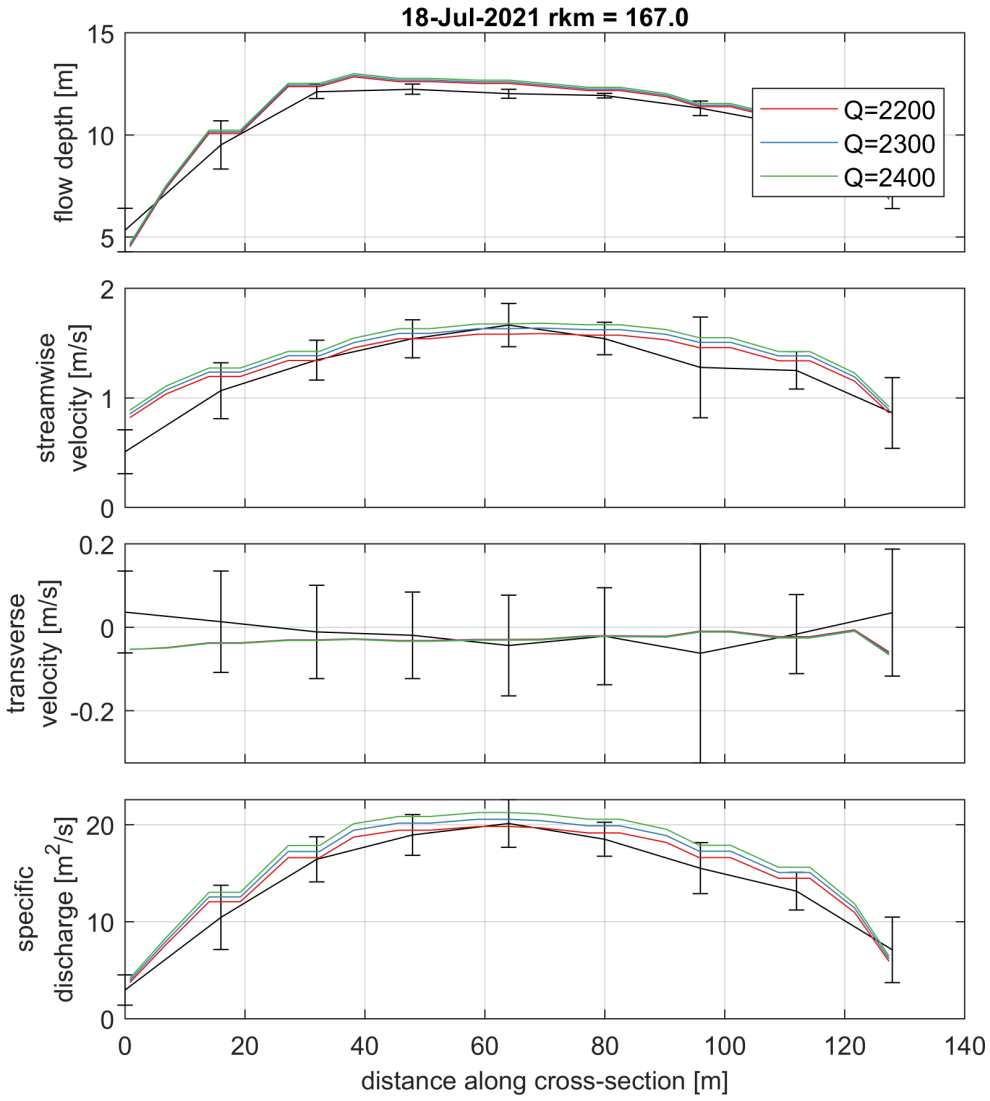

Figure C.2.65 Depth averaged velocity comparison for 18-7-2021 at river kilometre 167.0.

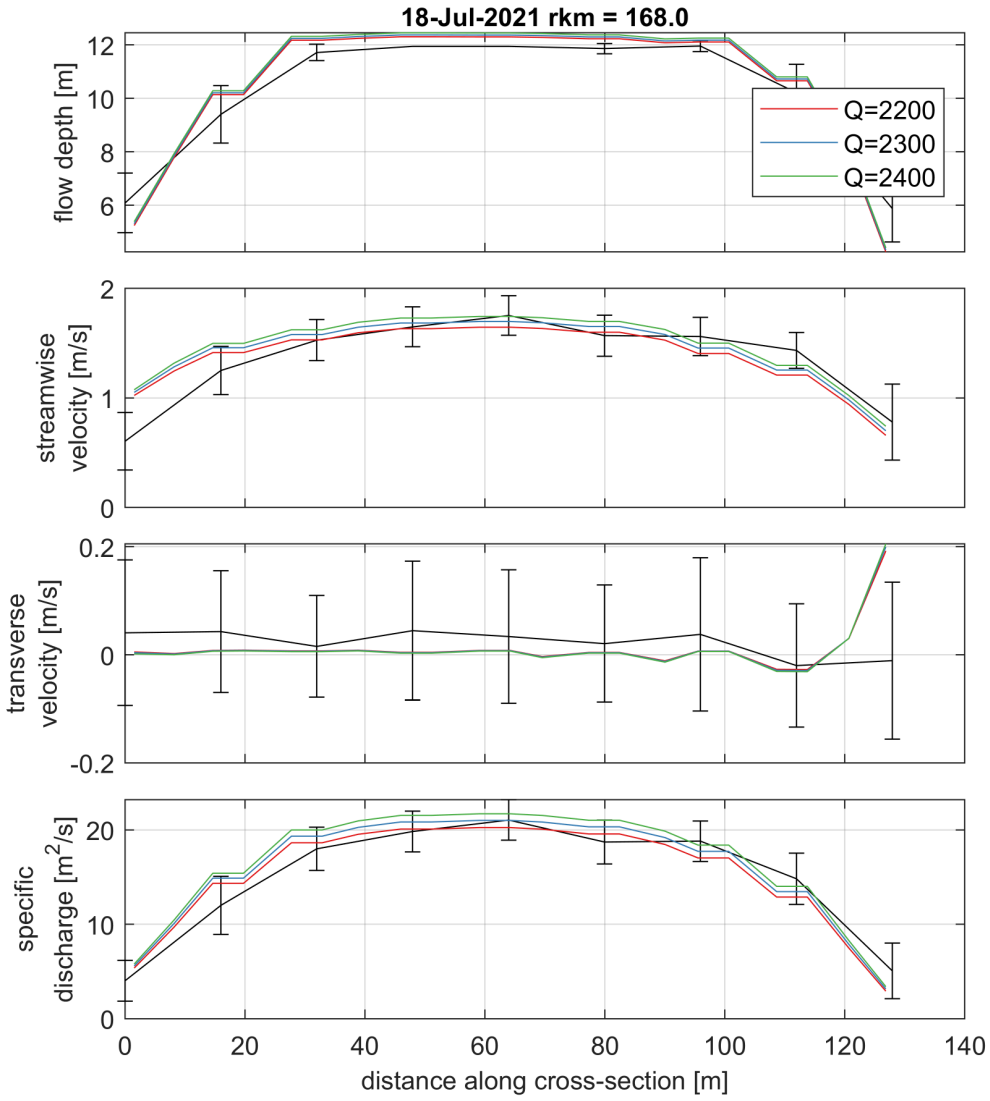

Figure C.2.66 Depth averaged velocity comparison for 18-7-2021 at river kilometre 168.0.

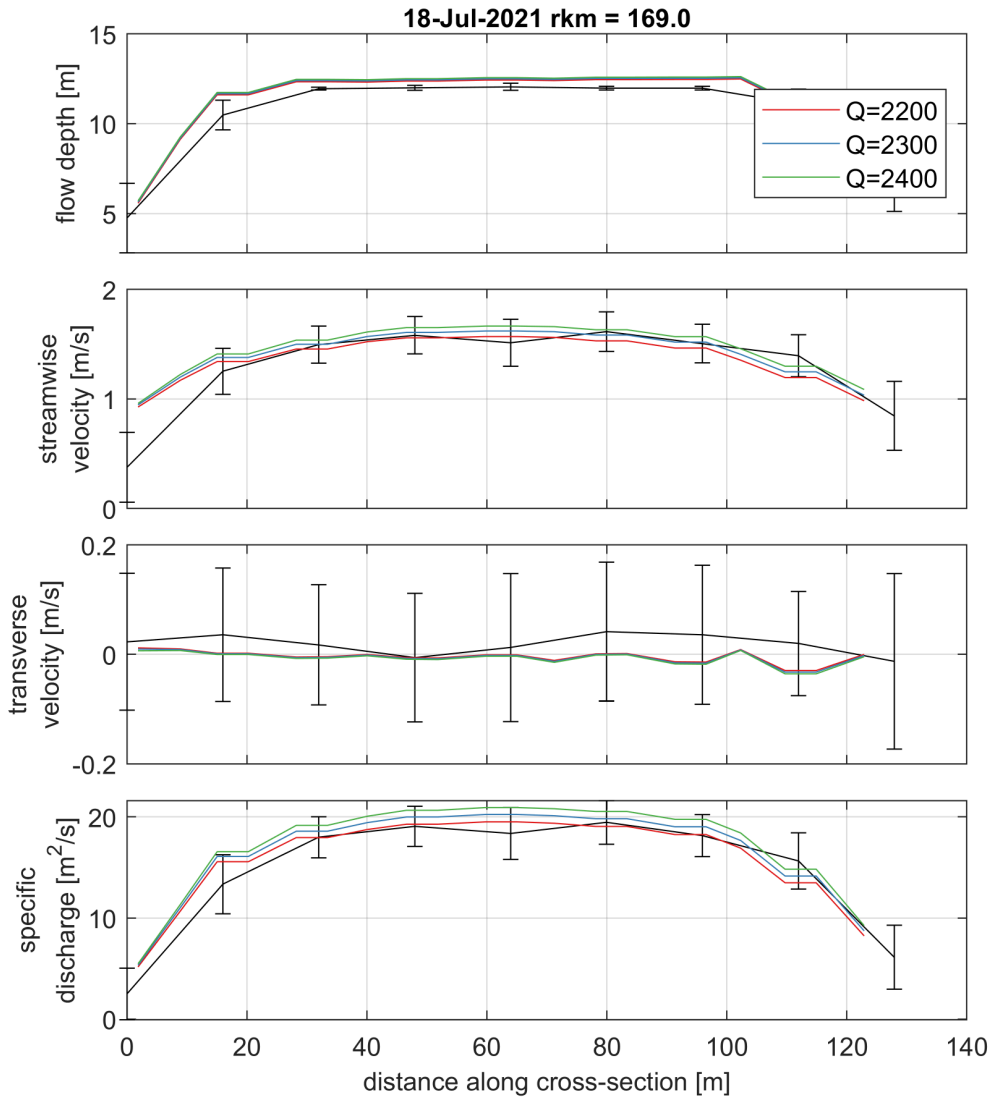

Figure C.2.67 Depth averaged velocity comparison for 18-7-2021 at river kilometre 169.0.

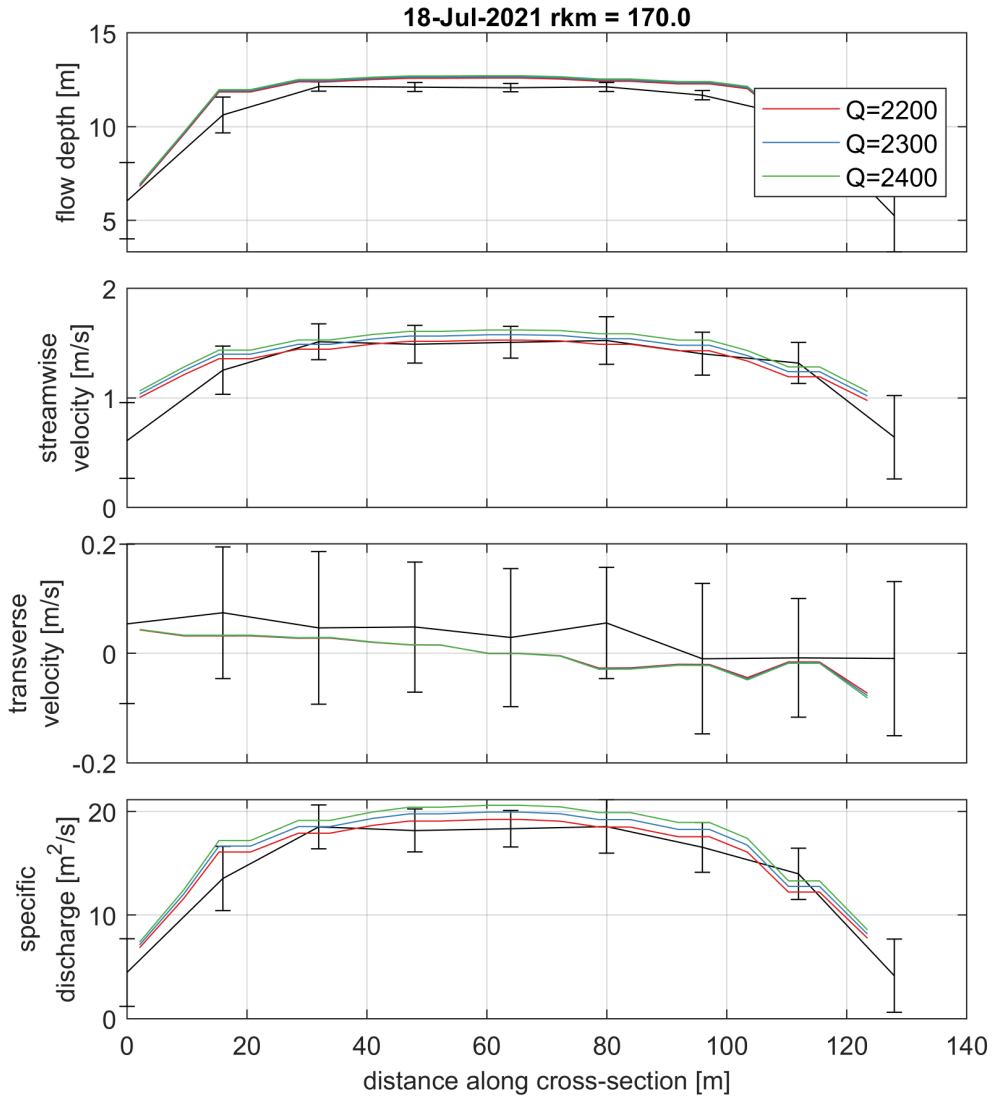

Figure C.2.68 Depth averaged velocity comparison for 18-7-2021 at river kilometre 170.0.

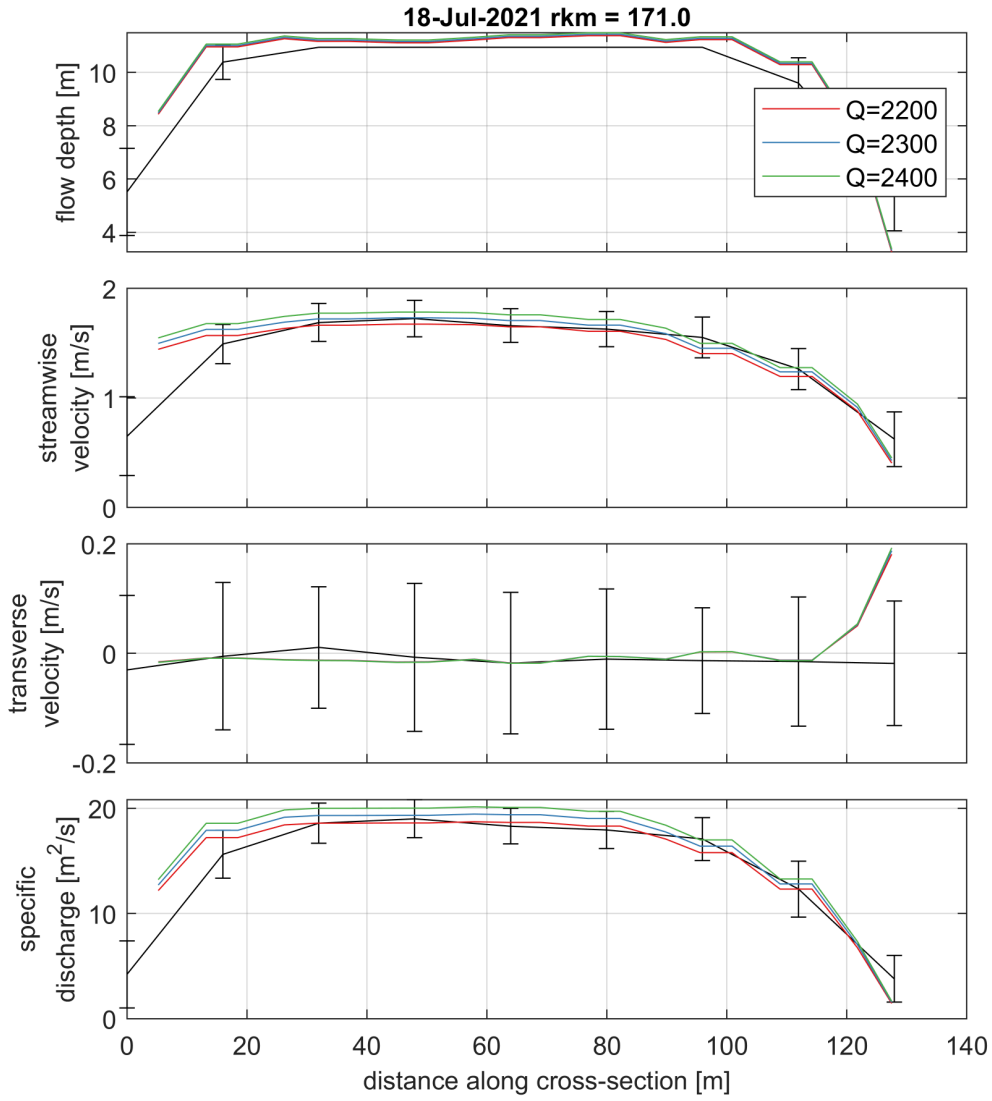

Figure C.2.69 Depth averaged velocity comparison for 18-7-2021 at river kilometre 171.0.

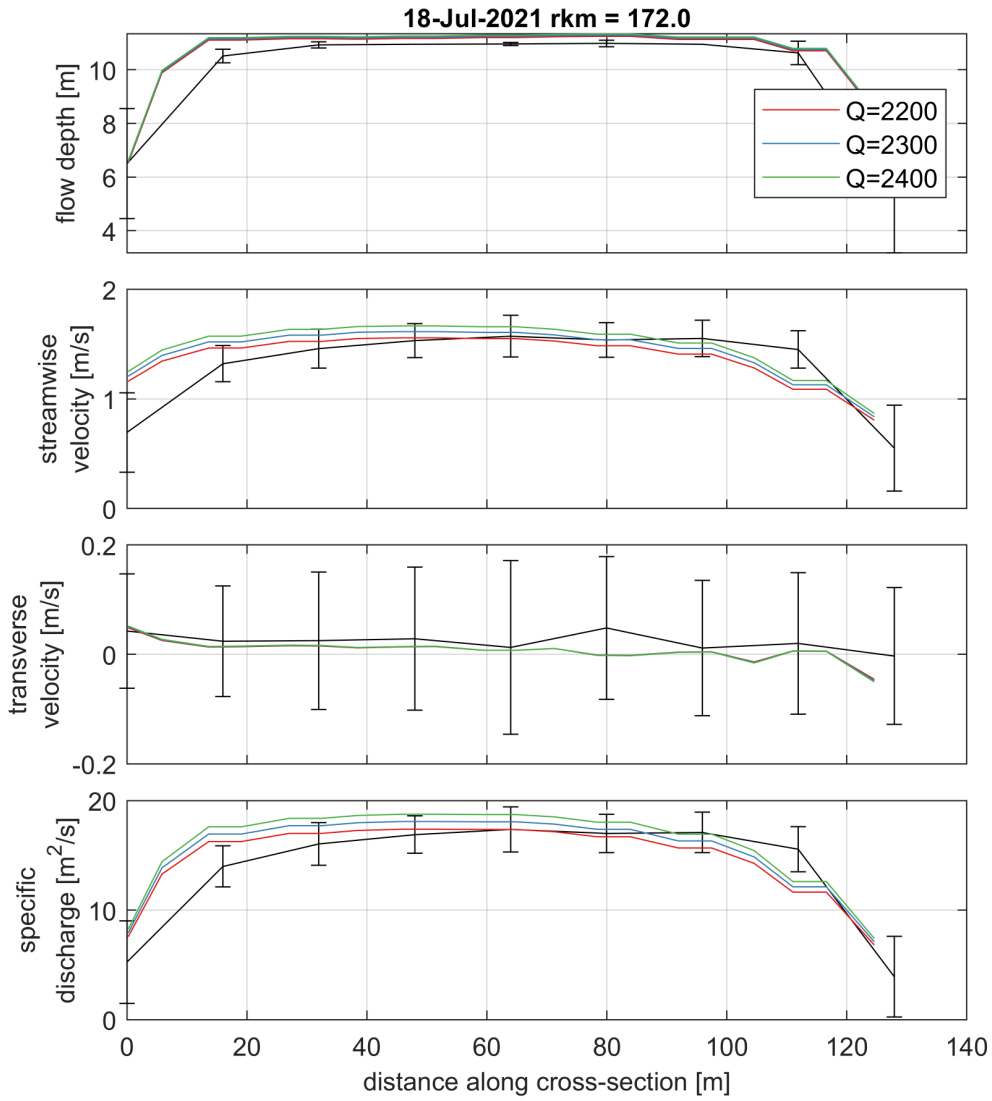

Figure C.2.70 Depth averaged velocity comparison for 18-7-2021 at river kilometre 172.0.

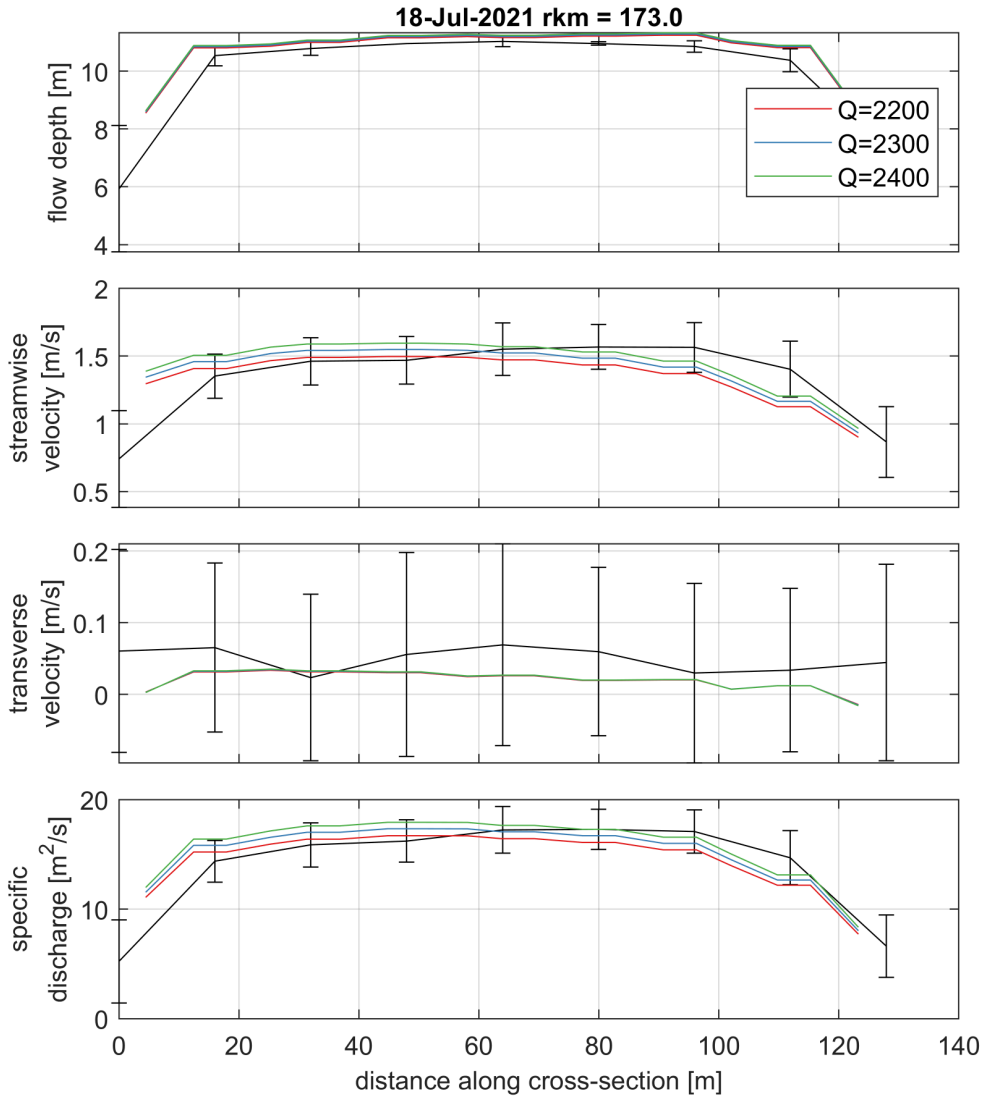

Figure C.2.71 Depth averaged velocity comparison for 18-7-2021 at river kilometre 173.0.

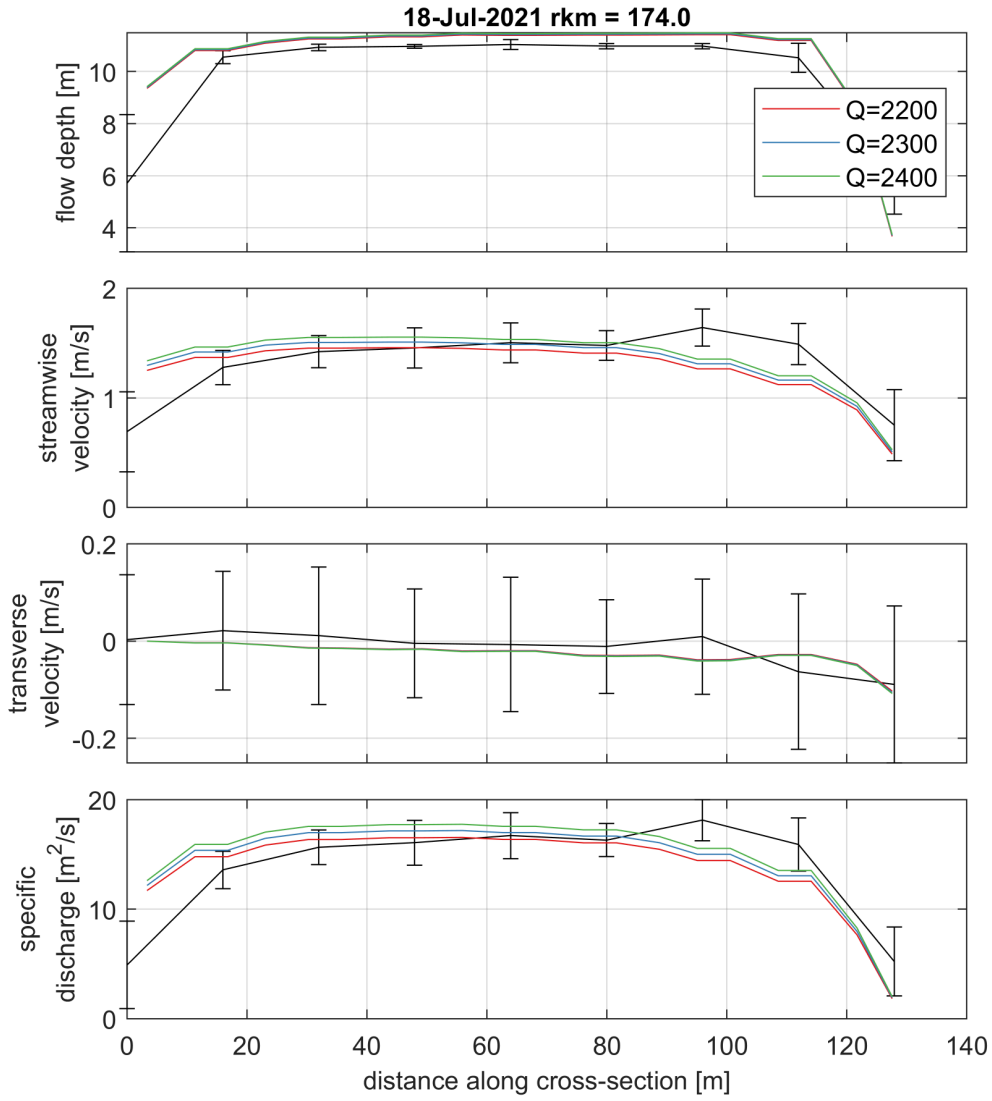

Figure C.2.72 Depth averaged velocity comparison for 18-7-2021 at river kilometre 174.0.

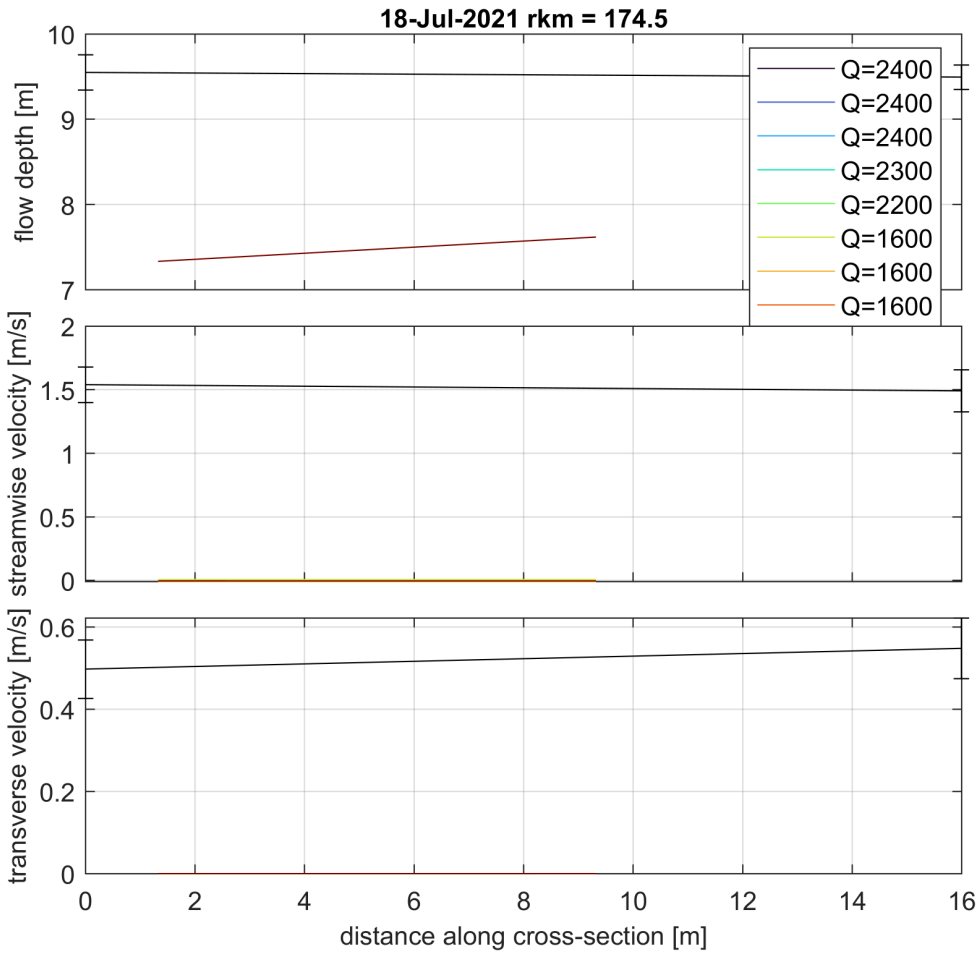

Figure C.2.73 Depth averaged velocity comparison for 18-7-2021 at river kilometre 174.5.

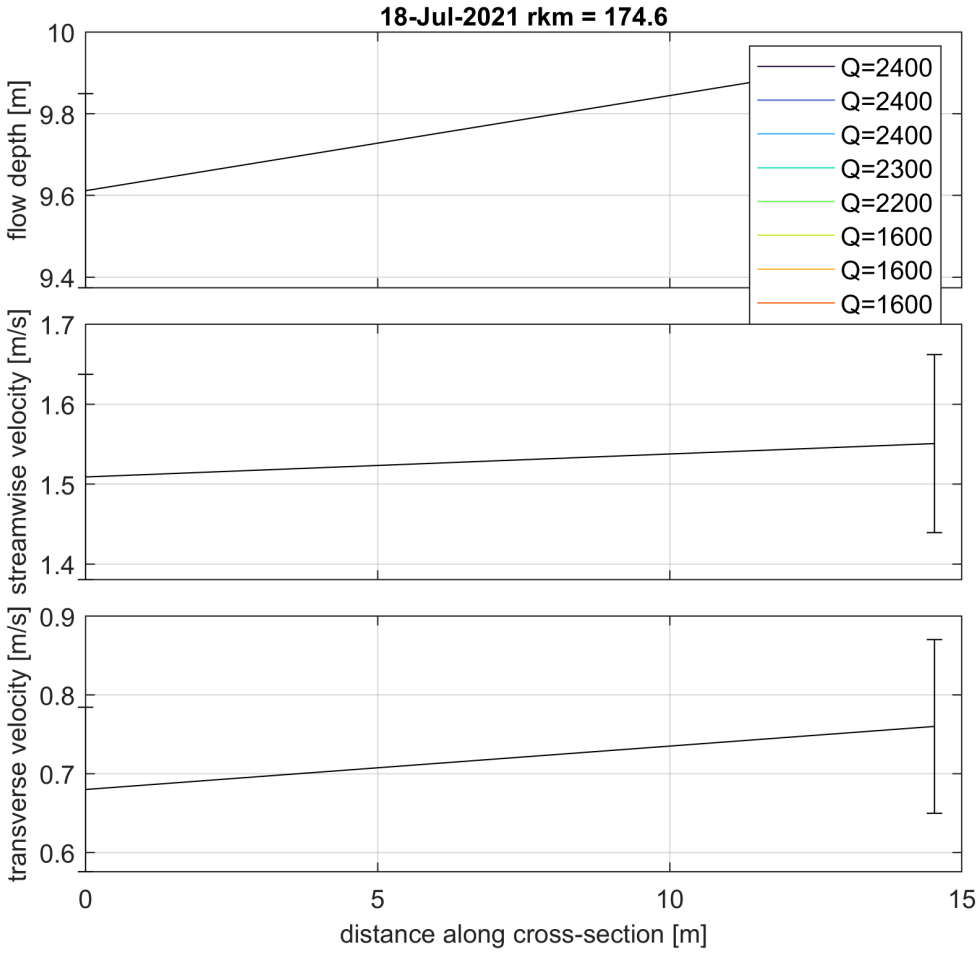

Figure C.2.74 Depth averaged velocity comparison for 18-7-2021 at river kilometre 174.6.

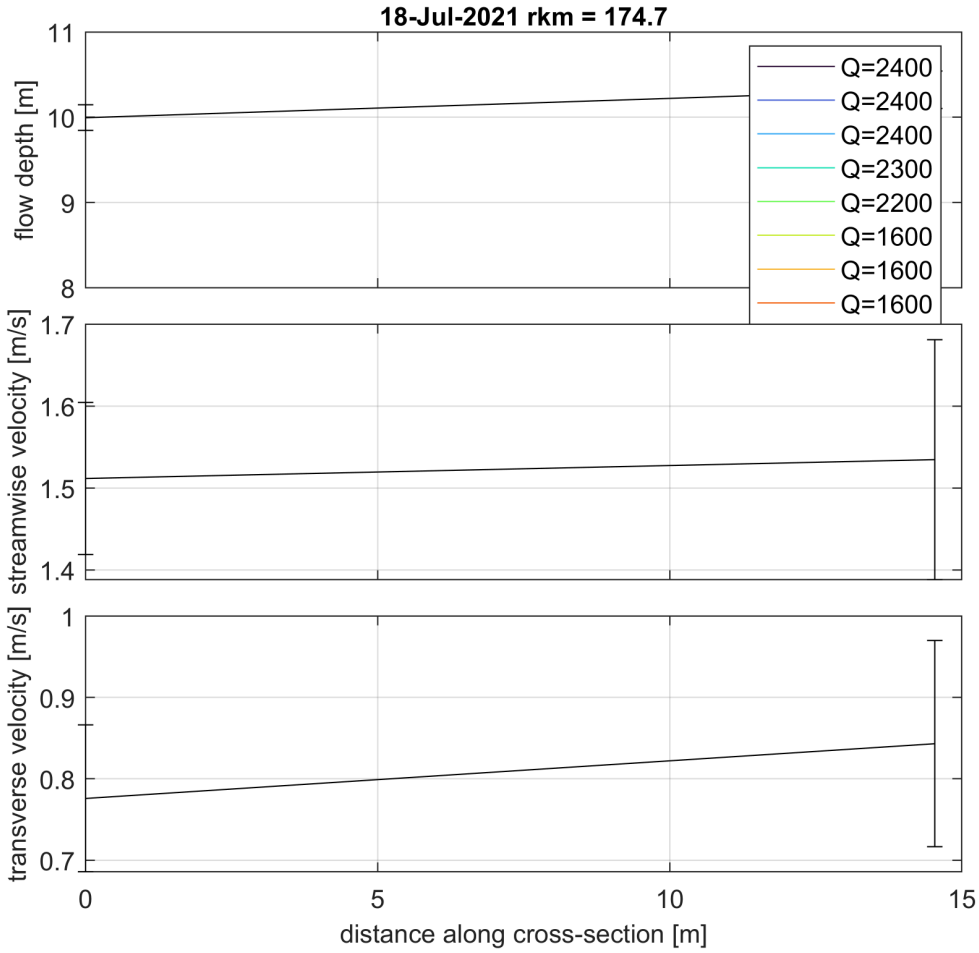

Figure C.2.75 Depth averaged velocity comparison for 18-7-2021 at river kilometre 174.7.

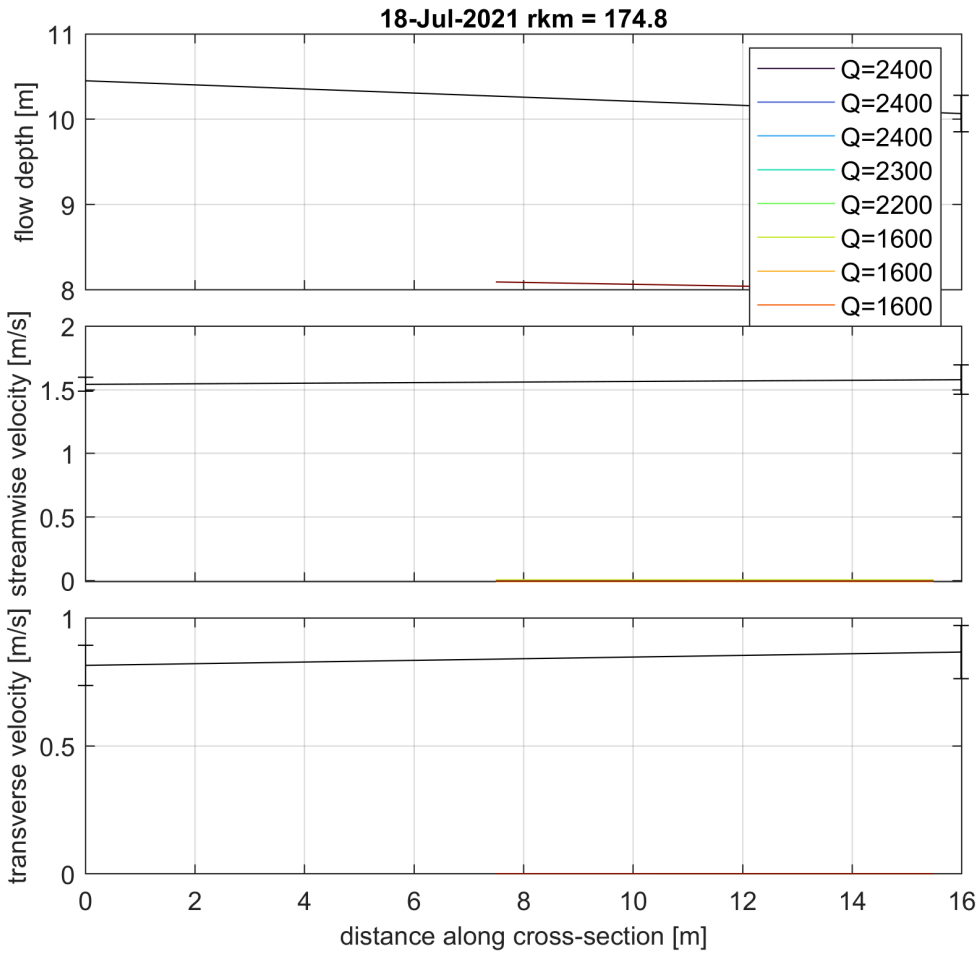

Figure C.2.76 Depth averaged velocity comparison for 18-7-2021 at river kilometre 174.8.

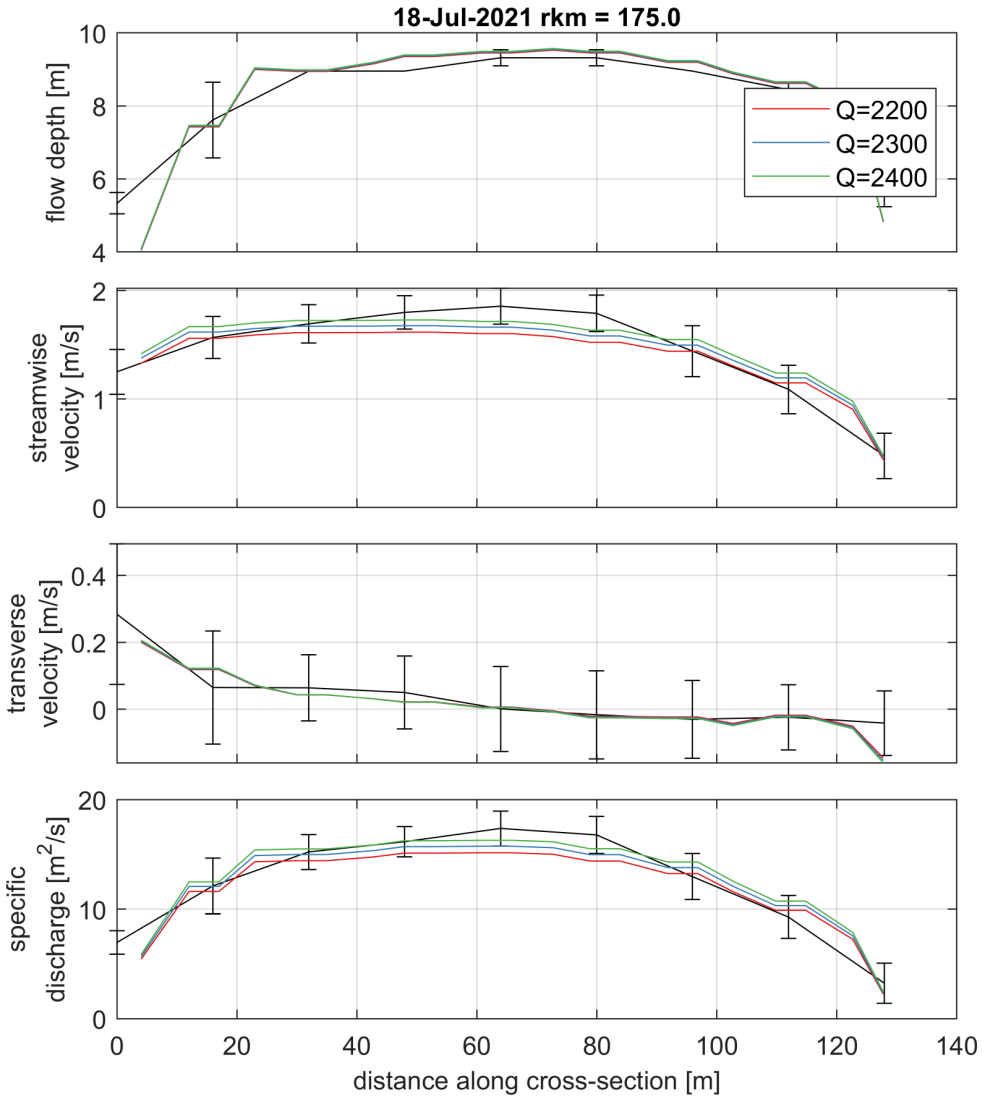

Figure C.2.77 Depth averaged velocity comparison for 18-7-2021 at river kilometre 175.0.

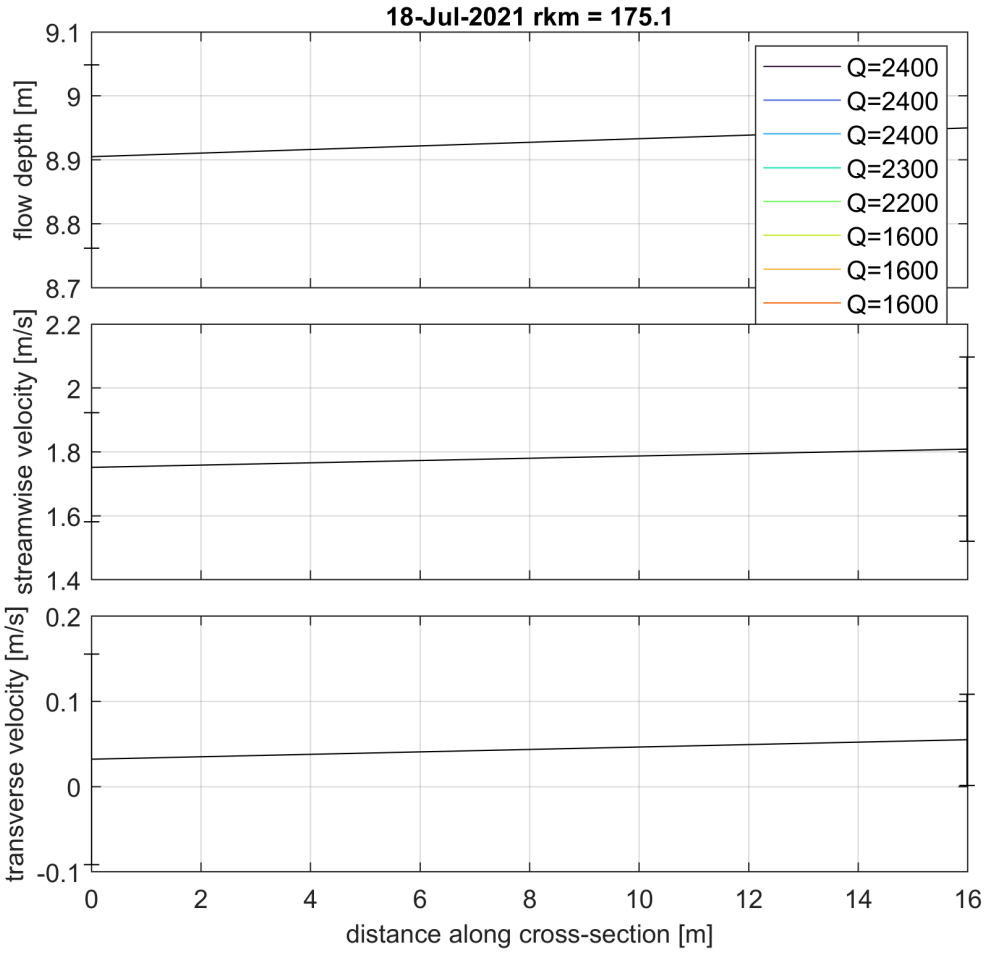

Figure C.2.78 Depth averaged velocity comparison for 18-7-2021 at river kilometre 175.1.

D Sediment availability

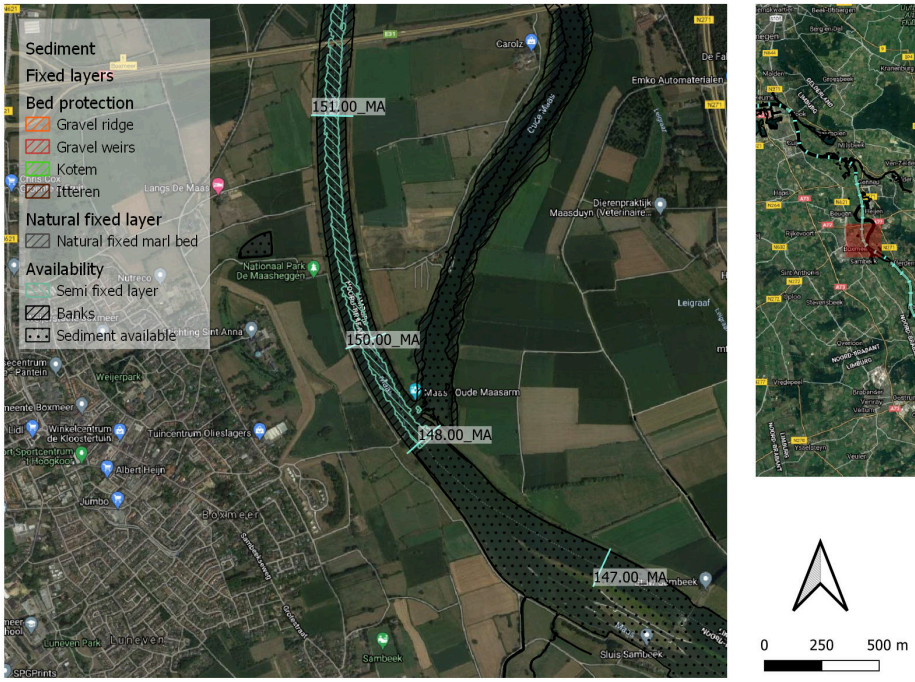

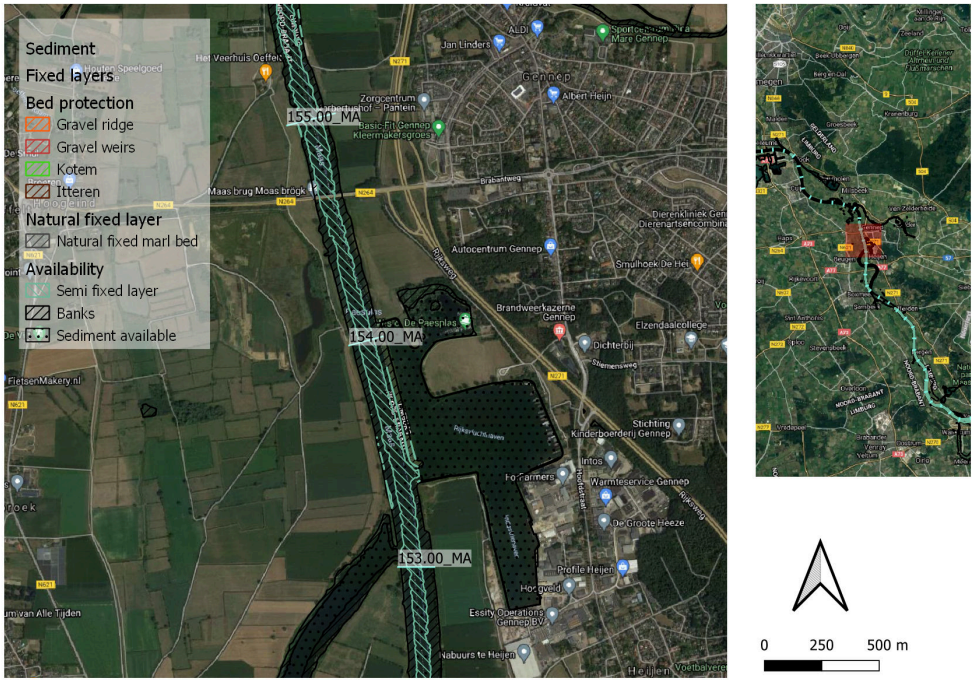
Sediment
Fixed layers
Bed protection
Gravel ridge
Gravel weirs
Kotem
Itteren
Natural fixed layer
Natural fixed marl bed
Availability
Semi fixed layer
Banks
Sediment available
155.00_MA
154.00_MA
153.00_MA
0
250
500 m

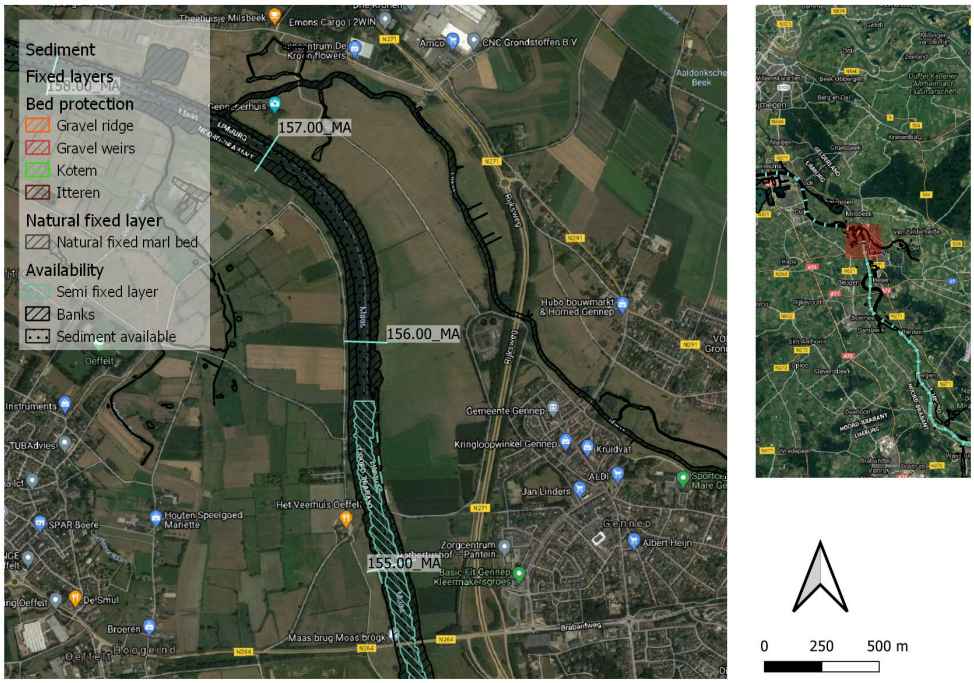
Sediment
Fixed layers
Bed protection
Gravel ridge
Gravel weirs
Kotem
Itteren
Natural fixed layer
Natural fixed marl bed
Availability
Semi fixed layer
Banks
Sediment available
157.00_MA
156.00_MA
155.00_MA
0
250
500 m


Sediment
Fixed layers
Bed protection
Gravel ridge
Gravel weirs
Kotem
Itteren
Natural fixed layer
Natural fixed marl bed
Availability
Semi fixed layer
Banks
Sediment available
159.00_MA
158.00_MA
157.00_MA
Millsbeek
Kwekerij Berns B.V.
Somlis Thai Massage & Spa
SPAR Willemsen
Bouwkringloop De Loods
Ovenberg
De Haas Verhuur
Meges Elektrotechniek
Act Organized
Van Huet Glass Logistics
Drie Kronen
Theehuisje Millsbeek
Emons Cargo | 2WIN
RSC Music & Design
De Rijtjes
Oeffelt
Inkerezi Spolders
0
250
500 m


Sediment
Fixed layers
Bed protection
Gravel ridge
Gravel weirs
Kotem
Itteren
Natural fixed layer
Natural fixed marl bed
Availability
Semi fixed layer
Banks
Sediment available
161.00_MA
160.00_MA
159.00_MA
Stichting Waterrecreatie Delfinarium
Kwekerbosch
Boathouse De Leopplank
Strandpaviljoen Dushi 2.0
Astrantia Sportvereniging
Heikant
Perfecto
De Zomereik | Houten Hekwerken
Garage Van Duijnhoven
Middelaar
J.H. Verheijen
Haarmode Jacqueline
Landschapspraamping Bos Kop
Speciale School voor Basisonderwijs De
Ink Rush
La Tertulia
Xtang Technologies B.V.
Sint-Agatha
Basisschool Lindekring
Voetbalvereniging VCA St. Agatha
Hendrikse Rozenkwekers VOF
RSC Music & Design
Graziosp webshop ruitersport
Hulij
A. Geerts B.V.
0
250
500 m

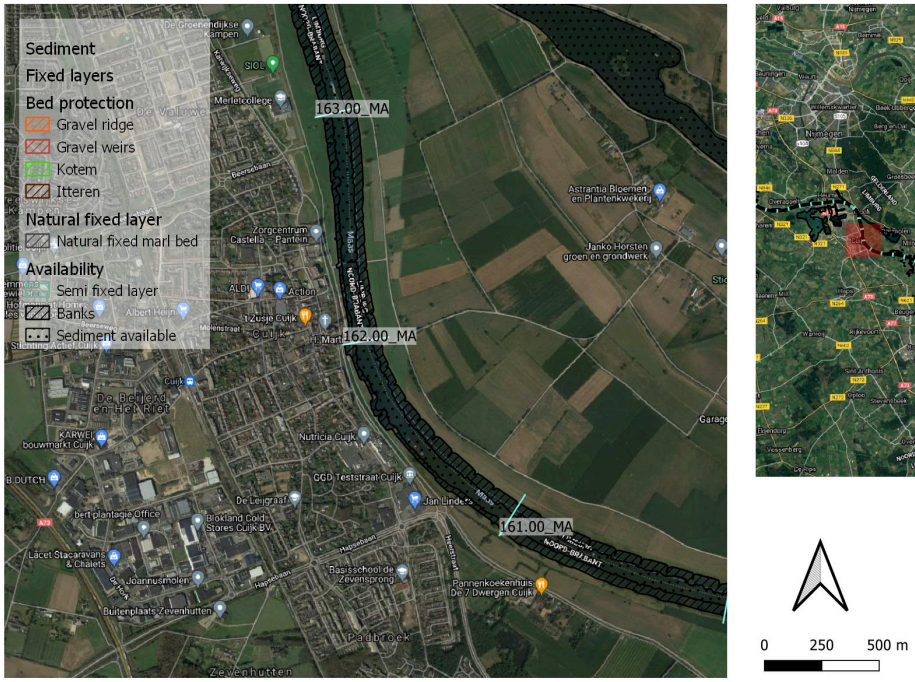
Sediment
Fixed layers
Bed protection
Gravel ridge
Gravel weirs
Kotem
Itteren
Natural fixed layer
Natural fixed marl bed
Availability
Semi fixed layer
Banks
Sediment available
163.00_MA
162.00_MA
161.00_MA
0
250
500 m


Sediment
Fixed layers
Bed protection
Gravel ridge
Gravel weirs
Kotem
Itteren
Natural fixed layer
Natural fixed marl bed
Availability
Semi fixed layer
Banks
Sediment available
165.00_MA
164.00_MA
163.00_MA
0
250
500 m


Sediment
Fixed layers
Bed protection
Gravel ridge
Gravel weirs
Kotem
Itteren
Natural fixed layer
Natural fixed marl bed
Availability
Semi fixed layer
Banks
Sediment available
166.00_MA
165.00_MA
164.00_MA
0
250
500 m

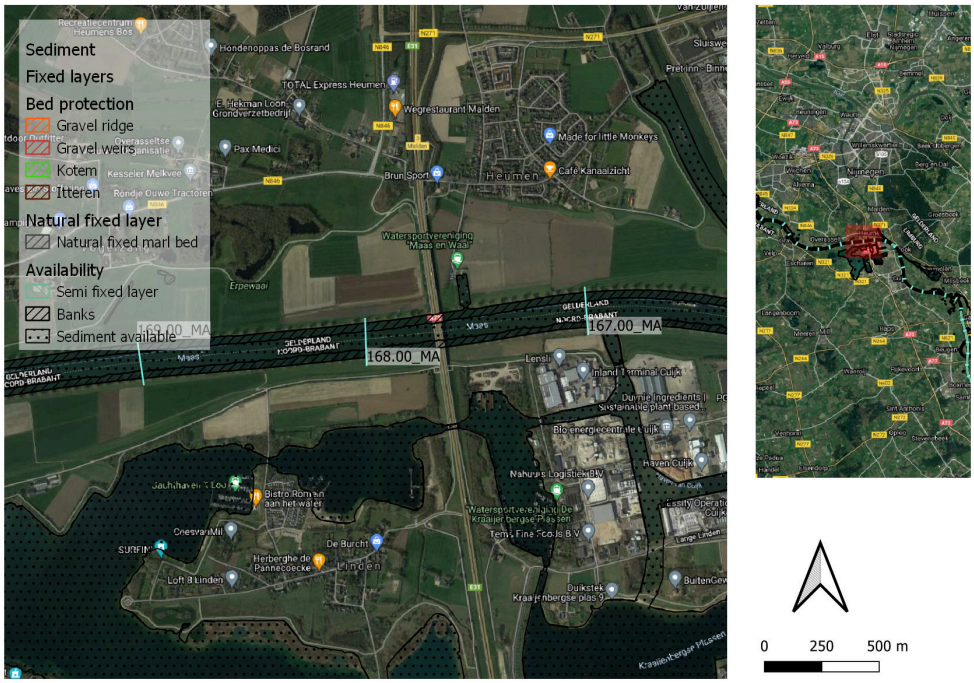
Sediment
Fixed layers
Bed protection
Gravel ridge
Gravel weirs
Kotem
Itteren
Natural fixed layer
Natural fixed marl bed
Availability
Semi fixed layer
Banks
Sediment available
168.00_MA
167.00_MA
0
250
500 m

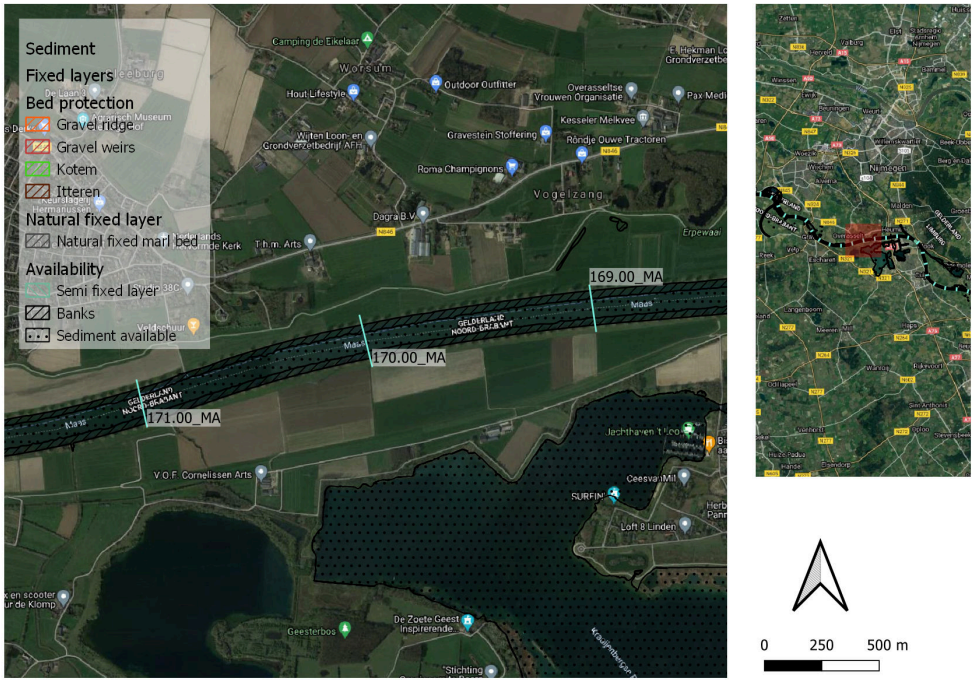
Sediment
Fixed layers
Bed protection
Gravel ridge
Gravel weirs
Kotem
Itteren
Natural fixed layer
Natural fixed marl bed
Availability
Semi fixed layer
Banks
Sediment available
169.00_MA
170.00_MA
171.00_MA
0
250
500 m


Sediment
Fixed layers
Bed protection
Gravel ridge
Gravel weirs
Kotem
Itteren
Natural fixed layer
Natural fixed marl bed
Availability
Semi fixed layer
Banks
Sediment available
172.00_MA
171.00_MA
0
250
500 m


Sediment
Fixed layers
Bed protection
Gravel ridge
Gravel weirs
Kotem
Itteren
Natural fixed layer
Natural fixed marl bed
Availability
Semi fixed layer
Banks
Sediment available
175.00_MA
174.00_MA
173.00_MA
0
250
500 m


Sediment
Fixed layers
Bed protection
Gravel ridge
Gravel weirs
Kotem
Itteren
Natural fixed layer
Natural fixed marl bed
Availability
Semi fixed layer
Banks
Sediment available
176.00_MA
175.00_MA
0
250
500 m

Deltares is an independent institute for applied research in the field of water and subsurface. Throughout the world, we work on smart solutions for people, environment and society.

Deltares

www.deltares.nl